Investigation of the Maisotsenko Cycle Based Air Conditioning Systems

By

Hamed Sadighi Dizaji

Supervisors

Associate Professor Eric Hu

Dr. Lei Chen

School of Mechanical Engineering

The University of Adelaide

This thesis is submitted for the degree of

Doctor of Philosophy

February 2021

Summary

Water evaporative based air coolers become more and more popular because of their lower energy consumption compared to the compressor-refrigerant based coolers. Low cooling capacity (theoretically wet-bulb temperature at 100% relative humidity), adding moisture to the product air and probable health issues due to the contaminated water droplets are the main shortcomings of direct evaporative air coolers. Although conventional indirect evaporative air cooler (which is direct evaporative cooler + a heat exchanger) overcomes some of the mentioned shortcomings (i.e. adding no moisture to the product air), the minimum achievable temperature would even be increased and remains as the main weakness of the indirect evaporative air coolers.

Maisotsenko-cycle (M-cycle) based indirect evaporative cooler (IEC) overcomes all mentioned problems as it is able to provide lower air temperature (below the wet-bulb temperature towards the dew point temperature) without adding moisture to the product air and without further energy consumption. Besides, M-cycle cooler does not have any negative impact on environment and it does not have any potential health issue due to the probable contaminated water droplets.

However, the research on M-cycle IEC is limited. No potential analytical model has been provided before for M-cycle IEC, and cumbersome time-consuming numerical simulations have been employed for design and analysis purposes. Hence, this research aims to develop better understanding on the thermal-exergetic behaviour of M-cycle cooler by developing new high-accurate quick analytical models for different working conditions. Experimental set-up is developed to validate the results of the programmed analytical models and then the

models are employed to perform a comprehensive sensitivity analysis of the key operation and design parameters of the M-cycle IEC.

Two high accurate quick solving analytical models are developed and presented for two main different working conditions of multi-stage Maisotsenko-cycle based indirect evaporative coolers termed water-spray mechanism and wet-surface mechanism. The models are able to generate cooling characteristics of the cooler very quick (compared to the numerical solutions) and accurate. The models are also able to provide temperature/humidity distribution (as a function of the locations inside the cooler) in addition to the outlet characteristics. Thus, the models can be considered as a strong research and design tool for M-cycle coolers. The models are further expanded to analyse the exergetic characteristics of the M-cycle cooler as well.

Although M-cycle IEC was first developed as the air conditioning system, other potential applications of M-cycle is proposed in this research as a novel air pre-cooling technology for gas turbine based power plants which suffer lower output power problem in summers (due to hot intake air temperature). The proposed system is based on a hybrid cycle of M-cycle and absorption chiller. The absorption chiller is powered by the released heat from the exhaust gas of the turbine, and the required water of M-cycle could be provided by the condensed water of the saturated air which make the system as an efficient air pre-cooling technology.

This thesis is presented in the form of a collection of the published papers which are the results of research. These five papers have been chosen to best demonstrate the study of M-cycle based air coolers. Additional background information is also provided in order to establish the context and significance of this work.

Acknowledgment

First of all, I would like to thank God almighty, the creator and the guardian, and to whom I owe my existence. God gives me the power to believe in myself and pursue my dreams. Apart from my efforts, the success of any project depends mostly on the encouragement and guidelines of many individuals. I take this opportunity to express my gratitude to my main supervisor A/Prof. Eric Hu for supervising my research using both his knowledge and experiences. I have been so lucky to have a supervisor from whom I learned many life lessons during my study. PhD study commonly is stressful period for students. However, I have been feeling calm and extreme peace of mind after any meeting with my supervisor. Briefly, it is impossible for me to show my sincere gratitude in few sentences to my supervisors. I highly thank again Eric for his support, valuable assistances, comments, guidelines and brilliant ideas. I also would like to express my gratitude to my co-supervisor Dr. Lei Chen for his valuable supports, patiently listening to my problems and guidelines. Lei always saw me immediately whenever I needed help. His guidelines have been so precious and facilitator for me during my PhD study. His efforts on fabrication process of my test-rig and through the all duration of my PhD study were significantly helpful. I highly thank again Lei for his supports and assistances. I also wish to thank the workshop staff members who helped me in fabrication of my test-rig. A special thank goes to my wife for giving me her deep love, encouragement and support during my studies.

Declaration

I certify that this work contains no material which has been accepted for the award of any other degree or diploma in my name in any university or other tertiary institution and, to the best of my knowledge and belief, contains no material previously published or written by another person, except where due reference has been made in the text. In addition, I certify that no part of this work will, in the future, be used in a submission in my name for any other degree or diploma in any university or other tertiary institution without the prior approval of the University of Adelaide and where applicable, any partner institution responsible for the joint award of this degree.

The author acknowledges that copyright of published works contained within this thesis resides with the copyright holders of those works. I give permission for the digital version of my thesis to be made available on the web, via the University's digital research repository, the Library Search and also through web search engines, unless permission has been granted by the University to restrict access for a period of time.

Hamed Sadighi Dizaji

Contents

Nomenclature

Nomenclature of each chapter has been provided at the beginning of each chapter (paper).

Chapter 1

Introduction

1.1. Background and introduction

A clean, fresh and temperate indoor condition directly affects people's productivity, well-being and tranquility in both their workplace and home. Moreover, recent issues due to the Covid-19 quarantines highlighted the significance of ventilation process and providing continuous fresh air. However, high energy cost and greenhouse gases emissions are still the main challenges in high quality heating, cooling and ventilation process for home/office users, electricity producers (power plants) and governments.

The required energy for heating process during the cold seasons is mainly supplied in the form of both electricity (heat pumps and electrical heater) and natural gas (oil fuels). That is why normally no peak electricity demand is shown in cold seasons of the year for air heating process. However, some countries consider the electrical heating as a safe and green method. Nonetheless, for countries with natural gas resources, heating by gas fuel is a basic, cheap and efficient method.

However, as all types of air coolers work based on electrical power, a critical situation is created for power plants (to work with higher or maximum capacity) to overcome the simultaneous electricity demand by all domestic, industrial and office buildings for air cooling process. Moreover, users have to pay more for electricity due to the high power consumption by the majority of the air coolers particularly compression based ones. Irrespective of electricity aspect, environmental issues such as using chlorofluorocarbons (Ozone destruction) by some cooling techniques are other major concerns discussed by environmental specialists.

Generally, three common cooling techniques exist for air cooling process including refrigerant compression method, air-water direct evaporative cooling

(swamp coolers) and air-water indirect evaporative cooling. The first group deals with chlorofluorocarbons and higher electricity consumption despite the enough cooling capacity. Moreover, their operation/maintenance cost is relatively higher than cost of the other techniques (because of moving parts, refrigerant required etc.).

Direct evaporative cooler works based on direct contact between air and water fluid. As shown in Fig. 1, the minimum achievable temperature in any direct evaporative cooling process is the wet-bulb temperature (occurs on saturation line, 100% relative humidity) of the inlet air entering to the channel.

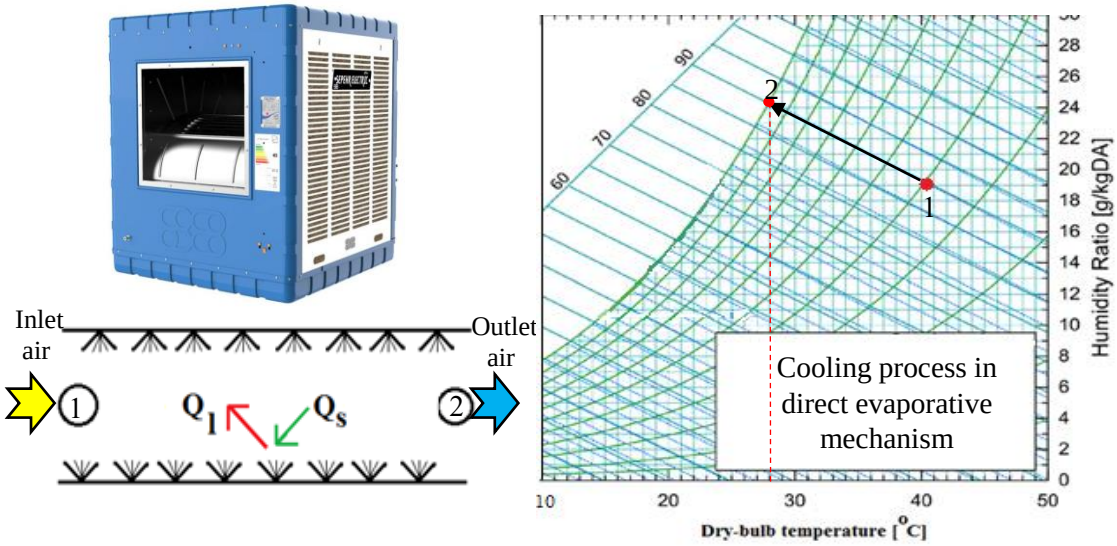

Fig. 1. Cooling process in direct evaporative cooler

For example, if the air inlet temperature is around 40 ^{o}C with humidity ratio of 19 g/kg (Point 1 in Fig. 1), the minimum theoretical outlet temperature is 28 ^{o}C (point 2 in Fig. 1). However, because of limitation of allowed humidity and also real efficiency of the cooler, the practical outlet temperature is warmer than this value. Although, direct evaporative cooler requires lower electricity power and has lower capital/maintenance cost, its cooling capacity is limited. Moreover, swamp cooler significantly increases the moisture of the product air which is not ideal. Besides, because of the direct contact between the product air and water droplets, clean

drinkable water must be employed in the cooling process to avoid health issues due to the probable contaminated water droplets (drinkable water is valuable and costly).

Indirect evaporative cooler (IEC), which is a direct evaporative cooler plus a heat exchanger (see Fig. 2), seems to be a solution for mentioned weaknesses as it does not add any moisture to the product air and does not require higher energy (compared to the compression based coolers). The working principle of the wet channel of the IEC is the same as direct evaporative cooler. Hence, the minimum achievable temperature of the wet-channel (which goes outside of the room) is wet-bulb temperature of the inlet air into the wet channel. As the inlet air into the wet-channel of the conventional IEC is ambient temperature, the minimum outlet temperature of the wet channel is wet-bulb temperature of the ambient temperature (Point 3 in Fig. 2). Hence, based on the principle of any heat exchanger, the outlet temperature of the dry channel (product air goes to the room) will be warmer than the outlet temperature of the wet-channel (Point 2 in Fig. 2). Thus, the product temperature of the conventional IEC is warmer than the product temperature of the direct evaporative cooler. That is why IEC was not commercialized in large scale as an air cooler.

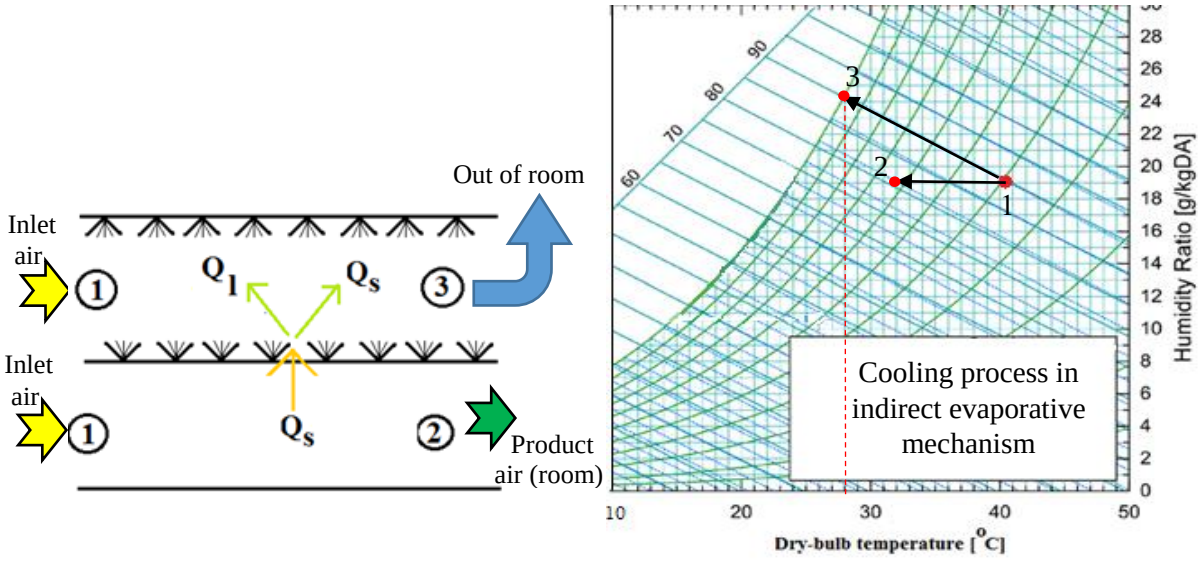

Fig. 2. Cooling process in conventional indirect evaporative coolers

Finally, Maisotsenko-cycle (see Fig. 3) revolutionized the whole indirect evaporative cooling process so that it is able to reduce the inlet air temperature below the wet-bulb temperature (toward the dew-point temperature). As can be seen in Fig. 3, a portion of the dry channel air is employed as the working fluid of wet-channel (instead of ambient air). It is mentioned that, the principle of direct evaporative cooling process (through the wet channel) is still valid i.e. the minimum achievable temperature along the wet channel is the wet-bulb temperature of its inlet air.

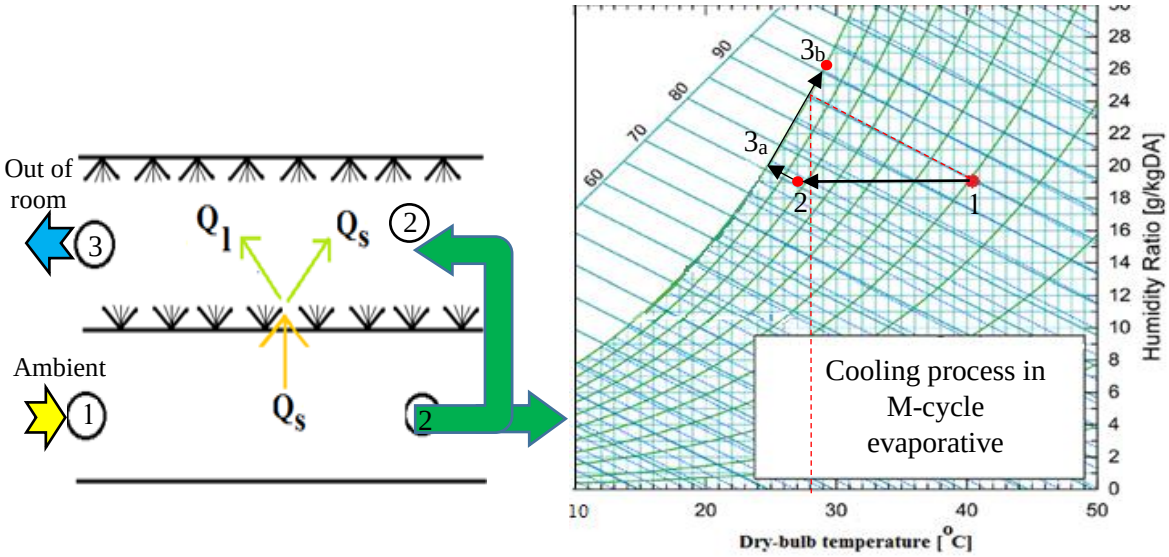

Fig. 3. Cooling process in M-cycle indirect evaporative coolers

However, it is clear that, the inlet air into the wet channel in M-cycle cooler is not ambient temperature and it is colder than the ambient temperature as it is first cooled through the dry channel (via the sensible and latent heat transfer). Hence, the air fluid through the wet-channel can be cooled until the wet-bulb temperature of number 2 (its inlet condition) via direct evaporative cooling process (Point 3_a in Fig. 3). As the wet-bulb temperature of number 2 is colder than the wet-bulb temperature of ambient air, the air fluid of dry channel can go below the wet-bulb temperature of the ambient air (its inlet air) due to the heat transfer principle of the heat exchangers.

The working principle of M-cycle is so interesting and requires deep thinking to be understandable. For example, the outlet temperature of wet channel can be either colder or warmer than its inlet temperature. Depending on the ambient condition, flow properties and the geometry of the channel, the cooling process through the wet channel can be finished at point 3_a or 3_b shown in Fig. 3. In the first option, the outlet temperature of the wet channel is colder than its inlet temperature while in the second option, the outlet temperature of the wet channel becomes warmer than its inlet temperature. In point 3_a, the air is fully saturated and hence it is not able to reduce its temperature by water evaporation. Nonetheless, as its temperature is colder than the inlet temperature of dry channel, the heat can still be transferred to the wet channel (from dry channel) via sensible heat transfer and increases the temperature of the working air (i.e process 3_a until 3_b occurs). However, the outlet temperature of the wet-channel is always colder than the ambient temperature (inlet temperature to the dry channel).

M-cycle system maintains the advantage of conventional direct evaporative cooling (i.e. lower power consumption) while overcomes its two major weaknesses (i.e. M-cycle does not add any moisture to the product air and the minimum achievable temperature by M-cycle is dew-point temperature rather than wet-bulb).

Fig. 4 shows a multi-stage M-cycle cooler in which the air fluid is gradually discharged into the wet channel instead of a sudden discharge at the end of the channel. This structure reduces the fluid pressure drop due to the gradual discharging process. The working principle of the perforated (multi-stage) cooler is the same as single-stage. The commercialized M-cycle coolers mainly work based on multi-stage structure in either counter flow (Fig. 4) or cross flow (Fig. 5) configuration. It is

mentioned that, cross flow configuration can only be in multi-stage structure (single stage structure is not meaningful for cross-flow configuration).

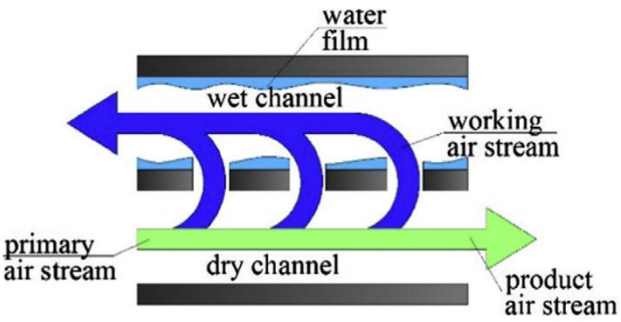

Fig. 4 Multi-stage M-cycle cooler

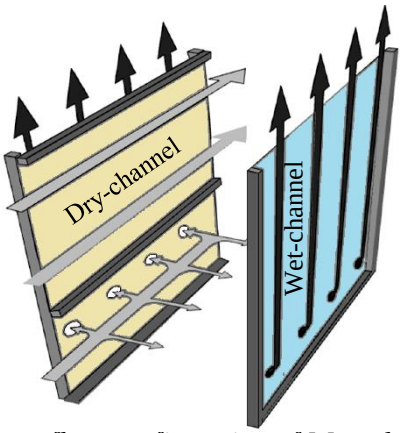

Fig. 5 Cross flow configuration of M-cycle cooler

Based on a comprehensive literature review, all previous investigations of multi-stage M-cycle coolers have been carried out using the numerical simulations or experimental techniques as no analytical solution has been proposed. Besides, the few provided analytical solutions for the single-stage M-cycle cooler were developed based on very simplified assumptions (constant wet plate temperature). Previous investigations of the M-cycle IEC are comprehensively discussed in the literature review section (Chapter 2).

In this dissertation, two high accurate analytical models are provided for two main different working principles of the multi-stage M-cycle cooler. These models are able to generate the cooling characteristics of the multi-stage M-cycle cooler so faster (compared to the numerical simulations) and accurately which means they can be employed as the strong design and optimization tools for these types of coolers in

both academic area and industrial sectors. Providing temperature/humidity distribution (in addition to the outlet characteristics) along the dry channel, wet channel and wet-surface as a function of location is another unique strong feature of the present validated models.

Sprayed-water mechanism and wet-surface mechanism are two possible working conditions of the M-cycle cooler. Sprayed water mechanism is the main working principle of the conventional M-cycle coolers while the wet-surface mechanism is mainly employed in the recent generations of the M-cycle coolers. In wet-surface mechanism, the water mass flow rate is as possible as small to only keep the middle-surface thoroughly wet (i.e. wet side of the middle surface). In other words, the water flow rate is the same as evaporated water which is replaced simultaneously (any further water stream reduces the efficiency of the cooler compared to the ideal wet-surface theory). Both latent and sensible heat transfers play key roles in the wet-surface theory and that is why the cooler is able to cool the air even if the water inlet temperature is the same as air inlet temperature. The M-cycle cooler can reach to its maximum capacity under this working condition as described in Chapter 4. In a real cooler, a specific ultra-thin material (curtain) is required as the middle plate to absorb the water fluid and keep the surface thoroughly wet in the wet-side (like a tissue or porous media) while stays dry and impermeable in the dry-side of the cooler. The recent invented material is discussed in mentioned Chapter 4 as well. However, instantaneous water replacement on the wet surface without further water streams is not practical (at least with current technology for water distribution systems) in real coolers and water flow rate has to be higher than the evaporated water to avoid creation of dry areas on the wet side of the surface. Hence, exact considerations are

required to make the efficiency of the cooler close to the theoretical wet-surface efficiency.

In sprayed-water mechanism, however, the water mass flow rate is large and is sprayed with a high pressure from the top side of the cooler and recirculates from the bottom side. Because of a continuous water fluid flow, the middle plate does not necessarily need to absorb the water and create a wet-surface. Hence, the material of the middle plate is not complicated (i.e. any ultra-thin impenetrable single material can be employed) which reduces the final cost of the cooler (and also the cooling capacity of the cooler). Because of the high water mass flow rate, the temperature of the middle plate is dominated by the water temperature and it has the same temperature as water. Sensible heat transfer plays a key role in this working condition and latent heat role becomes marginal. Hence, the water inlet temperature should be colder than the inlet air temperature (ambient air). The created noises due to the high-pressure water injection may make this working condition unsuitable for some inside-room applications. Indeed, this mechanism is only appropriate when cheap moderate cooling of hot air is expected without adding moisture to the product air (such as cooling process of a big exhibition through a hot day).

1.2.Aim and objectives

The aim of the present study is to develop better understanding of the thermal and exergetic characteristics of single and multi-stage Maisotsenko air cooler and then to improve its characteristics by addressing the research gaps identified.

The tasks (objectives) which have been taken in order to achieve the aforesaid aim are described in the following.

1. New high-accurate analytical model is developed and validated to investigate the cooling behaviour of the single and multi-stage M-cycle cooler.

2. The new model is programmed (via Maple programming software) and validated with the M-cycle test-rig (fabricated in the lab) at the University of Adelaide.

3. As no analytical parametric study has been provided before for multi-stage M-cycle cooler, a comprehensive analytical sensitivity analysis is performed by the new validated model to clarify the impact of various operational and design parameters on the performance of the M-cycle air cooler.

4. As extremely few exergetic evaluations have been performed for M-cycle air coolers (no exergetic study for multi-stage), a comprehensive exergetic analysis is performed for M-cycle air cooler to indicate how to enhance the performance of M-cycle from the viewpoint of the second law of thermodynamics.

5. Other probable application of M-cycle (beyond air conditioning systems) is investigated which resulted in proposition of a novel hybrid cycle of M-cycle and absorption chiller for air inlet temperature reduction of gas turbine power plants.

1.3. Thesis outline

This thesis is presented through several chapters. Each chapter (2 to 6) is based on a published paper. Chapter 1 is general concepts and the background of the research.

Chapter 2 provides a comprehensive literature review of Maisotsenko-cycle based air conditioning systems. All previous researches of M-cycle air coolers are classified based on research methodology including numerical simulation, analytical approach, statistical methods, parametric analysis and experimental techniques.

Chapter 3 provides an analytical model for perforated Maisotsenko air coolers based on the water-spray mechanism. The model validated with previous numerical/experimental research results in the same working conditions.

Chapter 4 provides a novel analytical model which is based on the wet-surface theory. This model is validated with the test-rig built at the University of Adelaide. Moreover, the impact of the key operational and design parameters of the cooler on cooling characteristics of the cooler is evaluated via the validated model.

Chapter 5 evaluates the M-cycle cooler from the viewpoint of the second law of thermodynamics. The validated model in Chapter 4 is employed to determine the outlet characteristics of the cooler and then the inlet and outlet characteristics are inserted to the exergetic model to evaluate the exergetic characteristics of the cooler.

Chapter 6 proposes a novel industrial application for M-cycle cooler (hybrid cycle of M-cycle and absorption chiller which can be used to reduce the air inlet temperature of gas turbine based power plants). Air temperature reduction causes increment of electrical power production by the power plant.

Chapter 7 provides a general conclusion and provides some recommendations for the future work.

1.4. Publications arising from this thesis

Based on the chapters described in the previous section, each chapter was published as a paper in high-rank international journals as listed in the following.

	List of Publications	Journal	Impact Factor
1	**Dizaji HS,** Hu EJ, Chen L. A comprehensive review of the Maisotsenko-cycle based air conditioning systems. Energy. 2018 Aug 1;156:725-49.	Energy (Published)	5.53 (Q1)
2	**Dizaji HS,** Hu EJ, Chen L, Pourhedayat S. Development and validation of an analytical model for perforated (multi-stage) regenerative M-cycle air cooler. Applied energy. 2018 Oct 15;228:2176-94.	Applied Energy (Published)	8.42 (Q1)
3	**Dizaji, H.S**., Hu, E.J., Chen, L. and Pourhedayat, S., 2020. Analytical/experimental sensitivity study of key design and operational parameters of perforated Maisotsenko cooler based on novel wet-surfac theory. Applied Energy, 262, p.114557.	Applied Energy (Published)	8.42 (Q1)
4	**Dizaji HS,** Hu EJ, Chen L, Pourhedayat S. Comprehensive exergetic study of regenerative Maisotsenko air cooler; formulation and sensitivity analysis. Applied Thermal Engineering. 2019 Apr 1;152:455-67.	Applied Thermal Engineering (Published)	4.02 (Q1)
5	**Dizaji HS,** Hu EJ, Chen L, Pourhedayat S. Using novel integrated Maisotsenko cooler and absorption chiller for cooling of gas turbine inlet air. Energy Conversion and Management. 2019 Sep 1;195:1067-78.	Energy Conversion and Management (Published)	7.18 (Q1)

1.5. Format

The thesis has been submitted as a portfolio of the publications, according to the formatting requirements of The University of Adelaide. The printed and online versions of this thesis are identical.

Chapter 2

Literature Review

This chapter has been published as

> Dizaji HS, Hu EJ, Chen L. A comprehensive review of the Maisotsenko-cycle based air conditioning systems. Energy. 2018 Aug 1;156:725-49.1;76:118-25 (DOI: 10.1016/j.energy.2018.05.086).

This chapter provides a comprehensive literature review of Maisotsenko-based air conditioning systems. All previous researches of M-cycle air coolers are classified based on research methodology including numerical simulation, analytical approach, statistical methods, parametric analysis and experimental techniques. It was found that no analytical solution was previously provided for multi-stage M-cycle cooler and analytical models for single stage M-cycle cooler have been significantly simplified with many assumptions.

Statement of Authorship

Title of Paper	A comprehensive review of the Maisotsenko-cycle based air conditioning systems
Publication Status	☑ Published ☐ Accepted for Publication ☐ Submitted for Publication ☐ Unpublished and Unsubmitted w ork w ritten in manuscript style
Publication Details	Dizaji HS, Hu EJ, Chen L. A comprehensive review of the Maisotsenko-cycle based air conditioning systems. Energy. 2018 Aug 1;156:725-49.1;76:118-25 (DOI: 10.1016/j.energy.2018.05.086).

Principal Author

Name of Principal Author (Candidate)	Hamed Sadighi Dizaji		
Contribution to the Paper	Performing the literature review, classification and organization of all previous models of M-cycle cooler and writing the manuscript.		
Overall percentage (%)	70%		
Certification:	This paper reports on original research I conducted during the period of my Higher Degree by Research candidature and is not subject to any obligations or contractual agreements with a third party that would constrain its inclusion in this thesis. I am the primary author of this paper.		
Signature		Date	

Co-Author Contributions

By signing the Statement of Authorship, each author certifies that:

i. the candidate's stated contribution to the publication is accurate (as detailed above);

ii. permission is granted for the candidate in include the publication in the thesis; and

iii. the sum of all co-author contributions is equal to 100% less the candidate's stated contribution.

Name of Co-Author	Eric Hu		
Contribution to the Paper	Supervising the work, assisting editing and finalising the manuscript.		
Signature		Date	

Name of Co-Author	Lei Chen		
Contribution to the Paper	Supervising the work, providing suggestions and recommendations.		
Signature	Ley Chen Digitally signed by Ley Chen DN: cn=Ley Chen, o, ou, email=Ley@mecheng.adelaide.edu.au, c=AU Date: 2021.01.12 16:23:00 +10'30'	Date	

Please cut and paste additional co-author panels here as required.

Energy 156 (2018) 725–749

Contents lists available at ScienceDirect

Energy

journal homepage: www.elsevier.com/locate/energy

A comprehensive review of the Maisotsenko-cycle based air conditioning systems

Hamed Sadighi Dizaji*, Eric Jing Hu, Lei Chen

School of Mechanical Engineering, The University of Adelaide, Adelaide, SA 5005, Australia

ARTICLE INFO

Article history:
Available online 17 May 2018

Keywords:
heat exchanger
Maisotsenko cycle
Evaporative
Dew-point
Wet-bulb
Air conditioner

ABSTRACT

Maisotsenko cycle (M-cycle) is a promising air cooling technique which can reduce the temperature of air flow until dew point which was not possible either in direct contact techniques or former indirect evaporative methods. M-cycle systems have been employed previously on gas turbines, air conditioning systems, cooling towers, electronic cooling etc. Simultaneous consideration of all of them prevents detailed presentation. For that reason and because of the wide application of air conditioning systems, this paper focuses only on the use of M-cycle on air conditioning systems. Moreover, former types of indirect evaporative air coolers which do not work based on Maisotsenko cycle are not considered in the present study. Researchers have evaluated the M-cycle characteristics via different methods including analytical solution, numerical simulation, statistical design methods and experimental-techniques all of which is divided into several categories as well. All said methods are organizedly discussed and compared in this paper. It has been tried to provide an evolutionary viewpoint for analytical solutions of M-cycle. Thus, analytical solutions were reorganized with unique abbreviations in order to become more understandable and comparable with each other. All M-cycle parameters (which have been analyzed via numerical or experimental ways) are coherently systematized and then a comprehensive-compact view of obtained results is presented. Finally, the current status of M-cycle industry is summarized and the future research direction on M-cycle is proposed.

Contents

* Corresponding author.
E-mail addresses: Hamed.SadighiDizaji@adelaide.edu.au, HamedSadighiDizaji@gmail.com (H. Sadighi Dizaji), eric.hu@adelaide.edu.au (E.J. Hu), lei.chen@adelaide.edu.au (L. Chen).

https://doi.org/10.1016/j.energy.2018.05.086
0360-5442/

Nomenclature

A	area (m^2)
c	Specific heat of moist air (Kj/Kg. ^oC)
h	Specific enthalpy (Kj/Kg)
h_g	Specific enthalpy of water vapor (J/Kg)
h_{fg}	Latent heat of vaporization of water (J/Kg)
k_p	Thermal conductivity of plate (W/m ^oC)
L	Length (m)
Le	Lewis factor
q	Heat transfer rate (W)
R	Thermal resistance (m^2K/W)
T	Temperature (^oC)
T_f	Water film temperature (^oC)
U	Overall heat transfer coefficient (Kw/m^2 ^oC)
$\dot{m}$	Mass transfer rate (Kg/s)
w	Humidity ratio (Kg moisture/Kg dry air)
W	Mass transfer between water film and moist air (Kg/s)

Special characters

ζ	Ratio between the change of enthalpy and wet-bulb temperature
δ_p	Thickness of plate (m)
δ_w	Thickness of water film (m)
α	Convective heat transfer coefficient (W/m^2 K)
β	Convective mass transfer coefficient (W/m K)

Subscripts

wa	Working air (secondary air)
Pa	Primary air (product air)
f	water film
wb	wet-bulb
s	saturated

1. Introduction

International Energy Outlook (2017) [1] has recently reported notable information regarding energy consumption by buildings. Rising standards of living in non-OECD (Organization for Economic Co-operation and Development) countries increase the demand for appliances, personal equipment, and commercial services [1]. It is projected that electricity use in buildings grows 2% annually, while total energy consumptions in buildings would increase by 32% between 2015 and 2040. The buildings sector (both commercial and residential), would account for almost twenty-one percent of the world's delivered energy consumption in 2040 [1]. Air conditioning systems are key energy consumer, using nearly fifty percent of the total consumed electricity in the buildings [2–4]. Hence, recognizing efficient air conditioning systems is required to reduce energy use in buildings.

Current air coolers especially compressor-based coolers increase significantly the electrical consumption in warm seasons, as they require electrical power to make cooling and circulate air. Most power-plants have to work with their maximum capacity in hot seasons in order to produce required extra electrical power which is mostly due to air conditioning systems. Moreover, increment of air temperature reduces gas-turbine-plants (one of the common powerhouses) performance which aggravates their working conditions. Subsequently, electrical power outage may occur in some regions of each country. Regardless the extra applied load on electrical power-plants, current air coolers increase the electrical power consumption cost for both home-users and industrial consumers as well. Hence, some governments have to allocate specific subsidies for electrical power consumers for some hot-weather regions of their country in summers. Obviously, this policy has its own economic issues and can't be considered as a permanent solution. Irrespective of economic features, all air coolers which work based on refrigerants may cause irreparable damages on our environment (particularly Ozone layer). Furthermore, burning of fossil fuels to generate extra electrical power causes air pollution too.

Employment of air-water direct contact coolers (Fig. 1a) instead of compressor-based systems may seem as a solution, as they only require electrical power for air circulation and cooling is made by water evaporation (into the air) without external power input. Although electrical consumption of direct contact evaporative air coolers (Fig. 1a) is usually less than the compressor-based coolers, they have some unavoidable disadvantages as below.

1. They are not able to reduce the air flow temperature less than wet-bulb temperature of inlet air. In other words, the minimum theoretical ideal temperature which can be achieved is wet-bulb temperature of inlet air (Fig. 1b).
2. Direct contact between the air and water fluid increases air-moisture which not only results in people's discomfort but also is harmful to electrical devices. Moreover, the water consumption of direct contact coolers is high and there is a possibility of health issues which can be due to unclean droplets of water fluid are evaporated by direct contact with the air.
3. This type of evaporator does not work on humid climate and the performance of such direct evaporative mechanisms significantly is affected by climates.

Because of different problems in both compressor-refrigerant based cooling techniques and direct-evaporative method (as mentioned above), researchers enthusiastically started to study on

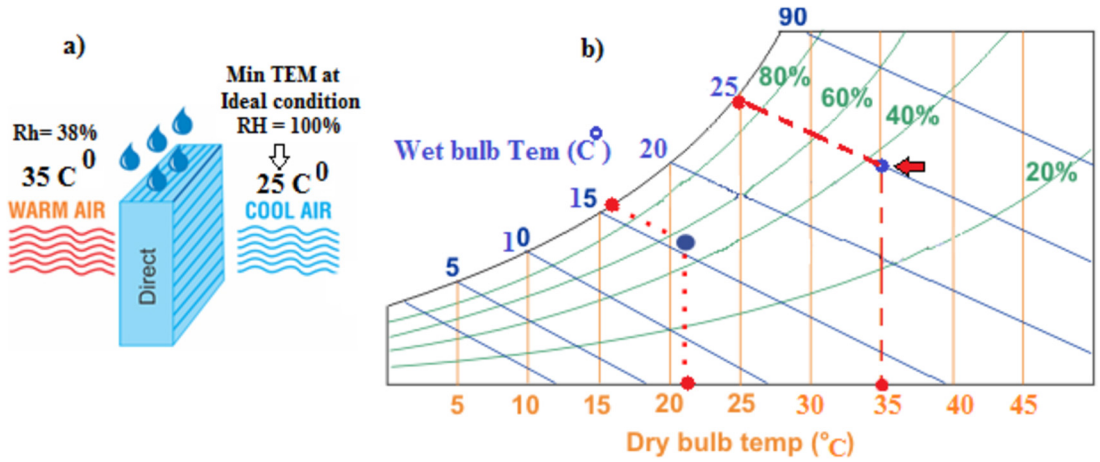

Fig. 1. Air-water direct contact mechanism a) general view b) process in psychometric chart.

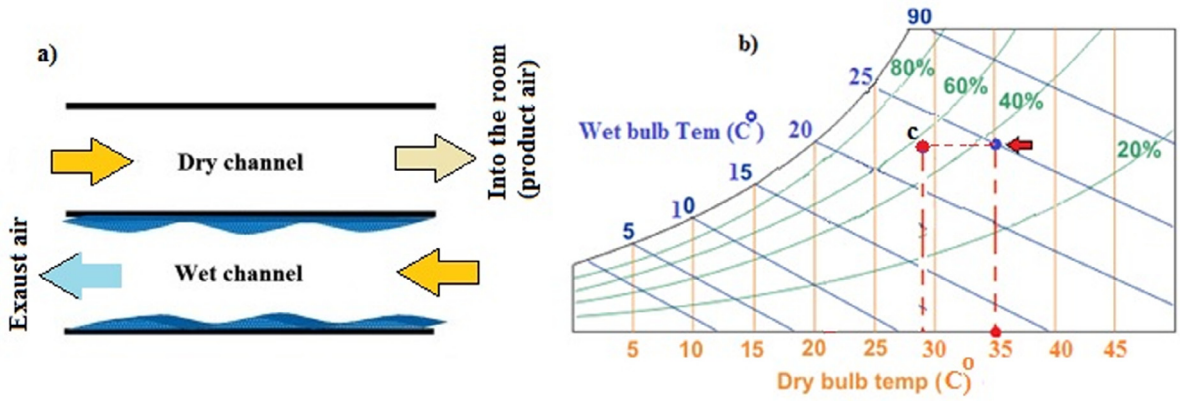

Fig. 2. Air-water indirect contact mechanism a) general view b) real process in psychometric chart.

indirect evaporative coolers (see Fig. 2a). Although the initial type of indirect evaporative cooler which basically combines a DEC and a heat exchanger (HE) as shown in Fig. 2a does not add any moisture to the product air, ie. overcomes the disadvantage 2 of DEC mentioned above, its performance is low in comparison with former direct contact evaporators. The outlet temperature of product air could reach the wet-bulb temperature of the incoming air theoretically [5]. Moreover, in completely ideal condition, outlet temperature of wet side of air flow could increase from its inlet wet-bulb temperature into the product air inlet dry bulb temperature (at saturated condition). Said ideal condition requires infinite amount of surface area and pure counter flow configuration. However, in real condition, temperature of dry side reaches only point "c" in Fig. 2b. Hence, for many years, indirect evaporative air coolers were not commercialized because of poor heat transfer rate which does not justify the excessive material and manufacturing cost.

Finally, Maisotsenko (at around 2000) presented a novel form of indirect evaporative exchanger in which all aforesaid problems of indirect evaporative method were solved. Based on Maisotsenko cycle, the wet side air fluid is pre-cooled before entering the wet channel. However, this precooling process can be occurred via different techniques. Fig. 3 (modified from Ref. [6]) illustrates different counter flow configurations of precooling process of wet side air flow by own wet channel. In Fig. 3a, wet channel air fluid is pre-cooled via another dry channel on the other side of wet channel. However, in Fig. 3b, a fraction of air-fluid of the main dry channel (which has been cooled) is returned into the wet channel at the end of the dry channel which is termed regenerative heat and mass exchanger. Maisotsenko technology causes reduction of dry side outlet air temperature under we-bulb temperature (until dew-point temperature) without adding any moisture. All other problems of direct contact evaporators and also former kind of indirect evaporative techniques have been solved in this novel form of indirect evaporative system. Psychometric chart related to Fig. 3b is illustrated in Fig. 3c from Ref. [10]. Fig. 4 [4–6] shows a perforation type of working channel in M-cycle heat exchanger which causes reduction of pressure drop across the exhaust channel [5].

Nonetheless, counter flow configuration of M-cycle air coolers was not commercialized for many years. Indeed, pure counter-flow configuration in a plate heat exchanger cannot be fabricated because of the geometry of the plates with air entering and evacuating on the same direction [5–7]. Hence, cross flow arrangement was presented which is easy to manufacture as a unit (see Fig. 5) and is produced by Coolerado Corporation [8] (see Fig. 6 [9] in which "1" is the primary air flow in dry channel, "2" is the working air stream which at first flow along the dry duct then it is delivered to the wet-channel, and "3" is the secondary air wet channel [4]).

As the working principle of M-cycle IEC, it could theoretically overcome disadvantages 1, 2 and 4 of DEC [10–12]. Hence, the main advantages of the novel M-cycle air conditioning systems can be described as below.

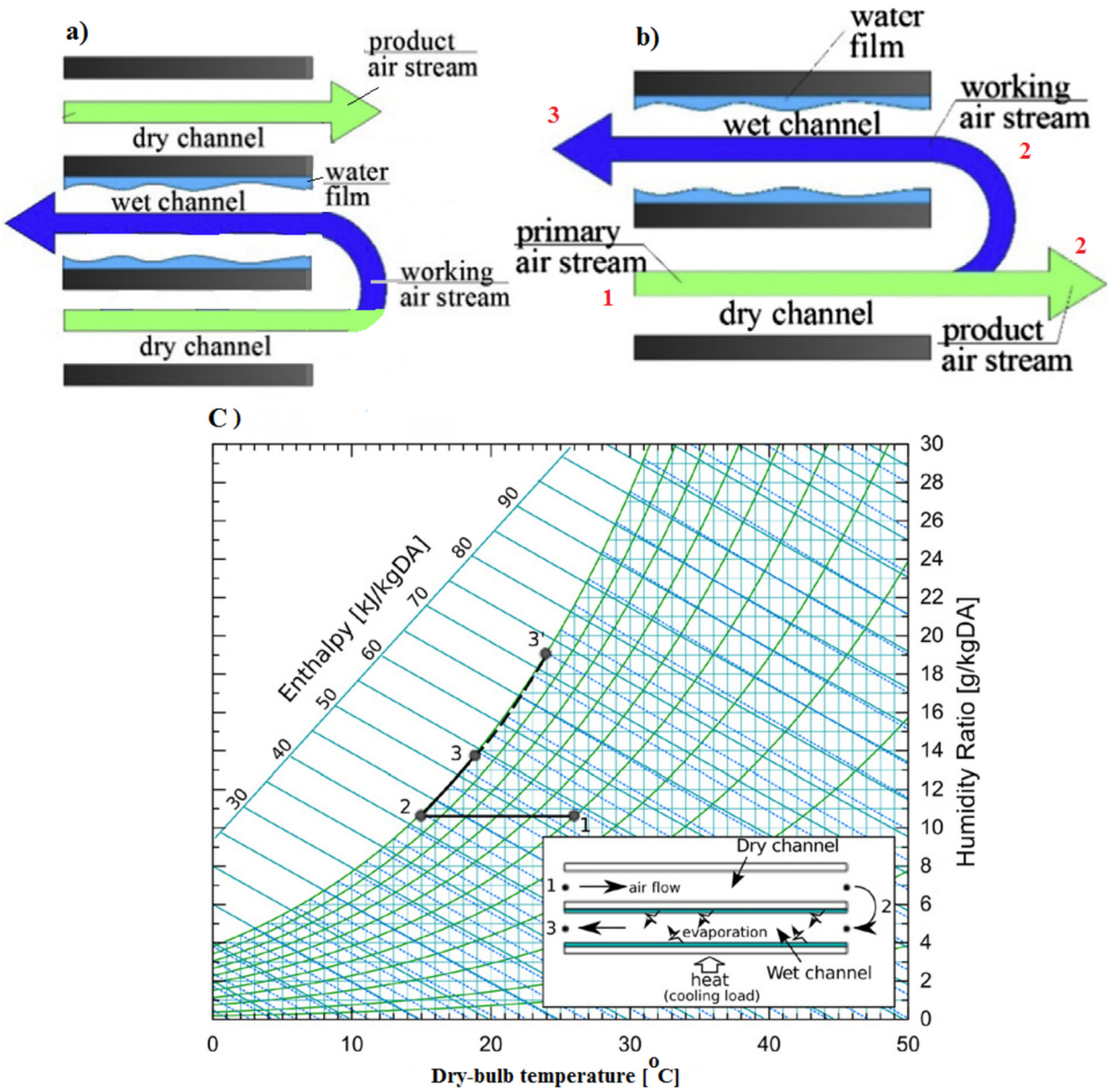

Fig. 3. Two main counter flow configurations of indirect evaporative based on main idea of M-cycle and the air conditions on the psychrometric chart [6–10].

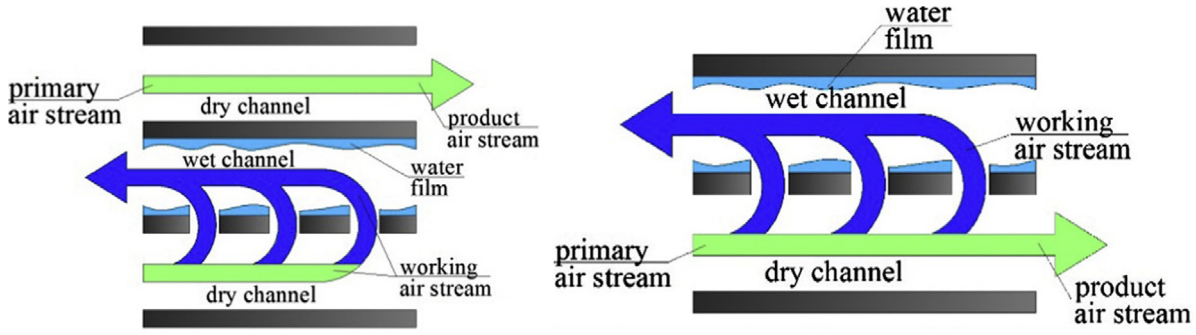

Fig. 4. Perforated type of counter flow configuration of indirect evaporative based on M-cycle [4,6].

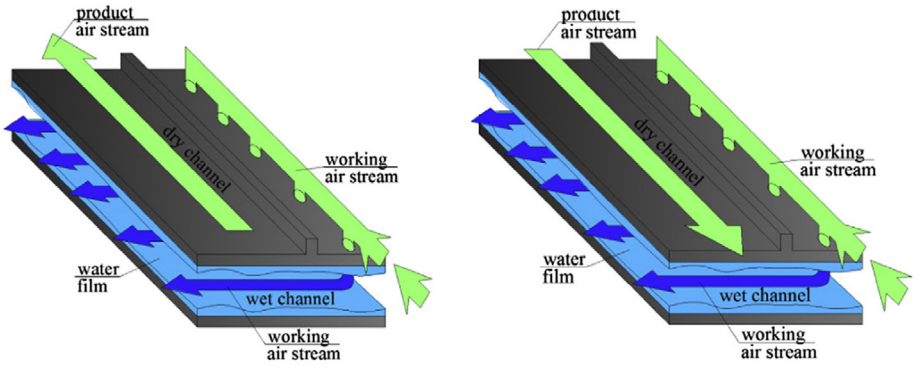

Fig. 5. Cross flow arrangement of M-cycle [6].

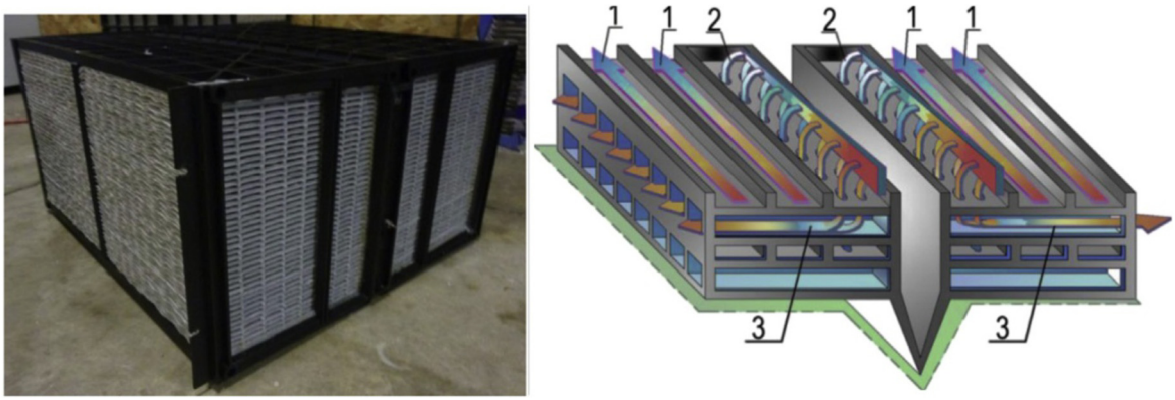

Fig. 6. Cross flow M-cycle HMX of Coolerado Corporation from Ref. [9].

1. M-cycle coolers are able to reduce the air temperature until dew-point temperature (which is not possible in DEC coolers) with very lower electrical-power-consumption in comparison with compressor-based air coolers.
2. Although both DEC coolers and M-cycle coolers use water fluid as a cooling mechanism, M-cycle coolers do not add any moisture to the product air stream. Moreover, in the same cooling power, M-cycle uses lesser water. Compressor-based coolers do not add moisture to the air as well. However, they use CFC in order to reach this aim not water fluid.
3. In comparison with DEC coolers, the possibility of health issues from contaminated water is zero in M-cycle coolers because of no direct contact between product air and water fluid.
4. M-cycle's cooling capacity enhances with increment of incoming air temperature [14].
5. As there is no compressor, condenser, evaporator, refrigerant etc. in M-cycle coolers, it has a very competitive initial and operating cost with compressor-based air coolers [14].
6. M-cycle coolers Provide healthier indoor atmosphere by incorporating 100% fresh air.

Nonetheless, some researchers believe that M-cycle is not appropriate for humid climates yet and it should be combined with desiccant systems in order to get higher efficiency. Thus, combination of liquid-desiccant or solid desiccant with M-cycle has been recently argued. These systems comprise of two processes: moisture removal by dehumidifier and sensible heat removal by M-cycle. Obviously, the effectiveness of the first stage impresses on the working quality of the second stage. Required power to drive desiccant system can be obtained by low-grade heat sources such as solar energy [16–19].

Despite the fact that the first idea of M-cycle evaporative cooler was developed around 1980, this type of M-cycle air coolers started to be developed and commercialized in this century [10–12]. Although Maisotsenko cycle is used in different applications such as gas turbine [20–31], cooling towers [32–35] and electronic cooling [36,37], this paper only focuses on the employment of M-cycle on air conditioning systems. Mahmood et al. [7] have presented the only review paper in any reputed journal on M-cycle systems in which the application of Maisotsenko cycle has been classified into 3 main parts (HVAC, cooling tower, gas turbine) and each part has been fundamentally discussed. However, present paper discusses only on Maisotsenko air conditioning systems in order to provide extra detail on this major application of M-cycle. Different evaluation methods of M-cycle air conditioning systems including analytical solution, numerical simulation, statistical design methods and experimental techniques which have been proposed by researchers are organized and discussed in this research. It has been tried to provide an evolutionary viewpoint for analytical solutions of M-cycle. Thus, analytical solutions were reorganized with unique abbreviations in order to become more understandable and comparable with each other. All M-cycle parameters (which have been analyzed via numerical or experimental ways) are systematized and then a comprehensive-compact view of obtained results is presented. Finally, the status of current M-cycle industry and the future research direction for M-cycle technology

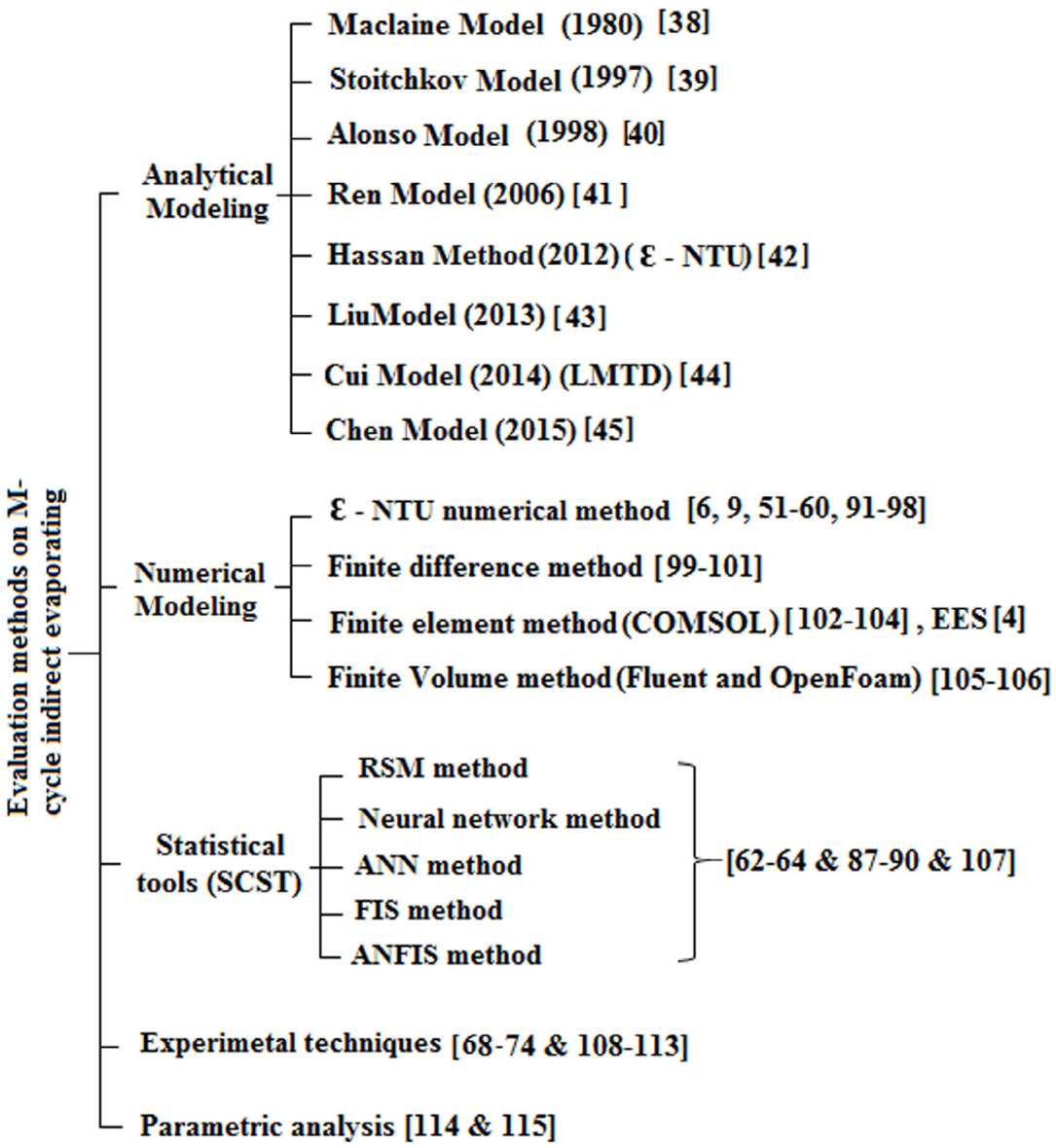

Fig. 7. Evaluation methods of M-cycle air conditioning systems [114,115].

are discussed.

2. Evaluation methods of indirect evaporative coolers

Generally, evaluation techniques of indirect M-cycle evaporative cooler can be classified into four main groups as shown in Fig. 7. Eight main analytical solutions of M-cycle are reorganized with unique abbreviations in order to become comparable with each other. The relationship between analytical solutions is discovered and discussed. Actually, it is tried to provide an evolutionary viewpoint for analytical solutions of M-cycle. M-cycle characteristics which have been evaluated by numerical or experimental techniques are discussed by some graphical representations.

3. Analytical approaches

The core of the M-cycle IEC modeling is to model/analyze heat and mass transfer on wet surface. Although some researches (Mickley [46] at 1949 and Pescod [47] at 1968) provided some basic theories on wet surface heat exchangers, it can be said that Makline-Cross theory [38] at 1980 is the leading general modeling of wet surface heat exchangers and its application to regenerative evaporative cooling. The main difference among analytical models is related to their assumptions. Indeed, some researchers prefer to simplify their modeling by considering some conditions while other researchers would not like to sacrifice accuracy for simplicity of the solution. Nonetheless, some of them have unique or new formulations (compared to the Maclaine model) which will be discussed with more detail of their formulations. Table 1 shows assumptions used in all analytical models reviewed, in which assumptions used in each modeling have been identified by "*" mark.

Lewis factor (assumption 7 in Table 1) plays a key role in evaluation of heat and mass transfer between liquids and gases. Lewis factor (Le) is a dimensionless number and generally is defined as the ratio of thermal diffusivity to mass diffusivity. Lewis [48] stated that the Le is approximately equal with "1" for air/water mixtures. Although according to [49,50] the proof given by Lewis was not strictly correct, this assumption has been used in most analytical

Table 1
Main assumptions of analytical modeling of indirect evaporative systems.

No	Assumptions	Maclaine [38]	Stoitchkov [39]	Alonso [40]	Ren [41]	Hassan [42]	Liu [43]	Cui [44]
1	Zero fluid thermal and moisture diffusivity in the flow directions	*	*	*	*	*	*	*
2	No heat transfer to the surrounding occurs	*	*	*	*	*	*	*
3	The passage walls are impervious to mass transfer	*	*	*	*	*	*	*
4	Pressures and mass flow rates are constant and uniform for both streams	*	*	*	*	*	*	*
5	c, h, α and U are constant and uniform;	*	*	*	*	–	–	*
6	The passage geometry is uniform throughout the heat exchanger	*	*	*	–	–	–	*
7	The Lewis relation is satisfied (Eq. (1))	*	*	–	–	*	*	*
8	The specific enthalpy of moist air h_{wa} is a linear function of T_{wa} and w_{wa}, thus $h_{wa} = a + c_{wa}T_{wa} + h_g w_{wa}$	*	–	–	–	–	–	–
9	The evaporating water film is stationary and continuously replenished at its surface with water at the same temperature.	*	–	–	–	–	–	–
10	The humidity ratio w_f of the air in equilibrium with the water surface is a linear function of the water surface temperature T_f so that the model saturation line is given by $w_f = d + eT_f$	*	–	–	*	–	–	–
11	Other type of 9: The water is distributed uniformly all over the channels and wets all the surface	*	–	–	–	–	*	*
12	Interface temperature is assumed to be the bulk water temperature	–	–	–	*	–	–	–
13	The interface between moist air and water film is saturated at the wate film temperature T_f	–	–	–	–	*	–	*
14	Air flow is laminar and also fully developed	–	–	–	–	–	–	*

Table 2
Heat exchanger type of each analytical model.

Models	Geometry of Heat exchanger
Maclaine [38]	Parallel and counter flow heat exchanger
Stoitchkov [39]	Cross flow plate heat exchanger
Alonso [40]	Cross flow heat exchanger
Ren [41]	Parallel and counter flow heat exchanger
Hassan [42]	Counter/parallel and usable for cross flow
Liu [43]	Counter flow heat exchanger
Cui [44]	Counter flow and expandable to cross flow
Chen [45]	Counter flow heat exchanger

models.

$$Le = \frac{\alpha}{\beta c_{wa}} = 1 \quad (1)$$

Thus:

$$\alpha = \beta\, c_{wa} \quad (2)$$

Where c_{wa} is the specific heat of moist air and $c_{wa} = 1.006 + 1.86w$. Eq. (2) creates a relationship between convective heat transfer coefficient (α) and convective mass transfer coefficient (β).

It should be mentioned that, each analytical model may focus on particular geometry (configuration) of direct contact heat exchangers. Thermal-flow configuration of each model has been provided in Table 2.

3.1. Maclaine-cross model

Maclaine and Banks [38] presented a general theory of wet surface heat exchanger and its application to regenerative evaporative cooling. They proposed a liner approximate model of wet surface heat exchanger by analogizing with dry surface heat exchanger [45]. Maclaine method proposed a linear approximate and graphical representation which can be employed to evaluate the wet surface heat exchanger effectiveness. A general view of wet surface heat exchanger is shown in Fig. 8.

Maclaine model is based on eight equations which four of them are based on assumptions (Table 1) and rest of them are based on conservation of energy or mass as below.

Conservation of energy for product air stream:

$$UA\left(T_f - T_{pa}\right) = \dot{m}_{pa} c_{pa} \frac{\partial T_{pa}}{\partial x} L_{pa} \quad (3)$$

Energy balance between two channels:

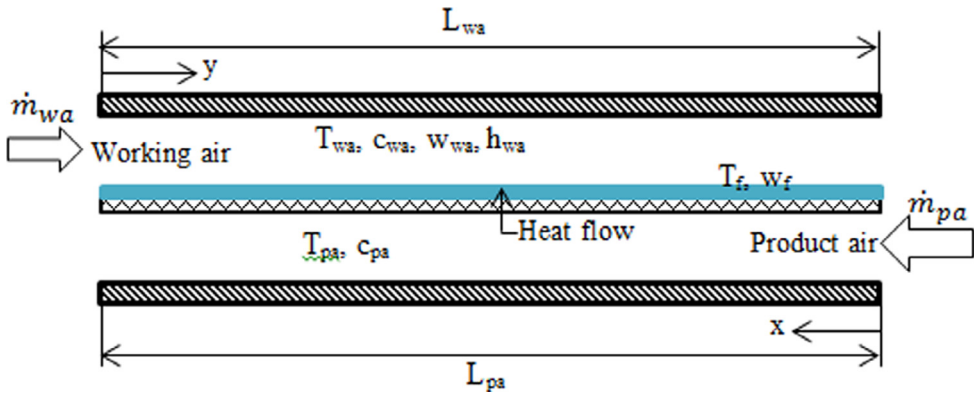

Fig. 8. A general view of wet surface heat exchanger (redrawn modified from Ref. [38]).

$$\alpha_{wa}A_{wa}\left(T_{wa}-T_f\right)+\beta A_{wa}h_{fg}\left(w_{wa}-w_f\right)+UA\left(T_{pa}-T_f\right)=0 \tag{4}$$

Conservation of water vapor in the moist air stream

$$\dot{m}_{pa}\,L_{wa}\frac{\partial w_{wa}}{\partial y}=\beta\,A_{wa}\left(w_f-w_{pa}\right) \tag{5}$$

Conservation of energy for working air:

$$\dot{m}_{wa}\frac{\partial h_{wa}}{\partial y}L_{wa}=\alpha_{wa}A_{wa}\left(T_f-T_{wa}\right)+\beta\,A_{wa}h_g\left(w_f-w_{pa}\right) \tag{6}$$

According to assumption 7, 8 and 10:

$$\alpha=\beta\,c_{wa} \tag{7}$$

$$h_{wa}=a+c_{wa}T_{wa}+h_g w_{wa} \tag{8}$$

$$w_f=d+eT_f \tag{9}$$

The approximation psychometric equation is written as below in which / indicates the adiabatic saturation state defined using the linearized or model saturation line of assumption 10.

$$w_{wa}=w'_{wa}+\left(T'_{wa}-T_{wa}\right)\frac{c_{wa}}{h_{fg}} \tag{10}$$

Inlet working air temperature and humidity ratio and also product air inlet temperature are constant and known as the boundary conditions of solving aforesaid eight equations.

Regarding to Eq. (9), although the actual saturation line in real psychometric chart is not linear, Maclaine assumed a linear behaviour (Eq. (9)) for saturation line (see Fig. 9). Indeed, if the constants "d" and "e" in Eq. (9) are chosen to give an approximate least square fit to the actual saturation line over the range of water surface temperature, this model can present actual performance. The recommended values for "d" and "e" by Maclaine are as below.

$$e=\frac{W_{f,max}-W_{f,min}}{T_{f,max}-T_{f,min}} \tag{11}$$

$$d=\frac{2\left(W_{f,min}+W_{f,mean}\right)-W_{f,max}}{3-eT_{f,min}} \tag{12}$$

Where $T_{f,\,min}$ and $T_{f,\,max}$ are the estimates of the minimum and maximum water surface temperature. $T_{f,\,mean}$ is the average of $T_{f,\,min}$ and $T_{f,\,max}$.

See Fig. 9 to understand graphical concepts of these values. Indeed, the estimated values of T_{fmin}, $T_{f\,max}$ and $T_{f\,mean}$ are used to plot the points W_{min}, W_{max} and W_f on the actual saturation line. The straight line joining W_{min} and W_{max} is drawn, then, parallel to this line and two-thirds of the way from it towards point $W_{\,mean}$, another line is drawn. This is Maclaine model saturation line [39]. Maclaine solved these eight equations by some methods found in literature in order to determine the thermal performance of characteristics of indirect evaporative exchanger.

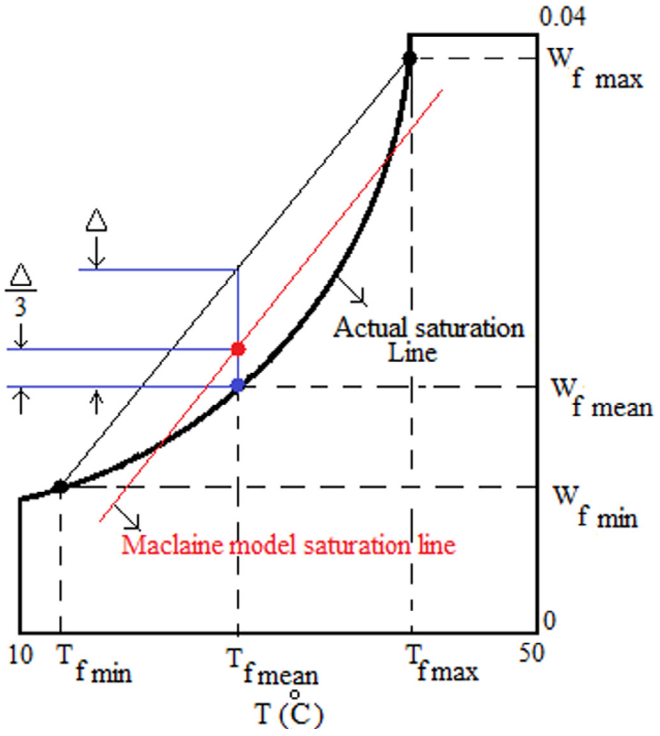

Fig. 9. Maclaine Model saturation line (modified redrawn from Ref. [38]).

3.2. Stoitchkov model

Stoitchkov [39] indicated three deficiencies for Maclaine model as listed below:

- Maclaine did not show how the mean surface temperature should be estimated.
- The values of total to sensible heat ratio for different mean surface temperatures given in a table are calculated for a barometric pressure of 101325 Pa. Hence, for other pressures, the outcomes will have a source of error.
- In Maclaine model, the evaporating water film is stationary and continuously replenished at with water at the same temperature (assumption 9 in Table 1). However, in a real heat exchanger, the evaporated water is much less than the mass flow rate of sprayed water which causes reduction of effectiveness of the wet surface heat exchanger compared to the Maclaine assumption.

Hence, Stoitchkov further improved the Maclaine model. However, this model focuses on cross flow plate heat exchanger. Stoitchkov and Dimitrov improved Maclaine method by following considerations:

- Determination of the mean surface temperature for any defined thermal and geometrical specification.
- Presenting a correlation (approach) to estimate the barometric pressure [39].

3.3. Alonso model

Alonso provided a user-friendly simplified model by providing an equivalent water temperature [45] in Maclaine solution. The model obtained based on the models developed by Maclaine [38].

3.4. Ren model

Ren and Yang [41] believed that previous simplified models sacrifice accuracy for simplicity of the solution. Most simplified models assume a unity Lewis factor and neglect the water losses due to evaporation. They indicated following deficiencies for all

previous modeling. All these deficiencies were applied to simplify the former models.

- The moisture content of the air has been considered a linear function of the water surface temperature.
- Lewis factor is satisfied
- The evaporating water film was stationary and continuously replenished with water.
- Wet surface is assumed completely wetted.

Hence, they expanded an analytical model for indirect evaporative cooler with parallel/counter flow configuration with variable surface wettability and Lewis factor [45]. Their model is sophisticated which is due to non-unity Lewis factor, surface wettability, varying spray water temperature and spray water enthalpy change [44]. Briefly, Ren model consists of below characteristics which can't be found in former analytical modes.

- Incomplete surface wetting condition: The wall surface cannot be entirely wetted because of low distance between the surface and high value of sprayed water which creates more tension. This leads to reduction of mass transfer area.
- Non-unity Lewis factor: Lewis factor is not necessary equal with unity even for entirely wetted surface [7].
- Consideration of spray water evaporation
- Consideration of spray water temperature variation
- Consideration of spray water enthalpy change through the heat exchanger

Nonetheless, humidity ratio is steel assumed to have a linear relationship with water surface temperature. However, the error of this condition can be minimized by choosing suitable values of “e” and “d” in Eq. (9). Assumptions of this model can be seen in Table 1. The effect of condition 12 (in Table 1) is minor because of very large heat transfer coefficient between water film and air-water interface [8,50].

After the development of the model, Ren compared the performance of four different configurations of indirect evaporative air cooler as shown in Fig. 10. The results evaluated by Ren model reviled higher performance for case “a” compared to the three other cases. However, with negligible spray water flow rate and complete wetting surface, case “a” and case “b” showed the same performance.

3.5. Cui model (LMTD)

Conventional LMTD method is a well-known method of evaluation of heat exchangers which deal with sensible heat transfer. The final aim in this technique is finding a correlation for total Q as $Q = A\,U\Delta T_{LMTD}$ in which the value of ΔT_{LMTD} is evaluated only by inlet and outlet temperatures. LMTD is appropriate for investigations in which temperature distribution is not considered as a main factor. In other words, LMTD works based on inlet/outlet, surface and some other bulk characteristics of heat exchangers. Contrary to numerical methods, this technique is neither cumbersome nor high time required. Nonetheless, conventional LMTD method should be modified in order to become usable in indirect evaporative systems. Indeed, latent heat transfer is an intrinsic feature of indirect evaporators which has not been applied in basic format of LMTD. For this reason, Cui et al. [44] presented a modified LMTD method to analyze counter flow indirect evaporative heat exchangers. This method provides better precision if the temperature variation in the heat exchanger is not linear and the maximum temperature difference at one end of the heat exchanger is higher than twice the temperature difference at the other end of the heat exchanger [44].

3.5.1. Assumptions of Cui method (LMTD)

As briefly stated in Table 1, the assumptions of this method are as below.

1) The distribution of water on the wet surface is uniform and even.
2) Heat and mass transfer occur in direction normal to the air flow.
3) Air flow is laminar and also fully developed and the system is well insulated.
4) Water fluid in the wet channel behaves as a thin static film because the water flow rate by convection is negligible (heat and mass transfer between water film and plate is assumed to be occurred only by conduction).
5) Thin moist air layer at the water-air interface is saturated at the water film temperature.
6) It is reasonable to assume that the enthalpy difference between two points has a linear function with wet bulb temperature difference for small operating range of temperatures. Indeed, on Psychrometric chart, the wet-bulb temperature lines are nearly parallel with constant enthalpy lines for small operating range

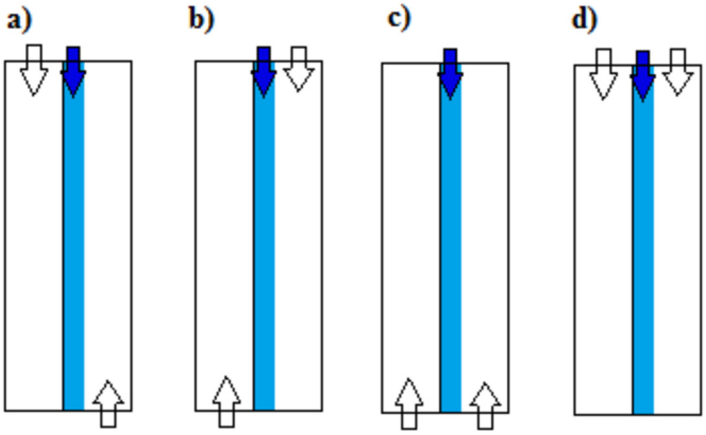

Fig. 10. Different arrangements evaluated by Ren analytical model [41].

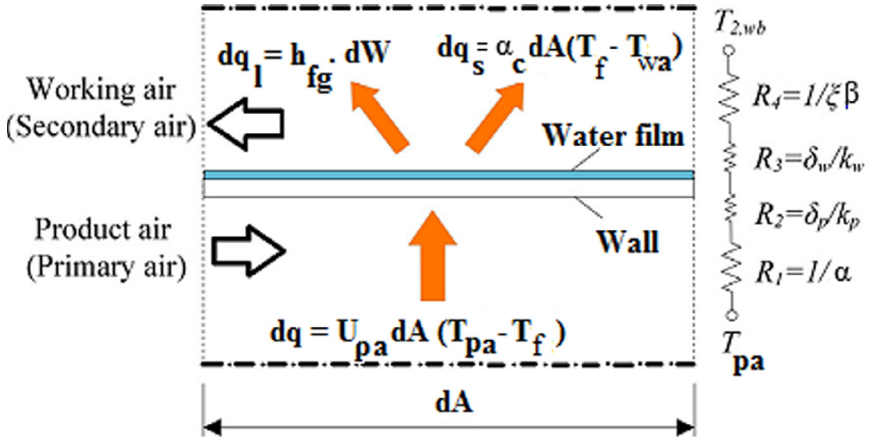

Fig. 11. One dimensional cross flow indirect heat exchanger [modified from 44].

of temperatures [44,45]. Hence, the parameter ξ is defined as the ratio between the change of enthalpy and the change of wet-bulb temperature $\left(\xi=\frac{\Delta h}{\Delta T_{wb}}\right)$ and is estimated by input and output condition of wet channel ($\Delta h=\xi\,\Delta T_{wb}$).

7) Lewis factor is unity

3.5.2. Mathematical development

Fig. 11 shows the defined computational element which comprises half of the product channel and working channel (due to geometrical symmetry) of a plate type indirect evaporative cooler [44]. Where U_{pa}, T_{pa}, T_f, T_{wa}, h_{fg} and α are overall heat transfer coefficient of primary air, temperature of primary air, temperature of water film, temperature of secondary air, latent heat of water evaporation and convection heat transfer coefficient respectively. δ_p, k_p, δ_w, k_w are thickness of plate, thermal conductivity of plate, thickness of water-film and thermal conductivity of water respectively.

According to conservation principle of energy for primary air, dry side heat transfer rate can be calculated from Eq. (13).

$$dq=-\dot{m}_{pa}c_{pa}dT_{pa}\overset{\text{yields}}{\Rightarrow}dT_{pa}=-\frac{dq}{\dot{m}_{pa}c_{pa}} \tag{13}$$

Besides, based on conservation principle of energy for working air and assumption "6", wet side heat transfer rate can be calculated from Eq. (14).

$$dq=-\dot{m}_{wa}dh_{wa}\approx-\dot{m}_{wa}\xi dT_{wa,wb}\overset{\text{yields}}{\Rightarrow}dT_{wa,wb}=-\frac{dq}{\dot{m}_{wa}\xi} \tag{14}$$

Subtracting Eq. (14) from Eq. (13) gives Eq. (15).

$$d\left(T_{pa}-dT_{wa,wb}\right)=-\left(\frac{1}{\dot{m}_{pa}c_{pa}}-\frac{1}{\dot{m}_{wa}\xi}\right)dq \tag{15}$$

Eq. (15) can't be integrated unless a correlation is found for dq. Hence, attempts are made to provide a correlation for dq as below.

Obviously, heat transfer rate between a fluid flow and a plate can be evaluated via Newton's Law of Cooling too. Thus, heat transfer on the dry side of heat exchanger (which is only sensible and occurs between product air and water-film) is evaluated by.

$$dq=U_{pa}dA\left(T_{pa}-T_f\right) \tag{16}$$

$$U_{pa}=\frac{1}{\frac{1}{\alpha}+\frac{\delta_p}{k_p}+\frac{\delta_f}{k_f}} \tag{17}$$

In wet side of heat exchanger, there are two types of heat transfer as below:

$$dq_{sensible}=\alpha\,dA\left(T_f-T_{wa}\right) \tag{18}$$

$$dq_{latent}=h_{fg}.\,dW \tag{19}$$

dq_{latent} is due to water evaporation in which dW is mass transfer rate between the water film and moist air and is calculated from Eq. (20) (β is mass transfer coefficient and w is humidity ratio).

$$dW=\beta\,dA\left(w_f-w_{wa}\right) \tag{20}$$

Hence, latent heat transfer is calculated by:

$$dq_{latent}=h_{fg}\,\beta\,dA\left(w_f-w_{wa}\right) \tag{21}$$

Total heat transfer rate on wet side is sum of the sensible heat and latent heat as below.

$$dq=dq_{sensible}+dq_{latent}=\alpha\,dA\left(T_f-T_{wa}\right)+h_{fg}\beta\,dA\left(w_f-w_{wa}\right) \tag{22}$$

According to Eq. (2) (from assumption "7"), Eq. (22) can be rewritten as below.

$$dq=\beta c_{wa}dA\left(T_f-T_{wa}\right)+h_{fg}\,\beta\,dA\left(w_f-w_{wa}\right)=\beta\,dA\left[\left(c_{wa}T_f+h_{fg}w_f-\left(c_{wa}T_{wa}+h_{fg}w_{wa}\right)\right)\right]$$
$$\xrightarrow{h=cT+h_{fg}w}dq=\beta\,dA\left[h_s\left(T_f\right)-h_{wa}\right] \tag{23}$$

$h_s(T_f)$ is saturation enthalpy of air fluid in water film temperature. According to Eq. (23), it can be said that, the driving force of total heat transfer in wet channel is calculated by enthalpy variation between the saturated air at water surface and the main moist air stream [11]. Eq. (23) can be rewritten based on assumption "6" ($\Delta h = \xi\,\Delta T_{wb}$) as follow (this is why modified thermal resistance in Fig. 10 is $1/\xi\,\beta$).

$$dq = \xi\,\beta\,dA\left(T_f - T_{wa,wb}\right) = U_{wa}dA\left(T_f - T_{wa,wb}\right) \tag{24}$$

U_{wa} is modified overall heat transfer coefficient in wet channel. If Eq. (16) is rearranged based on T_f and then is substituted for T_f in Eq. (24), yields,

$$dq = \frac{U_{pa}U_{wa}}{U_{pa}+U_{wa}}dA(T_{pa} - T_{wa,wb}) = U\,dA(T_{pa} - T_{wa,wb}) \tag{25}$$

U is the modified overall heat transfer coefficient which is related to both dry and wet channel.

$$U = \frac{1}{\frac{1}{\alpha_{pa}} + \frac{\delta_p}{k_p} + \frac{\delta_w}{k_w} + \frac{1}{\xi\,\beta}} \tag{26}$$

Now, Eq. (25) can be substituted for dq in Eq. (17) which yields Eq. (27).

$$\frac{d(T_{pa} - dTwa, wb)}{T_{pa} - T_{wa,wb}} = -U\left(\frac{1}{\dot{m}_{wa}c_{wa}} - \frac{1}{\dot{m}_{wa}\xi}\right)dA \tag{27}$$

Eq. (27) can now be integrated over the entire surface as below.

$$\int_0^A \frac{(T_{pa} - T_{wa,wb})}{T_{wa} - T_{wa,wb}} = -\int_0^A U\left(\frac{1}{\dot{m}_{wa}c_{wa}} - \frac{1}{\dot{m}_{wa}\xi}\right)dA \tag{28}$$

$$Ln(T_{pa} - T_{wa,wb})\Big|_0^A = -U\left(\frac{1}{\dot{m}_{wa}c_{wa}} - \frac{1}{\dot{m}_{wa}\xi}\right)A\Big|_0^A \tag{29}$$

$$Ln\frac{(T_{pa} - T_{wa,wb})_A}{(T_{pa} - T_{wa,wb})_0} = -U\left(\frac{1}{\dot{m}_{sa}c_{sa}} - \frac{1}{\dot{m}_{sa}\xi}\right)A \tag{30}$$

For a counter flow IEHX for example, Eq. (30) can be rewritten as below.

$$Ln\frac{T_{pa,outlet} - T_{wa,wb,inlet}}{T_{pa,inlet} - T_{wa,wb,outlet}} = -U\left(\frac{1}{\dot{m}_{wa}c_{wa}} - \frac{1}{\dot{m}_{wa}\xi}\right)A \tag{31}$$

Integrating Eq. (13) and Eq. (14) over the entire length of channel yields:

$$Q = \dot{m}_{pa}c_{pa}\left(T_{pa,\,inlet} - T_{pa,\,outlet}\right) \overset{\text{yields}}{\Rightarrow} \frac{1}{\dot{m}_{pa}c_{pa}} = \frac{Q}{T_{pa,\,inlet} - T_{pa,\,outlet}} \tag{32}$$

$$Q = \dot{m}_{wa}\xi(T_{wa,\,wb,\,outlet} - T_{wa,wb,\,inlet}) \overset{\text{yields}}{\Rightarrow} \frac{1}{\dot{m}_{wa}\xi} = \frac{Q}{(T_{wa,\,wb,\,outlet} - T_{sa,wb,\,inlet}} \tag{33}$$

Substituting Eq. (32) and Eq. (33) in Eq. (31) and after some simplification yields:

$$Q = U\,A\frac{\left(T_{pa,inlet} - T_{wa,wb,\,outlet}\right) - \left(T_{pa,outlet} - T_{wa,wb,inlet}\right)}{Ln\left(\frac{T_{pa,\,inlet} - T_{wa,\,wb,\,outlet}}{T_{pa,\,outlet} - T_{wa,wb,\,inlet}}\right)} \tag{34}$$

Eq. (34) is the final format of heat transfer rate of a counter flow indirect heat exchanger based on LMTD method (comparable with conventional LMDT method) in which:

$$LMTD = \frac{\left(T_{pa,inlet} - T_{wa,wb,outlet}\right) - \left(T_{pa,outlet} - T_{wa,wb,inlet}\right)}{Ln\left(\frac{T_{pa,\,inlet} - T_{wa,\,wb,\,outlet}}{T_{pa,\,outlet} - T_{wa,wb,inlet}}\right)} \tag{35}$$

3.6. Hassan [42] method (modified ε - NTU)

Hassan used modified analytical ε-NTU method to study the evaporative coolers and it may not be considered as a separate analytical model (usually "model" refers to a full distribution of the parameters inside the exchanger while "method" only allows to give outlet parameters on the basis of inlet parameters). Conventional ε-NTU is one of the well-known methods for solving heat transfer problems for sensible heat exchangers. Hasan [42] used the modified version of this technique which can be used for indirect evaporative heat exchangers. Sensible format of this technique can't be employed for indirect heat exchanger because of the existence of two gradients [42] including 1: temperature gradient between the air fluid in dry channel and water film and 2: enthalpy gradient between the saturated air-water film interface and the moist air. In the modified ε-NTU method attempts are made to create a connection between temperature of dry side channel and "h" in the wet channel by a unique gradient. As mentioned before in Table 1, the assumptions of this model are listed as below.

1) The cooler is well insulated to the surrounding.
2) Thermal conduction in the wall through longitudinal is neglected.
3) Heat and mass transfer coefficient inside each passage are constant.
4) Lewis number is unity.
5) Interface between moist air and water film is saturated at the water film temperature (T_f).

3.6.1. Mathematical development of ε - NTU model

The same equations (16–23) form LMTD method are the beginning mathematical process in this method too. Hence, Eq. (23) is rewritten here.

$$dq = \beta\,dA\left[h_s\left(T_f\right) - h_{wa}\right] \tag{36}$$

$h_s(T_f)$ is saturation enthalpy of air fluid in water film temperature. Totally, it can be assumed that, there is a linear relation between air saturation temperature and its enthalpy (saturated enthalpy) as below.

$$h_s(T) = aT + b \overset{so}{\Rightarrow} h_s\left(T_f\right) = aT_f + b \tag{37}$$

where $h_s(T)$ is saturated enthalpy of air at temperature of T and "a" is the slope of the saturation line (this assumption should not result in a significant error for small temperature ranges). Substituting Eq.

(37) into Eq, (36) gives:

$$dq = \beta\, dA\left(aT_f + b - h_{wa}\right) \tag{38}$$

Parameter T_f can be replaced with from Eq. (16).

$$dq = \beta\, dA\left(a\left(T_{pa} - \frac{dq}{UdA}\right) + b - h_{wa}\right) \overset{\text{yields}}{\Rightarrow} dq = \frac{aT_{pa} + b - h_{wa}}{\frac{a}{U} + \frac{1}{\beta}} dA \tag{39}$$

It should be noted that, according to Eq. (37), the term $(aT_{pa} + b)$ is $h_s(T_{pa})$ which means air saturated enthalpy at the primary air (dry side) temperature. Thus, Eq. (39) becomes

$$dq = \frac{1}{\frac{a}{U} + \frac{1}{\beta}} dA\left[h_s\left(T_{pa}\right) - h_{wa}\right] \tag{40}$$

$\frac{1}{\frac{a}{U} + \frac{1}{\beta}}$ is new transfer coefficient. Eq. (40) connects T_{pa} in dry channel with h_{wa} in the wet channel by one equation based on unique enthalpy gradient ($[h_s\,(T_{pa}) - h_{wa}]$). It should be noted that, the modified enthalpy form $[h_s\,(T_{pa})]$ represents the thermal content of air fluid flow in dry side. The value of this modified enthalpy at the inlet and outlet of dry channel are $h_s(T_{pa,\ inlet})$ and $h_s(T_{pa,outlet})$. Generally, the amount of heat transfer rate through dry channel is $dq = \dot{m}c\,(T_{inlet} - T_{outlet}) = \dot{m}(h_{inlet} - h_{outlet})$. However, $h_s(T_{pa,\ inlet})$ and $h_s(T_{pa,outlet})$ are modified enthalpy (not real enthalpy). Hence, a modified mass transfer rate should be defined which can be found from heat balance on dry air side as below.

$$\dot{m}_{pa}c_{pa}\left(T_{pa,\ inlet} - T_{pa,\ outlet}\right) = \dot{m}^*_{pa}\left[h_s\left(T_{pa,\ inlet}\right) - h_s\left(T_{pa,outlet}\right)\right] \tag{41}$$

Rearranging this equation:

$$\dot{m}^*_{pa} = \dot{m}_{pa}c_{pa}\frac{T_{pa,\ inlet} - T_{pa,outlet}}{h_s\left(T_{pa,inlet}\right) - h_s\left(T_{pa,outlet}\right)} = \frac{\dot{m}_{pa}c_{pa}}{a} \tag{42}$$

where "a" is the slope of the temperature-enthalpy saturation line. Conventional ε-NTU method of sensible heat exchangers is based on (T, c and $\dot{m}$). The correlations of ε-NTU method based on (T, c and $\dot{m}$) and its temperature profile is illustrated in Fig. 12. However, thermal profile of indirect evaporative was achieved based on modified enthalpy and modified mass flow rate as shown in Fig. 13a. It is mentioned that, these modified parameters can connect dry channel to wet channel via one equation and unique enthalpy gradient which is necessary in ε-NTU evaluation method.

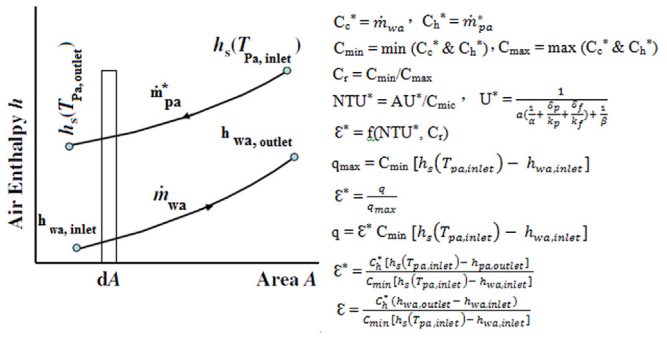

Fig. 12. Temperature profile and ε-NTU correlations in sensible heat exchangers [42].

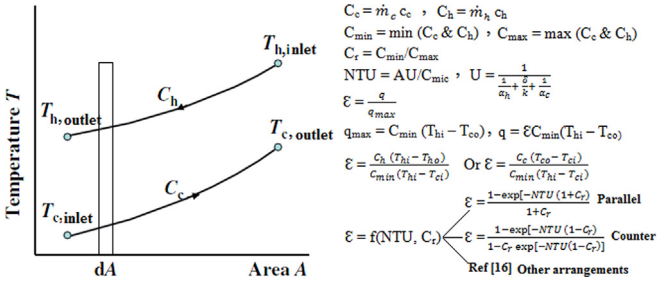

Fig. 13. Temperature profile and modified ε-NTU correlations in indirect heat exchangers [42].

And that is interest reason of this type of modified parameters. The ε-NTU method can be applied for indirect heat exchanger if proper redefining of sensible parameters is made by compering Figs. 12 and 13a. These adjustments are shown in Fig. 13b. The expression for the effectiveness $\varepsilon^* = f(NTU^*, C_r)$ takes similar forms as equations of sensible heat exchangers by replacing NTU by NTU^*. Heat transfer occurs from the fluid in dry side (hot air) to the fluid in wet side. Hassan method can be employed for different flow configurations in IEC coolers (regenerative, counter and parallel flow). Iteration is not necessary for counter and parallel flow configuration. However, for the regenerative configuration, iterations are needed because the wet side inlet air temperature is equal to the dry side outlet temperature which is unknown [42].

3.7. Liu model

Liu [43] stated two deficiencies for Hassan ε-NTU model as below:

- Hassan model introduced a coefficient "a" to present the slope of the saturation line and did not discussed how to evaluate this coefficient.
- Hassan's model has been validated only by one operation condition without discussing its verification with other operation condition.

Thus, Lui presented a simplified thermal modeling based on ε-NTU method and then validated utilizing experimental data from the literature in a wide range of operating conditions. The model highlights several improvements over the previous simplified models, including the detailed procedure for UA value calculation for laminar and turbulent IEHX channel flows [43].

The initial formulations of this model are the same equations used in Hassan model. Eq. (16) and Eq. (23) from Hassan's model are rewritten here.

$$dq = U_{pa}dA\left(T_{pa} - T_f\right) \tag{43}$$

$$dq = \frac{\alpha_{wa}}{c_{wa}}dA\left[\left(T_f\right) - h_{wa}\right] \tag{44}$$

Both Eq. (43) and Eq. (44) have the same functional form. If the enthalpies in Eq. (44) could be expressed as a function of temperature only, this equation can be used as a part of series heat transfer path with equation 43 [43].

For moist air, the enthalpy is expresed as Eq. (45) in which c_{pa} is specific heat of moist air and is calculating with $c_{pa} = 1.006 + 1.86$ W (Kj/Kg C) and h_{fg} is evaporation of water at 0 celsious. However, Liu approximated the enthalpy of moist air at its wet-bulb (saturation) temperature condition as seen in Eq. (46)).

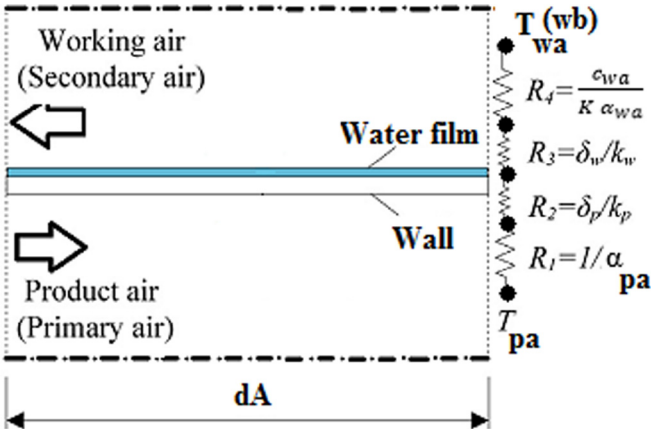

Fig. 14. Thermal resistance across the exchnager [43].

Liu used simmilar assumption for calculating of $h_s(T_f)$ which is enthalpy of saturated air-water interface layer (Eq. (47)).

$$h_{wa} = c_{pa}T + wh_{fg} \tag{45}$$

$$h_{wa} = c_{pa}T_{wa}(wb) + w_{wa}(wb)h_{fg} \tag{46}$$

$$h_s\left(T_f\right) = c_{pa}T_f + w_s\left(T_f\right)h_{fg} \tag{47}$$

Difference between Eq. (46) and Eq. (47) shows that $[h_s(T_f) - h_{wa}]$ in Eq. (44) can be expresed a linear equation of $T_f - T_{wa}(wb)$ as shown below.

$$dq = \frac{\alpha_{wa}}{c_{wa}}dA\left[h_s\left(T_f\right) - h_{wa}\right] \approx \frac{\alpha_{wa}}{c_{wa}}K(dA_s\left(T_f - T_{wa}(wb)\right) \tag{48}$$

where K is the slope of the enthalpy-saturation temperaturion curve. Eq. (48) reveales that the difference between water film temperature and working air wet-bulb temperature is the driving force for energy transfer from the water film to the working air stream [43]. If Eq. (48) and Newton's Law of Cooling is compared, it is obvious that the term $K\frac{\alpha_{wa}}{c_{wa}}$ is analogous to the local heat transfer coefficient between water film and working air. Hence, as shown in Fig. 14 (modified version of Fig. 2 from Ref. [43]), total, overall thermal resistance and its corresponding heat flux between primary air and working air are presented as Eq. (49) and Eq. (50) respectively.

$$\frac{1}{U} = \frac{1}{\alpha_{pa}} + \frac{\delta_p}{k_p} + \frac{\delta_f}{k_f} + \frac{c_{wa}}{K\alpha_{wa}} \tag{49}$$

$$dq = UdA(T_{pa} - T_{wa}(wb)) \tag{50}$$

Based on conservation of energy for working air:

$$q = \dot{m}_{wa}\left(h_{wa,\ outlet} - h_{wa,\ inlet}\right) \tag{51}$$

Parameter $\overline{K}$ (is diferent from K) is introduced and defined as the ratio of wet-bulb temperature difference between the wet side inlet and outlet and their enthalpy difference; Equation 51 can then be rewritten as:

$$q = \dot{m}_{wa}\overline{K}\left(T^{wb}_{wa,\ outlet} - T^{wb}_{wa,\ inlet}\right) \tag{52}$$

Based on conservation of energy for primary air:

$$q = \dot{m}_{pa}c_{pa}\left(T_{pa,\ inletr} - T_{Pa,\ outlet}\right) \tag{53}$$

Now, a modified ε-NTU method can be applied through equations 50, 52 and 53 as shown in Fig. 15. Indeed, modified C_c, C_h and other parameters of modified ε-NTU mehod is expressed by comparing equations 50, 52 and 53 with the sensible format of those equaions (for sensible heat exchnagers). The amount of α or other parametres for calculating U is definite and depends on flow regime etc. Hence, Liu [35] has discussed the method by which the value of U is evaluated for laminar or turbulante flow. Furthermore, determination of $\overline{K}$ has been presented as well by Liu for this model which can be found in Ref. [35].

3.8. Chen model

Chen [45] believed that none of previous analytical investigations has consider the effect of condensation on the performance of IEC units. Indeed, in humid area condensation may occur in the fresh air side which causes reduction of the cooler performance [45]. Former studies has not applied this consideration because of two reasons: 1) the humidity of the fresh air is low (indirect evaporative cooler is usually used in dry regions) and 2)

For sensible exchanger	For IEHx
$C_c = \dot{m}\,c_{pc}$, $C_h = \dot{m}\,c_{ph}$	$C_c = \dot{m}_{wa}\overline{K}$, $C_h = \dot{m}_{pa}\,c_{pa}$
$\frac{1}{U} = \frac{1}{\alpha_{hot}} + \frac{\delta_p}{k_p} + \frac{1}{\alpha_{cold}}$	$\frac{1}{U} = \frac{1}{\alpha_{pa}} + \frac{\delta_p}{k_p} + \frac{\delta_f}{k_f} + \frac{c_{wa}}{K\alpha_{wa}}$
$NTU = \frac{A\,U}{C_{min}}$	$\varepsilon = f(NTU, C_r)$
$C_{min} = \min(C_c \text{ and } C_h)$	$C_{max} = \max(C_c \text{ and } C_h)$

Fig. 15. Liu modified ε-NTU model.

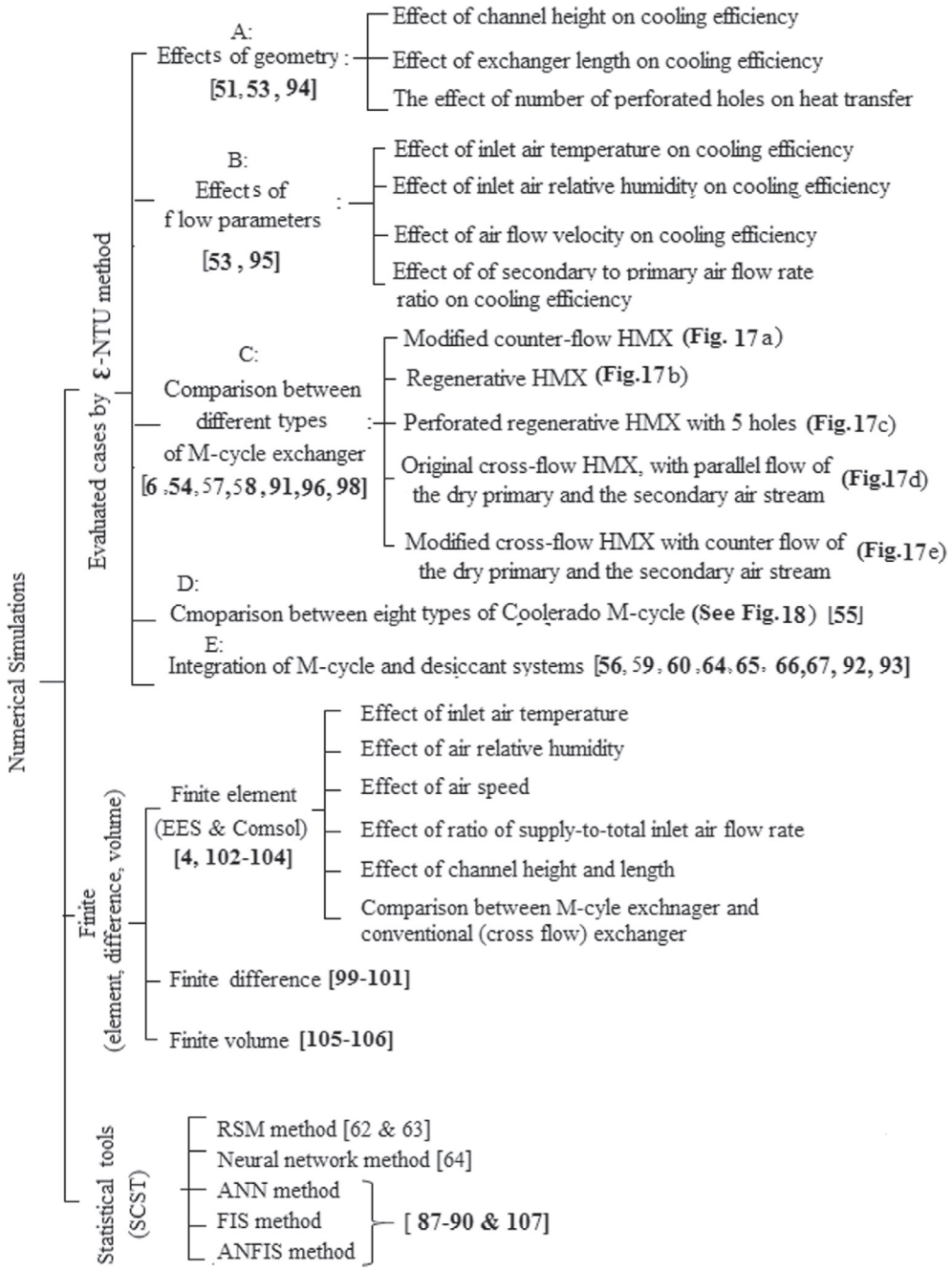

Fig. 16. A comprehensive compact view on investigated parameters of M-cycler via numerical simulations [51–67,88,90–99,107].

outdoor fresh air is used for both working air and primary air so that the plate surface temperature is higher than the dew point temperature of the air. Hence, Chen's model evaluates the performance of IEC form three viewpoints including non-condensation, totally condensation and partially condensation.

As a result, if a high-accurate analysis of M-cycle is required, Ren model will be the best model. However, this model is sophisticated and requires complex calculation. Maclaine-cross model and Stotichkov model is low accurate but quick-respond model and are appropriate for initial designing of M-cycle cooler. If the temperature distribution along the exchanger is not considered, Cui model (LMTD) will be useful which provides outlet specifications of M-cycle cooler based on inlet flow and geometric characteristics. Besides, Cui model can be used for both designing aim and calculating aim. In the first mode, an M-cycle cooler is designed by knowing the inlet/outlet condition of the cooler while in the second mode, the outlet parameters of a given cooler is determined. If the effect of condensation on the performance of M-cycle cooler is considered as an important parameter, Chen model will be the only helpful model. Both Hassan and Liu model are based on modified ε-NTU method will be suitable when the outlet temperature of the cooler are not known.

4. Numerical modeling

According to Fig. 16, M-cycle numerical modeling is classified into three main categories (based on analysis method) including ε-NTU, finite element/difference/volume, Statistical Design

Table 3
Effect of different parameters on cross-flow exchanger characteristics which have been evaluated by numerical ε-NTU method [51–58].

Parameters	Cooler characteristics		
	Output air temperature	Dew point effectiveness	Specific cooling capacity
Increment of air inlet temperature	+	+	+
Increment of inlet air relative humidity	+	+	−
Increment of inlet air humidity ratio	+	+	−
Increment of channel height	+	−	+
Increment of dry channel length	−	+	+
Increment of wet channel length	−	+	+
Increment of air flow velocity	+	−	−
Increment of secondary to primary air flow ratio	−	+	+
Increment of number of perforated holes	+	N	−

methods. However, Statistical Design Tool can be indicated as a distinct method (as seen in Fig. 7) and in this paper is discussed as a separate part. An overall-compact view on investigated parameters of M-cycle via all numerical simulations can be seen in Fig. 16. Numerical simulations revealed that the work of M-cycle exchanger is dependent on the interaction of many important factors including aerodynamic, hydrodynamic, thermodynamic, structure and others [51–53]. Perforations decrease the pressure loss of air which may allow for a significant reduction in the unit's operation costs [51]. However, it has lower cooling capacity which is due to the warm air inlet wet channel through the entire length of heat exchanger [51].

4.1. Numerical ε-NTU method

In most engineering applications, an engineer is interested in receiving bulk average values rather than variable distributions. For these cases, numerical ε-NTU method is preferred to other numerical simulations methods.

Most numerical analysis of M-cycle exchanger has been performed by ε-NTU technique. However, almost all ε-NTU-based evaluations have been carried out by one group of authors Sergey Anisimov and Demis Pandelidis [52] who tried to find different thermal features of M-cycle with their own ε-NTU modeling. Although the final formulations of the method have been presented in their publications, the references which have been cited for the origin of the formulations [74–77] are not online accessible.

A glimpse-view on the effect of different parameters on M-cycle characteristics (part A and B in Fig. 16 which have been evaluated by numerical ε-NTU method for cross-flow exchangers) is presented in Table 3. The signs "+" and "-"mean increment and decrement of that characteristics respectively. As can be seen in Table 3, increment of inlet humidity ratio or decrement of inlet air temperature reduces the cooling capacity of m-cycle air coolers which emphasize again the unsuitability of M-cycle coolers for humid and relatively cold climate conditions.

Regarding to part C in Fig. 16, the condition of comparison should be clearly stated because of the different structures of analyzed exchangers. Comparison has been carried out under real operating condition [6] of each exchanger. All exchangers have the same dimensions, the same plate thickness and the same channel height. Nonetheless, they have different secondary to primary air ratio. According to [53] the best air ratio (which provides higher effectiveness) for cross flow exchangers equals 1. However, it is

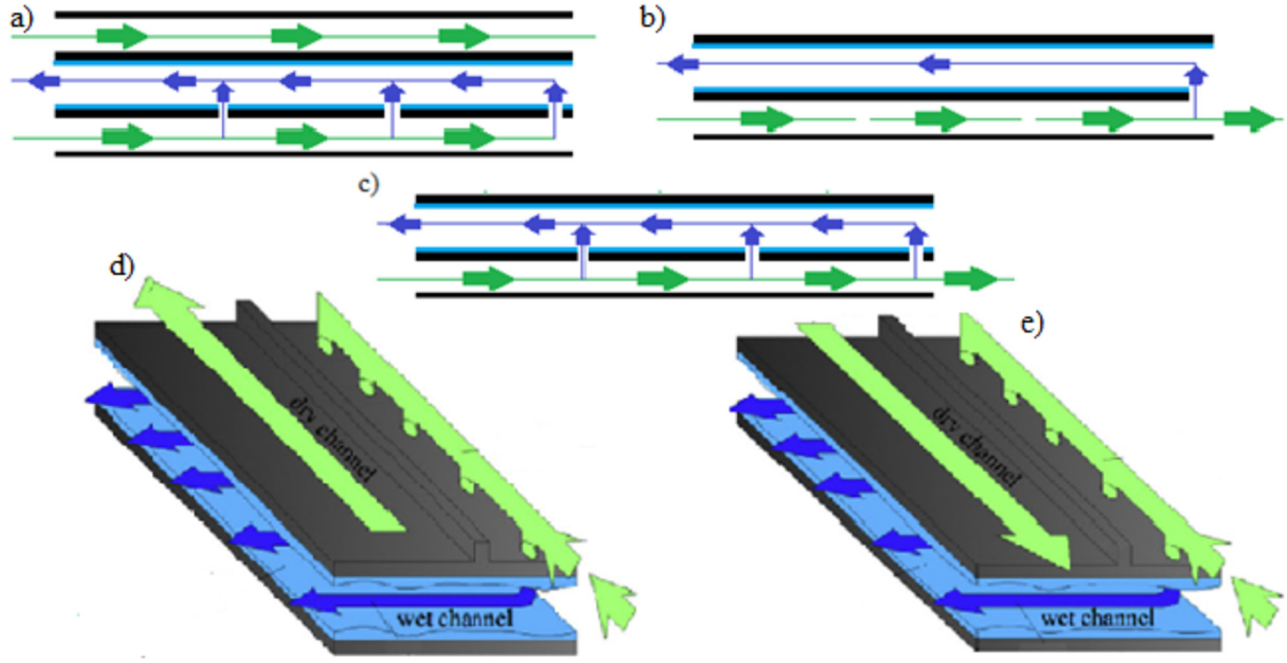

Fig. 17. Different types of M-cycle exchanger a) modified counter flow HMX, b) regenerative HMX c) perforated regenerative HMX d) cross flow HMX and e) modified cross flow HMX [6].

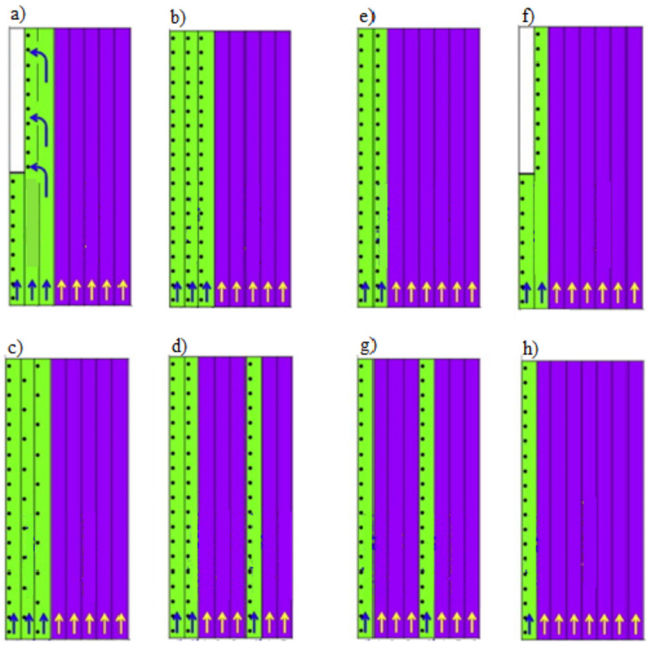

Fig. 18. Eight types of Coolerado corporation M-cycle HMX (See part D in Fig. 16) [55].

impossible to have the air ratio of 1 for regenerative exchangers (case "b" and "c" in Fig. 17) because of their construction. Indeed, all primary air streams from dry channel have to be delivered to wet side in order to have air ratio of 1 (but the cooling capacity of such would be zero). To that reason, the air ratio of case "b" and "c" was chosen around 0.3 which was suggested for these cases [13,78–81]. For all working condition (different inlet air temperature or different relative humidity) the arrange (order) of cooling capacity is shown in Fig. 19.

Different positions and arrangements of perforations in cross flow M-cycle (see Fig. 18) create different thermal characteristics of M-cycle. For each specific arrangement of perforation, changing of thermal-fluid condition causes creation of different output characteristics as well. However, maximum cooling capacity and wet-bulb effectiveness were obtained for case "h" (Fig. 18) and minimum values of said parameters were observed for case "a".

4.2. Finite element/difference/volume method

Table 4 shows a compact view of the numerical M-cycle investigations which have been studied via finite element/difference/volume method.

Zhang et al. [4], evaluated the specifications of the ISAW cooler [87] (which works based on M-cycle theory) using the finite-element method. The air flow through the channels was considered to be laminar. They varied each parameter while other parameters were remaining unchanged. According to finite element difference analysis of this air cooler, for desired supply air temperature (26 °C), air humidity, air velocity in dry channel and wet channels should not be higher than 65%, 1.77 m/s and 0.7 m/s respectively.

The main results (effect of different parameters on cooler characteristics) of finite element/volume/difference analysis of M-cycle cooler can be summarized as below.

- Increment of inlet air temperature increases product air temperature (warmer supply air) but it does not mean lower efficiency or cooling capacity.
- Increment of inlet air temperature improves cooling capacity, wet-bulb effectiveness and COP which shows M-cycle suitability for warm weather.
- Increment of air relative humidity enhances wet-bulb effectiveness and supply air temperature but decreases COP and cooling capacity. These results prove that, wet-bulb

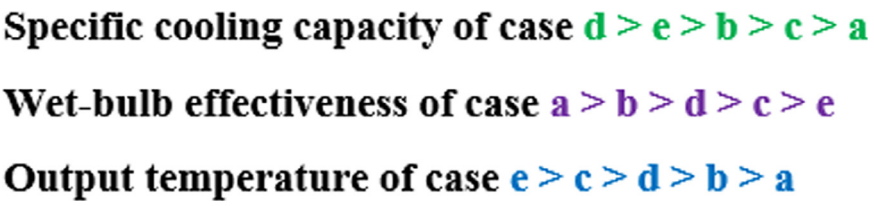

Fig. 19. Comparison between different types M-cycle exchanger (see Fig. 17).

Table 4
Numerical studies via finite element/difference/volume method.

Reference	year	Investigated method	Structure	Explanation
Zhang [4]	2011	Finite element	Cross flow	Effect of various parameters on cross-flow M-cycle performance
Cui [104]	2015	Finite element (Comsol)	Counter flow	Combination of indirect evaporative cooler and compression air cooler
Heidarianejad [100]	2015	Finite difference	Cross flow	Presenting a new model for M-cycle cross flow with consideration of spray water variation and wall longitudinal heat conduction along exchanger
Moshari [101]	2015	Finite difference (Matlab)	Counter& Cross	Performance comparison between counter flow, cross flow and four-stage indirect evaporative cooler with the same air and exchanger parameters
Cui [102]	2016	Finite element (EES)	Counter flow	Providing a performance correlation for counter flow regenerative M-cycle exchanger
Cui [103]	2016	Finite element (Comsol)	Counter flow	Combination of liquid desiccant dehumidification and regenerative M-cycle cooler
Jafarian [105]	2017	Finite Volume	Counter flow	Momentum, energy and mass transfer are simultaneously solved for counter flow M-cycle
Wan [106]	2017	Finite Volume	Counter flow	Providing a performance correlation for counter-flow M-cycle coolers

effectiveness should not be considered as an independent characterize the performance of the IEC.
- Increment of air speed (air flow rate) increases wet-bulb effectiveness and supply air temperature but decreases cooling capacity and COP.
- Increment of air passage height increases supply air temperature and reduces cooling capacity wet-bulb effectiveness. However, COP showed an ascending-descending behaviour. Nonetheless, the maximum point of COP should not be considered as the best condition because of very low cooling capacity and wet-bulb effectiveness in that point.
- Increment of dry channel or wet channel length decreases supply air temperature (colder air) and COP and increases cooling capacity and wet-bulb effectiveness.
- In comparison with conventional cross-flow exchanger (in which M-cycle has not been used), this exchanger provides 16% higher wet-bulb effectiveness and around 60 W higher cooling capacity in the same characteristics.

5. Statistical design methods

Response surface methodology (RSM), Fuzzy inference system (FIS), Adaptive neuro-fuzzy inference system (ANFIS), Multiple linear regression (MLR), Genetic programing (GP), Artificial neural network (ANN) are different type of statistical design method (SCST) [63] which can be used instead of numerical models to analyze the performance of Maisotsenko exchanger. The requirements of this method are: 1) basic knowledge of parameters that affect the system characteristics and 2) enough numerical or experimental data from the system operation. Some researchers have evaluated the indirect evaporative via SCST method as shown in Fig. 7. Pandelidis and Anisimov [4,62] believed that numerical models based on partial differential and algebraic equations require higher amount of calculation time and they are complex and cumbersome for everyday use [4]. Hence, an accurate fast mathematical model based on response surface regression procedure was developed as below which may be applied for engineers.

5.1. RSM method

This technique describes the basic performance of cross-flow M-cycle exchangers and can be used for optimization of M-cycle because of its lower calculation time.

As described in Ref. [82], Response surface methodology (RSM) comprises of some basic steps as below:

1) Screening: experiments are performed with the aim of providing the vital few control parameters.
2) Modeling: experiments are performed with the aim of modeling the quality characteristic of interest (response) as a function of control parameters;
3) Optimization: response model is evaluated to find the variable settings in which optimum conditions are obtained.

Detail explanations about Response Surface Methodology can be found in Refs. [82–86]. The analysis of M-cycle exchanger by RSM method can be classified into two main group as below.

- Describing (prediction) of the basic performance of cross flow M-cycle exchanger including outlet air flow temperature, dew point effectiveness, cooling capacity and COP
- Optimization of five influence factors including inlet temperature, relative humidity, primary air mass flow rate, working to primary air ratio and relative length of the initial part in order to determine the optimal range of operational and geometrical conditions.

The results obtained from this method are the same observed in numerical simulations. However, according to [61], optimization based on single performance factor is not suitable at all for M-cycle. In other words, it is impossible to optimize on the basis of single performance factor because the optimum value for one parameter is not favourable from the view point of other parameters. Hence, a compromise multi-optimization technique is required to determine an appropriate working condition for M-cycle air coolers. To that reason, a multi-parameter optimization was carried out in Ref. [62]. Authors [62] used the concepts of Harrington's desirability function and Compertz-curve for multivariate quality optimization (phase 3 of RSM method) in order to find suitable climate zones for the cross flow M-cycle exchanger. Gompertz curves show the effect of varying one parameter while keeping the others constant. More explanation about the concept of desirability function can be found in Ref. [82].

Based on RSM multi-optimization analysis, M-cycle is suitable for most of the typical climate condition. However, for really moist regions (more than 65% relative humidity) and also cold regions (around 25 °C) are considered as the unsuitable climates for M-cycle. Nonetheless, for hot and very moist weathers, combination of dehumidifier and M-cycle can solve the humidity problem. Cross flow M-cycle has a potential of wide application around the world [61].

Table 5
Experimental studies of M-cycle air conditioning systems.

Experimental investigations	Year	Description
Riangvilaikul & Kumar [78]	2010	Experimental study of a novel indirect evaporative air cooler
Zhan et al. [68]	2011	Comparison between counter-flow and cross-flow exchanger of M-cycle
Zube & Gillan [71]	2011	Evaluating a commercialized type of M-cycle air cooler
Gao et al. [73]	2014	Combination of liquid desiccant and indirect M-cycle cooler
Rogdakis et al. [72]	2014	Analysis of the M-cycle air cooler for Greek climate condition
Khalid et al. [69]	2016	Design and analysis of counter flow exchanger for M-cycle
Khalid et al. [70]	2016	Investigation of an improved M-cycle cooler under low velocity condition
Duan et al. [108]	2016	Analysis of the M-cycle air cooler for China climate condition
Antonellis et al. [109]	2016	Analysis of a cross flow indirect evaporative
Xu et al. [110]	2017	The use of an innovative exchanger for M-cycle air cooler
Duan et al. [111]	2017	Operational performance and impact factors of a counter-flow regenerative M-cycle
Antonellis et al. [112]	2017	Effect of wettability factor and adiabatic humidification on a cross flow heat exchanger
Lin et al. [113]	2017	Effect of dehumidification on cross-flow M-cycle cooler
Shahzad et al. [79]	2018	Combination of solid desiccant with cross flow M-cycle cooler

5.2. GMDG type neural network method

Group method of data handling-type neural network (GMDH) is a self-organizer predictive approach which is a subset of artificial neural network (ANN) family [63]. This technique was employed to perform a multi-objective performance optimization of Coolerado M50 M-cycle unit [63]. Average annual values of COP and cooling capacity were simultaneously maximized while inlet air velocity and working to air ratio were decision variables of optimizations. This optimization was carried out for twelve Koppen-Geigers classification. Koppen Geigers is one of the most widely used climate classification systems in all over the worlds. The GMDH model was used to predict the product air temperature as a function of inlet temperature, inlet humidity, inlet velocity and non-dimensional channel length. According to GMDH model, M-cycle is applicable for cooling season of all 12 classes of Koppen-Geigers climate classification system. Other results can be briefly described as below.an experimental study.

- Optimized velocity decreases with decrement of inlet air temperature
- Optimized velocity decreases with increment of inlet relative humidity
- M-50 Coolerado velocity is very close to the obtained optimum velocity range by GMDH model. Hence, there is no need to change the system's fan.
- Optimized working to air ratio decreased with reduction of inlet temperature or humidity.
- M-50 Coolerado working to air ratio is significantly higher than the achieved working to air ratio by GMD model.

6. Experimental investigations

The main experimental investigations on Maisotsenko type of indirect evaporative coolers ate illustrated in Table 5. It should be notes that, former type of indirect evaporative coolers (which are not worked based on Maisotsenko cycle) are not covered. As can be seen in Table 5, the previous experimental studies on M-cycle air coolers are mainly discussed below considerations.

- Comparison of cross flow and counter flow under various operating condition
- Evaluation of the current existence commercialized M-cycle coolers
- Investigation on the combination of M-cycle and desiccants
- Sensitivity (parametric) analysis of different types of M-cycle air cooler
- The use of existence M-cycle cooler for a defined region with specific climate
- Effect of wettability factor and dehumidification

Operating condition of each experimental investigation is different from each other. Characteristics of each experimental study and their operating parameters and key results are illustrated in Table 6. Type of cooling device, inlet condition including velocity and temperature, geometric specifications, obtained wet-bulb effectiveness and dew-point effectiveness are presented in this table.

Some researchers (for example [71]) have employed the commercialized M-cycle cooler for their experiments. However, most researchers have preferred to use unique test-rig for the test. A schematic view of some of the previously used experimental test-rigs is shown in Fig. 20.

Although each experimental study has different flow, thermal and geometrical condition, the curve behaviour of sensitive analysis (parametric study) are the same for all of them through a specific type of air cooler (single M-cycle or combination of M-cycle and desiccants). Hence, it is possible to provide a compact-comprehensive view of the results of parameter analysis of M-cycle air conditioning systems. In this regard, M-cycle experimental investigations can be classified into two main categories. In First category, the researchers have focused on the effect of various parameters on single M-cycle characteristics and in the second category, the effect of said parameters were studied on combined M-cycle-desiccant systems. A comprehensive compact view of the first and second categories and their results are shown in Fig. 21 and

Table 6
Experiment condition of each experimental study of M-cycle.

	Arrangement	Inlet air Tem	Inlet air humidity	Inlet air volume	Channel gap	Channel length	Channel width	Outlet Tem	Wet-bulb Eff	Dew-point Eff
Riangvilaikul [78]	Counter flow	25-45 °C	7-26 g/kg	1.5–6 m/s	5 mm	1200 mm	80 mm	15-32 °C	92-114%	58-84%
Zhan [68]	Counter &Cross flow	25-45 °C	11 g/kg	2000 m^3/h	5 mm	1000 mm	–	Counter: 16–18 °C Cross: 18–20 °C	Counter: 130–138% Cross: 110–120%	Counter: 70–80% Cross: 75–80%
Zube [71]	Couner	40 °C	0.128 m^3/s	–	–	–	–	–	–	–
Gao [73]	Cross flow	24-38 °C	14 g/kg	0.2 kg/s	2.2 mm	500 mm	500 mm	–	–	90-140%
Rogdakis [72]	Cross flow	32-36 °C	–	–	–	–	–	21–22.3 °C	–	–
Khalid [69]	Counter flow	25-45 °C	12-18 g/kg	0.88 –1.5 m/s	4 mm	900 mm	40 mm	18-25 °C	100-120%	70-80%
Khalid [70]	Cross flow	25-45 °C	11-19 g/kg	0.5 –1.1 m/s	4 mm	Dry:058 mm Wet:203 mm	25 mm	18-24 °C	90-120%	60-80%
Duan et al. [108]	Counter flow	27-37 °C	–	–	6 mm	900 mm	314 mm	18-28 °C	74-82%	–
Antonellis et al. [109]	Cross flow	30-36 °C	10 g/kg	1400 m^3/h	3.35 mm	500 mm	500 mm	23-24 °C	65-80%	–
Xu et al. [110]	Counter flow	30 –37.8 °C	–	750 m^3/h	–	1000 mm	800 mm	–	67-76%	–
Duan et al. [111]	Counter flow	24-34 °C	–	0.6–3 m/s	6 mm	900 mm	314 mm	19-24 °C	38-80%	20-45%
Antonellis et al. [112]	Cross flow	29-35 °C	10-11 g/kg	1400 m^3/h	3.21 mm	470 mm	470 mm	21-23 °C	–	–
Lin et al. [113]	Cross flow	30 °C	12-13 g/kg	2800 m^3/h	3 mm	–	–	20-28 °C	85%	62%
Shahzad [79]	Cross flow	25-45 °C	12-18 g/kg	660 kg/h	5 mm	900 mm	280 mm	17-25 °C	–	–

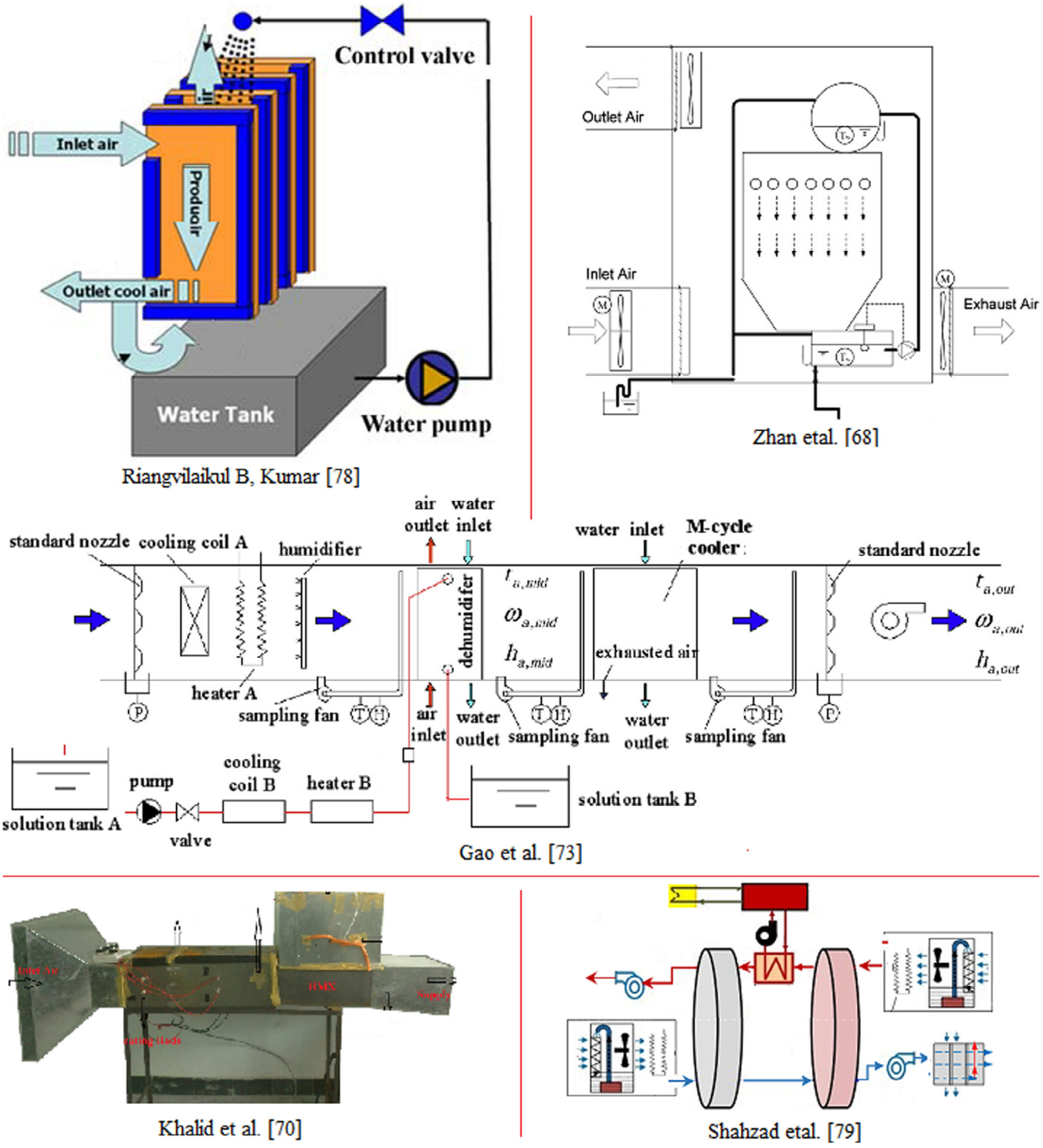

Fig. 20. Schematic view of some of the previously used experimental test-rigs [68,70,73,78,79].

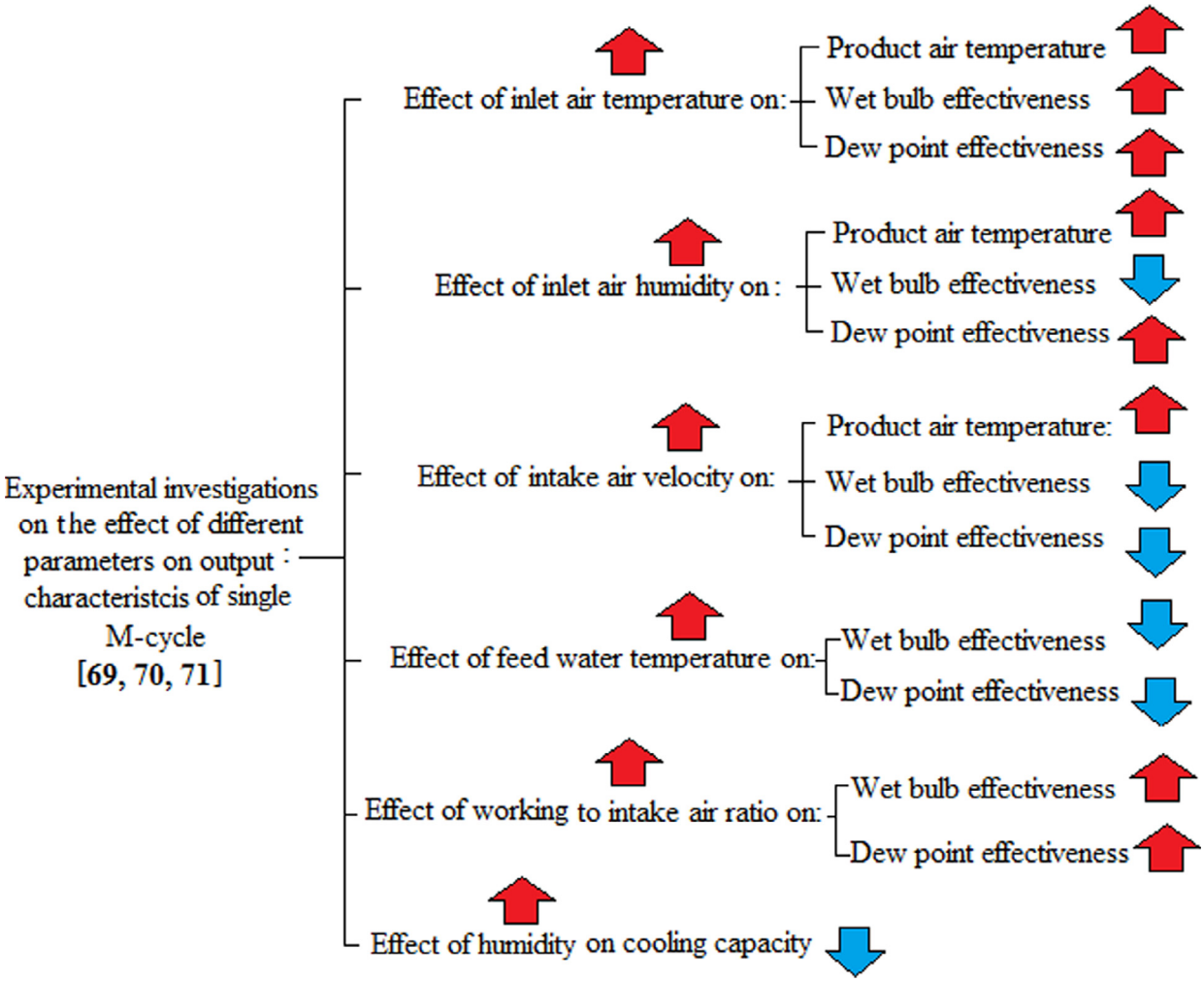

Fig. 21. The effect of various parameters on single M-cycle characteristics (experimental investigations).

Fig. 22 respectively which were extracted from [68–73] and [78,79]. For example, according to Fig. 21, increment of inlet air humidity causes enhancement of product air temperature and dew point effectiveness and causes reduction of wet bulb effectiveness. The results obtained from experiments are comparable with the numerical results mentioned above (in Table 3).

7. Industrial status of M-cycel air coolers

Maisotsenko cycle is protected by more than 200 patents all over the world [15]. Coolerado cooperation produced the first practical realization of the M-cycle cooler technology [17] for different aims including commercial, residential, solar and hybrid M-cycle air coolers. According to the experiments which were carried out by National Renewable Energy Laboratory (NREL), Coolerado's H-80 air cooler used 80% less energy than compressor-based air conditioning systems under hot and dry climate condition [17]. Coolerado air conditioners can be found in markets around the world. Coolerado products are classified into three main categories including HMX, M50 and C60. A general view of these air coolers can be seen in Figs. 23–25 which was extracted from Coolerado catalogs. Nowadays, other corporations such as Climate Wizards (Adelaide, Australia) etc. produced different types of M-cycle indirect evaporative air coolers particularly for big halls. Their applicability for big halls (which is installed on the roof of halls) is more prevalent than those for residential. Indirect evaporative cooler installed in the Hub central at the University of Adelaide is the first large IEC system utilization in Australia [89].

8. Future research direction

Through the literature review described above, it was found that, most of the previous analytical solutions of M-cycle air cooler have made several assumptions to simplify their model and reduce the calculation time, but sacrificing their accuracies. Moreover, previous analytical models are developed only on the simplest structure (without perforation) of M-cycle coolers. Therefore, researchers may interested in develop new analytical models for perforated or other more complex structures of M-cycle. Perforated M-cycle for example are investigated only via numerical or experimental methods which requires further time and cost. Obviously, formulations of current analytical model cannot be simply employed for complicated structures of M-cycle coolers.

Despite the importance of the second law of thermodynamic consideration in any thermodynamic process, extremely few analyses have been carried out for M-cycle coolers from the view point of the second law of thermodynamic. Hence, clarification of exergetic aspect of M-cycle system and developing (via either numerical or experimental techniques) is another research direction which should be bridged. Therefore, the research directions of the

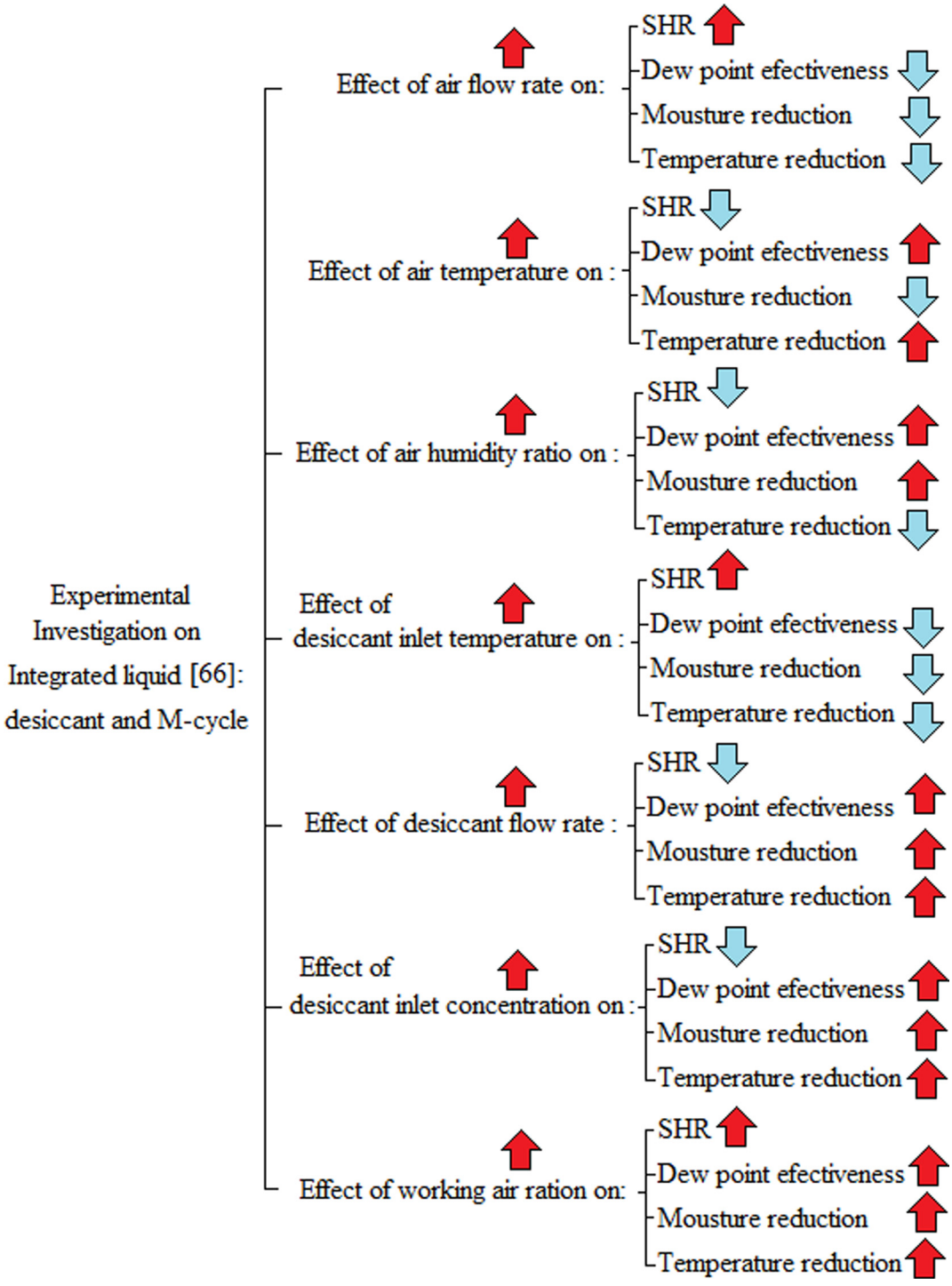

Fig. 22. The effect of various parameters on single desiccant M-cycle characteristics (experimental investigations).

M-cycle cooler can be briefly described as below.

- Lack of high accurate thermal analytical model for other structures of M-cycle cooler.
- Lack of enough M-cycle evaluation from the view point of the second law of thermodynamic.
- Lack of enough exergetic sensitive analysis of M-cycle.

Furthermore, it seems that, extra investigation is required to determine how M-cycle can be appropriately developed for residential aims in additional to big public places. In other words, it may be tried to reduce the size (weight) of M-cycle coolers without reduction of their performance so that it can be employed easily for any area. Moreover, the results of some investigations showed that the specifications of commercialized M-cycle coolers are not the best-optimized ones. Hence, further analysis and optimization via other methods is required. Although the use of perforation through the separator plate reduces the pressure drop, it reduces thermal

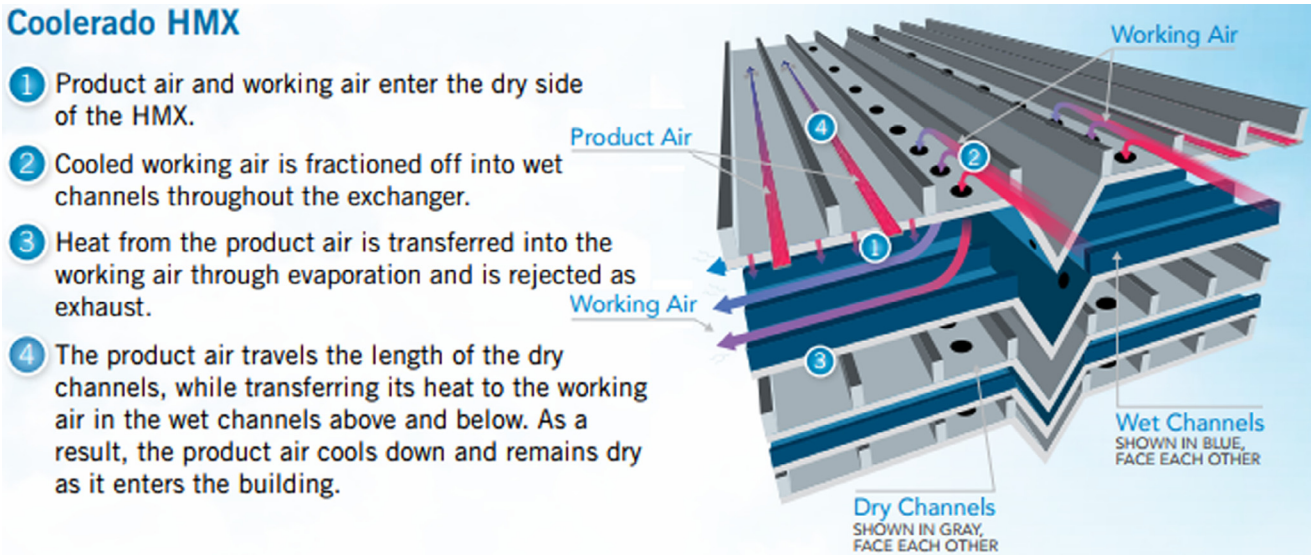

Fig. 23. HMX Coolerado air cooler [from brochure].

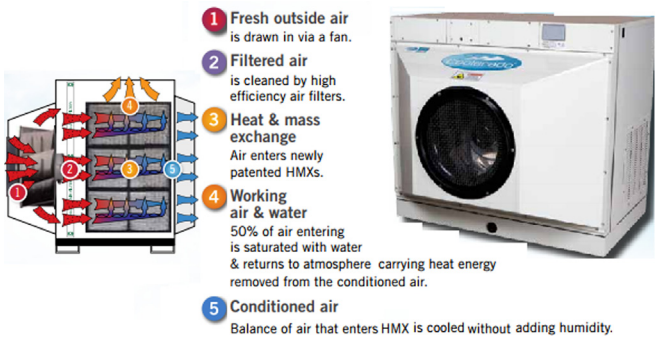

Fig. 24. C60 Coolerado air cooler [from brochure].

performance and causes complexity of manufacture and increment of production cost. Thus, other simple novel techniques should be developed in order to reduce the pressure drop along the exchanger. As a general result a lot of investigations should be carried out to find the best operational condition, geometry and other aspects of M-cycle air conditioning systems.

9. Conclusion

The present study provides a comprehensive review on Maisotsenko air conditioning systems, regarding its evaluation methods, obtained results, industrial situation and future research direction. The main analytical solutions of M-cycle (indirect evaporative) were evolutionary and briefly discussed. The relationship

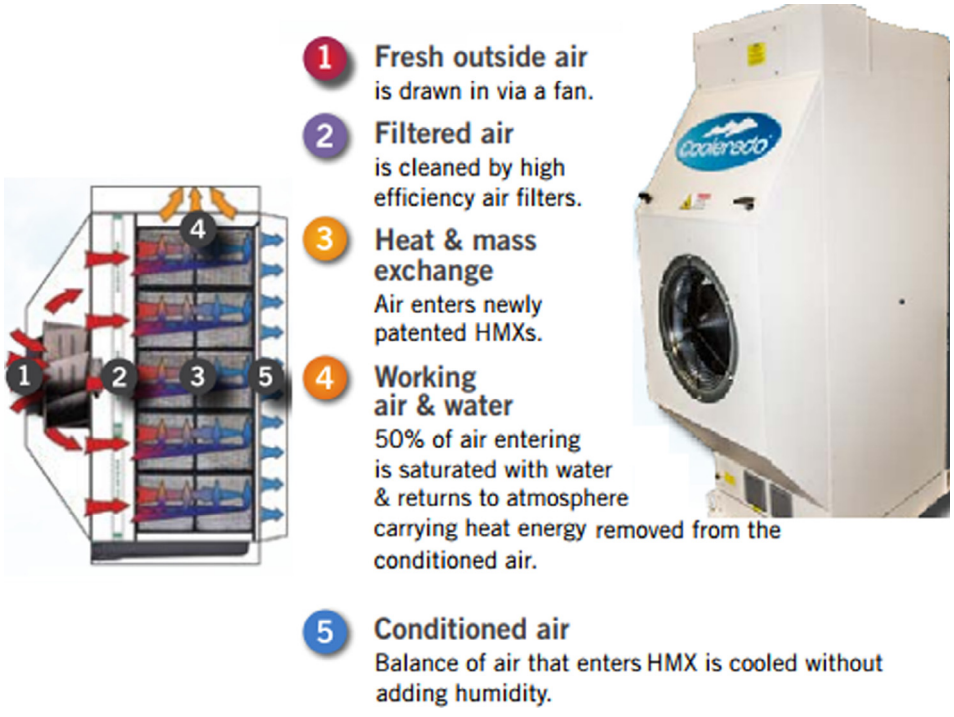

Fig. 25. M50 Coolerado air cooler [from brochure].

between analytical solutions was provided. The significant results which have been obtained from numerical simulation or experimental techniques were graphically presented. Statistical Design Tool is another analysis method for M-cycle which has been employed by some researchers. The application of said methods and their features (advantages) were explained. The current industrial situation of M-cycle air coolers was demonstrated. Coolerado-corporation which is the first corporation produced M-cycle coolers was chosen for this aim. The study concludes that, despite the commercialization of Maisotsenko air coolers, a lot of exact researches are required to improve the M-cycle coolers. A geometrical modification can be used instead of perforations to reduce the pressure drop through the exchanger. M-cycle should be evaluated from the view point of the second law of thermodynamic in addition to the first law of thermodynamic. Extremely few experimental investigations have been performed compared to the other methods.

References

[1] U.S. Department of Energy. Energy information administration. International Energy Outlook; 2017.
[2] Caliskan H, Dincer I, Hepbasli A. Exergetic and sustainability performance comparison of novel and conventional air cooling systems for building applications. Energy Build 2011;43:1461–72.
[3] Zhan C, Zhao X, et al. Comparative study of the performance of the M-Cycle counter-flow and cross-flow heat exchangers for indirect evaporative cooling– paving the path toward sustainable cooling of buildings. Energy 2011;36:6790–805.
[4] Zhan C, Zhao X, Smith S, Riffat SB. Numerical study of a M-Cycle cross-flow heat exchanger for indirect evaporative cooling. Build Environ 2011;46:657–68.
[5] Gillan L. Maisotsenko cycle for cooling processes. Int J Energy a Clean Environ (IJECE) 2008;9(1–3).
[6] Anisimov S, Pandelidis D, Danielewicz J. Numerical analysis of selected evaporative exchangers with the Maisotsenko cycle. Energy Convers Manag 2014 Dec 31;88:426–41.
[7] Mahmood MH, Sultan M, Miyazaki T, Koyama S, Maisotsenko VS. Overview of the Maisotsenko cycle–A way towards dew point evaporative cooling. Renew Sustain Energy Rev 2016 Dec 31;66:537–55.
[8] Weerts B. Coolerado and modeling an application of the maisotsenko cycle. Int J Energy a Clean Environ (IJECE) 2011;12(2–4).
[9] Anisimov S, Pandelidis D, Jedlikowski A, Polushkin V. Performance investigation of a M (Maisotsenko)-cycle cross-flow heat exchanger used for indirect evaporative cooling. Energy 2014 Nov 1;76:593–606.
[10] Miyazaki T, Akisawa A, Nikai I. The cooling performance of a building integrated evaporative cooling system driven by solar energy. Energy Build 2011 Sep 1;43(9):2211–8.
[11] Coolerado. CooleradoHMX (heat and mass exchanger) brochure. Arvada, Colorado, USA: Coolerado Corporation; 2006.
[12] ISAW. Natural air conditioner (heat and mass exchanger) catalogues. Hangzhou, China: ISAW Corporation Ltd.; 2005.
[13] Riangvilaikul B, Kumar S. Numerical study of a novel dew point evaporative cooling system. Energy Build 2010 Nov 30;42(11):2241–50.
[14] Wani C, Ghodke S. Performance analysis of a Maisotsenko cycle-based energy-efficient evaporative air conditioner. Int J Energy a Clean Environ (IJECE) 2011;12(2–4).
[15] Maisotsenko V, Treyger I. Way to energy abundance can be found through the Maisotsenko cycle. Int J Energy a Clean Environ (IJECE) 2011;12(2–4).
[16] Miyazaki T, Nikai I, Akisawa A. Simulation analysis of an open-cycle adsorption air conditioning system– numeral modeling of a fixed bed dehumidification unit and the maisotsenko cycle cooling unit. Int J Energy a Clean Environ (IJECE) 2011;12(2–4).
[17] Gillan L, Gillan A, Kozlov A, Kalensky D. An advanced evaporative condenser through the Maisotsenko cycle. Int J Energy a Clean Environ (IJECE) 2011;12(2–4).
[18] Reznikov M. Electrostatic enforcement of heat exchange in the Maisotsenkoâ€ cycle system. Int J Energy a Clean Environ (IJECE) 2011;12(2–4).
[19] Dirkes II JV. Energy simulation results for indirect Evaporativeâ€ assisted DX cooling systems. Int J Energy a Clean Environ (IJECE) 2011;12(2–4).
[20] Wicker K. Life below the wet bulb: the Maisotsenko cycle. Power 2003 Nov 1;147(9):29.
[21] Caliskan H, Dincer I, Hepbasli A. Assessment of maisotsenko combustion turbine cycle with compressor inlet cooler. In: In Progress in Clean Energy, Vol. 1; 2015. p. 41–55 [Springer International Publishing].
[22] Saghafifar M, Gadalla M. Thermo-economic optimization of hybrid solar Maisotsenko bottoming cycles using heliostat field collector: comparative analysis. Appl Energy 2017 Mar 15;190:686–702.
[23] Saghafifar M, Omar A, Erfanmoghaddam S, Gadalla M. Thermo-economic analysis of recuperated Maisotsenko bottoming cycle using triplex air saturator: comparative analyses. Appl Therm Eng 2017 Jan 25;111:431–44.
[24] Buyadgie D, Buyadgie O, Drakhnia O, Brodetsky P, Maisotsenko V. Solar low-pressure turbo-ejector Maisotsenko cycle-based power system for electricity, heating, cooling and distillation. Int J Low Carbon Technol 2015 May 12;10(2):157–64.
[25] Saghafifar M, Gadalla M. Innovative inlet air cooling technology for gas turbine power plants using integrated solid desiccant and Maisotsenko cooler. Energy 2015 Jul 1;87:663–77.
[26] Saghafifar M, Gadalla M. Analysis of Maisotsenko open gas turbine power cycle with a detailed air saturator model. Appl Energy 2015 Jul 1;149:338–53.
[27] Saghafifar M, Gadalla M. Analysis of Maisotsenko open gas turbine bottoming cycle. Appl Therm Eng 2015 May 5;82:351–9.
[28] Jenkins PE, Cerza Martin, Mohammad M, Saaid Al. Analysis of using the m-cycle regenerative-humidification process on a gas turbine. Proc ASME Turbo 2014:16–20.
[29] Jenkins PE, Carty J. The effects of the M-cycle on the performance of a gas turbine. 2012. HEFAT 2012.
[30] Guillet R. The humid combustion to protect environment and to save the fuel: the water vapor pump and Maisotsenko cycles examples. Int J Energy a Clean Environ (IJECE) 2011;12(2–4).
[31] Reyzin I. Evaluation of the Maisotsenko power cycle thermodynamic efficiency. Int J Energy a Clean Environ (IJECE) 2011;12(2–4).
[32] Sverdlin B, Tikhonov A, Gelfand R. Theoretical possibility of the Maisotsenko cycle application to decrease cold water temperature in cooling towers. Int J Energy a Clean Environ (IJECE) 2011;12(2–4).
[33] Anisimov S, Kozlov A, Glanville P, Khinkis M, Maisotsenko V, Shi J. Advanced cooling tower concept for commercial and industrial applications. In ASME 2014 power conference 2014 Jul 28 (pp. V002T10A001–V002T10A001). American Society of Mechanical Engineers.
[34] Morosuk T, Tsatsaronis G, Maisotsenko V, Kozlov A. Exergetic analysis of a maisotsenko-process-enhanced cooling tower. In: In ASME 2012 international mechanical engineering congress and exposition. American Society of Mechanical Engineers; 2012. p. 189–94. Nov 9.
[35] Morozyuk T, Tsatsaronis G. Advanced cooling tower concept based on the Maisotsenkoâ€ Cycle– an exergetic evaluation. Int J Energy a Clean Environ (IJECE) 2011;12(2–4).
[36] Maisotsenko V, Reyzin I. The Maisotsenko cycle for electronics cooling. In: In proceedings of the ASME/pacific rim technical conference and exhibition on integration and packaging of MEMS, NEMS, and electronic systems, vol. 22. San Francisco, CA, US: Advances in Electronic Packaging; 2005 Jul 17. 415e424. No. 2005.
[37] Khazhmuradov MA, Fedorchenko DV, Rudychev YV, Martynov S, Zakharchenko A, Prokhorets S, Skrypnyk AI, Krugol M, Yurkin A, Lukhanin AA, Lukhanin O. Analysis of the Maisotsenko cycle based cooling system for accumulator batteries. Int J Energy a Clean Environ (IJECE) 2011;12(2–4).
[38] Maclaine-Cross IL, Banks PJ. A general theory of wet surface heat exchangers and its application to regenerative evaporative cooling. J Heat Tran 1981 Aug 1;103(3):579–85.
[39] Stoitchkov NJ, Dimitrov GI. Effectiveness of crossflow plate heat exchanger for indirect evaporative cooling: efficacité des échangeurs thermiques à plaques, à courants croises pour refroidissement indirect évaporatif. Int J Refrig 1998 Sep 30;21(6):463–71.
[40] Alonso JS, Martinez FR, Gomez EV, Plasencia MA. Simulation model of an indirect evaporative cooler. Energy Build 1998 Dec 31;29(1):23–7.
[41] Chengqin R, Hongxing Y. An analytical model for the heat and mass transfer processes in indirect evaporative cooling with parallel/counter flow configurations. Int J Heat Mass Tran 2006 Feb 28;49(3):617–27.
[42] Hasan A. Going below the wet-bulb temperature by indirect evaporative cooling: analysis using a modified ε-NTU method. Appl Energy 2012 Jan 31;89(1):237–45.
[43] Liu Z, Allen W, Modera M. Simplified thermal modeling of indirect evaporative heat exchangers. HVAC R Res 2013 Apr 3;19(3):257–67.
[44] Cui X, Chua KJ, Islam MR, Yang WM. Fundamental formulation of a modified LMTD method to study indirect evaporative heat exchangers. Energy Convers Manag 2014 Dec 31;88:372–81.
[45] Chen Y, Luo Y, Yang H. A simplified analytical model for indirect evaporative cooling considering condensation from fresh air: development and application. Energy Build 2015 Dec 1;108:387–400.
[46] Mickley HS. Design of forced draft air conditioning equipment. Chem Eng Prog Dec. 1949;45(12):739–45.
[47] Pescod D. Unit air cooler using plastic heat exchanger with evaporatively cooled plates. Australian Refrig Air Condit Heat 1968;22(9):22–6. Sept.
[48] Lewis WK. The evaporation of a liquid into a gas. Trans. ASME 1922;44:325–40.
[49] Kloppers JC, Kröger DG. The Lewis factor and its influence on the performance prediction of wet-cooling towers. Int J Therm Sci 2005 Sep 1;44(9):879–84.
[50] Dreyer AA. Analysis of evaporative coolers and condensers. M.Eng. thesis. Stellenbosch, South Africa: University of Stellenbosch; 1988.
[51] Anisimov S, Pandelidis D. Numerical study of perforated indirect evaporative air cooler. Int J Energy a Clean Environ (IJECE) 2011;12(2–4).

[52] Anisimov S, Pandelidis D. Heat-and mass-transfer procesess in indirect evaporative air conditioners through the Maisotsenko cycle. Int J Energy a Clean Environ (IJECE) 2011;12(2–4).
[53] Anisimov S, Pandelidis D. Numerical study of the Maisotsenko cycle heat and mass exchanger. Int J Heat Mass Tran 2014 Aug 31;75:75–96.
[54] Pandelidis D, Anisimov S, Worek WM. Performance study of the Maisotsenko Cycle heat exchangers in different air-conditioning applications. Int J Heat Mass Tran 2015 Feb 28;81:207–21.
[55] Pandelidis D, Anisimov S. Numerical analysis of the heat and mass transfer processes in selected M-Cycle heat exchangers for the dew point evaporative cooling. Energy Convers Manag 2015 Jan 15;90:62–83.
[56] Pandelidis D, Anisimov S. Numerical analysis of the selected operational and geometrical aspects of the M-cycle heat and mass exchanger. Energy Build 2015 Jan 1;87:413–24.
[57] Pandelidis D, Anisimov S, Worek WM. Comparison study of the counter-flow regenerative evaporative heat exchangers with numerical methods. Appl Therm Eng 2015 Jun 5;84:211–24.
[58] Anisimov S, Pandelidis D, Maisotsenko V. Numerical study of heat and mass transfer process in the Maisotsenko cycle for indirect evaporative air cooling. Heat Tran Eng 2016 Nov 21;37(17):1455–65.
[59] Pandelidis D, Anisimov S, Worek WM, Drąg P. Numerical analysis of a desiccant system with cross-flow Maisotsenko cycle heat and mass exchanger. Energy Build 2016 Jul 1;123:136–50.
[60] Pandelidis D, Anisimov S, Worek WM, Drąg P. Analysis of different applications of Maisotsenko cycle heat exchanger in the desiccant air conditioning systems. Energy Build 2017 Apr 1;140:154–70.
[61] Pandelidis D, Anisimov S. Application of a statistical design for analyzing basic performance characteristics of the cross-flow Maisotsenko cycle heat exchanger. Int J Heat Mass Tran 2016 Apr 30;95:45–61.
[62] Pandelidis D, Anisimov S. Numerical study and optimization of the cross-flow Maisotsenko cycle indirect evaporative air cooler. Int J Heat Mass Tran 2016 Dec 31;103:1029–41.
[63] Sohani A, Sayyaadi H, Hoseinpoori S. Modeling and multi-objective optimization of an M-cycle cross-flow indirect evaporative cooler using the GMDH type neural network. Int J Refrig 2016 Sep 30;69:186–204.
[64] Buyadgie D, Buyadgie O, Drakhnia O, Sladkovskyi Y, Artemenko SV, Chamchine A. Theoretical study of the combined M-cycle/ejector air-conditioning system. Int J Energy a Clean Environ (IJECE) 2011;12(2–4).
[65] Saghafifar M, Gadalla M. Solid desiccant air conditioning systems using maisotsenko cooling cycle in UAE. In: The third international conference on water. Energy and Environment (ICWEE); 2015.
[66] Worek WM, Khinkis M, Kalensky D, Maisotsenko V. Integrated desiccant–indirect evaporative cooling system utilizing the Maisotsenko Cycle. In: ASME 2012 heat transfer summer conference collocated with the ASME 2012 fluids engineering division summer meeting and the ASME 2012 10th international conference on nanochannels, microchannels, and minichannels. American Society of Mechanical Engineers; 2012 Jul 8. p. 21–8.
[67] Saghafifar M, Gadalla M. Performance assessment of integrated PV/T and solid desiccant air-conditioning systems for cooling buildings using Maisotsenko cooling cycle. Sol Energy 2016 Apr 30;127:79–95.
[68] Zhan C, Duan Z, Zhao X, Smith S, Jin H, Riffat S. Comparative study of the performance of the M-cycle counter-flow and cross-flow heat exchangers for indirect evaporative cooling–paving the path toward sustainable cooling of buildings. Energy 2011 Dec 31;36(12):6790–805.
[69] Khalid O, Butt Z, Tanveer W, Rao HI. Design and experimental analysis of counter-flow heat and mass exchanger incorporating (M-cycle) for evaporative cooling. Heat Mass Tran 2017 Apr 1;53(4):1391–403.
[70] Khalid O, Ali M, Sheikh NA, Ali HM, Shehryar M. Experimental analysis of an improved Maisotsenko cycle design under low velocity conditions. Appl Therm Eng 2016 Feb 25;95:288–95.
[71] Zube D, Gillan L. Evaluating Coolerado Corportion's Heatâ€ mass exchanger performance through experimental analysis. Int J Energy a Clean Environ (IJECE) 2011;12(2–4).
[72] Rogdakis ED, Koronaki IP, Tertipis DN. Experimental and computational evaluation of a Maisotsenko evaporative cooler at Greek climate. Energy Build 2014 Feb 28;70:497–506.
[73] Gao WZ, Cheng YP, Jiang AG, Liu T, Anderson K. Experimental investigation on integrated liquid desiccant–Indirect evaporative air cooling system utilizing the Maisotesenko–Cycle. Appl Therm Eng 2015 Sep 5;88:288–96.
[74] Anisimov S, Żuchowicki J. Wymiana ciepła i masy w urządzeniach do pośredniego ochładzania powietrza za pomocą parowania wody przy mieszanym schemacie przepływu czynników, nowe Techniki w Klimatyzacji 2003. In: Proc. Of nowe techniki w Klimatyzacji conf; 2003. p. 13–20.
[75] Anisimov SM, Bolotin SA. Badania Krzyżowych wymienników ciepła do pośredniego ochładzania powietrza. Wiadomości Międzynarodowej Akademii Nauk Ochrony Środowiska- Ochrona Powietrza Atmosferycznego 1996;2:18–21.
[76] Bogosłowski VN, Poz MJ. Podstawy fizyki cieplnej urządzeń systemów ogrzewania. Moscow: Strojizdat: Wentylacji i Klimatyzacji; 1983.
[77] Pandelidis D, Polushkin V. Wymienniki do pośredniego ochładzania powietrza za pomocą odparowania cieczy. In: Anisimov S, editor. Współczesne metody i techniki w Badaniach systemów inżynieryjnych. Wrocław: Oficyna Wydawnicza Politechniki Wrocławskiej; 2011. p. 81–7.
[78] Riangvilaikul B, Kumar S. An experimental study of a novel dew point evaporative cooling system. Energy Build 2010;42:637–44.
[79] Shahzad MK, Chaudhary GQ, Ali M, Sheikh NA, Khalil MS, Rashid TU. Experimental evaluation of a solid desiccant system integrated with cross flow Maisotsenko cycle evaporative cooler. Appl Therm Eng 2018 Jan 5;128:1476–87.
[80] Zhao X, Li J, Riffat SB. Numerical study of a novel counter-flow heat and mass exchanger for dew point evaporative cooling. Appl Therm Eng 2008;28:1942–51.
[81] Anisimov S, Vasiljev V. Renewable energy utilization in indirect evaporative air coolers under combined airflow conditions. In: Proceedings of clima 2007 well being indoors, REHVA world congress, Helsinki, Finland, 10–14 June; 2007. p. 1650.
[82] Costa NR, Lourenço J, Pereira ZL. Desirability function approach: a review and performance evaluation in adverse conditions. Chemometr Intell Lab Syst 2011;107(2):234–44. Jul 31.
[83] Carley KM, Kamneva NY, Reminga J. Response surface, methodology, CASOS technical report. Carnegie Mellon University; October 2004. CMU-ISRI-04–136.
[84] Khuri AI, Mukhopadhyay S. Response surface methodology. WIREs Comp Stat 2010;2:128–49. 10.1002/wics.73.
[85] Myers Raymond H, Montgomery DC. Response Surface Methodology: process and product optimization using designed experiment. A Wiley-Interscience Publication; 2002.
[86] Khuri AI, Cornell JA. Response surfaces. second ed. New York: Marcel Dekker; 1996.
[87] Kiran TR, Rajput SP. An effectiveness model for an indirect evaporative cooling (IEC) system: comparison of artificial neural networks (ANN), adaptive neuro-fuzzy inference system (ANFIS) and fuzzy inference system (FIS) approach. Appl Soft Comput 2011 Jun 30;11(4):3525–33.
[88] ISAW. Natural air conditioner (heat and mass exchanger) catalogues. Hangzhou, China: ISAW Corporation Ltd; 2005.
[89] Chen ML, Liu XL, Hu E. Indirect Evaporative Cooling–an energy efficient way for air conditioning. In advanced materials research, vol. 608. Trans Tech Publications; 2013. p. 1198–203.
[90] Pandelidis D, Anisimov S, Drąg P, Sidorczyk M, Pacak A. Analysis of application of the M-Cycle heat and mass exchanger to the typical air conditioning systems in Poland. Energy Build 2018 Jan 1;158:873–83.
[91] Bolotin S, Vager B, Vasilijev V. Comparative analysis of the cross-flow indirect evaporative air coolers. Int J Heat Mass Tran 2015 Sep 30;88:224–35.
[92] Pandelidis D, Anisimov S, Worek WM, Drąg P. Comparison of desiccant air conditioning systems with different indirect evaporative air coolers. Energy Convers Manag 2016 Jun 1;117:375–92.
[93] Pandelidis D, Anisimov S, Worek WM. Drąg P. Numerical analysis of a desiccant system with cross-flow Maisotsenko cycle heat and mass exchanger. Energy Build 2016 Jul 1;123:136–50.
[94] Pandelidis D, Anisimov S. Numerical analysis of the selected operational and geometrical aspects of the M-cycle heat and mass exchanger. Energy Build 2015 Jan 1;87:413–24.
[95] Anisimov S, Pandelidis D, Danielewicz J. Numerical study and optimization of the combined indirect evaporative air cooler for air-conditioning systems. Energy 2015 Feb 1;80:452–64.
[96] Pandelidis D, Anisimov S, Rajski K, Brychcy E, Sidorczyk M. Performance comparison of the advanced indirect evaporative air coolers. Energy 2017 Sep 15;135:138–52.
[97] Pandelidis D, Anisimov S, Worek WM. Performance study of counter-flow indirect evaporative air coolers. Energy Build 2015 Dec 15;109:53–64.
[98] Anisimov S, Pandelidis D. Theoretical study of the basic cycles for indirect evaporative air cooling. Int J Heat Mass Tran 2015 May 31;84:974–89.
[99] Khafaji HQ, Ekaid AL, Terekhov VI. A numerical study of direct evaporative air cooler by forced laminar convection between parallel-plates channel with wetted walls. J Eng Thermophys 2015 Apr 1;24(2):113–22.
[100] Heidarinejad G, Moshari S. Novel modeling of an indirect evaporative cooling system with cross-flow configuration. Energy Build 2015 Apr 1;92:351–62.
[101] Moshari S, Heidarinejad G. Numerical study of regenerative evaporative coolers for sub-wet bulb cooling with cross-and counter-flow configuration. Appl Therm Eng 2015 Oct 5;89:669–83.
[102] Cui X, Islam MR, Mohan B, Chua KJ. Developing a performance correlation for counter-flow regenerative indirect evaporative heat exchangers with experimental validation. Appl Therm Eng 2016 Sep 5;108:774–84.
[103] Cui X, Islam MR, Mohan B, Chua KJ. Theoretical analysis of a liquid desiccant based indirect evaporative cooling system. Energy 2016 Jan 15;95:303–12.
[104] Cui X, Chua KJ, Islam MR, Ng KC. Performance evaluation of an indirect pre-cooling evaporative heat exchanger operating in hot and humid climate. Energy Convers Manag 2015 Sep 15;102:140–50.
[105] Jafarian H, Sayyaadi H, Torabi F. A numerical model for a dew-point counter-flow indirect evaporative cooler using a modified boundary condition and considering effects of entrance regions. Int J Refrig 2017 Dec 1;84:36–51.
[106] Wan Y, Ren C, Wang Z, Yang Y, Yu L. Numerical study and performance correlation development on counter-flow indirect evaporative air coolers. Int J Heat Mass Tran 2017 Dec 1;115:826–30.
[107] Zhu G, Chow TT, Lee CK. Performance analysis of counter-flow regenerative heat and mass exchanger for indirect evaporative cooling based on data-driven model. Energy Build 2017 Nov 15;155:503–12.
[108] Duan Z, Zhao X, Zhan C, Dong X, Chen H. Energy saving potential of a counter-flow regenerative evaporative cooler for various climates of China: experiment-based evaluation. Energy Build 2017 Aug 1;148:199–210.

[109] De Antonellis S, Joppolo CM, Liberati P, Milani S, Molinaroli L. Experimental analysis of a cross flow indirect evaporative cooling system. Energy Build 2016 Jun 1;121:130–8.
[110] Xu P, Ma X, Zhao X, Fancey K. Experimental investigation of a super performance dew point air cooler. Appl Energy 2017 Oct 1;203:761–77.
[111] Duan Z, Zhan C, Zhao X, Dong X. Experimental study of a counter-flow regenerative evaporative cooler. Build Environ 2016 Aug 1;104:47–58.
[112] De Antonellis S, Joppolo CM, Liberati P, Milani S, Romano F. Modeling and experimental study of an indirect evaporative cooler. Energy Build 2017 May 1;142:147–57.
[113] Lin J, Wang RZ, Kumja M, Bui TD, Chua KJ. Modelling and experimental investigation of the cross-flow dew point evaporative cooler with and without dehumidification. Appl Therm Eng 2017 Jul 5;121:1–3.
[114] Chen Y, Yang H, Luo Y. Parameter sensitivity analysis and configuration optimization of indirect evaporative cooler (IEC) considering condensation. Appl Energy 2017 May 15;194:440–53.
[115] Chauhan SS, Rajput SP. Parametric analysis of a combined dew point evaporative-vapour compression based air conditioning system. Alexandria Eng J 2016 Sep 30;55(3):2333–44.

Chapter 3

Analytical modelling (sprayed water theory)

This chapter has been published as

> Dizaji HS, Hu EJ, Chen L, Pourhedayat S. Development and validation of an analytical model for perforated (multi-stage) regenerative M-cycle air cooler. Applied energy. 2018 Oct 15;228:2176-94. (DOI: 10.1016/j.apenergy.2018.07.018).

This chapter provides an analytical model for perforated Maisotsenko air coolers. In this model, it is assumed that, the water flow rate is so higher than the air flow rate (sprayed water mechanism). The model is validated with previous numerical/experimental researches in the same working condition. It was concluded that the M-cycle cooler under sprayed water mechanism is not able to reach its maximum cooling capacity (compared to the dew-point temperature) and water inlet temperature plays a key role on cooling characteristics if the cooler as the impact of sensible heat transfer is major (in comparison with latent heat transfer). In this working condition, the temperature of the middle plate is dominated with water inlet temperature and that is why the water inlet temperature should be colder than the ambient temperature.

Statement of Authorship

Title of Paper	Development and validation of an analytical model for perforated (multi-stage) regenerative M-cycle air cooler
Publication Status	☑ Published ☐ Accepted for Publication ☐ Submitted for Publication ☐ Unpublished and Unsubmitted w ork w ritten in manuscript style
Publication Details	Dizaji HS, Hu EJ, Chen L, Pourhedayat S. Development and validation of an analytical model for perforated (multi-stage) regenerative M-cycle air cooler. Applied energy. 2018 Oct 15;228:2176-94. (DOI: 10.1016/j.apenergy.2018.07.018

Principal Author

Name of Principal Author (Candidate)	Hamed Sadighi Dizaji		
Contribution to the Paper	Developing the mathematical model and performing the parametric and sensitivity analysis, writing the manuscript.		
Overall percentage (%)	70%		
Certification:	This paper reports on original research I conducted during the period of my Higher Degree by Research candidature and is not subject to any obligations or contractual agreements with a third party that would constrain its inclusion in this thesis. I am the primary author of this paper.		
Signature		Date	

Co-Author Contributions

By signing the Statement of Authorship, each author certifies that:

i. the candidate's stated contribution to the publication is accurate (as detailed above);

ii. permission is granted for the candidate in include the publication in the thesis; and

iii. the sum of all co-author contributions is equal to 100% less the candidate's stated contribution.

Name of Co-Author	Eric Hu		
Contribution to the Paper	Supervising the work, continuous recommendations and assistances through the developing process of the model. Review and editing of the manuscript.		
Signature		Date	

Name of Co-Author	Lei Chen		
Contribution to the Paper	Supervising the work, continuous recommendations and assistances through the developing process of the model. Review and editing of the manuscript.		
Signature	Ley Chen Digitally signed by Ley Chen DN: cn=Ley Chen, o, ou, email=Ley@mecheng.adelaide.edu.au, c=AU Date: 2021.01.12 16:22:13 +10'30'	Date	

Please cut and paste additional co-author panels here as required.

Name of Co-Author	Samira Pourhedayat		
Contribution to the Paper	Validation of the analytical data with data available in literature.		
Signature		Date	

Applied Energy 228 (2018) 2176–2194

Contents lists available at ScienceDirect

Applied Energy

journal homepage: www.elsevier.com/locate/apenergy

Development and validation of an analytical model for perforated (multi-stage) regenerative M-cycle air cooler

Hamed Sadighi Dizaji, Eric Jing Hu*, Lei Chen, Samira Pourhedayat

School of Mechanical Engineering, The University of Adelaide, Adelaide, SA 5005, Australia

HIGHLIGHTS

- Previous analytical models of M-cycle cooler are reviewed.
- An analytical model is presented for multi-stage M-cycle cooler.
- The model is validated by numerical results.
- An application of the model is presented.

GRAPHICAL ABSTRACT

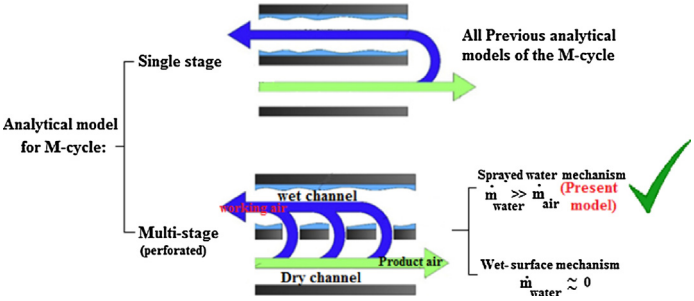

ARTICLE INFO

Keywords:
Heat exchanger
Maisotsenko cycle
Evaporative
Dew-point
Wet-bulb
Air conditioner
M-cycle

ABSTRACT

Maisotsenko cycle based coolers are able to reduce the air temperature below the wet-bulb temperature of the inlet air without adding any moisture to the product air and without the use of any compressor or refrigerant (CFC). These positive features of M-cycle have encouraged the researchers to enthusiastically consider the thermal-fluid characteristics of M-cycle cooler via numerical, analytical and experimental techniques. In this paper attempts are made to present an analytical solution for thermal behavior of perforated (multi-stage) regenerative M-cycle exchanger which has not been carried out before. Indeed, all previous analytical solutions of M-cycle have been provided for the simplest structure of M-cycle exchanger (single-stage, without perforation) and the perforated M-cycle cooler (multi-stage) has been investigated only via experimental and numerical techniques (including finite difference method, numerical ε-NTU technique, statistical design tools all of which are sophisticated and require high computational time). However, the precision aspect and analysis speed of analytical approach is undeniable and it is considered as the priority in most engineering problems. Hence, in this study, an analytical model is developed for three-stage regenerative M-cycle exchanger which can be developed for any number of perforations. All modeling process is described in detail (step by step) to make it ease understanding for readers. Evaluation methods of all required parameters are described in detail as well. Finally, the model is verified with numerical results.

1. Introduction

Generally, air cooling methods used in air conditioning systems can be classified into four main groups including compressor-based air coolers, air-water direct contact coolers, conventional air-water indirect air coolers and M-cycle indirect coolers. Very high electrical consumption, using of chlorofluorocarbons and complex moving parts which lead to higher maintenance costs are the main defectiveness of

* Corresponding author.
E-mail addresses: Hamed.SadighiDizaji@adelaide.edu.au, HamedSadighiDizaji@gmail.com (H. Sadighi Dizaji), Eric.Hu@Adelaide.edu.au (E.J. Hu), Lei.chen@adelaide.edu.au (L. Chen), Samira.Pourhedayat@gmail.com (S. Pourhedayat).

https://doi.org/10.1016/j.apenergy.2018.07.018
Received 26 February 2018; Received in revised form 19 June 2018; Accepted 4 July 2018
Available online 24 July 2018
0306-2619/

Nomenclature

a	geometry in Fig. 4
b	geometry in Fig. 4
B_1, B_2, B_3	defined in Eq. (33), (40), (41) respectively
A	area (m^2)
c	specific heat (kJ/kg °C)
c_a	specific heat of dry air (kJ/kg °C)
c_v	specific heat of water vapor (kJ/kg °C)
d_h	hydraulic diameter (m)
i_v	specific enthalpy of water vapor (kJ/kg)
i_{fg}	evaporation heat of water at 0 °C
c_f^*	defined in Eq. (8)
c_w^*	defined in Eq. (42)
k_p	thermal conductivity of plate (W/m^2 °C)
L	length (m)
L_a, L_b, L_c	lengths in Fig. 4 (m)
Le	Lewis factor
NTU	number of heat transfer units
Nu	Nusselt number
Pr	Prandtl Number
q	heat transfer rate (W)
r	defined in Eq. (7)
Re	Reynolds number
R_{cw}	defined in Eq. (43)
R	thermal resistance (m^2 K/W)
T	temperature (°C)
T_f	water film temperature (°C)
U	overall heat transfer coefficient (KW/m^2 °C)
V	velocity (m/s)
$\dot{m}$	mass transfer rate (kg/s)
P	atmospheric pressure of moist air
p_v	partial pressure of water vapor
w	humidity ratio (kg moisture/kg dry air)

Special characters

ε	mass transfer ratio between working and primary air
δ_p	thickness of the plate (m)
δ_w	thickness of water film (m)
α	convective heat transfer coefficient (W/m^2 K)
β	convective mass transfer coefficient (W/m K)
σ	wettability factor
ρ	density (kg/m^3)

Subscripts

1 or Pa	primary air (product air)
2 or wa	working air (secondary air)
f	water film
wb	wet-bulb
w	water
A, B, C	point A, B, C in Fig. 4
L_a, L_b, L_c	length L_a, L_b, L_c in Fig. 4

Superscripts

′	inlet
″	outlet

compressor-based air conditioning systems which has been explained in detail by Mahmood et al. [1] and Sadighi Dizaji et al. [2] as well. Although the power consumption of air-water direct contact coolers is less than the first group, they are not able to reduce the air temperature below the wet-bulb temperature of inlet air. Indeed, wet-bulb temperature is the minimum ideal theoretical temperature that can be reached by adding moist to the air (latent heat). Irrespective of cooling capacity, humidity-increment not only results in people's discomfort but also is harmful for electrical devises. Furthermore, water consumption of direct contact coolers is high and has potential health issues from contaminated water droplets entering spaces as well. Defectiveness of the first three groups (explained above) has recently encouraged both academic researchers and industrial sectors to further focus on M-cycle systems. As described in [1], M-cycle are protected by various patents all over the world and its application has been expanded to other aspects such as pollution control (i.e. NOx reduction in gas turbines) as well which shows the applicability and potential of M-cycle system.

Indirect evaporative cooling technique has neither the problems of compressor-based nor air-water direct contact coolers. Nonetheless, conventional indirect evaporative coolers (see Fig. 1a) was not able to reduce the air temperature significantly which prevented widespread application of this type of cooling method in air conditioning systems. Providing an ingenious idea by Professor Valeriy Maisotsenko converted the indirect evaporative cooling as a highly efficient cooling system. The principal aspect of this idea is precooling of the wet-side air fluid before entering to the working channel (see Fig. 1b).

Researchers presented different configurations of M-cycle exchanger as shown in Fig. 2. Generally, all investigations of M-cycle can be classified into four main categories including analytical approaches, numerical simulations, statistical design methods and experimental techniques. Each category is divided into some other classifications which is shown graphically on Fig. 3.

All configurations (in Fig. 2) have been studied via numerical or experimental techniques. Analytical solution has been presented only for the simplest structure of indirect evaporative-cooler (without perforation) as briefly described in the following.

Maclaine and Banks [3] presented a general theory of wet-surface heat exchanger. They proposed a liner approximate model of wet-surface heat exchanger by analogizing with dry surface heat exchanger. Maclaine method proposed a linear approximate and graphical representation which can be employed to evaluate the wet-surface heat

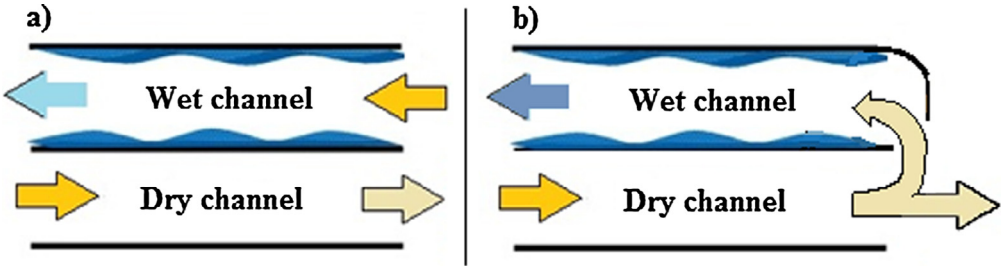

Fig. 1. (a) Conventional indirect evaporative cooling and (b) M-cycle indirect evaporative cooling.

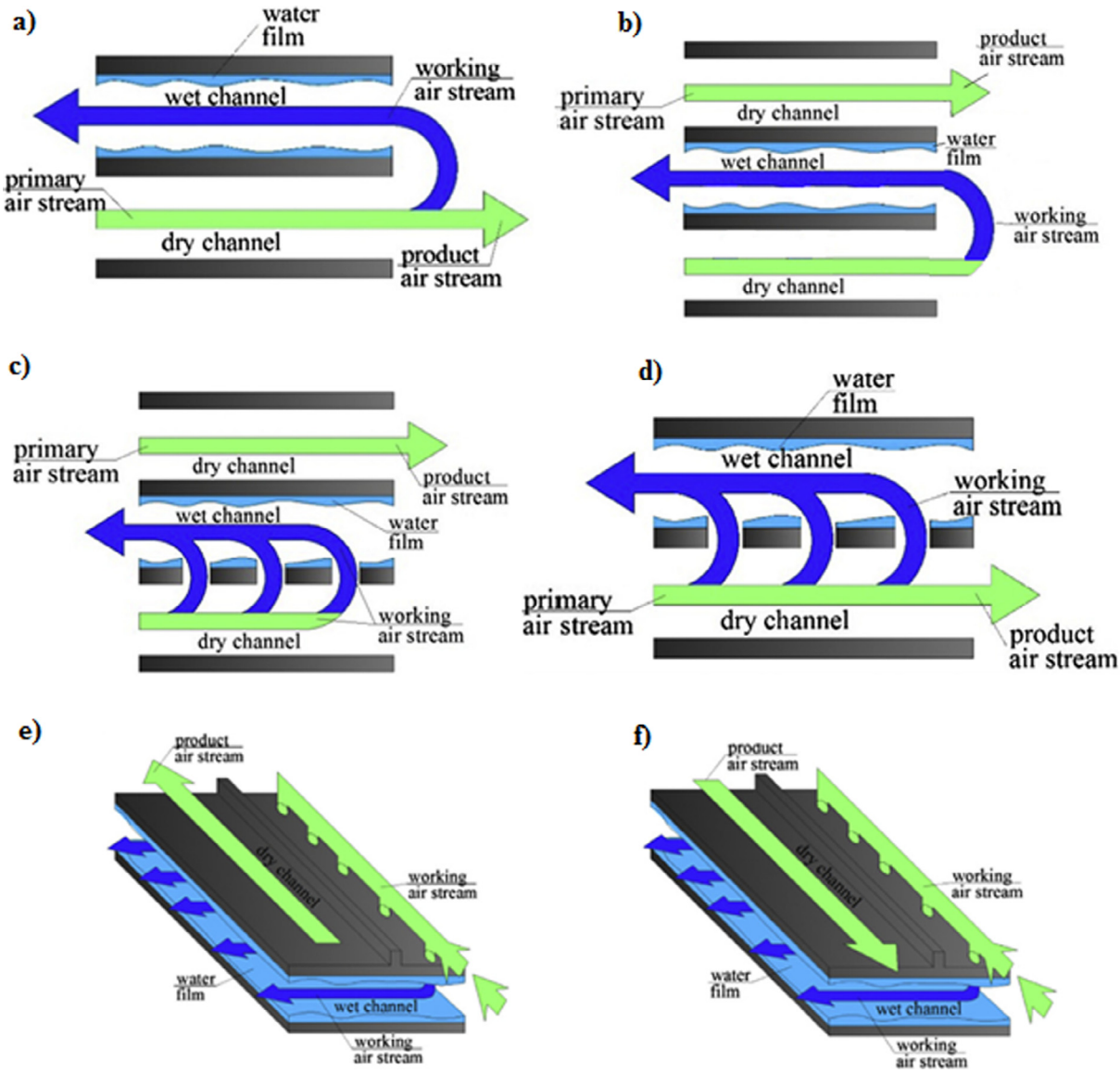

Fig. 2. Different M-cycle configurations modified from [2].

exchanger effectiveness. Maclaine model is based on eight equations which four of them are based on assumptions and rest of them are based on conservation of energy or mass.

Stoitchkov [4] indicated three deficiencies for Maclaine model as listed below:

- Maclaine did not show how the mean surface temperature should be estimated.
- The values of total to sensible heat ratio for different mean surface temperatures given in a table are calculated for a barometric pressure of 101,325 Pa. Hence, for other pressures, the outcomes will have a source of error.
- Maclaine model is based on a very important condition that the evaporating water film is stationary and continuously is replenished at its surface with water at the same temperature. However, in real heat exchanger, the mass flow rate of sprayed water is much more than that of the evaporated water which causes reduction of wet surface heat exchanger effectiveness compared to the Maclaine assumption.

Hence, Stoitchkov further improved the Maclaine model with an approach to determine the mean water-surface temperature with known geometrical and dry heat transfer characteristics, mass flow rate and initial temperature conditions. Alonso [5] developed a more user-friendly simplified model by introducing an equivalent water temperature in Maclaine solution. Ren and Yang [6] believed that all previous simplified models have sacrificed accuracy for simplicity of solution. Most simplified models assume unity Lewis factor and neglect the water losses due to evaporation. Hence, they developed an analytical model for IEC with parallel/counter flow configuration considering variable Lewis factor and surface wettability. Their model is sophisticated which is due to non-unity values of Lewis factor, surface wettability, varying spray water temperature and spray water enthalpy change. Briefly, Ren model consists of some characteristics which can't be found in previous analytical models including incomplete surface wetting condition, non-unity values of Lewis factor, consideration of spray water evaporation, consideration of spray water temperature variation, consideration of spray water enthalpy change along the heat exchanger surface. Hasan [7] presented a modified version of ε-NTU technique which can be used for indirect evaporative heat exchangers. Conventional sensible format of this technique can't be employed for indirect heat exchanger because of the existence of two gradients [7] including 1: temperature gradient between the air temperature in dry passage and the water film temperature and 2: enthalpy gradient

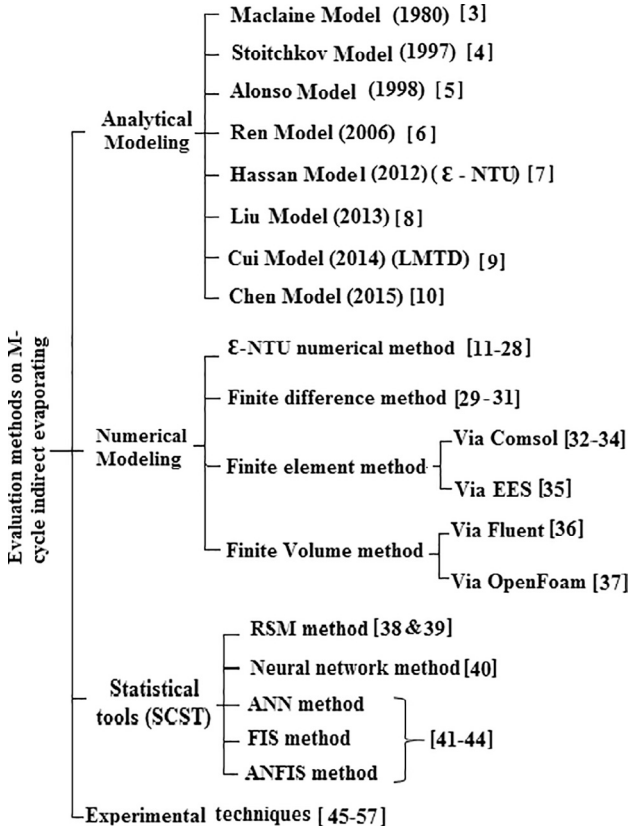

Fig. 3. Graphical view of the investigations of M-cycle [3–57].

between the saturated air-water film interface and the moist air. In the modified ε-NTU method attempts are made to create a connection between the temperature of dry side channel and "h" in the wet channel by a unique gradient. Liu [8] stated two deficiencies for Hassan ε-NTU model. Hassan model introduces a coefficient "a" to present the slope of the saturation line and does not discuss how to evaluate this coefficient. Hassan's model has been validated only by one operation condition without discussing its verification with other operation condition. Thus, Lui [8] presented a simplified thermal modeling based on ε-NTU method and then validated utilizing experimental data from the literature in a wide range of operating conditions. The model highlights several improvements over the previous simplified models, including the detailed procedure for "UA" value calculation for laminar and turbulent IEHX channel flows [8]. Cui et al. [9] presented a modified LMTD method to analyze counter flow indirect evaporative heat exchangers (IEHX). This method provides better accuracy when the temperature change in the IEHX (indirect evaporative heat exchanger) is non-linear and the greatest temperature difference at one end of the IEHX is more than twice the temperature difference at the other end of the IEHX [9].

The most recent selective investigations on indirect evaporative systems are presented as well. Kim et al. [58] evaluated the cooling performance of two different types of cross-flow indirect evaporative coolers including general type and regenerative type of cooler. They concluded that both of them provide similar cooling capacity per unit volume under equal primary and secondary air flow. Cui et al. [59] presented a novel energy-efficient dew-point evaporative air cooler which was designed based on a counter-flow closed-loop configuration consisting of separated working channels and product channels. Their cooler was able to obtain higher wet-bulb and dew-point effectiveness. Lin et al. [60] reminded that the method which have been used to estimate the heat/mass transfer coefficient in previous studied is the employment of Nusselt number and Sherwood number under constant condition of wet-surface which may not be the actual heat and mass transfer of the cooler. Hence, they tried to provide a mechanism to estimate the heat and mass transfer coefficient of M-cycle cooler. Chen et al. [61] reported a controller used in indirect evaporative cooler. Indeed, this controller causes a stable indoor temperature under different ambient air conditions.

As described above, analytical solutions of M-cycle have been presented only for the simplest structure of indirect evaporative cooler (without perforation) and no analytical model has yet been presented for perforated (multi-stage) M-cycle exchangers which are used in commercialized M-cycle air coolers. Thus, an analytical model is presented and verified for perforated M-cycle air cooler in this paper. Former evaluations of perforated M-cycle exchanger have been carried out only via elaborated numerical methods or experimental techniques which require further time, cost and energy. However, this paper shows that the thermal behavior of perforated regenerative M-cycle exchanger (Fig. 2d) can be analytically modeled and solved. The final outcomes of the model can be considered as a strong M-cycle initial-designing-tool so that the thermal characteristics of perforated M-cycle can be calculated very quickly by this model compared to the numerical or other techniques.

2. Physical modeling

Fig. 4a shows a schematic general view of a simple (without perforation) regenerative M-cycle exchanger, Fig. 4b illustrates a one-dimensional view of the regenerative M-cycle exchanger with two perforations (three-stage) and Fig. 4c represents a differential element in an arbitrary location along the exchanger. Temperature (T), humidity ratio (W) and mass flow rate ($\dot{m}$) of each point are illustrated in Table 1. Geometrical characteristics are shown in Fig. 4 as well. All parameters of primary air (dry channel) have been shown with subscripts "1" and all parameters of working air (wet channel) have been shown with subscript "2". It is also mentioned that, x' (in which "x" is any parameter) means the value of parameter "x" at the inlet of exchanger and x'' means the value of parameter x at the outlet of exchanger. For example, T_1' means temperature of primary air at inlet of dry channel, T_2'' means temperature of working air at the outlet of wet channel and T_1^A means the temperature of primary air at point A. The fraction of dry air which is discharged into the wet channel is shown with ε_a, ε_b and ε_c (for three stage) from the top side of exchanger respectively. Hence, for a three stage M-cycle $\varepsilon_a = \frac{\dot{m}_1^A}{\dot{m}_1'}$, $\varepsilon_b = \frac{\dot{m}_1^D}{\dot{m}_1'}$ and $\varepsilon_c = \frac{\dot{m}_2'}{\dot{m}_1'}$ and $\varepsilon_a + \varepsilon_b + \varepsilon_c < 1$.

The physical modeling of single-stage M-cycle can be explained as below.

(a) The inlet air of dry side (T_1') moves through the dry channel while its temperature is gradually reduced due to the sensible heat transfer process with wet channel. The humidity ratio of dry air never changes in this process because of no direct contact with water fluid. Obviously, the temperature of dry air at the outlet of dry channel (T_1'') has been reduced.
(b) A fraction of cooled dry air is discharged into the room and used as the product air and the remaining ($\dot{m}_1'\varepsilon_a$) returned into the wet channel and used as a working air. It is clear that the temperature and humidity ratio of working air at the inlet of the wet-channel are the same as product air. Working air flows along the wet channel. Contrary to the dry channel (in which the heat transfer process is occurred only via sensible format) energy variation of working air is occurred via both sensible and latent heat because of direct contact between working air and water film. Indeed, energy variation of working air is because of convective heat transfer (between working air and water film) and evaporation of water (latent heat). Although, the temperature of working air is reduced along the wet channel, its humidity ratio significantly increases as well.
(c) The outlet air from the wet channel is discharged into the outside of

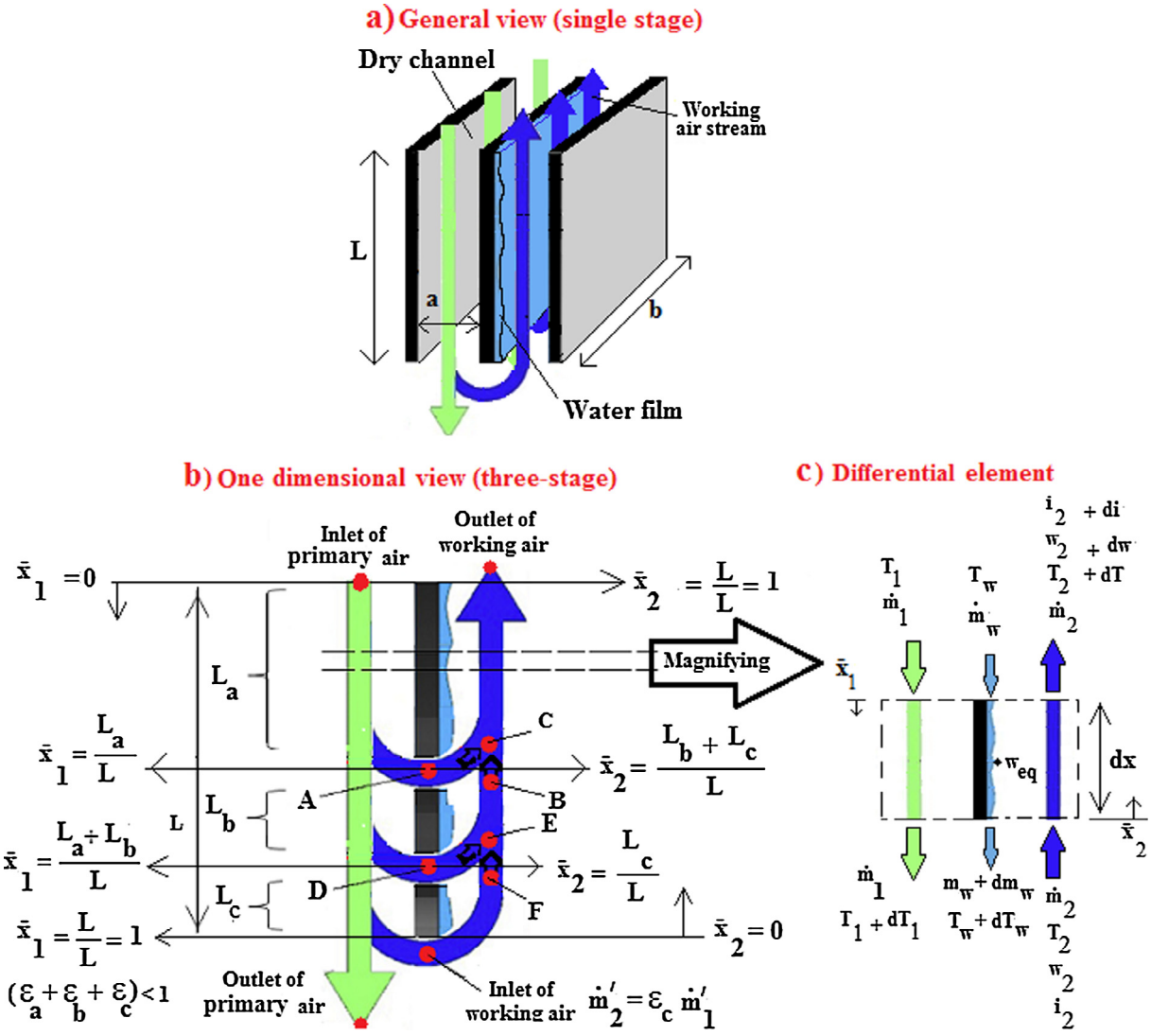

Fig. 4. (a) A general view of single stage M-cycle (b) one dimensional view of three-stage M-cycle and (c) differential element on an arbitrary location.

the air-conditioning room and that's why the M-cycle coolers have two exhausts one of which leads to the outside of the room by a chimney (related to working air) and the other is flowed into the room.

The physical modeling of perforated M-cycle cooler is similar to the single-stage M-cycle. However, in perforated M-cycle exchanger the dry air is gradually discharged into the wet-channel in order to reduce the pressure drop of heat exchanger. For example, according to Fig. 4b, a fraction of dry air (ε_a) is discharged into the wet-channel at point "A" and the remaining moves along the rest of the channel. This process is repeated again in point "B" and the end of the dry channel with two other value of ε_b and ε_c. It should be noted that, contrary to the bottom point of exchanger in which $T'_2 = T''_1$, there is a gas mixture between points A, B and C in the middle section of exchanger and that is why $T_c \neq T_A$ and $T_D \neq T_E$ (see Fig. 4). This explanation is valid for humidity ratio as well (note carefully to Table 1 for the value of each characteristic or parameter in each location).

3. Mathematical model

In this section analytical formulation is presented for three-stage M-cycle air cooler. $\dot{m}_w$ is water mass flow rate, $\dot{m}_1$ is mass flow rate of primary air, c_1 is specific heat of primary air, T_1 is temperature of primary air, U is overall heat transfer coefficient between primary air and water film, T_w is water film temperature, A_1 is interface area of primary

Table 1
Temperature, humidity ratio and mass flow rate of each point shown in Fig. 4b.

	Inlet of primary air	Outlet of primary air	Inlet of working air	Outlet of working air	A	B	C	D	E	F
T	T'_1	T''_1	$T'_2 = T''_1$	T''_2	T_1^A	T_2^B	T_2^C	T_2^D	T_2^E	T_2^F
W	W'_1	$W''_1 = W'_1$	$W'_2 = W''_1 = W'_1$	W''_2	$W_1^A = W'_1$	W_2^B	W_2^C	$W_1^D = W'_1$	W_2^E	W_2^F
$\dot{m}$	$\dot{m}'_1$	$\dot{m}''_1 = \dot{m}'_1$ $(1-\varepsilon_a-\varepsilon_b-\varepsilon_c)$	$\dot{m}'_2 = \varepsilon_c\dot{m}'_1$	$\dot{m}''_2 = \dot{m}'_1$ $(\varepsilon_a+\varepsilon_b+\varepsilon_c)$	$\dot{m}_1^A = \varepsilon_a\dot{m}'_1$	$\dot{m}_2^B = \dot{m}'_1$ $(\varepsilon_a+\varepsilon_b)$	$\dot{m}_2^C = \dot{m}'_1$ $(\varepsilon_a+\varepsilon_b+\varepsilon_c)$	$\dot{m}_1^D = \dot{m}'_1\varepsilon_b$	$\dot{m}_2^E = \dot{m}'_1$ $(\varepsilon_c+\varepsilon_b)$	$\dot{m}_2^F = \varepsilon_c\dot{m}'_1$

air, L_{pa} is flow length in direction of primary air and x_{pa} (or x_1) is space coordinate originated from the inlet of primary air. $\dot{m}_2$ is mass flow rate of working-air (humid air), i_2 is specific enthalpy of working air, α_2 is convective heat transfer coefficient of working air, i_υ is specific enthalpy of water vapor at water-film temperature, β is convective mass-transfer coefficient, w_{eq} is humidity ratio of working air where it is in equilibrium with water surface, w_2 is humidity ratio of working air, σ is wettability factor, A_2 is interface area of working air, L_{wa} is flow length in direction of working air and x_{wa} (or x_2) is space coordinate originated from the inlet of working air (for parallel and counter flow exchanger $L_{wa} = L_{pa} = L$). The perforations in an arbitrary locations along the exchanger have divided the exchanger into separate lengths termed L_a, L_b and L_c.

Energy balance of primary air, energy balance of wet channel, mass balance of working air and energy balance for all differential element should be written with regard to Fig. 4c. It is noted that the temperature of primary air (T_1), temperature of working air (T_2), water fluid temperature (T_w), and humidity ratio of working air (w_2) are the most significant parameters in the analysis of M-cycle system by which the performance characteristics of M-cycle cooler can be evaluated. Hence, it will be tried to arrange the differential-equations based on dT_2, dw_2, dT_1, dT_w and dw_{eq}. Furthermore, it is interested to arrange the equations as a function of Number of Thermal Units (NTU) (for wet channel) and Lewis factor (Le_f). Lewis factor plays a key role in the evaluation of heat and mass transfer between liquids and gases. Lewis factor is dimensionless number and generally is defined as the ratio of thermal diffusivity to mass diffusivity.

$$NTU = \frac{\alpha_2 A_2}{\dot{m}_2 c_a} \tag{1}$$

$$Le_f = \frac{\alpha_2}{\beta\, c_a} \tag{2}$$

The assumptions for expansion and solving of these differential equations are described as below in present study.

(1) Thermal diffusivity occurs only in the normal to flow direction and all system is entirely insulated.
(2) The value of mass transfer coefficient, heat transfer coefficient and specific heat of fluids are constant along exchanger surface.
(3) "w_{eq}" has a linear function with water surface temperature ($w_{eq} = F + eT_w$)
(4) Mass flow rate of sprayed water flow is so larger than the mass flow rate of working air flow ($\dot{m}_w \gg \dot{m}_2$). This assumption is applicable for the type of M-cycle coolers in which the spray-water is the mechanism for wetting the plate of exchanger. As described by Ren [6] as well, several previous analytical models of single-stage M-cycle were derived by assuming a constant or theoretically constant spray water temperature [62], similar to that reviewed by Erns and Dreyer [63] and utilized by Hasan [64,65] to interpretation of experimental data for getting the relevant heat and mass transfer coefficient [6]. This assumption was recommended for the evaluation of smaller systems and for initial design purpose. As the complexity of Multi-stage is much more than the single-stage, this model has been developed by that assumption as well.
(5) The whole surface of the plate is wetted ($\sigma = 1$) and Lewis factor is

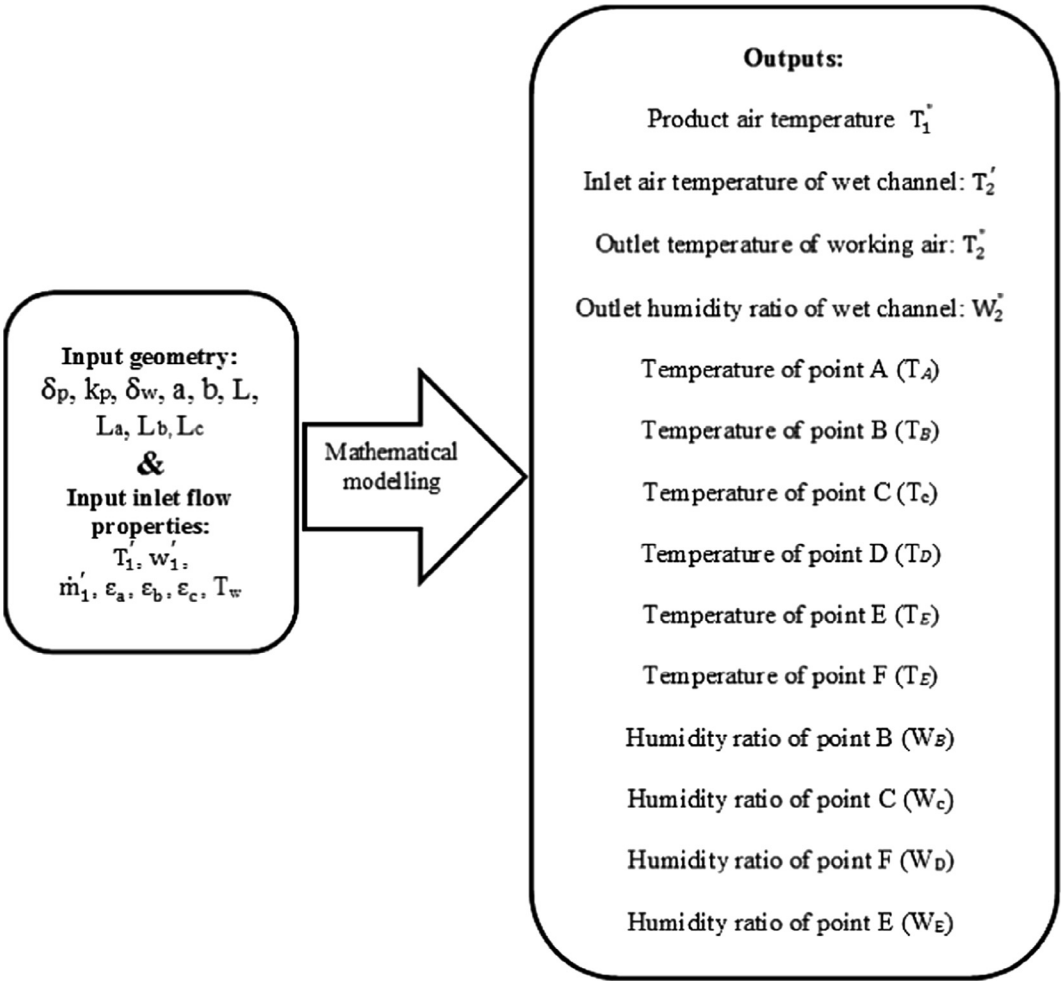

Fig. 5. Inputs and outputs of present analytical model.

satisfied which means $Le_f = \frac{\alpha_2}{\beta c_a} = 1$. Hence, $\frac{\sigma}{Le_f} = 1$ (as said above, Lewis factor is dimensionless number and generally is defined as the ratio of thermal diffusivity to mass diffusivity).

It should be noted that, Lewis [66] showed that the Le is approximately equal with unity for air/water mixtures and that's why most researchers have used this assumption in their models.

With this assumptions, the inputs and outputs of the model will be extracted as shown in Fig. 5.

According to Ren [6], the initial differential equations of energy and mass conservation for primary air (dry channel) and working air (wet channel) in a steady-state condition can be written as below.

Energy balance of primary air (dry channel) along differential element dx:

Obviously, for an insulated exchanger, energy variation of primary-air (along dx) equals with convective heat transfer rate between dry air and wall (water film) which is shown mathematically by Eq. (3).

$$\dot{m}_1 c_1 dT_1 = U(T_w - T_1)A_1\frac{dx_1}{L} \tag{3}$$

Rearrangement based on d T_1:

$$dT_1 = \frac{U}{\dot{m}_1 c_1}(T_w - T_1)A_1\frac{dx_1}{L_{pa}} \tag{4}$$

Rewritten based on NTU:

$$dT_1 = \left[\frac{\dot{m}_2 c_a}{\dot{m}_1 c_1} \times \frac{UA_1}{\alpha_2 A_2}\right]\frac{\alpha_2 A_2}{\dot{m}_2 c_a}(T_w - T_1)d\bar{x}_1 \tag{5}$$

$$dT_1 = \frac{r}{C_f^*}NTU(T_w - T_1)d\bar{x}_1 \tag{6}$$

$$\text{Where } r = \frac{UA_1}{\alpha_2 A_2} \tag{7}$$

$$C_f^* = \frac{\dot{m}_1 c_1}{\dot{m}_2 c_a} \tag{8}$$

$$d\bar{x}_1 = \frac{dx_1}{L_{pa}} \tag{9}$$

Mass balance of working air in wet channel (two equations):

$$\dot{m}_2\, dw_2 = \beta(w_{eq} - w_2)\sigma\, A_2\frac{dx_2}{L} \tag{10}$$

$$d\dot{m}_w = -\dot{m}_2 dw_2 \tag{11}$$

Eq. (10) is rearranged based on d w_2:

$$dw_2 = \frac{\beta}{\dot{m}_2}(w_{eq} - w_2)\sigma\, A_2\frac{dx_2}{L} \tag{12}$$

$$dw_2 = \frac{\sigma}{\frac{\alpha_2}{\beta c_a}}(w_{eq} - w_2)\frac{\alpha_2 A_2}{\dot{m}_2 c_a}d\bar{x}_2 \tag{13}$$

$$dw_2 = \frac{\sigma}{Le_f}(w_{eq} - w_2)\, NTU\, d\bar{x}_2 \quad \& \quad d\dot{m}_w = -\dot{m}_2 dw_2 \tag{14}$$

Energy balance of wet channel:

Contrary to dry channel in which energy variation occurs only in the form of sensible heat transfer, energy variation of working-air occurs in the form of both sensible and latent heat transfer. In other words, energy variation of working air has spent on convective heat transfer (between working air and water film) and evaporation of water (latent heat) which mathematically is shown by Eq. (15).

$$\dot{m}_2\, di_2 = [\alpha_2(T_w - T_2) + i_\upsilon\, \beta(w_{eq} - w_2)\sigma]A_2\frac{dx_2}{L_{wa}} \tag{15}$$

It should be noted that, i_2 is specific enthalpy of humid air which equals with the summation of specific enthalpy of dry air (i_a) and a coefficient of the specific enthalpy of water vapor (i_υ) as shown below.

$$i_2 = i_a + w_2 i_\upsilon \tag{16}$$

In Eq. (16) i_a is specific enthalpy of dry air and i_υ is specific enthalpy of water vapor at constant pressure which are calculated from Eq. (17) and (18) respectively.

$$i_a = c_a T_2 \tag{17}$$

$$i_\upsilon = c_\upsilon T_2 + i_{fg} \tag{18}$$

The constants c_a in Eq. (17), c_υ and i_{fg} in Eq. (18) are specific heat of dry air, specific heat of water vapor at constant pressure and evaporation heat of water at 0 °C.

c_a = 1 KJ/kg
c_υ = 1.84 KJ/kg
i_{fg} = 2501 KJ/kg

Substituting Eq. (17) and (18) in Eq. (16) yields;

$$i_2 = (c_a + w_2 c_\upsilon)T_2 + w_2 i_{fg} \tag{19}$$

Therefore, di_2 can be obtained from i_2 (Eq. (19)). It is noted that, both w_2 and T_2 are variable in direction of x, and differential of the first term (($c_a + w_2 c_\upsilon$) T_2) should be expanded via the "Product Rule for Derivatives" as shown in Eq. (20).

$$di_2 = (c_a + w_2 c_\upsilon)dT_2 + T_2 c_\upsilon dw_2 + i_{fg} dw_2 \tag{20}$$

$$di_2 = (c_a + w_2 c_\upsilon)dT_2 + dw_2(i_{fg} + T_2 c_\upsilon) \tag{21}$$

Now, di_2 can be substituted in Eq. (15) and rearranged based on d T_2:

$$\dot{m}_2[(c_a + w_2 c_\upsilon)dT_2 + (i_{fg} + T_2 c_\upsilon)dw_2] = [\alpha_2(T_w - T_2) + i_\upsilon\, \beta(w_{eq} - w_2)\sigma]A_2\frac{dx_2}{L} \tag{22}$$

$$dT_2 = [\alpha_2(T_w - T_2) + i_\upsilon\, \beta(w_{eq} - w_2)\sigma]\frac{A_2 dx_2}{(c_a + w_2 c_\upsilon)\dot{m}_2 L} - \frac{(i_{fg} + T_2 c_\upsilon)dw_2}{(c_a + w_2 c_\upsilon)} \tag{23}$$

$$dT_2 = \frac{\alpha_2(T_w - T_2)A_2 dx_2}{(c_a + w_2 c_\upsilon)\dot{m}_2 L} + \frac{i_\upsilon\, \beta(w_{eq} - w_2)\sigma A_2 dx_2}{(c_a + w_2 c_\upsilon)\dot{m}_2 L} - \frac{(i_{fg} + T_2 c_\upsilon)dw_2}{(c_a + w_2 c_\upsilon)}. \tag{24}$$

dw_2 can be replaced by Eq. (14) and $\frac{dx_2}{L} = d\bar{x}_2$

$$dT_2 = \frac{\alpha_2(T_w - T_2)A_2 dx_2}{(c_a + w_2 c_\upsilon)\dot{m}_2 L} + \frac{i_\upsilon\, \beta(w_{eq} - w_2)\sigma A_2 dx_2}{(c_a + w_2 c_\upsilon)\dot{m}_2 L} - \frac{(i_{fg} + T_2 c_\upsilon)\frac{\sigma}{Le_f}(w_{eq} - w_2)NTU\, d\bar{x}_2}{(c_a + w_2 c_\upsilon)} \tag{25}$$

$$dT_2 = \frac{\alpha_2(T_w - T_2)A_2 d\bar{x}_2}{(c_a + w_2 c_\upsilon)\dot{m}_2} + \frac{i_\upsilon\, \beta(w_{eq} - w_2)\sigma A_2 d\bar{x}_2}{(c_a + w_2 c_\upsilon)\dot{m}_2} - \frac{(i_{fg} + T_2 c_\upsilon)\frac{\sigma}{Le_f}(w_{eq} - w_2)NTU\, d\bar{x}_2}{(c_a + w_2 c_\upsilon)} \tag{26}$$

$$dT_2 = \frac{\alpha_2(T_w - T_2)A_2 d\bar{x}_2}{c_a\left(1 + w_2\frac{c_\upsilon}{c_a}\right)\dot{m}_2} + \frac{i_\upsilon\, \alpha_2\beta(w_{eq} - w_2)\sigma A_2 d\bar{x}_2}{\alpha_2 c_a\left(1 + w_2\frac{c_\upsilon}{c_a}\right)\dot{m}_2} - \frac{(i_{fg} + T_2 c_\upsilon)\frac{\sigma}{Le_f}(w_{eq} - w_2)NTU\, d\bar{x}_2}{c_a\left(1 + w_2\frac{c_\upsilon}{c_a}\right)} \tag{27}$$

After a time-consuming rearrangement of Eq. (27), following equation is obtained for dT_2.

$$dT_2 = \left[(T_w - T_2) + \frac{\frac{\sigma}{Le_f}(w_{eq} - w_2)(i_\upsilon - i_{fg} - T_2 c_\upsilon)}{c_a}\right]\frac{1}{\left(1 + w_2\frac{c_\upsilon}{c_a}\right)}NTU\, d\bar{x}_2 \tag{28}$$

According to Eq. (18) $i_\upsilon - i_{fg} = c_\upsilon T_2$, hence,

$$dT_2 = \left[(T_w - T_2) + \frac{\frac{\sigma}{Le_f}(w_{eq} - w_2)(0)}{c_a}\right]\frac{1}{\left(1 + w_2\frac{c_\upsilon}{c_a}\right)}NTU\, d\bar{x}_2 \quad (29)$$

$$dT_2 = [(T_w - T_2) + 0]\frac{1}{\left(1 + w_2\frac{c_\upsilon}{c_a}\right)}NTU\, d\bar{x}_2 \quad (30)$$

$$dT_2 = [(T_w - T_2)]\frac{1}{(1 + w_2\frac{c_\upsilon}{c_a})}NTU\, d\bar{x}_2 \quad (31)$$

$$dT_2 = [(T_w - T_2)]\frac{1}{B_1}NTU\, d\bar{x}_2 \quad (32)$$

where

$$B_1 = 1 + w_2\frac{c_\upsilon}{c_a} \quad (33)$$

It should be noted that, as the value of w_2 is so smaller than the unity (1), the value of B_1 is approximately equal to one.

Hence,

$$dT_2 = (T_w - T_2)NTU\, d\bar{x}_2 \quad (34)$$

Energy balance for differential element:

$$\dot{m}_w c_w\, dT_w + c_w T_w\, d\dot{m}_w + \dot{m}_1 c_1\, dT_1 + \dot{m}_2\, di_2 = 0 \quad (35)$$

Eq. (35) is rearranged based on d T_w:

$$dT_w = -\left[\frac{c_w T_w\, d\dot{m}_w}{\dot{m}_w c_w} + \frac{\dot{m}_1 c_1\, dT_1}{\dot{m}_w c_w} + \frac{\dot{m}_2\, di_2}{\dot{m}_w c_w}\right] \quad (36)$$

$d\dot{m}_w$, d T_1 and di_2 in Eq. (36) are substituted with Eq. (14), Eq. (6) and Eq. (20) respectively and $d\bar{x}_1 = -d\bar{x}_2$.

$$dT_w = -\left[\frac{-c_w T_w \dot{m}_2\, dw_2}{\dot{m}_w c_w} - \frac{\dot{m}_1 c_1 \frac{r}{C_f^*}NTU(T_w - T_1)d\bar{x}_2}{\dot{m}_w c_w} + \frac{\dot{m}_2[(c_a + w_2c_\upsilon)dT_2 + i_{fg}\, dw_2]}{\dot{m}_w c_w}\right] \quad (37)$$

dT_2 and dw_2 are substituted with Eq. (34) and Eq. (14) respectively.

$$dT_w = -\left[\frac{-c_w T_w \dot{m}_2\frac{\sigma}{Le_f}(w_{eq} - w_2)NTU\, d\bar{x}_2}{\dot{m}_w c_w} - \frac{\dot{m}_1 c_1\frac{r}{C_f^*}NTU(T_w - T_1)d\bar{x}_2}{\dot{m}_w c_w} + \frac{\dot{m}_2[(c_a + w_2c_\upsilon)\left(\frac{T_w}{B_0} - T_2\right)B_1 NTU\, d\bar{x}_2 + i_{fg}\frac{\sigma}{Le_f}(w_{eq} - w_2)NTU\, d\bar{x}_2]}{\dot{m}_w c_w}\right] \quad (38)$$

Rearrangement of Eq. (38) gives Eq. (39):

$$dT_w = \left[-B_2\frac{i_{fg}}{c_a}\frac{\sigma}{Le_f}(w_{eq} - w_2) - r(T_1 - T_w) - B_3(T_w - T_2)\right]\frac{1}{C_w^*}NTU\, d\bar{x}_2 \quad (39)$$

where

$$B_2 = 1 - \frac{R_{cw}T_w}{\frac{i_{fg}}{c_a}} \quad (40)$$

$$B_3 = 1 + w_2\frac{c_\upsilon}{c_a} \quad (41)$$

$$C_w^* = \frac{\dot{m}_w c_w}{\dot{m}_2 c_a} \quad (42)$$

$$R_{cw} = \frac{c_w}{c_a} \quad (43)$$

It is noted that, B_2 and B_3 can be approximated with unity as well and the equation can be written as below.

$$dT_w = \left[-\frac{i_{fg}}{c_a}\frac{\sigma}{Le_f}(w_{eq} - w_2) - r(T_1 - T_w) - (T_w - T_2)\right]\frac{1}{C_w^*}NTU\, d\bar{x}_2 \quad (44)$$

"w_{eq}" is the final parameter for which a relationship should be developed. Almost all analytical modeling of M-cycle have assumed that "w_{eq}" has a linear function with water surface temperature T_w as below where "F" and "e" are constant.

$$w_{eq} = F + eT_w \quad (45)$$

Hence, differential equation of w_{eq} can be illustrated as below.

$$dw_{eq} = e\, dT_w \quad (46)$$

Substituting Eq. (44) in Eq. (46) yields:

$$dw_{eq} = e\left[-\frac{i_{fg}}{c_a}\frac{\sigma}{Le_f}(w_{eq} - w_2) - r(T_1 - T_w) - (T_w - T_2)\right]\frac{1}{C_w^*}NTU\, d\bar{x}_2] \quad (47)$$

Eq. (6), (14), (34), (44) and (47) are five differential equations (written as a set of differential equations in Eq. (44)) which solving them through the exchanger from x = 0 to x = L ($\bar{x} = 0$ to $\bar{x} = 1$) can provide required thermal specifications of M-cycle. However, these equations should be further rearranged to get a systemized set of differential equations.

$$\begin{cases} dT_1 = \frac{r}{C_f^*}NTU(T_w - T_1)d\bar{x}_1 \\ dT_2 = NTU(T_w - T_2)d\bar{x}_2 \\ dw_2 = \frac{\sigma}{Le_f}(w_{eq} - w_2)NTU\, d\bar{x}_2 \\ dT_w = \left[-\frac{i_{fg}}{c_a}\frac{\sigma}{Le_f}(w_{eq} - w_2) - r(T_1 - T_w) - (T_w - T_2)\right]\frac{1}{C_w^*}NTU\, d\bar{x}_2 \\ dw_{eq} = \left[-\frac{i_{fg}}{c_a}\frac{\sigma}{Le_f}(w_{eq} - w_2) - r(T_1 - T_w) - (T_w - T_2)\right]\frac{e}{C_w^*}NTU\, d\bar{x}_2 \end{cases} \quad (48)$$

This system of equations can be solved for different operational conditions of M-cycle cooler which depends on real working condition of air cooler. However, according to assumption 4, the equations are solved for the condition in which the mass flow rate of water is so much than the mass flow rate of working air $\dot{m}_w \gg \dot{m}_2$. This condition is occurred for coolers in which the system is worked based on sprayed water. The concept of this condition is that the value of $C_w^* = \frac{\dot{m}_w c_w}{\dot{m}_2 c_a}$ tends to ∞. Under this condition $\frac{1}{C_w^*}$ tends to zero and the dT_w becomes equal with zero which means that the temperature variation of water film through the exchanger is zero and subsequently the water film along the exchanger has the same temperature of water inlet temperature. For this condition, wall temperature is the same temperature of water temperature. Moreover, the value of d w_{eq} is zero as well. Hence, the system of equations can be finally written as following.

$$\begin{cases} dT_1 = \frac{r}{C_f^*}NTU(T_w - T_1)d\bar{x}_1 \\ dT_2 = NTU(T_w - T_2)d\bar{x}_2 \\ dw_2 = \frac{\sigma}{Le_f}(w_{eq} - w_2)NTU\, d\bar{x}_2 \\ dT_w = 0 \xrightarrow{\text{yields}} T_w = \text{Constant} \\ dw_{eq} = \xrightarrow{\text{yields}} w_{eq} = \text{Constant} \end{cases} \quad (49)$$

In this condition, all differential equations are transformed into independent equations that can be integrated independently. It should be noted that, T_w and w_{eq} (in the first and the third equations) are not change along "x" (which is clear in the fourth and fifth equations). By applying the assumption 6 and some rearrangements the system of equations (49) is rewritten as below.

$$\begin{cases} \frac{dT_1}{(T_w - T_1)} = \frac{r}{C_f^*}NTU\, d\bar{x}_1 \\ \frac{dT_2}{(T_w - T_{wa})} = NTU\, d\bar{x}_2 \\ \frac{dw_2}{(w_{eq} - w_2)} = NTU\, d\bar{x}_2 \\ T_w = Constant \\ w_{eq} = Constant \end{cases} \quad (50)$$

For a given cooler, inlet temperature of dry air (T_1', ambient temperature), T_w (water inlet temperature), w_1' (humidity ratio of inlet air) and geometrical characteristics are known-input parameters. NTU, "r" and w_{eq} should be determined before the solving of the equations as described in the following. These equations can be used vice versa as well. Indeed, if the value of NTU and outlet conditions are given, the geometries of cooler is determinable.

It is noted that, according to Fig. 4, the directions of $\bar{x}_{wa}$ and $\bar{x}_{pa}$ which were chosen based on flow direction are vice versa ($d\bar{x}_{wa} = -d\bar{x}_{pa}$). In other words, $\bar{x}_{pa} = 1$ is the top side of exchanger and $\bar{x}_{wa} = 1$ is the bottom side of exchanger.

4. Solving the model for three-stage exchanger

Generally, Eq. (50) can be integrated from $\bar{x} = \gamma_1$ until $\bar{x} = \gamma_2$ via the mathematical integration rule shown in Eq. (51) if the flow parameter of working air ($\dot{m}_2$) does not change between γ_1 and γ_2 in order to have an exclusive NTU in that distance. For example, for a single-stage exchanger all equations of Eq. (50) can be integrated from $\bar{x} = 0$ until $\bar{x} = 1$ via the mathematical integration rule shown in Eq. (51). It is noted that the flow parameter of working air (i.e. $\dot{m}_2$) is not changed between $\bar{x} = 0$ and $\bar{x} = 1$ in a single stage M-cycle and then it is possible to consider a unit NTU for all exchanger.

$$\int_{\gamma_1}^{\gamma_2} \frac{c}{ax + b}dx = \frac{c}{a}Ln\frac{a\gamma_2 + b}{a\gamma_1 + b} \quad (51)$$

However, for a perforated M-cycle exchanger the Eq. (50) cannot be integrated along the whole exchanger ($\bar{x} = 0$ until $\bar{x} = 1$) all at once. Therefore, the differential equations should be integrated through separated lengths (between any two consecutive perforations) as shown mathematically in Eq. (52).

$$\int_{\bar{x}=0}^{\bar{x}=1} \text{Function} = \int_0^{\gamma_1} \text{Function} + \int_{\gamma_1}^{\gamma_2} \text{Function} + \cdots + \int_{\gamma_n}^{1} \text{Function} \quad (52)$$

In other words, the equations is firstly integrated from the beginning of the plate until the first perforation (L_a) and then from the first perforation to the second perforation (L_b) etc. The thermal fluid condition of each point were shown in Fig. 4 and Table 1 before. Now, equations should be integrated for each three length separately. Eq. (51) should be integrated for L_a, L_b and L_c.

Integration from top side of exchanger until the end of L_a:

$$L_a: \begin{cases} \int_{\bar{x}_1=0}^{\bar{x}_1=\frac{L_a}{L}} \frac{dT_1}{(T_w - T_1)} = \frac{r_{La}}{C_{f_{La}}^*}NTU_{La}\int_{\bar{x}_1=0}^{\bar{x}_1=\frac{L_a}{L}} d\bar{x}_1 \\ \int_{\bar{x}_{2=\frac{L_b+L_c}{L}}}^{\bar{x}_2=1} \frac{dT_2}{(T_w - T_2)} = NTU_{La}\int_{\bar{x}_{2=\frac{L_b+L_c}{L}}}^{\bar{x}_2=1} d\bar{x}_2 \\ \int_{\bar{x}_{2=\frac{L_b+L_c}{L}}}^{\bar{x}_2=1} \frac{dw_2}{(w_{eq} - w_2)} = NTU_{La}\int_{\bar{x}_{2=\frac{L_b+L_c}{L}}}^{\bar{x}_2=1} d\bar{x}_2 \\ T_w = Constant \\ w_{eq} = Constant \end{cases} \quad (53)$$

Integration for L_b:

$$L_b: \begin{cases} \int_{\bar{x}_{1=\frac{L_a}{L}}}^{\bar{x}_{1=\frac{L_a+L_b}{L}}} \frac{dT_1}{(T_w - T_1)} = \frac{r_{Lb}}{C_{f_{Lb}}^*}NTU_{Lb}\int_{\bar{x}_{1=\frac{L_a}{L}}}^{\bar{x}_{1=\frac{L_a+L_b}{L}}} d\bar{x}_1 \\ \int_{\bar{x}_{2=\frac{L_c}{L}}}^{\bar{x}_{2=\frac{L_b+L_c}{L}}} \frac{dT_2}{(T_w - T_2)} = NTU_{Lb}\int_{\bar{x}_{2=\frac{L_c}{L}}}^{\bar{x}_{2=\frac{L_b+L_c}{L}}} d\bar{x}_2 \\ \int_{\bar{x}_{2=\frac{L_c}{L}}}^{\bar{x}_{2=\frac{L_b+L_c}{L}}} \frac{dw_2}{(w_{eq} - w_2)} = NTU_{Lb}\int_{\bar{x}_{2=\frac{L_c}{L}}}^{\bar{x}_{2=\frac{L_b+L_c}{L}}} d\bar{x}_2 \\ T_w = Constant \\ w_{eq} = Constant \end{cases} \quad (54)$$

Integration for L_c:

$$L_c: \begin{cases} \int_{\bar{x}_{1=\frac{L_a+L_b}{L}}}^{\bar{x}_1=1} \frac{dT_1}{(T_w - T_1)} = \frac{r_{Lc}}{C_{f_{Lc}}^*}NTU_{Lc}\int_{\bar{x}_{1=\frac{L_a+L_b}{L}}}^{\bar{x}_1=1} d\bar{x}_1 \\ \int_{\bar{x}2=0}^{\bar{x}_{2=\frac{L_c}{L}}} \frac{dT_2}{(T_w - T_2)} = NTU_{Lc}\int_{\bar{x}2=0}^{\bar{x}_{2=\frac{L_c}{L}}} d\bar{x}_2 \\ \int_{\bar{x}2=0}^{\bar{x}_{2=\frac{L_c}{L}}} \frac{dw_2}{(w_{eq} - w_2)} = NTU_{Lc}\int_{\bar{x}2=0}^{\bar{x}_{2=\frac{L_c}{L}}} d\bar{x}_2 \\ T_w = Constant \\ w_{eq} = Constant \end{cases} \quad (55)$$

Now, the integrations can be solved in accordance with the Eq. (51) (for left sides) as shown below.

$$\text{Solving, } L_a: \begin{cases} Ln\frac{T_w - T_{1|\bar{x}_1=\frac{L_a}{L}}}{T_w - T_{1|\bar{x}1=0}} = -\frac{r_{La}}{C_{f_{La}}^*}NTU_{La}\left(\frac{L_a}{L} - 0\right) \\ Ln\frac{T_w - T_{2|\bar{x}_2=1}}{T_w - T_{2\ |\bar{x}_2=\frac{L_b+L_c}{L}}} = -NTU_{La}\left(1 - \frac{L_b + L_c}{L}\right) \\ Ln\frac{w_{eq} - w_{2|\bar{x}_2=1}}{w_{eq} - w_{2\ |\bar{x}_2=\frac{L_b+L_c}{L}}} = -NTU_{La}\left(1 - \frac{L_b + L_c}{L}\right) \\ T_w = Constant \\ w_{eq} = Constant \end{cases} \quad (56)$$

$$\text{Solving, } L_b: \begin{cases} \text{Ln}\frac{T_w - T_{1\ |\bar{x}_1=\frac{L_a+L_b}{L}}}{T_w - T_{1\ |\bar{x}_1=\frac{L_a}{L}}} = -\frac{r_{Lb}}{C_{f_{Lb}}^*}NTU_{Lb}\left(\frac{L_a + L_b}{L} - \frac{L_a}{L}\right) \\ \text{Ln}\frac{T_w - T_{2\ |\bar{x}_2=\frac{L_b+L_c}{L}}}{T_w - T_{2\ |\bar{x}_2=\frac{L_c}{L}}} = -NTU_{Lb}\left(\frac{L_b + L_c}{L} - \frac{L_c}{L}\right) \\ \text{Ln}\frac{w_{eq} - w_{2\ |\bar{x}_2=\frac{L_b+L_c}{L}}}{w_{eq} - w_{2\ |\bar{x}_2=\frac{L_c}{L}}} = -NTU_{Lb}\left(\frac{L_b + L_c}{L} - \frac{L_c}{L}\right) \\ T_w = Constant \\ w_{eq} = Constant \end{cases} \quad (57)$$

$$\text{Solving, } L_c: \begin{cases} \text{Ln}\frac{T_w - T_{1|\bar{x}_1=1}}{T_w - T_{1\ |\bar{x}_1=\frac{L_a+L_b}{L}}} = -\frac{r_{Lc}}{C_{f_{Lc}}^*}NTU_{Lc}\left(1 - \frac{L_a + L_b}{L}\right) \\ \text{Ln}\frac{T_w - T_{2\ |\bar{x}_2=\frac{L_c}{L}}}{T_w - T_{2|\bar{x}_2=0}} = -NTU_{Lc}\left(\frac{L_c}{L} - 0\right) \\ \text{Ln}\frac{w_{eq} - w_{2|\bar{x}_2=\frac{L_c}{L}}}{w_{eq} - w_{2|\bar{x}_2=0}} = -NTU_{Lc}\left(\frac{L_c}{L} - 0\right) \\ T_w = Constant \\ w_{eq} = Constant \end{cases} \quad (58)$$

It is noted that again, the concept of $T_{1|\bar{x}1=1}$ is the amount of T_1 at $\bar{x}_1 = 1$. Moreover, NTU_{La}, r_{La} and $C_{f_{La}}^*$ mean the amount of NTU, r and C_f^* for section L_a. The symbols of parameters are substituted according to Fig. 4c (For example, $T_{2|\bar{x}2=0} = T_2' = T_1''$ and $T_{2\ |\bar{x}_2=\frac{L_b}{L}} = T_B$) and the equations are rearranged based on exponential function as shown below.

$$L_a:\begin{cases} T_A = T_w - \left[(T_w - T_1')e^{-\frac{r_{L_a}}{C^*_{f_{L_a}}}NTU_{L_a}(\frac{L_a}{L})}\right] \\ T_2'' = T_w - \left[(T_w - T_c)e^{-NTU_{L_a}(1-\frac{L_b+L_c}{L})}\right] \\ w_2'' = w_{eq} - \left[(w_{eq} - w_c)e^{-NTU_{L_a}(1-\frac{L_b+L_c}{L})}\right] \\ T_w = \text{Constant} \\ w_{eq} = \text{Constant} \end{cases} \quad (59)$$

$$L_b:\begin{cases} T_D = T_w - \left[(T_w - T_A)e^{-\frac{r_{L_b}}{C^*_{f_{L_b}}}NTU_{L_b}(\frac{L_b}{L})}\right] \\ T_B = T_w - \left[(T_w - T_E)e^{-NTU_{L_b}(\frac{L_b}{L})}\right] \\ W_B = w_{eq} - \left[(w_{eq} - w_E)e^{-NTU_{L_b}(\frac{L_b}{L})}\right] \\ T_w = \text{Constant} \\ w_{eq} = \text{Constant} \end{cases} \quad (60)$$

$$L_c:\begin{cases} T_1'' = T_w - \left[(T_w - T_D)e^{-\frac{r_{L_c}}{C^*_{f_{L_c}}}NTU_{L_c}(1-\frac{L_a+L_b}{L})}\right] \\ T_F = T_w - \left[(T_w - T_1'')e^{-NTU_{L_c}(\frac{L_c}{L})}\right] \\ W_F = w_{eq} - \left[(w_{eq} - w_1')e^{-NTU_{L_c}(\frac{L_c}{L})}\right] \\ T_w = \text{Constant} \\ w_{eq} = \text{Constant} \end{cases} \quad (61)$$

Therefore, obtained equations (algebraic equations) can be summarized as below.

$$\begin{cases} T_A = T_w - \left[(T_w - T_1')e^{-\frac{r_{L_a}}{C^*_{f_{L_a}}}NTU_{L_a}(\frac{L_a}{L})}\right] \\ T_2'' = T_w - \left[(T_w - T_c)e^{-NTU_{L_a}(1-\frac{L_b+L_c}{L})}\right] \\ w_2'' = w_{eq} - \left[(w_{eq} - w_c)e^{-NTU_{L_a}(1-\frac{L_b+L_c}{L})}\right] \\ T_D = T_w - \left[(T_w - T_A)e^{-\frac{r_{L_b}}{C^*_{f_{L_b}}}NTU_{L_b}(\frac{L_b}{L})}\right] \\ T_B = T_w - \left[(T_w - T_E)e^{-NTU_{L_b}(\frac{L_b}{L})}\right] \\ W_B = w_{eq} - \left[(w_{eq} - w_E)e^{-NTU_{L_b}(\frac{L_b}{L})}\right] \\ T_1'' = T_w - \left[(T_w - T_D)e^{-\frac{r_{L_c}}{C^*_{f_{L_c}}}NTU_{L_c}(1-\frac{L_a+L_b}{L})}\right] \\ T_F = T_w - \left[(T_w - T_1'')e^{-NTU_{L_c}(\frac{L_c}{L})}\right] \\ W_F = w_{eq} - \left[(w_{eq} - w_1')e^{-NTU_{L_c}(\frac{L_c}{L})}\right] \\ T_w = \text{Constant} \\ w_{eq} = \text{Constant} \end{cases} \quad (62)$$

As can be seen in Eq. (62), there are thirteen unknown parameters including T_A, T_2'', w_2'', T_1'', T_B, W_B, T_c, w_c, T_D, T_E, w_E, T_F and w_F. However, there are only nine equations with said parameters. Hence, four other equations should be arranged in order to become solvable the above system of equations. These four new equations can be found from the enthalpy balance and moisture balance between the points A, B, C and D, E, F as below.

Enthalpy balance between A, B and C:

$$\dot{m}_c i_c = \dot{m}_A i_A + \dot{m}_B i_B \quad (63)$$

In which specific enthalpy of air (i) can be evaluated by:

$$i_A = (c_a + w_A c_\upsilon)T_A + w_A i_{fg} \quad (64)$$

$$i_B = (c_a + w_B c_\upsilon)T_B + w_B i_{fg} \quad (65)$$

$$i_C = (c_a + w_c c_\upsilon)T_c + w_c i_{fg} \quad (66)$$

So,

$$\dot{m}_c[(c_a + w_c c_\upsilon)T_c + w_c i_{fg}] = \dot{m}_A[(c_a + w_A c_\upsilon)T_A + w_A i_{fg}] + \dot{m}_B[(c_a + w_B c_\upsilon)T_B + w_B i_{fg}] \quad (67)$$

Mass transfer of each point is substituted.

$$(\varepsilon_a + \varepsilon_b + \varepsilon_c)\dot{m}_1'[(c_a + w_c c_\upsilon)T_c + w_c i_{fg}] = \varepsilon_a \dot{m}_1'[(c_a + w_A c_\upsilon)T_A + w_A i_{fg}] + \dot{m}_1'(\varepsilon_c + \varepsilon_b)[(c_a + w_B c_\upsilon)T_B + w_B i_{fg}] \quad (68)$$

Removing $\dot{m}_1'$ and replacing w_1' with w_A yields:

$$T_c = \frac{\varepsilon_a[(c_a + w_1' c_\upsilon)T_A + w_1' i_{fg}] + (\varepsilon_c + \varepsilon_b)[(c_a + w_B c_\upsilon)T_B + w_B i_{fg}] - (\varepsilon_a + \varepsilon_b + \varepsilon_c)w_c i_{fg}}{(\varepsilon_a + \varepsilon_b + \varepsilon_c)(c_a + w_c c_\upsilon)} \quad (69)$$

Moisture balance:

$$\dot{m}_c w_c = \dot{m}_A w_A + \dot{m}_B w_B \quad (70)$$

$$(\varepsilon_a + \varepsilon_b + \varepsilon_c)w_c = \varepsilon_a w_1' + (\varepsilon_c + \varepsilon_b)w_B \quad (71)$$

$$W_c = \frac{\varepsilon_a w_1' + (\varepsilon_c + \varepsilon_b)w_B}{(\varepsilon_a + \varepsilon_b + \varepsilon_c)} \quad (72)$$

Enthalpy balance between D, F and E:

$$\dot{m}_D i_D + \dot{m}_F i_F = \dot{m}_E i_E \quad (73)$$

In which specific enthalpy of air (i) can be evaluated by:

$$i_D = (c_a + w_D c_\upsilon)T_D + w_D i_{fg} \quad (74)$$

$$i_F = (c_a + w_F c_\upsilon)T_F + w_F i_{fg} \quad (75)$$

$$i_E = (c_a + w_E c_\upsilon)T_E + w_E i_{fg} \quad (76)$$

So,

$$\dot{m}_D[(c_a + w_D c_\upsilon)T_D + w_D i_{fg}] + \dot{m}_F[(c_a + w_F c_\upsilon)T_F + w_F i_{fg}] = \dot{m}_E[(c_a + w_E c_\upsilon)T_E + w_E i_{fg}] \quad (77)$$

Mass transfer of each point is substituted.

$$\varepsilon_b \dot{m}_1'[(c_a + w_D c_\upsilon)T_D + w_D i_{fg}] + \dot{m}_1'(\varepsilon_c)[(c_a + w_F c_\upsilon)T_F + w_F i_{fg}] = (\varepsilon_c + \varepsilon_b)\dot{m}_1'[(c_a + w_E c_\upsilon)T_E + w_E i_{fg}] \quad (78)$$

Removing $\dot{m}_1'$ and replacing w_1' with w_D yields:

$$T_E = \frac{\varepsilon_b[(c_a + w_1' c_\upsilon)T_D + w_1' i_{fg}] + (\varepsilon_c)[(c_a + w_F c_\upsilon)T_F + w_F i_{fg}] - (\varepsilon_c + \varepsilon_b)w_E i_{fg}}{(\varepsilon_c + \varepsilon_b)(c_a + w_E c_\upsilon)} \quad (79)$$

Moisture balance:

$$\dot{m}_D w_D + \dot{m}_F w_F = \dot{m}_E w_E \quad (80)$$

$$\varepsilon_b w_1' + (\varepsilon_c)w_F = (\varepsilon_c + \varepsilon_b)w_E \quad (81)$$

$$W_E = \frac{\varepsilon_b w_1' + (\varepsilon_c)w_F}{(\varepsilon_c + \varepsilon_b)} \quad (82)$$

Therefore, thirteen final algebraic equations can be written a below which can be solved easily now.

Answers for three-stage

$$\begin{cases} T_A = T_w - \left[(T_w - T_1') e^{-\frac{r_{L_a}}{C_{f_{L_a}}^*} NTU_{L_a} (\frac{L_a}{L})} \right] \\ T_D = T_w - \left[(T_w - T_A) e^{-\frac{r_{L_b}}{C_{f_{L_b}}^*} NTU_{L_b} (\frac{L_b}{L})} \right] \\ W_F = w_{eq} - \left[(w_{eq} - w_1') e^{-NTU_{L_c} (\frac{L_c}{L})} \right] \\ T_1'' = T_w - \left[(T_w - T_D) e^{-\frac{r_{L_c}}{C_{f_{L_c}}^*} NTU_{L_c} (1 - \frac{L_a + L_b}{L})} \right] \\ T_F = T_w - \left[(T_w - T_1'') e^{-NTU_{L_c} (\frac{L_c}{L})} \right] \\ W_E = \frac{\varepsilon_b w_1' + (\varepsilon_c) w_F}{(\varepsilon_c + \varepsilon_b)} \\ W_B = w_{eq} - \left[(w_{eq} - w_E) e^{-NTU_{L_b} (\frac{L_b}{L})} \right] \\ W_c = \frac{\varepsilon_a w_1' + (\varepsilon_a + \varepsilon_b) w_B}{(\varepsilon_a + \varepsilon_b + \varepsilon_c)} \\ w_2'' = w_{eq} - \left[(w_{eq} - w_c) e^{-NTU_{L_a} (1 - \frac{L_b + L_c}{L})} \right] \\ T_E = \frac{\varepsilon_b [(c_a + w_1' c_v) T_D + w_1' i_{fg}] + (\varepsilon_c) [(c_a + w_F c_v) T_F + w_F i_{fg}] - (\varepsilon_c + \varepsilon_b) w_E i_{fg}}{(\varepsilon_c + \varepsilon_b)(c_a + w_E c_v)} \\ T_B = T_w - \left[(T_w - T_E) e^{-NTU_{L_b} (\frac{L_b}{L})} \right] \\ T_c = \frac{\varepsilon_a [(c_a + w_1' c_v) T_A + w_1' i_{fg}] + (\varepsilon_a + \varepsilon_b) [(c_a + w_B c_v) T_B + w_B i_{fg}] - (\varepsilon_a + \varepsilon_b + \varepsilon_c) w_c i_{fg}}{(\varepsilon_a + \varepsilon_b + \varepsilon_c)(c_a + w_c c_v)} \\ T_2'' = T_w - \left[(T_w - T_c) e^{-NTU_{L_a} (1 - \frac{L_b + L_c}{L})} \right] \\ T_w = \text{Constant} \\ w_{eq} = \text{Constant} \end{cases} \quad (83)$$

It is noted that, each required parameter to evaluate a defined characteristic is calculated in previous lines. For example, wE should be known to calculate" WB". Hence, wE has been evaluated in former line. Thus, the model should be employed in the arrangements shown in Eq. (83) to become ease solvable.

5. Evaluation of NTU, r, C_f^* and w_{eq}

5.1. Evaluation of NTU

Evaluation of NTU $= \frac{\alpha_2 A_2}{\dot{m}_2 c_a}$ means the evaluation of α_2 that should be evaluated for each separate section of exchanger. The value of α_2 for laminar flow is different from that for turbulent flow. Thus, it should be discussed separately. The example is related to the three-stage.

5.1.1. Evaluation of NTU for laminar flow

Generally, the flow regime between the plates of M-cycle cooler is turbulent flow because of the so small width of the channels and high air flow rates. Nonetheless, in order to generalize the current model, evaluation of NTU for laminar flow is presented as well. For any laminar flow between two parallel plates with uniform wall temperature it has been demonstrated that the amount of Nusselt number is constant 7.54 [67]. Hence, the value of α_2 can be calculated as below.

$$Nu = \frac{\alpha d_h}{K} \overset{so}{\rightarrow} \alpha_2 = \frac{K\, Nu}{d_h} \overset{so}{\rightarrow} \alpha_{2,La} = \alpha_{2,Lb} = \alpha_{2,Lc} = \alpha_2 = 7.54 \times \frac{K}{d_h} \quad (84)$$

K is the thermal conductivity of air fluid. The mount of K for air fluid between temperature of 20 °C and 40 °C is around 0.026 W/m°C. d_h is hydraulic dimeter of channel (with rectangular cross-section) and is calculated with $d_h = \frac{4 \times A}{P} = \frac{4ab}{2(a+b)} = \frac{2ab}{a+b}$

$$\alpha_2 = \frac{0.196}{\frac{2ab}{a+b}} = \frac{0.098(a+b)}{ab} \quad (85)$$

Although the value of α_2 is the same for all sections (if flow regime is laminar in all of them), mass flow rate of working air ($\dot{m}_2$) is different for each section. Hence, the amount of NTU for each section should be evaluated separately which were termed NTU_{L_a}, NTU_{L_a} and NTU_{L_c} previously in equations. Thus, NTU_{L_a}, NTU_{L_b} and NTU_{L_c} are expanded as below.

$$A_{L_a} = b \times L_a \quad (86)$$

$$A_{L_b} = b \times L_b \quad (87)$$

$$A_{L_c} = b \times L_c$$

$$\dot{m}_{2,L_a} = \dot{m}_1'(\varepsilon_a + \varepsilon_b + \varepsilon_c) \quad (88)$$

$$\dot{m}_{2,L_b} = \dot{m}_1'(\varepsilon_b + \varepsilon_c) \quad (89)$$

$$\dot{m}_{2,L_c} = \dot{m}_1' \varepsilon_c \quad (90)$$

$$NTU_{L_a} = \frac{\alpha_2 A_{L_a}}{\dot{m}_{2,L_a} c_a} = \frac{\frac{0.098(a+b)}{ab} b \times L_a}{\dot{m}_1'(\varepsilon_a + \varepsilon_b + \varepsilon_c) c_a} = \frac{0.098(a+b) \times L_a}{a \dot{m}_1'(\varepsilon_a + \varepsilon_b + \varepsilon_c) c_a} \quad (91)$$

$$NTU_{L_b} = \frac{\alpha_2 A_{L_b}}{\dot{m}_{2,L_b} c_a} = \frac{\frac{0.098(a+b)}{ab} b \times L_b}{\dot{m}_1'(\varepsilon_b + \varepsilon_c) c_a} = \frac{0.098(a+b) \times L_b}{a \dot{m}_1'(\varepsilon_b + \varepsilon_c)} \quad (92)$$

$$NTU_{L_c} = \frac{\alpha_2 A_{L_c}}{\dot{m}_{2,L_c} c_a} = \frac{\frac{0.098(a+b)}{ab} b \times L_c}{\dot{m}_1' \varepsilon_c c_a} = \frac{0.098(a+b) \times L_b}{a c_a \dot{m}_1' \varepsilon_c} \quad (93)$$

Specific heat capacity of dry air (c_a) for temperature range of air conditioning systems can be estimated by unity with a very good accuracy.

5.1.2. Evaluation of NTU for turbulent flow

In the case of turbulent air flow between two parallel plates, Nusselt number correlation of circular tube is employed to evaluate the Nusselt number of plates by replacing the tube diameter by effective diameter [68]. Although for $0.1 < Pr < 10^4$ the accuracy of said method is logical [68], a correlation which has been exclusively developed for parallel plates is used in present research.

Depending on the working condition of M-cycle air cooler, Nusselt number (heat transfer coefficient) of turbulent flow between two parallel plates can be calculated via different empirical correlations. Uniform heat flux and uniform wall-temperature are two main working conditions for which various empirical correlations have been provided in literate. In this study wall temperature was assumed to be equal with water inlet temperature (because of large mass flow rate of spread water). Hence, uniform wall temperature condition is preferred in present work.

For uniform wall-temperature, Shibni and Ozisik [68] presented a solution (correlation) for Nusselt number of turbulent heat transfer flow between parallel plates as shown in Eq. (94).

$$Nu = 12 + 0.03 Re^{a_1} Pr^{a_2}, \quad 0.1 < Pr < 10^4, \quad 10^4 < Re < 10^6 \quad (94)$$

$$a_1 = 0.88 - \frac{0.24}{(3.6 + Pr)} \quad (95)$$

$$a_2 = 0.33 + 0.5 e^{-0.6 Pr} \quad (96)$$

The value of *Pr* for air fluid varies between 0.715 and 0.703 in temperature range of 0–100 °C. Thus, for air conditioning systems a constant value of air Prandtl number (0.7) can be employed. The mount of Reynolds number can be evaluated via:

$$Re = \frac{\rho V d_h}{\mu} \quad (97)$$

$$d_h = \frac{2ab}{a+b} \tag{98}$$

$$V = \frac{\dot{m}}{\rho\, ab} \tag{99}$$

Hence, convective heat transfer coefficient can be calculated from Eq. (101) and (103):

$$\alpha_2 = \frac{K\, Nu}{d_h} \tag{100}$$

$$\alpha_{2,L_a} = \frac{K\, Nu_{2,L_a}}{d_h} \tag{101}$$

$$\alpha_{2,L_b} = \frac{K\, Nu_{2,L_b}}{d_h} \tag{102}$$

$$\alpha_{2,L_b} = \frac{K\, Nu_{2,L_c}}{d_h} \tag{103}$$

It should be noted that, although all Nu_{2,L_a} and Nu_{2,L_b}, Nu_{2,L_c} are calculated via Eq. (94), each section has its own value of Reynolds number that should be replaced in Eq. (94). In other words, the value of Nusselt number is different for each section. After evaluation of α_{2,L_a}, α_{2,L_b} and α_{2,L_c} the amounts of NTU_{L_a}, NTU_{L_b} and NTU_{L_c} can be found from below equations.

$$NTU_{L_a} = \frac{\alpha_2 A_{L_a}}{\dot{m}_{2,L_a} c_a} \tag{104}$$

$$NTU_{L_b} = \frac{\alpha_2 A_{L_b}}{\dot{m}_{2,L_b} c_a} \tag{105}$$

$$NTU_{L_c} = \frac{\alpha_2 A_{L_c}}{\dot{m}_{2,L_c} c_a} \tag{106}$$

5.2. Evaluation of r, C_f^*

For a parallel or counter flow the value of A_1 and A_2 is the same. Hence, the amount of "r" can be determined via Eq. (107).

$$r = \frac{UA_1}{\alpha_2 A_2} = \frac{U}{\alpha_2} \tag{107}$$

The overall heat transfer coefficient between primary air and water film (U) can be estimated from Eq. (108).

$$U = \frac{1}{\frac{1}{\alpha_1} + \frac{\delta_p}{k_p} + \frac{\delta_w}{k_w}} \tag{108}$$

where α_1 is the heat transfer coefficient of primary air, δ_p, δ_w, k_p and k_w are thickness of plate, thickness of water film, thermal conductivity of plate and thermal conductivity of water respectively. The value of α_1 can be calculated from the same method which was used to determine the heat transfer coefficient of the working air. Thermal conductivity of water is around 0.6 W/m°C. Overall heat transfer coefficient should be evaluated for L_a, L_b and L_c separately if the value of α_1 is different for each length (in turbulent flow). Therefore, r_{L_a} and r_{L_b} can be calculated via below equations.

$$r_{L_a} = \frac{U_{L_a}}{\alpha_{2,L_a}} \tag{109}$$

$$r_{L_b} = \frac{U_{L_b}}{\alpha_{2,L_b}} \tag{110}$$

$$r_{L_c} = \frac{U_{L_c}}{\alpha_{2,L_c}} \tag{111}$$

C_f^* for each section $C_{f_{La}}^*$ and $C_{f_{L_b}}^*$ can be determined via ($c_a = 1$):

$$C_f^* = \frac{\dot{m}_1 c_1}{\dot{m}_2 c_a} \tag{112}$$

$$C_{f_{L_a}}^* = \frac{\dot{m}_{1,L_a} c_1}{\dot{m}_{2,La}} \tag{113}$$

$$C_{f_{L_b}}^* = \frac{\dot{m}_{1,L_b} c_1}{\dot{m}_{2,L_b}} \tag{114}$$

$$C_{f_{L_b}}^* = \frac{\dot{m}_{1,L_c} c_1}{\dot{m}_{2,L_c}} \tag{115}$$

5.3. Evaluation of w_{eq}

Humidity ratio of saturated air at inlet water temperature (w_{eq}) can be directly extracted from psychometric chart or can be evaluated based on Ideal Gas Law from below correlation.

$$w_{eq} = 0.621945 \frac{P_\upsilon}{P - P_\upsilon} \tag{116}$$

where P_υ is partial pressure of water-vapor in moist air and P is atmospheric pressure of moist air (in wet channel). For the zone in which working air is in equilibrium with water surface (w_{eq}), P_υ is saturation pressure (P_{sat}) and can be calculated from Hyland and Wexler formula as below and P can be assumed equal with the standard atmospheric pressure (101,325 Pa).

$$\begin{aligned} \mathrm{Ln}P_{sat} = {} & \left(\frac{-0.58002206 \times 10^4}{T_w}\right) + (1.3914993) - (0.048640239 \times T_w) \\ & + (0.41764768 \times 10^{-4} \times T_w^2) - (0.14452093 \times 10^{-7} \times T_w^3) \\ & + (0.65459673 \times 10 \times \mathrm{Ln}T_w) \end{aligned} \tag{117}$$

T is in Kelvin in Eq. (117). Specific heat of primary air (c_1) which generally comprises of dry air and water vapor can be evaluated as below (primary air is not necessarily completely dry).

$$c_1 = \frac{1}{1 + w_1'} c_a + \frac{w_1'}{1 + w_1'} c_\upsilon \tag{118}$$

where c_a and c_υ are specific heat of dry air and specific heat of water vapor and are calculated as below.

$$c_a = 1.0029 + (5.4 \times 10^{-5} T_1') \tag{119}$$

$$c_\upsilon = 1.856 + (2 \times 10^{-4} T_1') \tag{120}$$

6. Flowchart of the analytical model

Programming flow-chart is presented in Fig. 6.

It is noted that, the recognition of flow regime in this model is based on Reynolds number. Hence, if the flow regime of L_c in the wet channel is turbulent, the flow regime of the rest of the channel (L_b and L_a) are turbulent as well. Because, the flow rate of L_b and L_a in the wet channel is higher than the flow rate of L_b. However, if the flow regime of L_b is laminar, no conclusion can be considered about the flow regime of the rest of the channel. There is a similar condition in dry channel as well. Indeed, if the flow regime of L_a in dry channel is laminar, the flow regime of the rest of the channel (L_b and L_c) are laminar as well. This principle has been used in flowchart.

7. Model validation

Equations obtained from analytical solution (Eq. (83)) is validated from the results obtained from numerical solving of Eq. (50) and some results from Pandelidis et al. [27] as described in the following.

Differential Eq. (50) (which was obtained from governing equations) is true for any single-stage M-cycle. Thus, it was written (as presented in Eq. (121)) for each section (L_a, L_b and L_c)and then solved

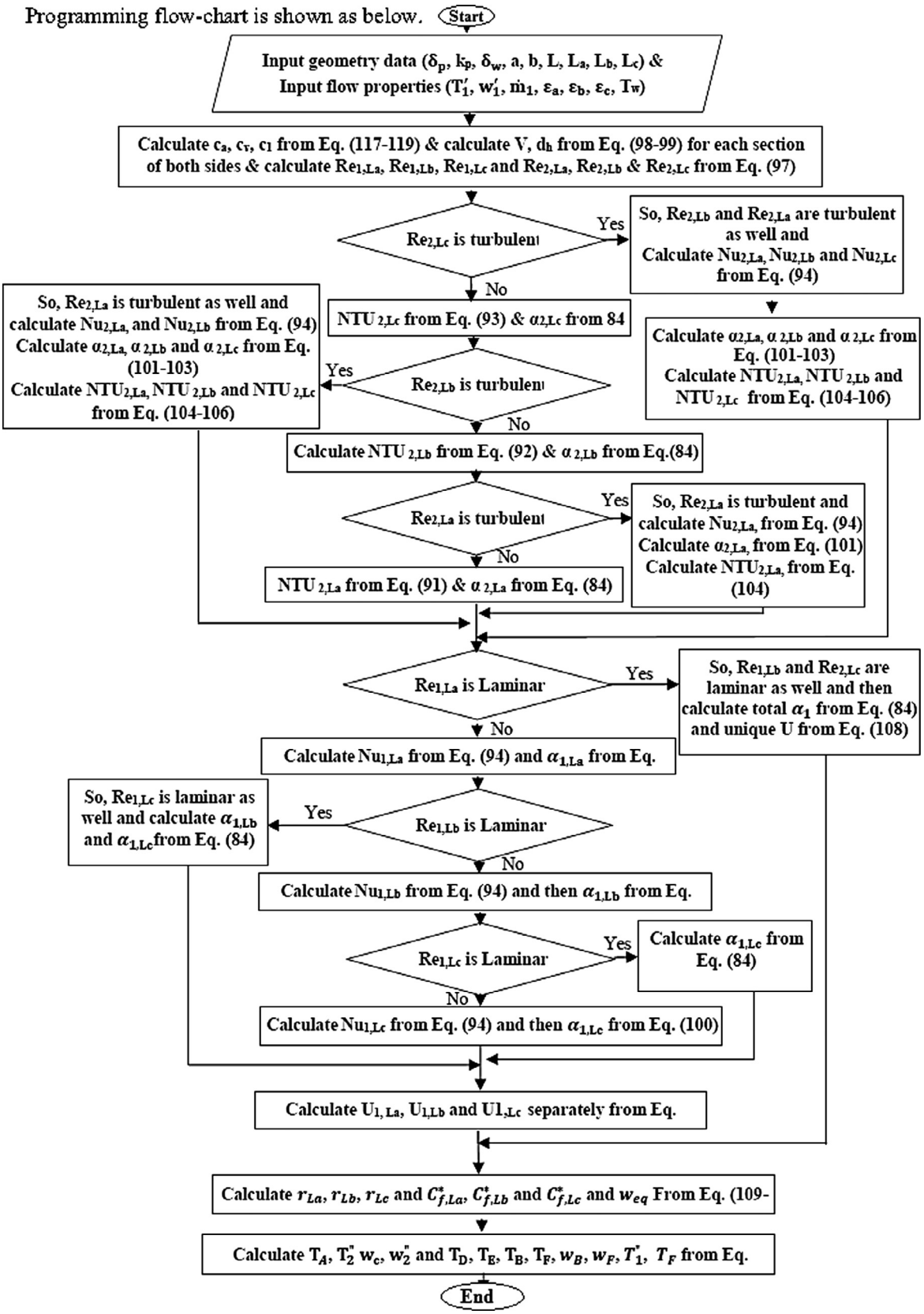

Fig. 6. Flowchart of three-stage regenerative M-cycle.

numerically (via Matlab software) simultaneously with their own boundary conditions provided in Eq. (122). The limitation of each set of differential equations can be seen in Eq. (121) too. The results obtained from numerical solution are compared with the curve trend obtained from the analytical model in two modes. In the first mode, the inlet air temperature was kept constant and the water inlet temperature was

Table 2
Input parameters of analytical/numerical simulation.

Parameter	Value
a (m)	0.003
b (m)	0.5
L (m)	0.7
L_a (m)	0.231
L_b (m)	0.231
L_c (m)	0.238
Inlet air temperature (C)	40 or variant
Humidity ratio of inlet air kg/kg	0.006
Inlet-air velocity (m/s)	3
ε_a	0.066
ε_b	0.066
ε_c	0.066

changed in five different values. In the second mode, the water-inlet temperature was remained in a constant value and the inlet air temperature was varied at five different values. The input parameters for which the numerical solution and analytical model were solved are shown in Table 2.

Input flow and thermal parameters (Table 2) are the same used in Pandelidis et al. [27]. Some results for three-stage M-cycle have been provided in their study [27] (Fig. 5 in [27]). They validated their results with experimental results performed by Riangvilaikul and Kumar [69]. Hence, the results of present model are compared with [27] as well. As they do not change the water inlet temperature, the comparison is performed only for the second mode in which the water-inlet temperature is constant and the inlet air is varied.

Comparison between numerical results and analytical results is presented in Fig. 7 which shows a good agreement between numerical solution, analytical model and Pandelidis [27]. The deviation between the model and results from Pandelidis [27] most probably is related to the assumption 4 used in present model.

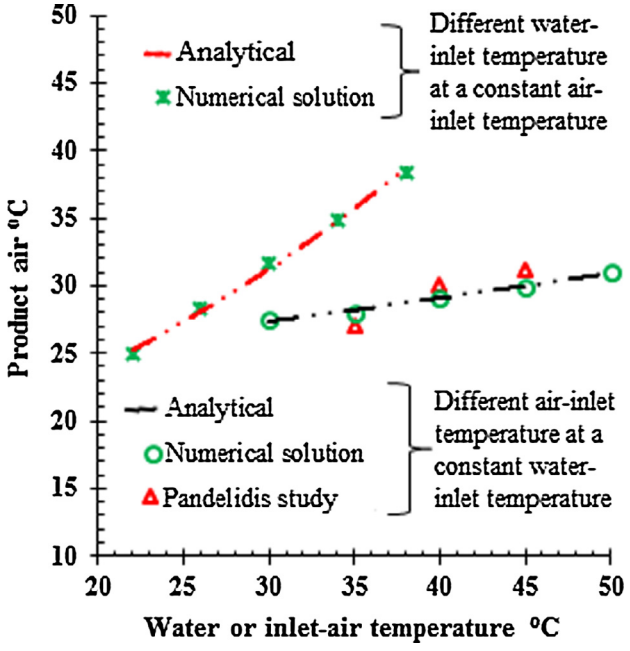

Fig. 7. Comparison between numerical solution, analytical model and Pandelidis study [27]

Differential equations

$$\begin{cases} L_a \begin{cases} \frac{dT_1}{(T_w - T_1)} = \frac{r}{C_1^*} NTU_{La} d\bar{x}_1 \\ \frac{dT_2}{(T_w - T_{wa})} = NTU_{La} d\bar{x}_2 \\ \frac{dw_2}{(w_{eq} - w_2)} = NTU_{La} d\bar{x}_2 \end{cases} & 0 < \bar{x}_1 < \frac{L_a}{L}, \frac{L_b + L_c}{L} < \bar{x}_2 < 1 \\ L_b \begin{cases} \frac{dT_1}{(T_w - T_1)} = \frac{r_{Lb}}{C^*_{fLb}} NTU_{Lb} d\bar{x}_1 \\ \frac{dT_2}{(T_w - T_{wa})} = NTU_{Lb} d\bar{x}_2 \\ \frac{dw_2}{(w_{eq} - w_2)} = NTU_{Lb} d\bar{x}_2 \end{cases} & \frac{L_a}{L} < \bar{x}_1 < \frac{L_a + L_b}{L}, \frac{L_c}{L} < \bar{x}_2 < \frac{L_b + L_c}{L} \\ L_c \begin{cases} \frac{dT_1}{(T_w - T_1)} = \frac{r_{Lc}}{C^*_{fLc}} NTU_{Lc} d\bar{x}_1 \\ \frac{dT_2}{(T_w - T_{wa})} = NTU_{Lc} d\bar{x}_2 \\ \frac{dw_2}{(w_{eq} - w_2)} = NTU_{Lc} d\bar{x}_2 \end{cases} & \frac{L_a + L_b}{L} < \bar{x}_1 < 1, 0 < \bar{x}_2 < \frac{L_c}{L} \end{cases} \quad (121)$$

Boundary conditions

$$\begin{cases} L_a \begin{cases} T_1(\bar{x}_1 = 0) = T_{inlet} \\ T_2\left(\bar{x}_2 = \frac{L_b + L_c}{L}\right) = T_c \\ w_2\left(\bar{x}_2 = \frac{L_b + L_c}{L}\right) = w_c \end{cases} \\ L_b \begin{cases} T_1\left(\bar{x}_1 = \frac{L_a}{L}\right) = T_A \\ T_2\left(\bar{x}_2 = \frac{L_c}{L}\right) = T_E \\ w_2\left(\bar{x}_2 = \frac{L_c}{L}\right) = w_E \end{cases} \\ L_c \begin{cases} T_1\left(\bar{x}_1 = \frac{L_a + L_b}{L}\right) = T_D \\ T_2(\bar{x}_2 = 0) = T_1(\bar{x}_1 = 1) \\ w_2(\bar{x}_2 = 0) = w_{inlet} \end{cases} \end{cases} \quad (122)$$

8. Application analysis (an example)

As an application example of the model, two important parameters of Multi-stage M-cycle air coolers including (L_a, L_b, L_c) and (ε_a, ε_b, ε_c) are discussed. Variations of "L" and "ε" are presented in Table 3. In case 1, all perforations are in similar distance with each other. In Case2 and Case 3 perforations (point "A" and "D" in Fig. 4) are closer to the bottom side of exchanger. In Case4 and Case5, perforations are closer to the top side of exchanger. Similar explanation is valid for "ε" as well. The results of this evaluation is shown in Fig. 8a and b.

The programming code to simulate the model (written by Visual Basic) is presented in Appendix which may help other researchers who are interested to analyse the perforated M-cycle exchanger via this analytical model.

As can be seen in Fig. 8a, case 5 and case 4 in which the perforations (point "A" and "D") are closer to the top side of exchanger, provides better (lower) product air temperature. Case 2 and case 3 in which the

Table 3
Variation of separated lengths and returned air flows.

	Case 1	Case 2	Case 3	Case 4	Case 5
Effect of location of perforations (all ε = 0.2 and $\dot{m}'_1$ = 1 kg/s)					
L_a	1	2	2.5	0.5	0.25
L_b	1	0.5	0.25	0.5	0.25
L_c	1	0.5	0.25	2	2.5
Effect of allocation of each ε (all L_x = 1 and $\dot{m}'_1$ = 1 kg/s)					
ε_a	0.2	0.4	0.5	0.1	0.05
ε_b	0.2	0.1	0.05	0.1	0.05
ε_c	0.2	0.1	0.05	0.4	0.5

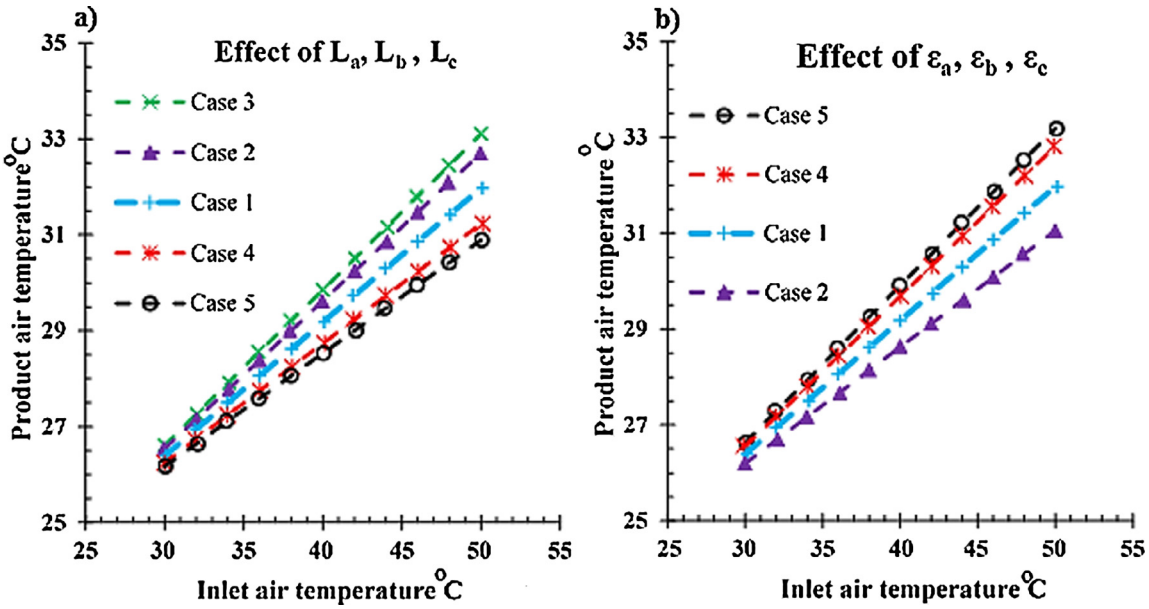

Fig. 8. (a) Effect of the locations of perforations and (b) effect of returned air flows to wet-channel.

perforations are closer to the bottom side exchanger provides higher product temperature. Case 1 obtains product temperature between these two groups. It is clear that the location of perforations significantly influence the outlet temperature of the cooler. It is noted that, it is not expected to achieve the same results for other primary air mass flow rates because other flow rates may create turbulent or laminar flows which provides different heat transfer coefficient. In other words, the location arrangements of the perforations can be different for laminar and turbulent flows. On the other hand, various values of "ε" may create different conditions in each section of exchanger. Indeed, the flow pattern may act as a turbulent or laminar regime flow in each section because of different flow rates in each section. It is obvious that, all these criteria should be considered simultaneously to achieve an optimum design condition. Hence, further exact studied are required in this regard.

9. Conclusion

The present study provides an analytical modeling for multi-stage (perforated) M-cycle air cooler. All former analytical modeling of M-cycle coolers have been presented only for single-stage (without perforation) M-cycle cooler and multi-stage coolers have been evaluated only via numerical or experimental methods which require further time, cost and energy. The present model can provide the specifications of any multi-stage M-cycle cooler very quickly. The comparison between analytical model, numerical solution and previous studies showed a good agreement between them. Present model can be considered as powerful initial design utility. Furthermore, with significant reduction of calculation time, this analytical model can be easily employed as an optimization utility as well by other researchers or industrial sectors. However, further study is required to eliminate the main assumption of this model (assumption 5) to consider the water temperature variation along the exchanger. The eliminating of this assumption significantly increases the complexity of the model and no analytical model (solution) is presented for multi-stage M-cycle cooler in which the water (wall) temperature is varied along the exchanger.

Appendix A. Programming code by Visual Basic

```
Private Sub Command1_Click()
ThicknessOfPlate = Val(Text1.Text)
PlateThermalConductivity = Val(Text2.Text)
WaterFilmThicness = Val(Text3.Text)
a = Val(Text4.Text)
b = Val(Text5.Text)
L = Val(Text6.Text)
La = Val(Text7.Text)
Lb = Val(Text8.Text)
Lc = Val(Text9.Text)
InletAirTem = Val(Text10.Text)
InletHumidity = Val(Text11.Text)
InletairMassflow = Val(Text12.Text)
InletWaterTem = Val(Text13.Text)
Ea = Val(Text14.Text)
Eb = Val(Text15.Text)
Ec = Val(Text16.Text)
mdat1La = InletairMassflow
mdat1Lb = InletairMassflow * (1 - Ea)
```

```
mdat1Lc = InletairMassflow * (1 - Ea - Eb)
mdat2La = InletairMassflow * (Ea + Eb + Ec)
mdat2Lb = InletairMassflow * (Eb + Ec)
mdat2Lc = InletairMassflow * (Ec)
ca = 1.0029 + (5.4 * InletAirTem * (10 ^ -5))
cv = 1.856 + (2 * InletAirTem * 10 ^ -4)
c1 = (ca * (1/(1 + InletHumidity))) + (cv * (InletHumidity/(1 + InletHumidity)))
ifg = 2501 'Kj/kg
Miuoo = 1.8 * (10 ^ -5) 'Ns/m2
Pr = 0.7
K = 0.026/1000 'air KW/m0C
dh = (2 * a * b)/(a + b)
Kwater = 0.6/1000 'water KW/m0C
Ro = ((1 + InletHumidity)/(461.56 * (0.62195 + InletHumidity))) * (101325/(InletAirTem + 273.15)) 'm3/kg
V1La = (mdat1La/(Ro * a * b))
V1Lb = (mdat1Lb/(Ro * a * b))
V1Lc = (mdat1Lc/(Ro * a * b))
V2La = (mdat2La/(Ro * a * b))
V2Lb = (mdat2Lb/(Ro * a * b))
V2Lc = (mdat2Lc/(Ro * a * b))
Re1La = (Ro * V1La * dh)/Miuoo
Re1Lb = (Ro * V1Lb * dh)/Miuoo
Re1Lc = (Ro * V1Lc * dh)/Miuoo
Re2La = (Ro * V2La * dh)/Miuoo
Re2Lb = (Ro * V2Lb * dh)/Miuoo
Re2Lc = (Ro * V2Lc * dh)/Miuoo
ALa = b * La
Alb = b * Lb
Alc = b * Lc
If Re2Lc > 10 Then
Nu2La = 12 + ((0.03 * (Re2La ^ ((0.88 - (0.24/(3.6 + Pr)))))) * (Pr ^ ((0.33 + (0.5 * (2.7182 ^ (-0.6 * Pr))))))
Nu2Lb = 12 + ((0.03 * (Re2Lb ^ ((0.88 - (0.24/(3.6 + Pr)))))) * (Pr ^ ((0.33 + (0.5 * (2.7182 ^ (-0.6 * Pr))))))
Nu2Lc = 12 + ((0.03 * (Re2Lc ^ ((0.88 - (0.24/(3.6 + Pr)))))) * (Pr ^ ((0.33 + (0.5 * (2.7182 ^ (-0.6 * Pr))))))
Alfa2La = (K * Nu2La)/dh
Alfa2Lb = (K * Nu2Lb)/dh
Alfa2Lc = (K * Nu2Lc)/dh
NTU2La = (Alfa2La * ALa)/(mdat2La * ca)
NTU2Lb = (Alfa2Lb * Alb)/(mdat2Lb * ca)
NTU2Lc = (Alfa2Lc * Alc)/(mdat2Lc * ca)
Else
Alfa2Lc = (0.107 * (a + b))/(a + b)
NTU2Lc = (((0.107 * (a + b))/(a * b)) * Alc)/(mdat2Lc * ca)
If Re2Lb > 10 Then
Nu2La = 12 + ((0.03 * (Re2La ^ ((0.88 - (0.24/(3.6 + Pr)))))) * (Pr ^ ((0.33 + (0.5 * (2.7182 ^ (-0.6 * Pr))))))
Nu2Lb = 12 + ((0.03 * (Re2Lb ^ ((0.88 - (0.24/(3.6 + Pr)))))) * (Pr ^ ((0.33 + (0.5 * (2.7182 ^ (-0.6 * Pr))))))
Alfa2La = (K * Nu2La)/dh
Alfa2Lb = (K * Nu2Lb)/dh
ALa = b * La
Alb = b * Lb
NTU2La = (Alfa2La * ALa)/(mdat2La * ca)
NTU2Lb = (Alfa2Lb * Alb)/(mdat2Lb * ca)
Else
Alfa2Lb = (0.107 * (a + b))/(a + b)
NTU2Lb = (((0.107 * (a + b))/(a * b)) * Alb)/(mdat2Lb * ca)
If Re2La > 10 Then
Nu2La = 12 + ((0.03 * (Re2La ^ ((0.88 - (0.24/(3.6 + Pr)))))) * (Pr ^ ((0.33 + (0.5 * (2.7182 ^ (-0.6 * Pr))))))
Alfa2La = (K * Nu2La)/dh
ALa = b * La
NTU2La = (Alfa2La * ALa)/(mdat2La * ca)
Else
Alfa2La = (0.107 * (a + b))/(a + b)
NTU2La = (((0.107 * (a + b))/(a * b)) * ALa)/(mdat2La * ca)
End If
End If
End If
If Re1La < 10 Then
```

```
Alfa1La = (0.107 * (a + b))/(a * b)
Alfa1Lb = Alfa1La
Alfa1Lc = Alfa1La
U1La = 1/((1/Alfa1La) + (ThicknessOfPlate/PlateThermalConductivity) + (WaterFilmThicness/Kwater))
U1Lb = U1La
U1Lc = U1La
Else
Nu1La = 12 + ((0.03 * (Re1La ^ ((0.88 - (0.24/(3.6 + Pr)))))) * (Pr ^ ((0.33 + (0.5 * (2.7182 ^ (-0.6 * Pr)))))))
Alfa1La = (K * Nu1La)/dh
If Re1Lb < 10 Then
Alfa1Lb = (0.107 * (a + b))/(a * b)
Alfa1Lc = (0.107 * (a + b))/(a * b)
Else
Nu1Lb = 12 + ((0.03 * (Re1Lb ^ ((0.88 - (0.24/(3.6 + Pr)))))) * (Pr ^ ((0.33 + (0.5 * (2.7182 ^ (-0.6 * Pr)))))))
Alfa1Lb = (K * Nu1Lb)/dh
If Re1Lc < 10 Then
Alfa1Lc = (0.107 * (a + b))/(a * b)
Else
Nu1Lc = 12 + ((0.03 * (Re1Lc ^ ((0.88 - (0.24/(3.6 + Pr)))))) * (Pr ^ ((0.33 + (0.5 * (2.7182 ^ (-0.6 * Pr)))))))
Alfa1Lc = (K * Nu1Lc)/dh
End If
End If
U1La = 1/((1/Alfa1La) + (ThicknessOfPlate/PlateThermalConductivity) + (WaterFilmThicness/Kwater))
U1Lb = 1/((1/Alfa1Lb) + (ThicknessOfPlate/PlateThermalConductivity) + (WaterFilmThicness/Kwater))
U1Lc = 1/((1/Alfa1Lc) + (ThicknessOfPlate/PlateThermalConductivity) + (WaterFilmThicness/Kwater))
End If
RLa = U1La/Alfa2La
RLb = U1Lb/Alfa2Lb
RLc = U1Lc/Alfa2Lc
CstarFLa = (mdat1La * c1)/(ca * mdat2La)
CstarfLb = (mdat1Lb * c1)/(ca * mdat2Lb)
CstarfLc = (mdat1Lc * c1)/(ca * mdat2Lc)
Pv = 2.7182 ^ ((-0.58002206 * (10 ^ 4)/(InletWaterTem + 273.15)) + (1.39149) - (0.048640239 * (InletWaterTem + 273.15)) + (0.417647 *
    (10 ^ -4) * ((InletWaterTem + 273.15) ^ 2)) - (0.14452 * (10 ^ -7) * ((InletWaterTem + 273.15) ^ 3)) + (0.654596 * 10 * Ln(InletWaterTem +
    273.15)))
Weq = 0.621945 * (Pv/(101325 - Pv))
TA = InletWaterTem - ((InletWaterTem - InletAirTem) * (2.7182 ^ (-1 * ((RLa/CstarFLa) * NTU2La * (La/L)))))
TD = InletWaterTem - ((InletWaterTem - TA) * (2.7182 ^ (-1 * ((RLb/CstarfLb) * NTU2Lb * (Lb/L)))))
WF = Weq - ((Weq - InletHumidity) * (2.7182 ^ (-1 * (NTU2Lc * (Lc/L)))))
Tzegon1 = InletWaterTem - ((InletWaterTem - TD) * (2.7182 ^ (-1 * ((RLc/CstarfLc) * NTU2Lc * (1 - ((La + Lb)/L))))))
TF = InletWaterTem - ((InletWaterTem - Tzegon1) * (2.7182 ^ (-1 * (NTU2Lc * (Lc/L)))))
WE = ((Eb * InletHumidity) + (WF * (Ec)))/(Ec + Eb)
WB = Weq - ((Weq - WE) * (2.7182 ^ (-1 * (NTU2Lb * (Lb/L)))))
gg = Ea * InletHumidity
hh = WB * (Ec + Eb)
Wc = ((gg) + (hh))/(Ec + Eb + Ec)
Wzegon2 = Weq - ((Weq - Wc) * (2.7182 ^ (-1 * (NTU2La * (1 - ((Lb + Lc)/L))))))
aa = ((ca + (InletHumidity * cv)) * TD) + (InletHumidity * ifg)
bb = ((ca + (WF * cv)) * TF) + (WF * ifg)
TE = ((Eb * [aa]) + ((Ec) * [bb]) - ((Ec + Eb) * WE * ifg))/((Ec + Eb) * (ca + (WE * cv)))
TB = InletWaterTem - ((InletWaterTem - TE) * (2.7182 ^ (-1 * (NTU2Lb * (Lb/L)))))
aaa = ((ca + (InletHumidity * cv)) * TA) + (InletHumidity * ifg)
bbb = ((ca + (WB * cv)) * TB) + (WB * ifg)
Tc = ((Ea * [aaa]) + ((Ec + Eb) * [bbb]) - ((Ec + Eb + Ec) * Wc * ifg))/((Ea + Ec + Eb) * (ca + (Wc * cv)))
Tzegon2 = InletWaterTem - ((InletWaterTem - Tc) * (2.7182 ^ (-1 * (NTU2La * (1 - ((Lb + Lc)/L))))))
Text17.Text = TA
Text18.Text = TD
Text19.Text = WF
Text20.Text = Tzegon1
Text21.Text = TF
Text22.Text = WE
Text23.Text = WB
Text24.Text = Wc
Text25.Text = Wzegon2
Text26.Text = TE
Text27.Text = TB
```

```
Text28.Text = Tc
Text29.Text = Tzegon2
End Sub
Public Function Ln(x)
Ln = Log(x)/Log(2.718281)
End Function
```

References

[1] Mahmood MH, Sultan M, Miyazaki T, Koyama S, Maisotsenko VS. Overview of the Maisotsenko cycle–a way towards dew point evaporative cooling. Renew Sustain Energy Rev 2016(66):537–55.
[2] Dizaji HS, Hu EJ, Chen L. A comprehensive review of the Maisotsenko-cycle based air conditioning systems. Energy 2018.
[3] Maclaine-Cross IL, Banks PJ. A general theory of wet surface heat exchangers and its application to regenerative evaporative cooling. J Heat Transf 1981;103(3):579–85.
[4] Stoitchkov NJ, Dimitrov GI. Effectiveness of crossflow plate heat exchanger for indirect evaporative cooling: efficacité des échangeurs thermiques à plaques, à courants croises pour refroidissement indirect évaporatif. Int J Refrig 1998 30;21(6):463–71.
[5] Alonso JS, Martinez FR, Gomez EV, Plasencia MA. Simulation model of an indirect evaporative cooler. Energy Build 1998;29(1):23–7.
[6] Chengqin R, Hongxing Y. An analytical model for the heat and mass transfer processes in indirect evaporative cooling with parallel/counter flow configurations. Int J Heat Mass Transf 2006;49(3):617–27.
[7] Hasan A. Going below the wet-bulb temperature by indirect evaporative cooling: analysis using a modified ε-NTU method. Appl Energy 2012;89(1):237–45.
[8] Liu Z, Allen W, Modera M. Simplified thermal modeling of indirect evaporative heat exchangers. HVAC&R Res 2013;19(3):257–67.
[9] Cui X, Chua KJ, Islam MR, Yang WM. Fundamental formulation of a modified LMTD method to study indirect evaporative heat exchangers. Energy Convers Manage 2014;31(88):372–81.
[10] Chen Y, Luo Y, Yang H. A simplified analytical model for indirect evaporative cooling considering condensation from fresh air: Development and application. Energy Build 2015;108:387–400.
[11] Anisimov S, Pandelidis D, Danielewicz J. Numerical analysis of selected evaporative exchangers with the Maisotsenko cycle. Energy Convers Manage 2014;88:426–41.
[12] Anisimov S, Pandelidis D, Jedlikowski A, Polushkin V. Performance investigation of a M (Maisotsenko)-cycle cross-flow heat exchanger used for indirect evaporative cooling. Energy 2014;76:593–606.
[13] Anisimov S, Pandelidis D. Numerical study of perforated indirect evaporative air cooler. Int J Energy Clean Environ 2011;12(2–4).
[14] Anisimov S, Pandelidis D. Heat-and mass-transfer processess in indirect evaporative air conditioners through the Maisotsenko cycle. Int J Energy Clean Environ 2011;12(2–4).
[15] Anisimov S, Pandelidis D. Numerical study of the Maisotsenko cycle heat and mass exchanger. Int J Heat Mass Transf 2014;75:75–96.
[16] Pandelidis D, Anisimov S, Worek WM. Performance study of the Maisotsenko Cycle heat exchangers in different air-conditioning applications. Int J Heat Mass Transf 2015;81:207–21.
[17] Pandelidis D, Anisimov S. Numerical analysis of the heat and mass transfer processes in selected M-Cycle heat exchangers for the dew point evaporative cooling. Energy Convers Manage 2015;90:62–83.
[18] Pandelidis D, Anisimov S. Numerical analysis of the selected operational and geometrical aspects of the M-cycle heat and mass exchanger. Energy Build 2015;87:413–24.
[19] Pandelidis D, Anisimov S, Worek WM. Comparison study of the counter-flow regenerative evaporative heat exchangers with numerical methods. Appl Therm Eng 2015;84:211–24.
[20] Anisimov S, Pandelidis D, Maisotsenko V. Numerical study of heat and mass transfer process in the Maisotsenko cycle for indirect evaporative air cooling. Heat Transf Eng 2016;37(17):1455–65.
[21] Pandelidis D, Anisimov S, Worek WM, Drąg P. Numerical analysis of a desiccant system with cross-flow Maisotsenko cycle heat and mass exchanger. Energy Build 2016;123:136–50.
[22] Pandelidis D, Anisimov S, Worek WM, Drąg P. Analysis of different applications of Maisotsenko cycle heat exchanger in the desiccant air conditioning systems. Energy Build 2017;140:154–70.
[23] Bolotin S, Vager B, Vasilijev V. Comparative analysis of the cross-flow indirect evaporative air coolers. Int J Heat Mass Transf 2015;30(88):224–35.
[24] Pandelidis D, Anisimov S, Worek WM, Drąg P. Comparison of desiccant air conditioning systems with different indirect evaporative air coolers. Energy Convers Manage 2016;117:375–92.
[25] Anisimov S, Pandelidis D, Danielewicz J. Numerical study and optimization of the combined indirect evaporative air cooler for air-conditioning systems. Energy 2015;80:452–64.
[26] Pandelidis D, Anisimov S, Rajski K, Brychcy E, Sidorczyk M. Performance comparison of the advanced indirect evaporative air coolers. Energy 2017;135:138–52.
[27] Pandelidis D, Anisimov S, Worek WM. Performance study of counter-flow indirect evaporative air coolers. Energy Build 2015;109:53–64.
[28] Anisimov S, Pandelidis D. Theoretical study of the basic cycles for indirect evaporative air cooling. Int J Heat Mass Transf 2015;84:974–89.
[29] Khafaji HQ, Ekaid AL, Terekhov VI. A numerical study of direct evaporative air cooler by forced laminar convection between parallel-plates channel with wetted walls. J Eng Thermophys 2015;24(2):113–22.
[30] Heidarinejad G, Moshari S. Novel modeling of an indirect evaporative cooling system with cross-flow configuration. Energy Build 2015;92:351–62.
[31] Moshari S, Heidarinejad G. Numerical study of regenerative evaporative coolers for sub-wet bulb cooling with cross-and counter-flow configuration. Appl Therm Eng 2015;89:669–83.
[32] Cui X, Islam MR, Mohan B, Chua KJ. Developing a performance correlation for counter-flow regenerative indirect evaporative heat exchangers with experimental validation. Appl Therm Eng 2016;108:774–84.
[33] Cui X, Islam MR, Mohan B, Chua KJ. Theoretical analysis of a liquid desiccant based indirect evaporative cooling system. Energy 2016;95:303–12.
[34] Cui X, Chua KJ, Islam MR, Ng KC. Performance evaluation of an indirect pre-cooling evaporative heat exchanger operating in hot and humid climate. Energy Convers Manage 2015;102:140–50.
[35] Zhan C, Zhao X, Smith S, Riffat SB. Numerical study of a M-Cycle cross-flow heat exchanger for indirect evaporative cooling. Build Environ 2011;46:657–68.
[36] Wan Y, Ren C, Wang Z, Yang Y, Yu L. Numerical study and performance correlation development on counter-flow indirect evaporative air coolers. Int J Heat Mass Transf 2017;115:826–30.
[37] Jafarian H, Sayyaadi H, Torabi F. A numerical model for a dew-point counter-flow indirect evaporative cooler using a modified boundary condition and considering effects of entrance regions. Int J Refrig 2017;84:36–51.
[38] Pandelidis D, Anisimov S. Numerical study and optimization of the cross-flow Maisotsenko cycle indirect evaporative air cooler. Int J Heat Mass Transf 2016;103:1029–41.
[39] Pandelidis D, Anisimov S. Application of a statistical design for analyzing basic performance characteristics of the cross-flow Maisotsenko cycle heat exchanger. Int J Heat Mass Transf 2016;95:45–61.
[40] Sohani A, Sayyaadi H, Hoseinpoori S. Modeling and multi-objective optimization of an M-cycle cross-flow indirect evaporative cooler using the GMDH type neural network. Int J Refrig 2016;69:186–204.
[41] Kiran TR, Rajput SP. An effectiveness model for an indirect evaporative cooling (IEC) system: Comparison of artificial neural networks (ANN), adaptive neuro-fuzzy inference system (ANFIS) and fuzzy inference system (FIS) approach. Appl Soft Comput 2011;11(4):3525–33.
[42] ISAW. Natural Air Conditioner (Heat and Mass Exchanger) Catalogues. Hang-zhou, China: ISAW Corporation Ltd; 2005.
[43] Chen ML, Liu XL, Hu E. Indirect evaporative cooling–an energy efficient way for air conditioning. Advanced materials research 2013. Trans Tech Publications; 2013. p. 1198–203.
[44] Pandelidis D, Anisimov S, Drąg P, Sidorczyk M, Pacak A. Analysis of application of the M-Cycle heat and mass exchanger to the typical air conditioning systems in Poland. Energy Build 2018;158:873–83.
[45] Zhan C, Duan Z, Zhao X, Smith S, Jin H, Riffat S. Comparative study of the performance of the M-cycle counter-flow and cross-flow heat exchangers for indirect evaporative cooling–paving the path toward sustainable cooling of buildings. Energy 2011;36(12):6790–805.
[46] Khalid O, Butt Z, Tanveer W, Rao HI. Design and experimental analysis of counter-flow heat and mass exchanger incorporating (M-cycle) for evaporative cooling. Heat Mass Transf 2017;53(4):1391–403.
[47] Khalid O, Ali M, Sheikh NA, Ali HM, Shehryar M. Experimental analysis of an improved Maisotsenko cycle design under low velocity conditions. Appl Therm Eng 2016;95:288–95.
[48] Zube D, Gillan L. Evaluating coolerado corportion's heat mass exchanger performance through experimental analysis. Int J Energy Clean Environ 2011;12(2–4).
[49] Rogdakis ED, Koronaki IP, Tertipis DN. Experimental and computational evaluation of a Maisotsenko evaporative cooler at Greek climate. Energy Build 2014;70:497–506.
[50] Gao WZ, Cheng YP, Jiang AG, Liu T, Anderson K. Experimental investigation on integrated liquid desiccant–Indirect evaporative air cooling system utilizing the Maisotesenko-Cycle. Appl Therm Eng 2015;88:288–96.
[51] Anisimov S, Żuchowicki J. Wymiana Ciepła i Masy w Urządzeniach do Pośredniego Ochładzania Powietrza za Pomocą Parowania Wody przy Mieszanym Schemacie Przepływu Czynników, Nowe Techniki w Klimatyzacji 2003. In: Proc. of Nowe Techniki w Klimatyzacji Conf.; 2003. p. 13–20.
[52] Duan Z, Zhao X, Zhan C, Dong X, Chen H. Energy saving potential of a counter-flow regenerative evaporative cooler for various climates of China: experiment-based evaluation. Energy Build 2017;148:199–210.
[53] De Antonellis S, Joppolo CM, Liberati P, Milani S, Molinaroli L. Experimental analysis of a cross flow indirect evaporative cooling system. Energy Build 2016;121:130–8.
[54] Xu P, Ma X, Zhao X, Fancey K. Experimental investigation of a super performance

dew point air cooler. Appl Energy 2017;203:761–77.
[55] Duan Z, Zhan C, Zhao X, Dong X. Experimental study of a counter-flow regenerative evaporative cooler. Build Environ 2016;104:47–58.
[56] De Antonellis S, Joppolo CM, Liberati P, Milani S, Romano F. Modeling and experimental study of an indirect evaporative cooler. Energy Build 2017;142:147–57.
[57] Lin J, Wang RZ, Kumja M, Bui TD, Chua KJ. Modelling and experimental investigation of the cross-flow dew point evaporative cooler with and without dehumidification. Appl Therm Eng 2017;121:1–3.
[58] Kim HJ, Ham SW, Yoon DS, Jeong JW. Cooling performance measurement of two cross-flow indirect evaporative coolers in general and regenerative operation modes. Appl Energy 2017;195:268–77.
[59] Cui X, Chua KJ, Yang WM. Numerical simulation of a novel energy-efficient dew-point evaporative air cooler. Appl Energy 2014;136:979–88.
[60] Lin J, Bui DT, Wang R, Chua KJ. On the fundamental heat and mass transfer analysis of the counter-flow dew point evaporative cooler. Appl Energy 2018;217:126–42.
[61] Chen Y, Yan H, Yang H. Comparative study of on-off control and novel high-low control of regenerative indirect evaporative cooler (RIEC). Appl Energy 2018;225:233–43.
[62] Peterson D, Glasser D, Williams D, Ramsden R. Predicting the performance of an evaporative condenser. ASME J Heat Transf 1988;110:748–53. 61.
[63] Erens PJ, Dreyer AA. Modelling of indirect evaporative coolers. Int J Heat Mass Transfer 1993;36(1):17–26. 62.
[64] Hasan A, Siren K. Performance investigation of plain and finned tube evaporatively cooled heat exchangers. Appl Thermal Eng 2003;23(3):325–40.
[65] Hasan A, Siren K. Performance investigation of plain circular and oval tube evaporatively cooled heat exchangers. Appl Therm Eng 2004;24(5–6):779–90.
[66] Lewis WK. The evaporation of a liquid into a gas. Trans ASME 1922;44:325–40.
[67] Kays WM, Crawford ME. Convection heat and mass transfer. 3rd ed. New York: McGraw-Hill; 1993.
[68] Shibani AA, Özisik MN. A solution to heat transfer in turbulent flow between parallel plates. Int J Heat Mass Transf 1977;20(5):565–73.
[69] Riangvilaikul B, Kumar S. An experimental study of a novel dew point evaporative cooling system. Energy Build 2010;42(5):637–44.

Chapter 4

Analytical modelling (wet-surface theory), related experiments and sensitivity analysis

This chapter has been submitted as

Dizaji, H.S., Hu, E.J., Chen, L. and Pourhedayat, S., 2020. Analytical/experimental sensitivity study of key design and operational parameters of perforated Maisotsenko cooler based on novel wet-surface theory. Applied Energy, 262, p.114557.

This chapter provides a novel analytical model which is based on the proposed wet-surface theory as described in the introduction section. This model is validated with our test-ring at the University of Adelaide in this chapter. Moreover, the impact of key operational and design parameters of the cooler on cooling characteristics of the cooler is evaluated via validated model in this chapter as well. The model works based on wet-surface theory in which the water flow rate is as possible as small to only keep the whole surface wetly while the cooler is working (any further water flow rate causes reduction of cooling capacity which will discuss in the paper).

The maximum cooling capacity of M-cycle cooler is achieved under this working condition in which the latent heat transfer plays a key role because of a high surface evaporation due to ultra-thin water film. Specific porous material is required in real application to instantly absorb the water and create the mentioned thin water film (without water stream). M-cycle under wet-surface theory is able to reduce the air temperature even if the water inlet temperature is the same as air inlet temperature. Moreover, contrary to the sprayed-water mechanism, the temperature of the middle plate is not constant along the plate and is dominated by water evaporation rate (which subsequently is dominated by thermal fluid condition through the cooler).

Statement of Authorship

Title of Paper	Analytical/experimental sensitivity study of key design and operational parameters of perforated Maisotsenko cooler based on novel wet-surface theory
Publication Status	☑ Published ☐ Accepted for Publication ☐ Submitted for Publication ☐ Unpublished and Unsubmitted w ork w ritten in manuscript style
Publication Details	Dizaji, H.S., Hu, E.J., Chen, L. and Pourhedayat, S., 2020. Analytical/experimental sensitivity study of key design and operational parameters of perforated Maisotsenko cooler based on novel wet-surface theory. Applied Energy, 262, p.114557.

Principal Author

Name of Principal Author (Candidate)	Hamed Sadighi Dizaji		
Contribution to the Paper	Developing the mathematical model and performing the parametric and sensitivity analysis, writing the manuscript. Designing the experimental set-up and performing related experiments. Programming the model with Maple.		
Overall percentage (%)	70		
Certification:	This paper reports on original research I conducted during the period of my Higher Degree by Research candidature and is not subject to any obligations or contractual agreements with a third party that would constrain its inclusion in this thesis. I am the primary author of this paper.		
Signature		Date	

Co-Author Contributions

By signing the Statement of Authorship, each author certifies that:

i. the candidate's stated contribution to the publication is accurate (as detailed above);

ii. permission is granted for the candidate in include the publication in the thesis; and

iii. the sum of all co-author contributions is equal to 100% less the candidate's stated contribution.

Name of Co-Author	Eric Hu		
Contribution to the Paper	Supervising the work, continuous recommendations and assistances through the developing process of the model. Review and editing of the manuscript.		
Signature		Date	

Name of Co-Author	Lei Chen		
Contribution to the Paper	Supervising the work, continuous recommendations and assistances through the developing process of the model. Review and editing of the manuscript.		
Signature	Ley Chen	Date	

Name of Co-Author	Samira Pourhedayat		
Contribution to the Paper	Validation of the analytical data with experimental data.		
Signature		Date	

Applied Energy 262 (2020) 114557

Contents lists available at ScienceDirect

Applied Energy

journal homepage: www.elsevier.com/locate/apenergy

Analytical/experimental sensitivity study of key design and operational parameters of perforated Maisotsenko cooler based on novel wet-surface theory

Hamed Sadighi Dizaji*, Eric Jing Hu*, Lei Chen, Samira Pourhedayat

School of Mechanical Engineering, The University of Adelaide, Adelaide, SA 5005, Australia

HIGHLIGHTS

- A new analytical model is presented for M-cycle based on novel we-surface theory.
- The model is able to generate temperature/humidity distribution.
- The validated model was employed for sensitivity analysis of key parameters.
- Given M-cycle obtains its maximum cooling capacity under Wet-Surface theory.

GRAPHICAL ABSTRACT

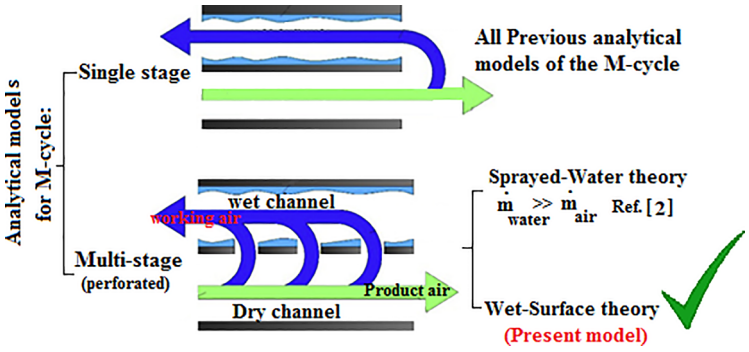

ARTICLE INFO

Keywords:
Maisotsenko cycle
Experimental
Sensitivity analysis
M-cycle
Air cooler
HVAC
Wet-Surface theory

ABSTRACT

Only one analytical model was previously proposed for multi-stage M-cycle cooler which is based on Sprayed-Water Theory in which the temperature of the wet plate was assumed constant, equal to water inlet temperature, (as the water flow rate was assumed so high). Said preliminary model was only able to predict outlet characteristics of the cooler (not parameters distribution along the cooler). This paper presents a new model for multi-stage M-cycle cooler based on the novel Wet-Surface theory in which the temperature of the wet-plate varies along the cooler (real working condition) and the model is able to generate the temperature/humidity distribution in addition to the outlet characteristics. The concept of the novel Wet-Surface theory and its potentials are discussed in the paper. Maximum theoretic cooling capacity of a given M-cycle cooler is obtained when it works based on Wet-Surface Theory. The model is experimentally validated with a unique test-rig and then the impacts of key operation and design parameters of multi-stage M-cycle cooler (i.e. inlet temperature, humidity ratio, mass flow rate, mass flow ratio, channel gap, channel length, channel height and the location of perforation) on its cooling characteristics (including outlet temperatures, outlet humidity ratio, wet-bulb effectiveness and dew-point effectiveness) are studied by the validated model.

1. Introduction

As can be seen in Fig. 1(a), all indirect evaporative coolers deal with two channels so-called working (secondary or wet) channel and product (primary or dry) channel. Contrary to conventional indirect evaporative coolers (Fig. 1(a)) in which the air fluid of the working channel is

* Corresponding authors.
E-mail addresses: HamedSadighiDizaji@gmail.com, Hamed.SadighiDizaji@adelaide.edu.au (H. Sadighi Dizaji), Eric.Hu@Adelaide.edu.au (E.J. Hu).

https://doi.org/10.1016/j.apenergy.2020.114557
Received 20 October 2019; Received in revised form 22 November 2019; Accepted 24 January 2020
Available online 06 February 2020

Nomenclature

a	gap between plates (m) (Fig. 5)
b	width of the channel
A	area (m^2)
c	specific heat (KJ/kg °C)
c_a	specific heat of dry air (KJ/kg °C)
c_v	specific heat of water vapor (KJ/kg °C)
c_f^*	$\frac{\dot{m}_1 c_1}{\dot{m}_2 c_a}$
c_w^*	$\frac{\dot{m}_w c_w}{\dot{m}_2 c_a}$
d_h	hydraulic diameter (m)
e	in defined of w_{eq} (Fig. 6) or Napier number
F	in defined of w_{eq} (Fig. 6)
i_v	specific enthalpy of water vapor (KJ/kg)
i_{fg}	evaporation heat of water at 0 °C
$\bar{i}_{fg}$	i_{fg}/c_a
k_p	thermal conductivity of plate (W/m^2 °C)
L	length of the channel in flow direction, (m)
L_a, L_b	refer to Fig. 5
Le	Lewis factor($\frac{\alpha_2}{\beta c_a}$)
NTU	number of heat transfer units
Nu	Nusselt number
Pr	Prandtl Number
q	heat transfer rate (W)
r	$\frac{UA_1}{\alpha_2 A_2}$
Re	Reynolds number
R_{cw}	$\frac{c_w}{c_a}$
R	thermal resistance (m^2K/W)
T	temperature (°C)
T_f	water film temperature (°C)
U	overall heat transfer coefficient (KW/m^2 °C)
V	velocity (m/s)
$\dot{m}$	mass transfer rate (kg/s)
P	atmospheric pressure of moist air
p_v	partial pressure of water vapor
w	humidity ratio (kg moisture/kg dry air)
w_{eq}	humidity ratio of moist air in equilibrium with water surface (kg moisture/kg dry air)
ε	mass transfer ratio
δ_p	thickness of the plate (m)
δ_w	thickness of water film (m)
α	coefficient of convective heat transfer (KW/m^2 °C)
β	coefficient of convective mass transfer (W/m K)
σ	wettability factor
ρ	density (kg/m^3)
η	$1 + e\bar{i}_{fg}$

Subscripts

1 or Pa	primary air (product air)
2 or wa	working air (secondary air)
dp	dew point
f	water film
wb	wet-bulb
w	water
A, B, C	refer to Fig. 5
L_a, L_b	refer to Fig. 5

Superscripts

′	inlet
″	outlet

provided from the ambient air, the air fluid of working channel in M-cycle (Fig. 1b and c) coolers is supplied from the cooled down primary air [1] which prevents cooling loss by existence heat in the ambient air. In other words, as both sensible and latent heat transfer participate in cooling mechanism of indirect evaporative air cooler, lower temperature of the secondary air at the inlet of the working channel increases the quality of the sensible heat (from primary air into the secondary air) along the cooler.

Main analytical models of indirect evaporative cooler are illustrated in Fig. 2. The concept of Sprayed Water Theory (previous analytical model by Sadighi Dizaji et al. [2] for multi-stage M-cycle cooler) is first summarized in the following and then the concept of the present Wet-Surface Theory is described.

The quality of latent heat transfer depends on the water evaporation rate and consequently depends on the material of wet plate (the effect of material will be explained). It is noted that, higher water flow rate does not means higher water evaporation rate or higher cooling capacity. Indeed, higher water flow rate increases the thickness of the water film and significantly reduces the water evaporation rate and cooling capacity of the cooler. In such condition (in which water flow rate is so higher than the air flow rate), the temperature of the wet-plate can be assumed constant (equal to the water inlet temperature) and approximately only sensible heat transfer participates in cooling process. Under this condition, which is termed Sprayed-Water Theory, water inlet temperature should be colder than the air inlet temperature. Otherwise, the cooler will not be able to reduce the air temperature because of weak water evaporation rate (which results in weak latent heat transfer). In Sprayed-Water Theory, the water temperature dominates the wet-plate temperature; and air flow condition is not able to affect the temperature distribution along wet-plate. Moreover, obtained cooling capacity of the cooler is away from the ideal condition and it severely depends on water inlet temperature (the concept of the present Wet-Surface Theory is described as below).

Contrary to the previous sprayed-water theory [2], in Wet-Surface Theory, the mass flow rate of the water is theoretically zero (compared to the air flow rate) while the wet-plate is continuously wet (without water stream on it) and the water evaporation from the surface does not make it dry (in other words, the evaporated water from the surface is continuously replenished). Practically (in real working condition), a specific wet-plate material is required to comply the wet-surface theory.

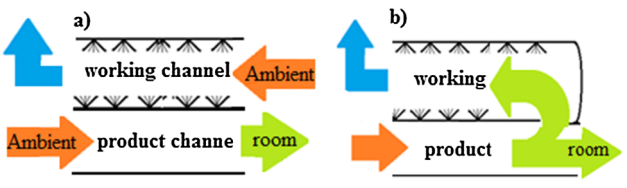

Fig. 1. (a) Conventional indirect evaporative cooler and (b) Single stage M-cycle indirect evaporative cooler.

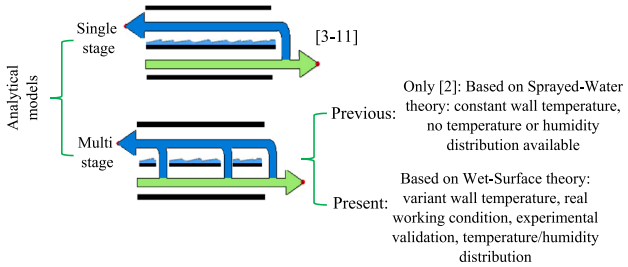

Fig. 2. Previous analytical models on indirect evaporative coolers.

This material should be able to absorb the water and remain itself thoroughly wet (like a tissue) and the evaporated water from the wet-surface should be replenished with a small water mass flow rate (the water mass flow rate is as possible as small to only keep the whole plate continuously wetly without creation of water stream on the surface). Under wet-surface theory, the rate of water evaporation is so high and latent heat transfer plays a key role of heat transfer process. Besides, in wet-surface theory, the temperature of the wet-plate varies along the channel and it is not affected by water temperature. Contrary to the Sprayed Water Theory, in Wet-Surface Theory, the air fluid flow dominates the water evaporation rate and consequently dominates the temperature distribution along the wet plate. In Wet-Surface Theory, the cooler is able to reduce the air temperature even if the water inlet temperature is the same as air inlet temperature. An ultra-thin specific material (0.4 mm thickness) was employed in this research to comply the wet-surface theory in real working condition and will be described in the experimental section.

As the methodologies of the present work are analytical and experimental, the main analytical investigations of indirect evaporative air coolers are summarized in the following. Maclaine and Banks model [3] is one of the main initial analytical models of indirect evaporative air cooler. Stotichkov [4], Alonso [5] and Ren [6] tried to expand the Maclaine model by eliminating some of the assumptions. Hassan [7] suggested a modified version of ε-NTU method which can be applicable for indirect evaporative cooling. Liu [8] worked further on Hassan model and tried to improve the model by removing some vague features of the Liu model. Cui [9] employed a modified version of the well-known LMTD technique (which is utilized in heat exchangers deals with only sensible heat transfer) for M-cycle exchanger. Chen [10] considered the effect of condensation of air fluid in the performance of the cooler which has not been applied in the previous models. Nonetheless, all mentioned analytical models have been developed for single-stage M-cycle cooler and they do not provide temperature/humidity distribution along the channels. Recently, Dizaji et al. [2] provided an analytical model for multi-stage M-cycle cooler for the first time. However, it was developed based on sprayed-water theory (as described above) and similar to previous models it only is able to provide outlet characteristics of the cooler without temperature/humidity distribution through the channels. The main numerical and experimental studies of M-cycle have been summarised in the review paper by Dizaji et al. [1] and it is highlighted in Table 1.

Present research shows how an analytical model can be developed and solved for multi-stage M-cycle cooler based on real working condition (variant wet-plate temperature). The model was developed based on wet-surface theory which was explained above. Besides, this model is able to generate temperature/humidity distribution along the dry channel, wet channel and wet plate for multi-stage M-cycle cooler. The model is validated with a unique experimental test-rig and then is employed to clarify the effect of all key design and operational parameters on cooling characteristic of the multi-stage M-cycle cooler. All key operational and design characteristics are covered in this study which can be applicable for real industrial-based applications. The test-rig was built transparent to exactly clarify the working principle of the M-cycle cooler.

2. Analytical model based on the novel Wet-Surface Theory

The concept of Wet-Surface Theory was explained completely in introduction section. Fig. 4 illustrates a general parallel configuration of indirect evaporative cooler. The related main governing equations of the cooler (shown in Fig. 3) are presented in Eq. (1).

$$\begin{cases} \text{Energy balance of primary air: } \dot{m}_1 c_1 dT_1 = U(T_w - T_1)A_1 d\bar{x} \\ \text{Mass balance of working air:} \\ \dot{m}_2 dw_2 = \beta(w_{eq} - w_2)\sigma A_2 \frac{dx_2}{L} \text{ and } d\dot{m}_w = -\dot{m}_2 dw_2 \\ \text{Energy balance of wet channel:} \\ \dot{m}_2 di_2 = [\alpha_2(T_w - T_2) + i_v\beta(w_{eq} - w_2)\sigma]A_2\frac{dx_2}{L_{wa}} \\ \text{Energy balance for differential element:} \\ \dot{m}_w c_w dT_w + c_w T_w d\dot{m}_w + \dot{m}_1 c_1 dT_1 + \dot{m}_2 di_2 = 0 \\ \text{linear function between } W_{eq} \text{ water surface temperatur} \\ \text{e: } w_{eq} = F + eT_w \end{cases} \quad (1)$$

Similar to the long simplification process presented by Dizaji et al. [2] (Eqs. (1) to (48) in [2]), Eq. (1) can be rewritten as Eq. (2). In wet-surface theory (present model), the water flow rate is as possible as small to only the plate wetly without further water stream. The mathematical concept of wet-surface theory is that the value of $C_w^* = \dot{m}_w c_w / \dot{m}_2 c_a$ tends to zero. By consideration of wet-surface theory the Eq. (2) can be rewritten as Eq. (3).

Table 1
Some main experimental, theoretical and numerical researches on Maisotsenko coolers.

Ref.	Studying on	Evaluation method
[18]	Proposing an improved M-cycle cooler	Experimental
[19]	Effect of geometry on M-cycle performance	Numerical ε-NTU method
[20]	Proposing a control technique for M-cycle to reduce power consumption	Theoretical
[16]	Comparison between eight types of Coolerado M-cycle coolers	Numerical ε-NTU method
[21]	Effect of flow/geometric parameters on M-cycle performance	Numerical finite element
[22]	Performance correlation for counter-flow M-cycle cooler	Numerical/Experimental
[23]	General study on M-cycle	Numerical finite volume
[24]	Experimental research of a novel indirect evaporative air cooler	Experimental
[25]	Counter-flow and cross-flow configurations are compared with each other	Experimental
[26]	Analysis of a commercialized M-cycle cooler	Experimental
[27]	Application of liquid desiccant for M-cycle coolers	Experimental
[28]	Analysis of M-cycle air cooler under Greek climate condition	Experimental
[29]	Proposing and analysis of a counter flow exchanger for Maisotsenko coolers	Experimental
[30]	Studying of an modified Maisotsenko cooler under low velocity condition	Experimental
[17]	Analysis of M-cycle air cooler under china climate condition	Experimental
[31]	Investigation of the cross-flow exchanger of M-cycle	Experimental
[32]	Providing an innovative exchanger for Maisotsenko coolers	Experimental
[33]	Operational performance and impact factors of a counter-flow M-cycle	Experimental
[34]	Consideration of wettability factor on M-cycle exchangers	Experimental
[35]	Impact of dehumidification on cross-flow exchangers of Maisotsenko cooler	Experimental
[36]	Application of solid desiccant for cross flow exchangers of M-cycle cooler	Experimental

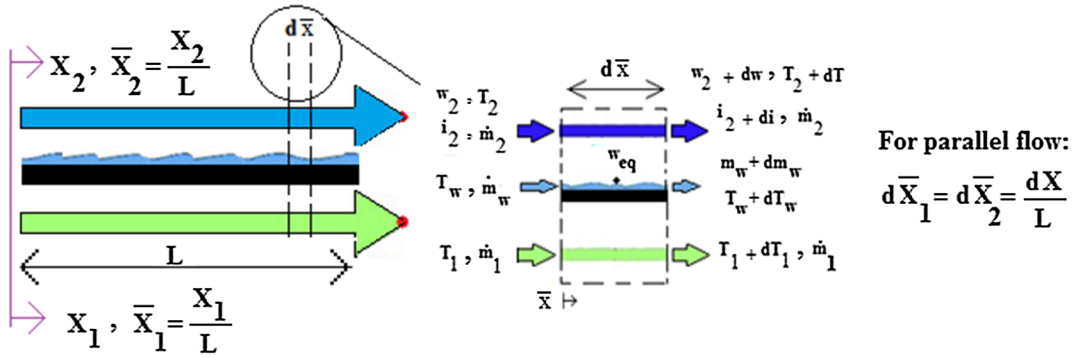

Fig. 3. General view of the conventional indirect evaporative cooler.

$$\begin{cases} dT_1 = (T_w - T_1)\frac{r}{C_f^*}NTUd\bar{x} \\ dT_2 = (T_w - T_2)NTUd\bar{x} \\ dw_2 = \frac{\sigma}{Le_f}(w_{eq} - w_2)NTUd\bar{x} \\ dT_w = [-\frac{i_{fg}}{c_a}\frac{\sigma}{Le_f}(w_{eq} - w_2) + r(T_1 - T_w) \\ \quad - (T_w - T_2)]\frac{1}{C_w^*}NTUd\bar{x} \\ dw_{eq} = [-\frac{i_{fg}}{c_a}\frac{\sigma}{Le_f}(w_{eq} - w_2) + r(T_1 - T_w) \\ \quad - (T_w - T_2)]\frac{e}{C_w^*}NTUd\bar{x} \end{cases} \quad (2)$$

$$\begin{cases} dT_1 = (T_w - T_1)\frac{r}{C_f^*}NTUd\bar{x} \\ dT_2 = (T_w - T_2)NTUd\bar{x} \\ dw_2 = \frac{\sigma}{Le_f}(w_{eq} - w_2)NTUd\bar{x} \\ -\frac{i_{fg}}{c_a}\frac{\sigma}{Le_f}(F + eT_w - w_2) + r(T_1 - T_w) - (T_w - T_2) = 0 \end{cases} \quad (3)$$

where NTU is Number of Heat Transfer Units ($\frac{\alpha_2 A_2}{\dot{m}_2 c_a}$), C_f^* is defined as $\frac{\dot{m}_1 c_1}{\dot{m}_2 c_a}$, " r" is defined as $\frac{UA_1}{\alpha_2 A_2}$, C_w^* is calculated by$\frac{\dot{m}_w c_w}{\dot{m}_2 c_a}$ and Le_f is Lewis factor ($\frac{\alpha_2}{\beta c_a}$). If the latest correlation of Eq. (3) rearranged as a function of T_w and replaced in the first two correlations, Eq. (3) will be appeared in the form of Eq. (4) (by applying a couple of assumptions including satisfying of Lewis factor ($\frac{\sigma}{Le_f} = 1$) and $w_{eq} = F + eT_w$ and some arrangements.

$$\begin{cases} \frac{dT_1}{d\bar{x}} = \{\bar{i_{fg}}F - \bar{i_{fg}}w_2 - T_2 + \eta T_1\}\frac{-r}{C_f^*(r+\eta)} \\ \frac{dT_2}{d\bar{x}} = \{\bar{i_{fg}}F - \bar{i_{fg}}w_2 - (1 - r - \eta)T_2 - rT_1\}\frac{-1}{(r+\eta)}NTU \\ \frac{dw_2}{d\bar{x}} = \{F(\bar{i_{fg}} - \frac{(r+\eta)}{e}) - (\bar{i_{fg}} - \frac{(r+\eta)}{e})w_2 - t_2 - rt_1\}\frac{-e}{(r+\eta)}NTU \end{cases} \quad (4)$$

where $\eta = 1 + e\bar{i_{fg}}$ and$\bar{i_{fg}} = i_{fg}/c_a$. Unlike Fig. 3 (which is parallel flow), M-cycle cooler works in counter flow configuration (see Fig. 4). Hence, for M-cycle cooler, the Eq. (4) is rewritten as shown in Eq. (5) based on flow direction of dry air ($\bar{x}_1$).

$$\begin{cases} \frac{dT_1}{d\bar{x}_1} = \{\bar{i_{fg}}F - \bar{i_{fg}}w_2 - T_2 + \eta T_1\}\frac{-r}{C_f^*(r+\eta)}NTU \\ \frac{dT_2}{d\bar{x}_1} = \{\bar{i_{fg}}F - \bar{i_{fg}}w_2 - (1 - r - \eta)T_2 - rT_1\}\frac{1}{(r+\eta)}NTU \\ \frac{dw_2}{d\bar{x}_1} = \{F(\bar{i_{fg}} - \frac{(r+\eta)}{e}) - (\bar{i_{fg}} - \frac{(r+\eta)}{e})w_2 - t_2 - rt_1\}\frac{e}{(r+\eta)}NTU \end{cases} \quad (5)$$

Eq. (5) can be written in a general form as shown in Eq. (6.1). Analytical solution methods such as Laplace Transformations Technique or Euler Technique can be employed to solve the Eq. (6) as it is a first order linear differential equation which contains constant coefficients. It is noted that, the coefficients "G, …, Q" are calculated for any given cooler and then are replaced in Eq. (6.1). By solving the Eq. (6.1), the temperature and humidity of the channels are obtained as the functions of $\bar{x}_1$ (temperature and humidity distribution). Eq. (6.3) is the boundary condition for Eq. (6.1) for single stage M-cycle cooler.

$$\begin{cases} \frac{dT_1}{d\bar{x}_1} = G + Hw_2 + IT_2 + JT_1 \\ \frac{dT_2}{d\bar{x}_1} = K + Lw_2 + MT_2 + NT_1 \quad 0 < \bar{x}_1 < 1 \\ \frac{dW_2}{d\bar{x}_1} = O + Zw_2 + VT_2 + QT_1 \end{cases} \quad (6.1)$$

$$\begin{cases} G = \frac{-r}{C_f^*(r+\eta)}NTU\bar{i_{fg}}F \\ H = \frac{r}{C_f^*(r+\eta)}NTU\bar{i_{fg}} \\ I = \frac{r}{C_f^*(r+\eta)}NTU \\ J = \frac{-r\eta}{C_f^*(r+\eta)}NTU \\ K = \bar{i_{fg}}\frac{F}{(r+\eta)}NTU \\ L = \bar{i_{fg}}\frac{-1}{(r+\eta)}NTU \\ M = \frac{-(1-r-\eta)}{(r+\eta)}NTU \\ N = \frac{-r}{(r+\eta)}NTU \\ O = F\left(\bar{i_{fg}} - \frac{r+\eta}{e}\right)\frac{e}{(r+\eta)}NTU \\ Z = (\bar{i_{fg}} - \frac{r+\eta}{e})\frac{-e}{(r+\eta)}NTU \\ V = \frac{-e}{(r+\eta)}NTU \\ Q = \frac{-er}{(r+\eta)}NTU \end{cases} \quad (6.2)$$

$$\begin{cases} T_1(\bar{x}_1 = 0) = T_{inlet} = T'_1 \\ T_2(\bar{x}_1 = 1) = T''_1 \\ W_2(\bar{x}_1 = 1) = W'_1 \end{cases} \quad (6.3)$$

For a multi-stage M-cycle as shown in Fig. 5, (the aim of present study), Eq. (6) should be written and solved separately for each section of cooler (L_a and L_b) with their own unique boundary conditions. Moreover, the value of the parameters "G" to "Q" is different for each section that is calculated separately for each section with its own characteristics (the calculation process of the required parameters to evaluate the constant coefficients G,…,Q are shown graphically in

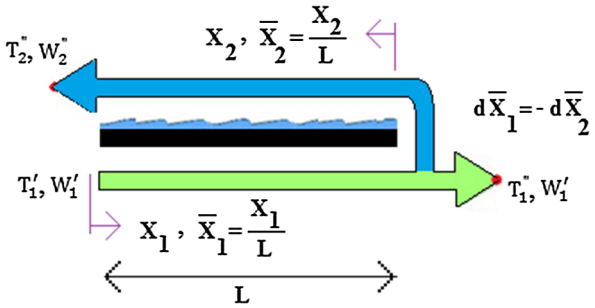

Fig. 4. General view of the M-cycle air cooler.

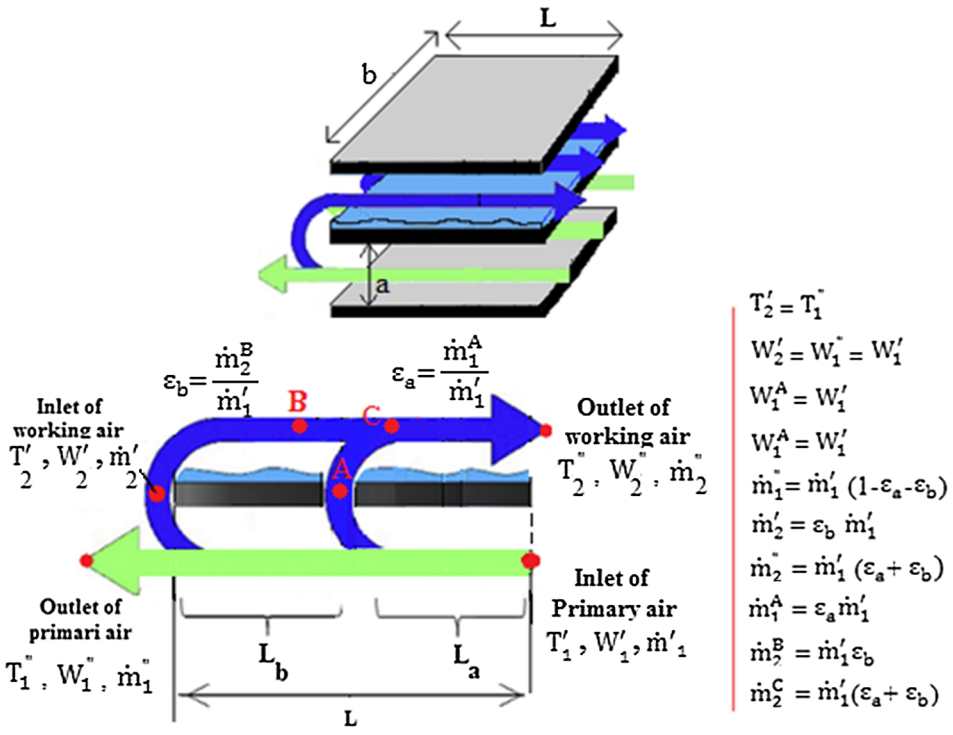

Fig. 5. A general view of two-stage M-cycle cooler.

Fig. 6). Hence, Eq. (6) is written for a two-stage M-cycle as shown in Eq. (7). It is noted that, the boundary condition of each section is different and should be specified carefully (see Fig. 5). For example, the humidity ratio of the inlet of working channel for section L_b is the same as the humidity ratio of inlet primary air. However, the humidity ratio of the inlet of working channel for section L_a is equal with W_c which has still unknown value.

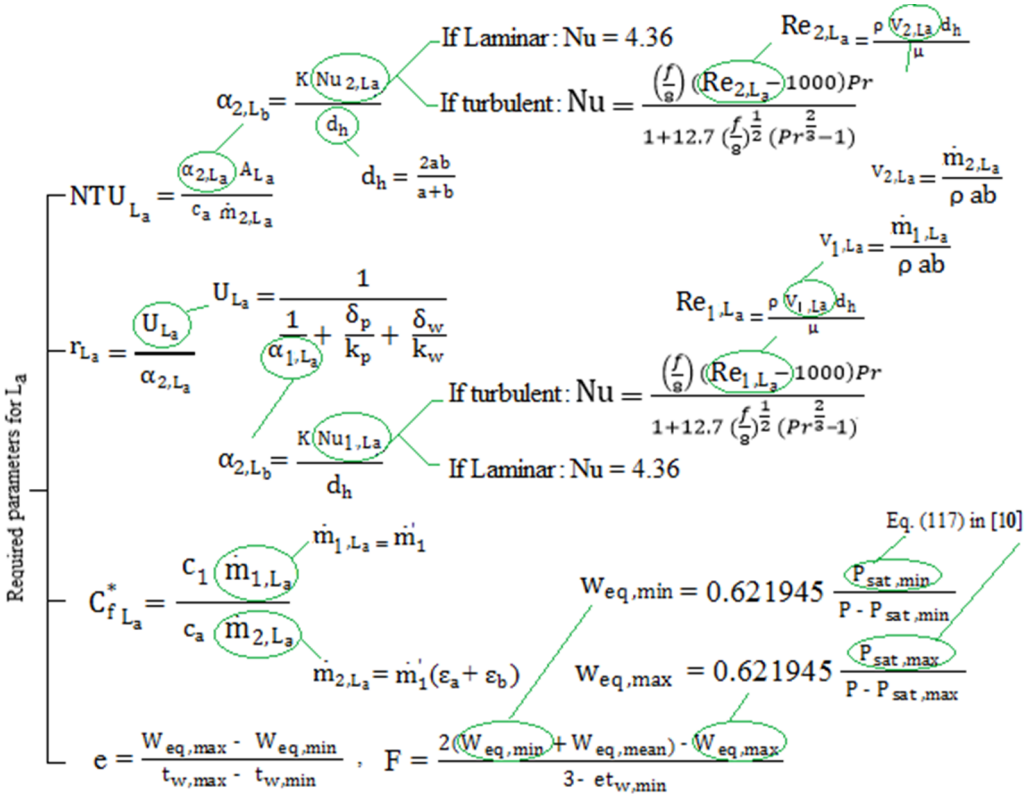

Fig. 6. Calculation process of required parameters to evaluate the coefficients G, …, Q (example for L_a).

Table 2
Input parameters of the given two-stage M-cycle cooler.

Parameter	Value
a (m)	0.005
b (m)	0.2
L (m)	1
$\mathbf{L_a}$(m)	0.5
$\mathbf{L_b}$(m)	0.5
Inlet air temperature (°C)	35
Humidity ratio of inlet air kg/kg	0.016
Inlet-air mass flow rate (Kg/s)	0.009
$\varepsilon_\mathbf{a}$	0.25
$\varepsilon_\mathbf{b}$	0.25
$\mathbf{k_p}$	0.00250 kW/m^{2}C
$\delta_\mathbf{p}$	0.0005 m
$\mathbf{k_w}$	0.6 × 10^{-3} kW/m^{2}C
$\delta_\mathbf{w}$	0.0001 m

$$\begin{cases} L_a \begin{cases} \frac{dT_1}{d\bar{x}_1} = G' + H'w_2 + I't_2 + J't_1 \\ \frac{dT_2}{d\bar{x}_1} = K' + L'w_2 + M't_2 + N't_1 \\ \frac{dW_2}{d\bar{x}_1} = O' + Z'^{w_2} + Vt_2 + Qt_1 \end{cases} & 0 < \bar{x}_1 < \frac{L_a}{L} \text{or} \frac{L_b}{L} < \bar{x}_2 < 1 \\ L_b \begin{cases} \frac{dT_1}{d\bar{x}_1} = G'' + H''w_2 + I''t_2 + J''t_1 \\ \frac{dT_2}{d\bar{x}_1} = K'' + L''w_2 + M''t_2 + N''t_1 \\ \frac{dW_2}{d\bar{x}_1} = O + Zw_2 + Vt_2 + Qt_1 \end{cases} & \frac{L_a}{L} < \bar{x}_1 < 1 or 0 < \bar{x}_2 < \frac{L_b}{L} \end{cases} \tag{7.1}$$

$$\begin{cases} G' = \frac{-r_{La}}{C^*_{f,La}(r_{La}+\eta)} NTU_{La} \bar{i_{fg}} F & G'' = \frac{-r_{Lb}}{C^*_f(r+\eta)} NTU_{Lb} \bar{i_{fg}} F \\ H' = \frac{r_{La}}{C^*_f(r_{La}+\eta)} NTU_{La} \bar{i_{fg}} & H'' = \frac{r_{Lb}}{C^*_f(r+\eta)} NTU_{Lb} \bar{i_{fg}} \\ I' = \frac{r_{La}}{C^*_f(r_{La}+\eta)} NTU_{La} & I'' = \frac{r_{Lb}}{C^*_f(r+\eta)} NTU_{Lb} \\ J' = \frac{-r_{La}\eta}{C^*_f(r_{La}+\eta)} NTU_{La} & J'' = \frac{-r_{Lb}\eta}{C^*_f(r+\eta)} NTU_{Lb} \\ K' = \bar{i_{fg}} \frac{F}{(r_{La}+\eta)} NTU_{La} & K'' = \bar{i_{fg}} \frac{F}{(r_{Lb}+\eta)} NTU_{Lb} \\ L' = \bar{i_{fg}} \frac{-1}{(r_{La}+\eta)} NTU_{La} & L'' = \bar{i_{fg}} \frac{-1}{(r_{Lb}+\eta)} NTU_{Lb} \\ M' = \frac{-(1-r_{La}-\eta)}{(r_{La}+\eta)} NTU_{La} & M'' = \frac{-(1-r_{Lb}-\eta)}{(r_{Lb}+\eta)} NTU_{Lb} \\ N' = \frac{-r_{La}}{(r_{La}+\eta)} NTU_{La}, & N'' = \frac{-r}{(r_{Lb}+\eta)} NTU_{Lb} \\ O' = F\left(\bar{i_{fg}} - \frac{r_{La}+\eta}{e}\right) \frac{e}{(r_{La}+\eta)} NTU_{La} & O'' = F\left(\bar{i_{fg}} - \frac{r_{Lb}+\eta}{e}\right) \frac{e}{(r_{Lb}+\eta)} NTU_{Lb} \\ Z' = (\bar{i_{fg}} - \frac{r_{La}+\eta}{e}) \frac{-e}{(r_{La}+\eta)} NTU_{La} & Z'' = (\bar{i_{fg}} - \frac{r_{Lb}+\eta}{e}) \frac{-e}{(r_{Lb}+\eta)} NTU_{Lb} \\ V' = \frac{-e}{(r_{La}+\eta)} NTU_{La} & V'' = \frac{-e}{(r_{Lb}+\eta)} NTU_{Lb} \\ Q' = \frac{-er}{(r_{La}+\eta)} NTU_{La} & Q'' = \frac{-er_{Lb}}{(r_{Lb}+\eta)} NTU_{Lb} \end{cases} \tag{7.2}$$

$$\begin{cases} L_a \begin{cases} T_1(\bar{x}_1 = 0) = T_{inlet} = T'_1 \\ T_2\left(\bar{x}_1 = \frac{L_a}{L}\right) = T_c \\ W_2\left(\bar{x}_1 = \frac{L_a}{L}\right) = W_c \end{cases} \\ L_b \begin{cases} T_1\left(\bar{x}_1 = \frac{L_a}{L}\right) = T_A \\ T_2(\bar{x}_1 = 1) = T_1(\bar{x}_2 = 1) \\ W_2(\bar{x}_1 = 1) = W_{inlet} = W'_1 \end{cases} \end{cases} \tag{7.3}$$

For multi-stage cooler, after solving the Eq. (7) by analytical Laplace Transforms Method the obtained results still contain some unknown parameters including T_A, T_c and W_c. They can be calculated from the enthalpy balance and moisture balance between the points A, B, C as described in [2] which resulted in below correlations for T_c and W_c (Eqs. (8) and (9)). By replacement of T_c and W_c in the analytical result, all unknown parameters will be evaluated. Solving of Eq. (7) provides the temperature of the dry channel, working channel and water temperature as a function of dimension (x) which is temperature/humidity distribution. For obtaining the temperature of any location of the exchanger (for example outlet characteristics), the value of dimension "x" of that location is placed in the equation.

$$T_c = \frac{\varepsilon_a[(c_a + w'_1 c_v)T_A + w'_1 i_{fg}] + (\varepsilon_b)[(c_a + w_B c_v)T_B + w_B i_{fg}] - (\varepsilon_a + \varepsilon_b)w_c i_{fg}}{(\varepsilon_a + \varepsilon_b)(c_a + w_c c_v)} \tag{8}$$

$$W_c = \frac{\varepsilon_a w'_1 + \varepsilon_b w_B}{(\varepsilon_a + \varepsilon_b)} \tag{9}$$

3. Sample solving of the model

The model is solved for a given two-stage M-cycle cooler with characteristics shown in Table 2.

Required constants (including r_{La}, r_{Lb}, $C^*_{f,La}$, $C^*_{f,Lb}$, NTU_{La}, NTU_{Lb} e nad F) to evaluate the coefficients of (G′, … , Q′)can be calculated for the information provided in Table 2 as was shown schematically in Fig. 6. The coefficients related to L_b i.e. G″, … , Q″ is similar to L_a (note that all characteristics should be extracted from the characteristics of L_b). After the calculation of required parameters for both L_a and L_b (in two-stage), the coefficients of (G′, … , Q′ and G″, … , Q″) are simply evaluated for that given cooler by Eq. (7.2). The obtained values of coefficients are replaced in Eq. (7) which yields Eq. (10.1) as differential equation and 10.2 as the boundary conditions.

$$\begin{cases} L_a \begin{cases} \frac{dT_1}{d\bar{x}_1} = -3.62 + 131w_2 + 0.05T_2 - 0.27T_1 \\ \frac{dT_2}{d\bar{x}_1} = 2 - 72.37w_2 + 0.22T_2 + 0.1T_1 \\ \frac{dW_2}{d\bar{x}_1} = -0.0037 + 0.13w_2 - 4.8 \times 10^{-5}T_2 - 1.7 \times 10^{-4}T_1 \end{cases} & 0 \\ < \bar{x}_1 < 0.5 & \\ L_b \begin{cases} \frac{dT_1}{d\bar{x}_1} = -4 + 147.7w_2 + 0.06T_2 - 0.3T_1 \\ \frac{dT_2}{d\bar{x}_1} = 4.4 - 160.57w_2 + 0.45T_2 + 0.18T_1 \\ \frac{dW_2}{d\bar{x}_1} = -0.0067 + 0.24w_2 - 1.08 \times 10^{-4}T_2 - 3 \times 10^{-4}T_1 \end{cases} & 0.5 \\ < \bar{x}_1 < 1 & \end{cases} \tag{10.1}$$

$$\begin{cases} L_a \begin{cases} T_1(\bar{x}_1 = 0) = T_{inlet} = 35 \\ T_2\left(\bar{x}_1 = \frac{1}{2}\right) = T_c \\ W_2\left(\bar{x}_1 = \frac{1}{2}\right) = W_c \end{cases} \\ L_b \begin{cases} T_1\left(\bar{x}_1 = \frac{1}{2}\right) = T_A \\ T_2(\bar{x}_1 = 1) = T_1(\bar{x}_2 = 1) \\ W_2(\bar{x}_1 = 1) = W_{inlet} = 0.016 \end{cases} \end{cases} \tag{10.2}$$

Eq. (10.1) can be solved via analytical Laplace transformations Technique (Maple software is helpful) and the temperature of dry side, wet side and humidity of wet side are achieved as a function of $\bar{x}_1$ as shown in Eq. (11) ("e" is Napier number in these equations). Hence, in order to calculate the value of T_A, T''_2, W''_2, T''_1, T_B and W_B, their location (i.e. $\bar{x}_1 = 0$ and $\frac{1}{2}$ for L_a and $\bar{x}_1 = \frac{1}{2}$ and 1 for L_b) should be substituted in Eq. (11) which yields Eq. (12).

$$
\begin{cases}
\text{La}\begin{cases}
T_1(\bar{x}_1) = (-0.05 - 0.003T_c + 0.89W_c)e^{0.25\bar{x}_1} \\
\quad - (18.32 + 0.2T_c - 445W_c)e^{0.047\bar{x}_1} \\
\quad + (52 - 0.19T_c - 445W_c)e^{-0.21\bar{x}_1} + 1.3 \\
T_2(\bar{x}_1) = (12.2 + 0.79T_c - 205W_c)e^{0.25\bar{x}_1} \\
\quad + (-6.9 - 0.07T_c + 167W_c)e^{0.047\bar{x}_1} \\
\quad + (-7.8 - 0.03T_c + 67.4W_c)e^{-0.21\bar{x}_1} + 0.27 \\
W_2(\bar{x}_1) = (-0.004 - 3\times10^{-4}T_c + 0.08W_c)e^{0.25\bar{x}_1} \\
\quad + (-0.041 + 4\times10^{-4}T_c + 1.01W_c)e^{0.047\bar{x}_1} \\
\quad + (0.02 - 9\times10^{-5}T_c - 0.2W_c)e^{-0.21\bar{x}_1} + 0.03
\end{cases} \\
\text{Lb}\begin{cases}
T_1(\bar{x}_1) = (0.008 - 0.003T_A)e^{0.51\bar{x}_1} - (5.6 + 0.08T_A)e^{0.09\bar{x}_1} \\
\quad + (5.18 + 1.2T_A)e^{-0.21\bar{x}_1} + 1.25 \\
T_2(\bar{x}_1) = (1.9 + 0.63T_A)e^{0.51\bar{x}_1} - (3.3 + 0.049T_A)e^{0.09\bar{x}_1} \\
\quad - (0.6 + 0.14T_A)e^{-0.21\bar{x}_1} + 0.17 \\
W_2(\bar{x}_1) = (-0.0007 - 0.0002T_A)e^{0.51\bar{x}_1} \\
\quad - (0.01 + 0.0002T_A)e^{0.09\bar{x}_1} \\
\quad + (0.003 + 0.0007T_A)e^{-0.21\bar{x}_1} + 0.02
\end{cases}
\end{cases}
\tag{11}
$$

$$
\begin{cases}
\text{La}\begin{cases}
T_A = T_1\left(\frac{1}{2}\right) = 0.023T_c + 59.7W_c + 28.9 \\
T''_2 = T_2(0) = 0.89T_c + 31.76w_c - 2.38 \\
W''_2 = w_2(0) = 0.00002T_c + 0.93w_c + 0.0043
\end{cases} & 0 < \bar{x}_1 < 0.5 \\
\text{Lb}\begin{cases}
T''_1 = T'_2 = T_1(1) = -0.47 + 0.88T_A \\
T_B = T_2\left(\frac{1}{2}\right) = 0.63T_A - 0.88 \\
W_B = w_2\left(\frac{1}{2}\right) = 0.00017T_A + 0.02
\end{cases} & 0.5 < \bar{x}_1 < 1
\end{cases}
\tag{12}
$$

It is clear that the amount ofT_c, W_c, T_A (which comes from boundary conditions) are still unknown and should be evaluated by Eqs. (8)–(9). By calculation of T_c, W_c, T_A and substitution in Eq. (12), the final value of T''_1, T''_2 and W''_2 will be 26.5 °C, 20 °C and 0.023 respectively. Moreover, By substitution of T_c, W_c, T_A in Eq. (11), the temperature/humidity distribution along the channel will be obtained as the functions of "$\bar{x}_1$" as show in Eq. (13) which can be graphically drawn as seen in Fig. 7 as well. It is noted that curve trends can vary depending on operational and design parameters which will be discussed in the next sections.

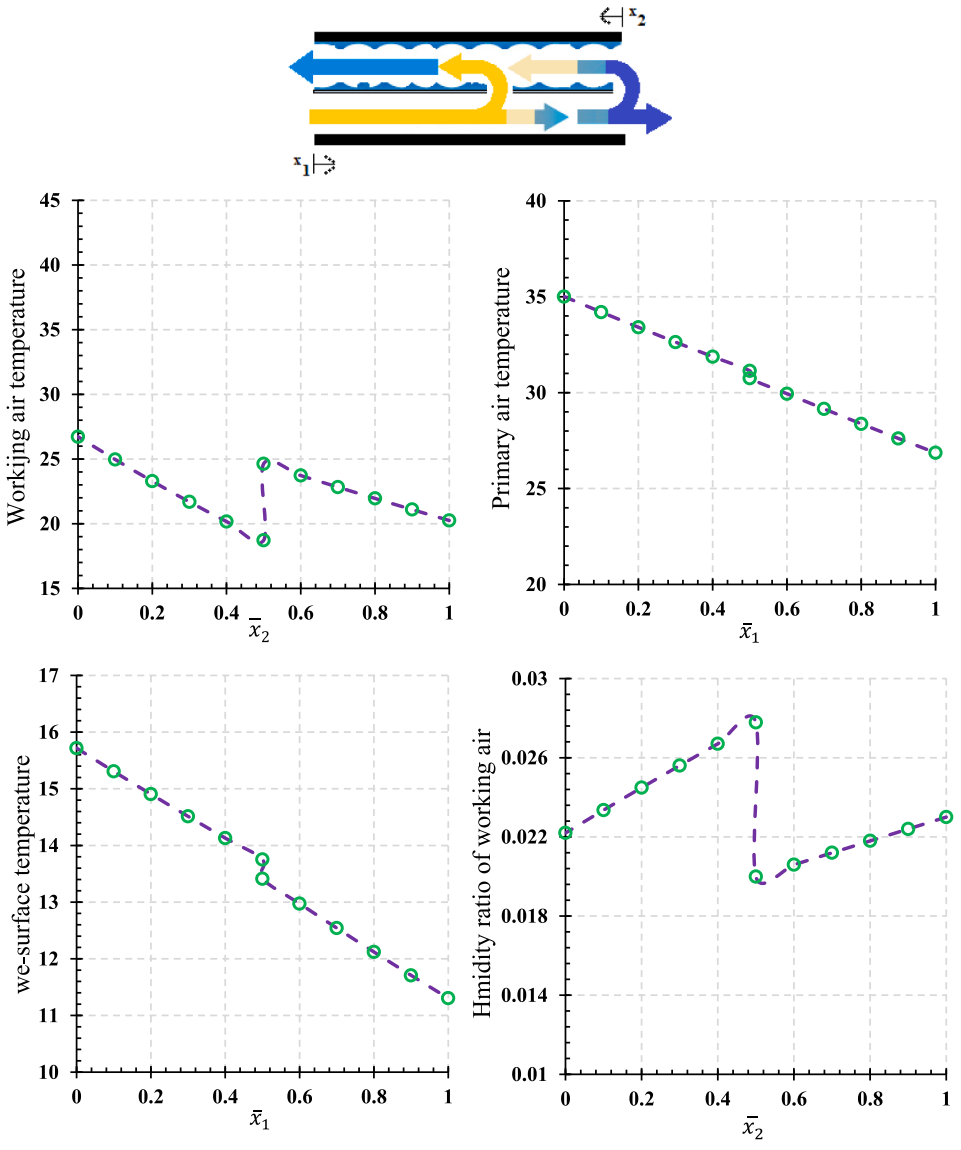

Fig. 7. Distribution for a two-stage M-cycle (a) primary air temperature, (b) working air temperature, (c) working air humidity ratio and (d) wet-surface temperature.

$$F(\bar{x}_1)\begin{cases} L_a \begin{cases} T_1(\bar{x}_1) = -0.11e^{0.25\bar{x}_1} + 39.8e^{-0.21\bar{x}_1} - 4.34e^{-0.05\bar{x}_1} - 0.34 \\ T_2(\bar{x}_1) = 28.07e^{0.25\bar{x}_1} - 6.05e^{-0.21\bar{x}_1} - 1.7e^{-0.05\bar{x}_1} - 0.07 \\ W_2(\bar{x}_1) = -0.011e^{0.25\bar{x}_1} + 0.018e^{-0.21\bar{x}_1} - 0.01e^{-0.05\bar{x}_1} + 0.026 \end{cases} & \frac{1}{2} < \bar{x}_2 < 1 \\ L_b \begin{cases} T_1(\bar{x}_1) = 0.09e^{0.51\bar{x}_1} - 6.5e^{0.09\bar{x}_1} + 40.19e^{-0.21\bar{x}_1} + 1.25 \\ T_2(\bar{x}_1) = 20.73e^{0.51\bar{x}_1} - 3.8e^{0.09\bar{x}_1} - 4.71e^{-0.21\bar{x}_1} + 0.18 \\ W_2(\bar{x}_1) = -0.007e^{0.51\bar{x}_1} - 0.015e^{0.09\bar{x}_1} + 0.025e^{-0.21\bar{x}_1} + 0.03 \end{cases} & 0 < \bar{x}_2 < \frac{1}{2} \end{cases} \quad (13)$$

4. Experiments and model validation

To validate the analytical model based on wet-surface theory, a unique test-rig was developed which is able to simulate M-cycle working condition based on wet-surface theory. The concept of wet-surface theory was described in the introduction section. Fig. 8 shows a general view of the test rig. The middle wet plate of the cooler is a specific ultra-thin surface. One side of this material is similar to a tissue while the other side is an impermeable nylon (see Fig. 8c). The tissue side can absorb and remain the water on itself which (working channel) avoid requirement of continuous water stream on the surface. The inlet of the cooler was designed by 3-D printer (inside of the inlet contains parallel plates) in order to provide uniform air flow through the channel (see Fig. 8b).

The air fluid in the working channel goes through the tissue side and causes evaporation of the water film which significantly reduces the temperature of the wet plate (similarly, a cooling sense is felt on our skin when a rubbing alcohol is spread on it is because of alcohol evaporation and latent heat). That is why it can be said that in wet-surface theory, the fluid flow condition (which affects the water evaporation) controls the temperature distribution on the wet-surface (not water inlet temperature). A minimum water flow rates is required to keep the surface wetly. In this case, the role of water distribution mechanism which should continuously replenish the evaporated water on the surface (with the minimum possible flow rate) is very important. Although the minimum required water flow rate can be calculated, its

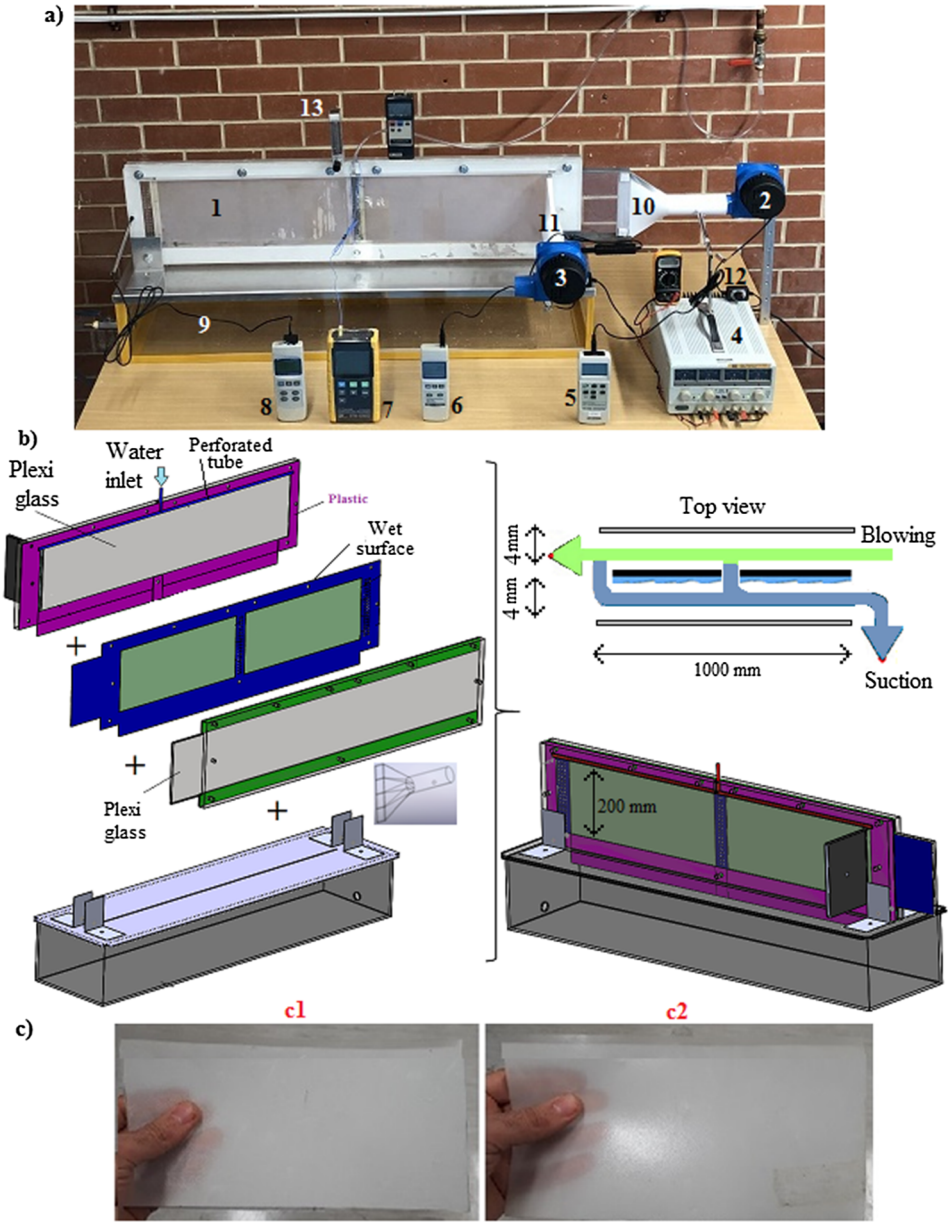

Fig. 8. (a) Experimental set-up including 1: Test-rig, 2: Blower, 3: Suction, 4: Dc supplier, 5: Hot-wire flow meter, 6: Humidity meter, 7: Temperature data logger, 8: Hot-wire flow meter, 9: Water reservoir, 10: Air inlet, 11: Working air outlet, 12: Fan speed controller, 13: Water Rota-meter (b) parts of the test-rig and (c) Wet-surface material (c1) tissue side (c2) nylon side.

distribution method is a problem in the real application. In wet-surface theory, lack of appropriate water distributer system may cause some dry parts on the wet-surface. It is mentioned again that, although larger water flow rate can rapidly replenish the water on the wet-surface, it will reduce the role of the surface evaporation (latent heat) and subsequently reduces the cooling capacity of the cooler.

As can be seen in Fig. 8, the primary air is injected to the dry channel via an air fan. The speed of fan is controlled by a dimmer to adjust arbitrary air flow rate. The body of the test-rig was made from 2-cm thickness Plexiglass to provide a transparent insulator wall. The dry air is going through the primary channel. A percentage of the air is discharged into the working channel in the mid and at the end of the channel. However, if the perforations in the middle of the channel are covered, the cooler will work as a single-stage cooler. The water fluid is spread on the wet-surface by a perforated tube (placed in a created groove in the body of plexiglass) with a small flow rate. Another fan at the end of the working channel sucks the working air. Another dimmer controls the speed of this fan to provide different values of "ε". The water is collected into a reservoir. The temperature and air flow rate in the primary and working channels (at inlets and outlets) are measured by hot-wire mechanism and K-type thermocouples. The humidity ratio of the working air at the end of the channel is recorded by a humidity meter. A hair drier was employed to provide warmer inlet temperature. A DC supplier was employed to apply Dc voltage to the air fans. The name and characteristics of the instruments can be seen in Table 3. All data was recorded at steady-state condition for different air flow rates and inlet temperatures.

The geometric characteristics (see Fig. 8) and flow parameters (see Fig. 9) of the experiments were put in the model and the outlet temperatures and humidity ratio were evaluated and then were compared with experimental measurements. The comparison is illustrated in Fig. 9 which shows a good agreement with maximum deviation of 5% for outlet temperature and maximum deviation of 14% for humidity ratio. The model predicts higher cooling capacity (colder outlet temperature and higher outlet humidity ratio) compared to the experimental results. It is noted that, wet-surface theory (current model) provides the maximum water evaporation rate because of lack of any physical water stream on the surface and its other features described in the introduction section. However, in real experimental condition, it is not possible (at least with current technology) to ideally make the wet-surface theory as water mass flow rate should be more than the evaporated water to prevent the creation of dry areas on the surface (which makes water streams on the surface and causes reduction of the water evaporation rate compared to the theoretical model). That is why outlet humidity during the experiments is smaller than the analytical model (poor water evaporation compared to the model). Moreover, the direction of the water stream is the same as air flow in the model. However, in the test-rig the water comes down from top side of the plate and therefore its direction is normal to the air flow direction (design limitations) which may increase the experimental errors. Besides, some heat losses is always unavoidable during the experiments. Hence, in real working condition, it should be tried to provide the practical wet-surface as close as to the theoretical concept with novel ideas on water distribution mechanisms (as described before, in Wet-Surface theory, the wet plate is always thoroughly wet and water evaporation does not make it dry at all).

5. Sensitivity analysis

After the validation, the model was employed to clarify the impact of all operational and design parameters (presented in Table 4) on cooling characteristics of a two-stage M-cycle cooler. The impact of all parameters on outlet temperatures/humidity, wet-bulb and dew-point effectiveness (so-called dry-bulb effectiveness) are studied where wet-bulb and dew-point effectiveness are defined as $\frac{T_1^{'}-T_1^{''}}{T_1^{'}-T_{1,wb}^{'}}$ and $\frac{T_1^{'}-T_1^{''}}{T_1^{'}-T_{1,dp}^{'}}$ respectively. Refer to Fig. 5 to see the definition of design parameters.

5.1. Impact of operational parameters

Temperature, humidity, mass flow rate, mass flow ratios (ε_a and ε_b) are the main operational parameters of M-cycle cooler. The impact of said parameters on outlet temperature of primary air, outlet temperature of working air, outlet humidity of working air, wet-bulb effectiveness and dew-point effectiveness are evaluated and the results are provided in Figs. 10–12.

As shown in Fig. 10(a), increment of primary air inlet temperature ($T_1^{'}$) increases the outlet temperature of both primary air and working air which is logical. However, it is noted that the temperature difference between the inlet and outlet temperature of primary air ($T_1^{'} - T''_1$) has increased. In other words, the cooling capacity of M-cycle cooler is increased by increment of environment temperature (inlet temperature into the cooler). The increment slope of T''_1 (outlet of primary air) is more than the increment slope of T''_2 because of the higher evaporation rate in higher temperature. In other words, the portion of the heat (in working air) which is allocated to water evaporation (latent heat) increases with increment of air inlet temperature into the working channel and that is why the humidity ratio at at the outlet of the working channel has been increases by increment of $T_1^{'}$ as well. Actually, higher inlet temperature through the working channel increases the water evaporation rate along the wet channel.

Although the cooling capacity of the cooler has enhanced with increment of air inlet temperature, the wet-bulb effectiveness of the cooler has been decreased. It is noted that, although the value of $T_1^{'} - T''_1$ (numerator of effectiveness) increases with increment of $T_1^{'}$, the amount of $T_1^{'} - T_{1,wb}^{'}$ (denominator of effectiveness) increases as well with severer slope (as can be seen in Fig. 13) which leads to reduction of wet-bulb effectiveness. However, obtained curve behavior is not a constant rule. Generally, the effectiveness of the cooler may enhance, decrease or even remain constant with increment of air inlet temperature depending on other effective factors which can be seen in previous studies. For example, Fig. 9 in [11], Fig. 8 in [12] and Fig. 9 in [13] show that the increment of air inlet temperature reduces the amount of wet-bulb effectiveness while Fig. 10(c) in [14] shows a constant value of wet-bulb effectiveness for different values of air inlet temperatures. However, wet bulb effectiveness has increased with increment of air inlet temperature based on Fig. 11(a) in [15] (for relative humidity of 30%). In the same figure (Fig. 11 (a) in [15]), wet bulb effectiveness has reduced and remained constant with increment of air inlet temperature for humidity ratio of 50% and 70% respectively.

As shown in Fig. 10(b), increment of air inlet humidity ratio causes increment of outlet temperature of both primary air and working air which is predictable. Humidity ratio through the working channel has intensified as well. Indeed, higher inlet humidity reduces the heat absorbing capacity (latent heat) in the working channel. However, warmer outlet temperature at the outlet of primary channel does not mean smaller value of effectiveness as can be seen in Fig. 10(b). As was explained before by [16] (Fig. 14(b) in that paper), enhancement of wet bulb effectiveness with the increment of air inlet humidity can be explained by the nonlinearity of the saturation line (refer to Fig. 14(c) in

Table 3
Instruments used through the experiments.

Item	Type	Accuracy	Resolution
Air fan	TAFENG/D20R50	–	–
12-channel data logger	MTM-4208	0.5 °C	0.1 °C
Anemometer	YK-2004AH	5%	0.1 m/s
Humidity meter	YK-90HT	3%	0.01%
Water flow meter	ROTA-METER	0.5 LPM	0.5 LPM

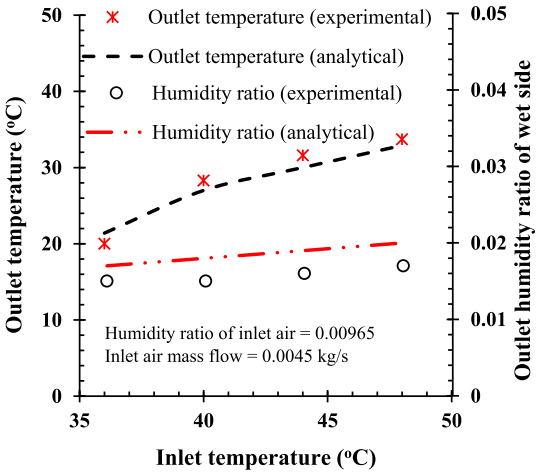

Fig. 9. Comparison between analytical results and experimental data.

[16]). Indeed, increment of air inlet humidity (for a constant air inlet temperature) increases its wet bulb temperature with nonlinearity behaviour (while increment of outlet air temperature is linear). Hence, increment of humidity of the inlet air reduces the numerator of effectiveness equation with linear behavior and denominator with nonlinearity trend which results in the increment of wet bulb effectiveness. It is mentioned that, other researches have provided other behaviour for the variation of wet-bulb effectiveness with inlet humidity. For instance, Fig. 10 (d) in [14] shows almost constant value of wet bulb effectiveness for different values of inlet air humidity. However, Fig. 18 (a) in [17] shows a descending and ascending trend for wet bulb effectiveness against inlet humidity for counter flow and cross flow heat exchanger respectively. Fig. 10 shows the effect of ε_a and ε_b on cooling characteristic of the cooler while the other parameters of the cooler are constant as shown in Table 4. As can be seen Fig. 11 (a), some peak points have been created through the curves of outlet temperature of the primary channel and working channel which can be discussed as following.

It is obvious that, any change of ε_a or ε_b directly impresses the value of Reynolds number in each part of channel. As can be seen in Fig. 5, whole cooler can be divided into four parts including $L_{a,1}$ (dry channel, section a), $L_{b,1}$ (dry channel, section b), $L_{a,2}$ (wet channel, section a) and $L_{b,2}$ (wet channel section b). The Reynolds number of said parts are shown with Re_{1La}, Re_{1Lb}, Re_{2La} and Re_{2La} respectively. Based on the Reynolds number criteria, the flow regime of each part can be laminar flow or turbulent flow. For each value of ε_a and ε_b the flow regime of each part is provided in Fig. 13 (b). Fig. 13 (a) shows an example curve behaviour extracted from Fig. 11. It is clear that, the flow regime through the channels justifies the curve trends of Fig. 11. For example, outlet temperature of working channel is increased with increment of $\varepsilon_a$in the range of $0.1 < \varepsilon_a < 0.3$ in which the flow regime through the all dry channel is turbulent and flow regime through the all wet channel is laminar. By further increment of ε_a, the Reynolds number of part $L_{a,2}$ changes to turbulent flow as well which causes a sudden reduction of outlet temperature of working channel. The reason of any peak point which is shown in Fig. 11 is the variation of flow regime through one or two parts of the cooler. Despite the ascending-descending behaviour of outlet temperatures, no sharp change was observed for effectiveness. Both wet-bulb and dew-point effectiveness increase with a small ascending slope for all value of air ε_a or ε_b which means that the numerator and denominator of effectiveness change with almost the same behaviour. Humidity ratio of working air is generally decreased with increment of ε_a or ε_b which is logical. Indeed, higher ε_a or ε_b increases the weight of existent dry air through the working channel which results in the reduction of working air humidity ratio. Fig. 12 illustrates the variation of cooling characteristics of the cooler against the primary air inlet mass flow rate. It is clear that, higher mass flow rate increases the outlet temperature of the dry channel (as the cooling capacity of the cooler is the same). Mass flow rate of the primary air does not show significant effect on the effectiveness and humidity ratio of working air.

5.2. Impact of design parameters

Channel gap (a), channel height (b), channel length (L) and the location of perforation (L_a/L) are the design parameters which are studied in present study (refer to Fig. 5 for definition of the design parameters). The range of all parameters was provided in Table 4. The impacts of “a”, “b” on cooling characteristics are presented in Fig. 14 and the impact of “L” and “ L_a/L” is illustrated on Fig. 15.

Based on Fig. 14 (a), increment of channel gap (a), increases (warmer) the outlet temperature of the cooler (both outlet temperature of primary channel and working channel) which is predictable. In a constant air inlet mass flow rate, increment of channel gap reduces the air velocity (Reynolds number) through the channels which results in the reduction of heat transfer rates between two channels. Humidity ratio through the working channel has been reduced which shows that the increment of channel gap reduces the water evaporation rate which is another reason for the reduction of heat transfer rate (latent heat). Both wet-bulb effectiveness and dew-point effectiveness has been reduced with increment of channel gap as well. Hence, it seems that, channel gap plays a key role in the improvement of the cooling capacity of the cooler.

Although, for a constant mass flow rate, increment of “b” reduces the air velocity and Reynolds number (negative feature) of the fluid flow, it increases the heat transfer area (positive feature). Hence, contrary to the channel gap, channel height does not impress sharply on cooling parameters. Nonetheless, higher value of “b” has provided colder outlet temperature and higher effectiveness which means that

Table 4
Sensitivity analysis, related parameters and their ranges.

		Operational parameters					Design parameters			
		T'_1 (°C)	W'_1 (g/kg)	$\dot{m}'_1$ (kg/s)	$\varepsilon_a = \frac{\dot{m}_1^A}{\dot{m}_1}$	$\varepsilon_b = \frac{\dot{m}_2^B}{\dot{m}_1}$	a (mm)	b (m)	L (m)	$\frac{L_a}{L}$
Impact of operational parameters	impact of T'_1	**25–55**	15	0.01	0.2	0.2	5	0.2	1	0.5
	impact of W'_1	45	**5–25**	0.01	0.2	0.2	5	0.2	1	0.5
	impact of $\dot{m}'_1$	45	15	**0.01–0.09**	0.2	0.2	5	0.2	1	0.5
	impact of ε_a	45	15	0.01	**0.1–0.7**	0.2	5	0.2	1	0.5
	impact of ε_b	45	15	0.01	0.2	**0.1–0.7**	5	0.2	1	0.5
Impact of design parameters	impact of a	45	15	0.01	0.2	0.2	**1–5**	0.2	1	0.5
	impact of b	45	15	0.01	0.2	0.2	5	**0.2–0.6**	1	0.5
	impact of L	45	15	0.01	0.2	0.2	5	0.2	**0.4–1.2**	0.5
	impact of $\frac{L_a}{L}$	45	15	0.03	0.2	0.2	5	0.2	1	**0.2–0.7**

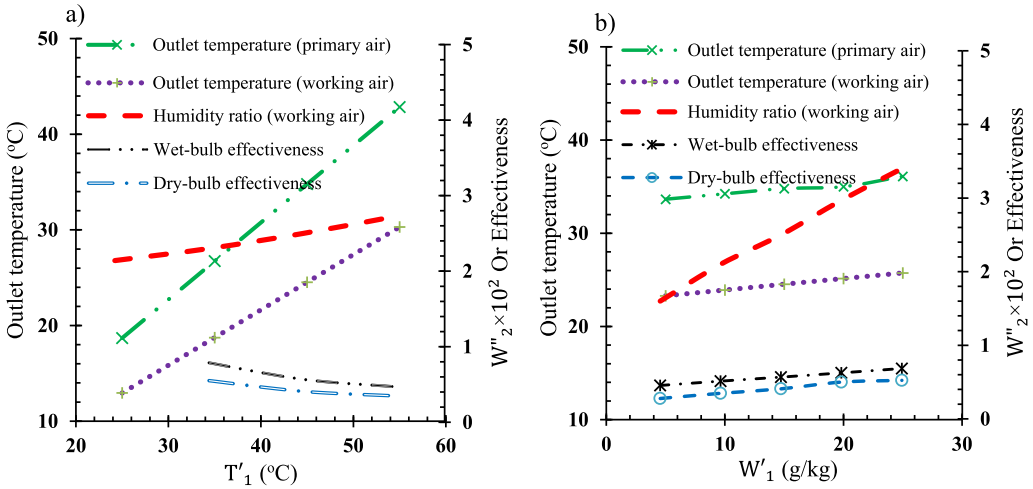

Fig. 10. (a) The impact of T'_1 on T''_1, T''_2, W''_2, wet-bulb effectiveness and dry-bulb effectiveness and (b) The impact of W'_1 on T''_1, T''_2, W''_2, wet-bulb effectiveness and dry-bulb effectiveness.

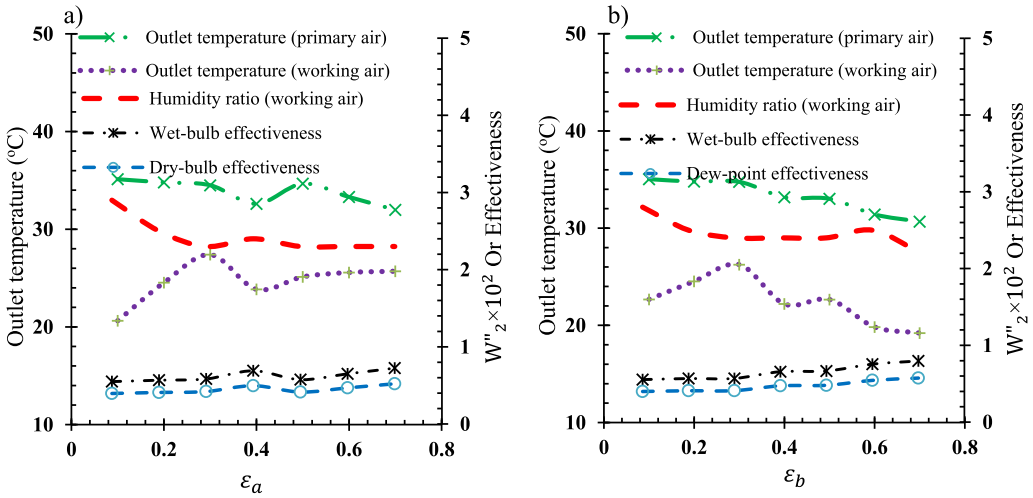

Fig. 11. (a) The impact of ε_a on T''_1, T''_2, W''_2, wet-bulb effectiveness and dry-bulb effectiveness and (b) the impact of ε_b on T''_1, T''_2, W''_2, wet-bulb effectiveness and dry-bulb effectiveness.

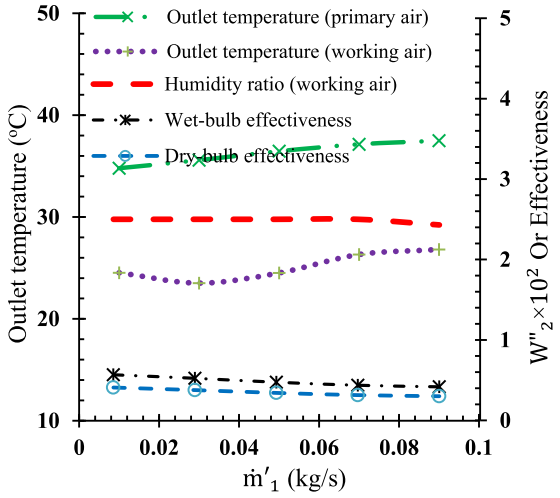

Fig. 12. (a) The impact of $\dot{m}'_1$ on T''_1, T''_2, W''_2, wet-bulb effectiveness and dry-bulb effectiveness.

the positive feature of the larger "b" overweight its negative feature. Humidity ratio of the working air is increased with increment of "b" which is due to the larger contact area between working air and wet plate. However, its increment slope is small because of the smaller air velocity in larger channel height.

As can be seen in Fig. 15 (a), larger channel length (in direction of fluid flow) reduces the outlet temperature of the cooler which its reason is larger heat transfer area again. The effect of channel length on outlet temperature is linear. Humidity ratio of the working air has been enhanced which means higher water evaporation. Higher water evaporation is because of the further residence time of the air fluid along the channel. Larger channel length has provided higher effectiveness as well. However, it is mentioned that, larger channel length makes the cooler bigger and heavier and the optimized value of channel length should be selected. The impact of the location of middle perforation (L_a/L) is provided in Fig. 15(b). Larger L_a/L means that the perforation is closer to the end of the product channel. Both outlet temperature of primary air and working air increase (warmer) and then decrease (colder) with increment of L_a/L. It is noted that, one of the important

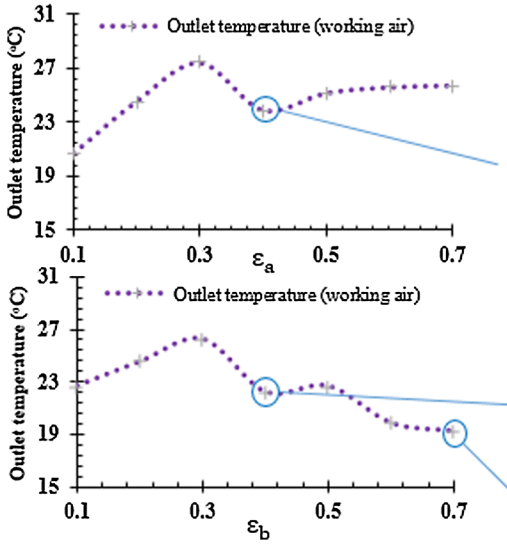

ε_a	Re1La	Re1Lb	Re2La	Re2Lb
$\varepsilon_a = 0.1$	Turbulent	Turbulent	Laminar	Laminar
$\varepsilon_a = 0.2$	Turbulent	Turbulent	Laminar	Laminar
$\varepsilon_a = 0.3$	Turbulent	Turbulent	Laminar	Laminar
$\varepsilon_a = 0.4$	Turbulent	Turbulent	Turbulent	Laminar
$\varepsilon_a = 0.5$	Turbulent	Laminar	Turbulent	Laminar
$\varepsilon_a = 0.6$	Turbulent	Laminar	Turbulent	Laminar
$\varepsilon_a = 0.7$	Turbulent	Laminar	Turbulent	Laminar

ε_b	Re1La	Re1Lb	Re2La	Re2Lb
$\varepsilon_b = 0.1$	Turbulent	Turbulent	Laminar	Laminar
$\varepsilon_b = 0.2$	Turbulent	Turbulent	Laminar	Laminar
$\varepsilon_b = 0.3$	Turbulent	Turbulent	Laminar	Laminar
$\varepsilon_b = 0.4$	Turbulent	Turbulent	Turbulent	Laminar
$\varepsilon_b = 0.5$	Turbulent	Turbulent	Turbulent	Laminar
$\varepsilon_b = 0.6$	Turbulent	Turbulent	Turbulent	Turbulent
$\varepsilon_b = 0.7$	Turbulent	Turbulent	Turbulent	Turbulent

Fig. 13. Flow regime of each part of the cooler based on Reynolds criteria.

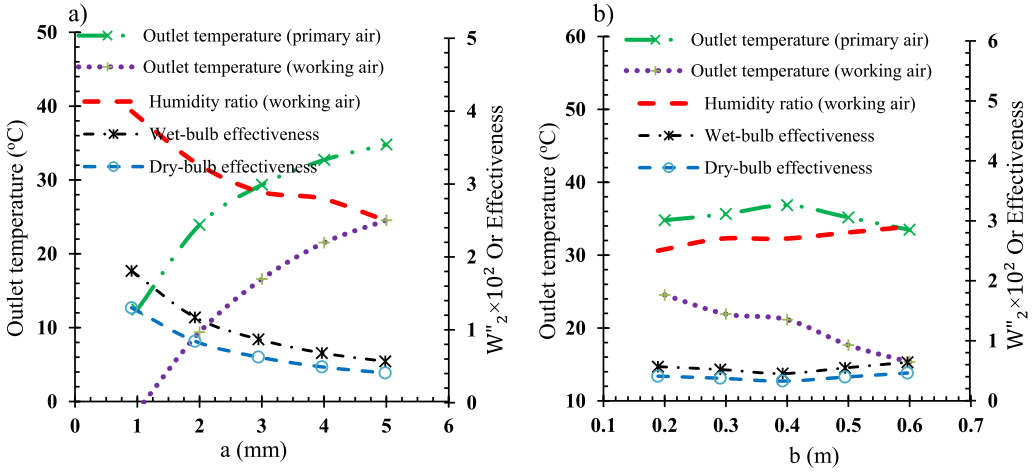

Fig. 14. (a) The impact of "a" on and "b" on cooling characteristics of the cooler.

advantages of perforated M-cycle cooler "compared to the single stage" is its smaller pressure drop. However, as in single stage M-cycle, the residence time of fluid in through both dry channel and working channel is higher (compared to the multi stage), its cooling capacity is better. That's why when the perforation of the present cooler (two-stage) is closer to the beginning or end of the channel it works similar to a single stage and provides colder outlet temperature. When the location of the perforation is closer to the end of the channel, larger length

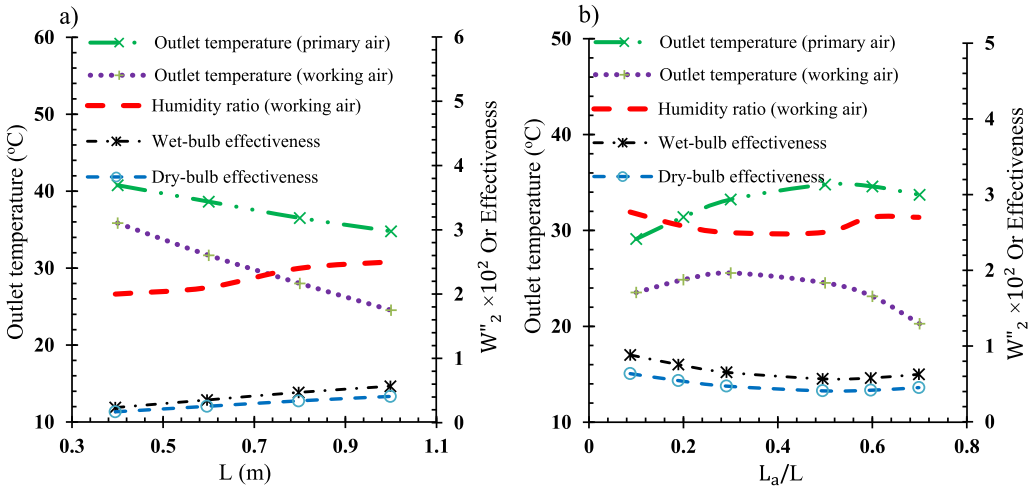

Fig. 15. (a) The impact of "L" and L_a/L on cooling characteristics of the cooler.

of the working channel deals with higher air flow rate (Reynolds number) and causes higher water evaporation and colder outlet temperature at the end of the working channel. If the perforation is placed in the middle of the plate, the outlet temperature of the dry side will be higher. However, it does not mean that the middle location is not appropriate because of the frictional parameter role. Generally, the designing process of the perforations should be performed based on both thermal and frictional characteristics.

6. Conclusion

A new analytical model has been developed for multi-stage M-cycle cooler in this paper based on novel wet-surface theory and then validated with a unique M-cycle test-rig. After validation, the impacts of key operational and design parameters on the performance of a two-stage M-cycle cooler were studied. The model works based on wet-surface theory in which the wet plate is continuously wet without water stream on the surface and the water evaporation does not make the wet surface dry i.e. the evaporated water is continuously replenished on the wet plate (practically, it requires a specific material for wet-plate which is able to absorb the water and keep itself wet while the evaporated water is replenished with a water flow rate as possible as small). The model is able to generate the temperature/humidity distribution through the channels. The effects of inlet temperatures, humidity, mass flow rate, mass flow ratio, channel gap, channel length, channel height and the location of perforation on the cooling performance of the cooler have been studied which can be employed as an optimization tool in either industrial sectors or academic researches as summarized below.

- Although the increment of the ambient temperature increases the outlet temperature of the product air (going to room), the obtained temperature-drop is enhanced which means increment of air cooling capacity for warmer ambient temperatures.
- Despite the increment of temperature-drop (cooling capacity) for warmer ambient temperatures, the wet-bulb effectiveness was reduced. Nonetheless, for other conditions, the wet-bulb effectiveness may enhance or remain constant with increment of ambient temperature as described in the paper.
- Changing of the discharged air into the wet channel, can increase or decrease the outlet product temperature depending on the created Reynolds number for each part of the cooler which varies based on mass flow ratios.
- Smaller channel gap provides colder outlet temperature with a sharp curve behavior. However, channel height does not impress the cooling capacity as severity as channel gap.
- By moving the middle perforation towards the end of the dry channel, the outlet temperature of product air is first increased and then decreased so that the maximum (warmer) temperature occurs when the perforation is in the middle of the channel.

Generally, the effect of each operational or design parameter may vary depending on the values of other parameters which were specified. Hence, the multiple optimization and simultaneous parameters variation are required to comprehensively clarify the behavior of M-cycle cooler.

CRediT authorship contribution statement

Hamed Sadighi Dizaji: Conceptualization, Data curation, Investigation, Methodology, Software, Validation, Writing - original draft. **Eric Jing Hu:** Supervision, Data curation, Writing - review & editing. **Lei Chen:** Supervision, Resources, Writing - review & editing. **Samira Pourhedayat:** Writing - review & editing, Validation, Data curation

Declaration of Competing Interest

The authors declare that they have no known competing financial interests or personal relationships that could have appeared to influence the work reported in this paper.

References

[1] Dizaji HS, Hu EJ, Chen L. A comprehensive review of the Maisotsenko-cycle based air conditioning systems. Energy 2018.
[2] Dizaji HS, Hu EJ, Chen L, Pourhedayat S. Development and validation of an analytical model for perforated (multi-stage) regenerative M-cycle air cooler. Appl Energy 2018;15(228):2176–94.
[3] Maclaine-Cross IL, Banks PJ. A general theory of wet surface heat exchangers and its application to regenerative evaporative cooling. J Heat Transfer 1981;103(3):579–85.
[4] Stoitchkov NJ, Dimitrov GI. Effectiveness of crossflow plate heat exchanger for indirect evaporative cooling: Efficacité des échangeurs thermiques à plaques, à courants croises pour refroidissement indirect évaporatif. Int J Refrig 1998;21(6):463–71.
[5] Alonso JS, Martinez FR, Gomez EV, Plasencia MA. Simulation model of an indirect evaporative cooler. Energy Build 1998;29(1):23–7.
[6] Chengqin R, Hongxing Y. An analytical model for the heat and mass transfer processes in indirect evaporative cooling with parallel/counter flow configurations. Int J Heat Mass Transf 2006;49(3):617–27.
[7] Hasan A. Going below the wet-bulb temperature by indirect evaporative cooling: analysis using a modified ε-NTU method. Appl Energy 2012;89(1):237–45.
[8] Liu Z, Allen W, Modera M. Simplified thermal modeling of indirect evaporative heat exchangers. HVAC&R Res 2013;19(3):257–67.
[9] Cui X, Chua KJ, Islam MR, Yang WM. Fundamental formulation of a modified LMTD method to study indirect evaporative heat exchangers. Energy Convers Manage 2014;31(88):372–81.
[10] Chen Y, Luo Y, Yang H. A simplified analytical model for indirect evaporative cooling considering condensation from fresh air: Development and application. Energy Build 2015;1(108):387–400.
[11] Cui X, Yang X, Sun Y, Meng X, Jin L. Energy efficient indirect evaporative air cooling. In: Advanced Cooling Technologies and Applications 2018 Nov 5. IntechOpen.
[12] Wan Y, Lin J, Chua KJ, Ren C. Similarity analysis and comparative study on the performance of counter-flow dew point evaporative coolers with experimental validation. Energy Convers Manage 2018;1(169):97–110.
[13] Min Y, Chen Y, Yang H. Numerical study on indirect evaporative coolers considering condensation: A thorough comparison between cross flow and counter flow. Int J Heat Mass Transf 2019;1(131):472–86.
[14] Pakari A, Ghani S. Comparison of 1D and 3D heat and mass transfer models of a counter flow dew point evaporative cooling system: Numerical and experimental study. Int J Refrig 2019;1(99):114–25.
[15] Zheng B, Guo C, Chen T, Shi Q, Lv J, You Y. Development of an experimental validated model of cross-flow indirect evaporative cooler with condensation. Appl Energy 2019;15(252):113438.
[16] Pandelidis D, Anisimov S. Numerical analysis of the heat and mass transfer processes in selected M-Cycle heat exchangers for the dew point evaporative cooling. Energy Convers Manage 2015;15(90):62–83.
[17] Rogdakis ED, Koronaki IP, Tertipis DN. Experimental and computational evaluation of a Maisotsenko evaporative cooler at Greek climate. Energy Build 2014;28(70):497–506.
[18] Shahzad MW, Burhan M, Ybyraiymkul D, Oh SJ, Ng KC. An improved indirect evaporative cooler experimental investigation. Appl Energy 2019;15(256):113934.
[19] Zhu G, Chen W, Lu S. Modelling of a dew-point effectiveness correlation for Maisotsenko cycle heat and mass exchanger. Chem Eng Process-Process Intensification 2019;1(145):107655.
[20] Chen Y, Yan H, Yang H. Comparative study of on-off control and novel high-low control of regenerative indirect evaporative cooler (RIEC). Appl Energy 2018;1(225):233–43.
[21] Zhan C, Zhao X, Smith S, Riffat SB. Numerical study of a M-Cycle cross-flow heat exchanger for indirect evaporative cooling. Build Environ 2011;46:657–68.
[22] Cui X, Islam MR, Mohan B, Chua KJ. Developing a performance correlation for counter-flow regenerative indirect evaporative heat exchangers with experimental validation. Appl Therm Eng 2016;5(108):774–84.
[23] Khafaji HQ, Ekaid AL, Terekhov VI. A numerical study of direct evaporative air cooler by forced laminar convection between parallel-plates channel with wetted walls. J Eng Thermophys 2015;24(2):113–22.
[24] Heidarinejad G, Moshari S. Novel modeling of an indirect evaporative cooling system with cross-flow configuration. Energy Build 2015;1(92):351–62.
[25] Moshari S, Heidarinejad G. Numerical study of regenerative evaporative coolers for sub-wet bulb cooling with cross-and counter-flow configuration. Appl Therm Eng 2015;5(89):669–83.
[26] Wan Y, Ren C, Wang Z, Yang Y, Yu L. Numerical study and performance correlation development on counter-flow indirect evaporative air coolers. Int J Heat Mass Transf 2017;1(115):826–30.
[27] Riangvilaikul B, Kumar S. An experimental study of a novel dew point evaporative cooling system. Energy Build 2010;42:637–44.
[28] Zhan C, Duan Z, Zhao X, Smith S, Jin H, Riffat S. Comparative study of the

performance of the M-cycle counter-flow and cross-flow heat exchangers for indirect evaporative cooling–paving the path toward sustainable cooling of buildings. Energy. 2011;36(12):6790–805.
[29] Zube D, Gillan L. Evaluating Coolerado Corportion's heat mass exchanger performance through experimental analysis. Int J Energy Clean Environ 2011;12(2–4).
[30] Gao WZ, Cheng YP, Jiang AG, Liu T, Anderson K. Experimental investigation on integrated liquid desiccant–Indirect evaporative air cooling system utilizing the Maisotesenko-Cycle. Appl Therm Eng 2015;5(88):288–96.
[31] Khalid O, Butt Z, Tanveer W, Rao HI. Design and experimental analysis of counter-flow heat and mass exchanger incorporating (M-cycle) for evaporative cooling. Heat Mass Transf 2017;53(4):1391–403.
[32] Khalid O, Ali M, Sheikh NA, Ali HM, Shehryar M. Experimental analysis of an improved Maisotsenko cycle design under low velocity conditions. Appl Therm Eng 2016;25(95):288–95.
[33] Duan Z, Zhao X, Zhan C, Dong X, Chen H. Energy saving potential of a counter-flow regenerative evaporative cooler for various climates of China: Experiment-based evaluation. Energy Build 2017;1(148):199–210.
[34] De Antonellis S, Joppolo CM, Liberati P, Milani S, Molinaroli L. Experimental analysis of a cross flow indirect evaporative cooling system. Energy Build 2016;1(121):130–8.
[35] Xu P, Ma X, Zhao X, Fancey K. Experimental investigation of a super performance dew point air cooler. Appl Energy 2017;1(203):761–77.
[36] Duan Z, Zhan C, Zhao X, Dong X. Experimental study of a counter-flow regenerative evaporative cooler. Build Environ 2016;1(104):47–58.

Chapter 5

Exergetic Study of M-cycle cooler

This chapter has been published as

Dizaji HS, Hu EJ, Chen L, Pourhedayat S. Comprehensive exergetic study of regenerative Maisotsenko air cooler; formulation and sensitivity analysis. Applied Thermal Engineering. 2019 Apr 1;152:455-67. (DOI: 10.1016/j.applthermaleng.2019.02.067).

This chapter evaluates the M-cycle cooler from the viewpoint of the second law of thermodynamics (Exergetic Study). The validated model Chapter 4 is employed to determine the outlet characteristics of the cooler and then the inlet and outlet characteristics are inserted to the exergetic model to evaluate the exergetic characteristics. The provided model is able to predict the exergetic characteristics of the M-cycle cooler successfully through the very short processing time (compared to the numerical simulation). Key operating and design parameters are varied to identify their impacts on exergetic factors of the M-cycle cooler. It is concluded that all geometric factors of the cooler should be selected through the optimisation process to minimise the exergy destruction of the cooling process.

Statement of Authorship

Title of Paper	Comprehensive exergetic study of regenerative Maisotsenko air cooler; formulation and sensitivity analysis
Publication Status	☑ Published ☐ Accepted for Publication ☐ Submitted for Publication ☐ Unpublished and Unsubmitted w ork w ritten in manuscript style
Publication Details	Dizaji HS, Hu EJ, Chen L, Pourhedayat S. Comprehensive exergetic study of regenerative Maisotsenko air cooler; formulation and sensitivity analysis. Applied Thermal Engineering. 2019 Apr 1;152:455-67. (DOI: 10.1016/j.applthermaleng.2019.02.067.

Principal Author

Name of Principal Author (Candidate)	Hamed Sadighi Dizaji		
Contribution to the Paper	Developing the mathematical model and performing the parametric and sensitivity analysis, writing the manuscript. Programming the model with Maple.		
Overall percentage (%)	70%		
Certification:	This paper reports on original research I conducted during the period of my Higher Degree by Research candidature and is not subject to any obligations or contractual agreements with a third party that would constrain its inclusion in this thesis. I am the primary author of this paper.		
Signature		Date	

Co-Author Contributions

By signing the Statement of Authorship, each author certifies that:

i. the candidate's stated contribution to the publication is accurate (as detailed above);

ii. permission is granted for the candidate in include the publication in the thesis; and

iii. the sum of all co-author contributions is equal to 100% less the candidate's stated contribution.

Name of Co-Author	Eric Hu		
Contribution to the Paper	Supervising the work, continuous recommendations and assistances through the developing process of the model. Review and editing of the manuscript.		
Signature		Date	

Name of Co-Author	Lei Chen		
Contribution to the Paper	Supervising the work, continuous recommendations and assistances through the developing process of the model. Review and editing of the manuscript.		
Signature	Ley Chen	Date	

Name of Co-Author	Samira Pourhedayat		
Contribution to the Paper	Assisting in the programming of the model.		
Signature		Date	

Applied Thermal Engineering 152 (2019) 455–467

Contents lists available at ScienceDirect

Applied Thermal Engineering

journal homepage: www.elsevier.com/locate/apthermeng

Research Paper

Comprehensive exergetic study of regenerative Maisotsenko air cooler; formulation and sensitivity analysis

Hamed Sadighi Dizaji*, Eric Jing Hu*, Lei Chen, Samira Pourhedayat

School of Mechanical Engineering, The University of Adelaide, Adelaide, SA 5005, Australia

HIGHLIGHTS

- A new exergetic analysis is provided for M-cycle cooler.
- Outlet characteristics of cooler is evaluated via analytical solution.
- Impact of all thermal/flow parameters on exergetic characteristics are discussed.
- Lower air flow rates provided higher exergetic efficiency.
- Higher air inlet temperature or flow rate increased exergy destruction.

ARTICLE INFO

Keywords:
Maisotsenko cycle
Exergy analysis
Air conditioner
M-cycle
Indirect evaporative

ABSTRACT

Great achievements have been made in the researches of thermal characteristics of Maisotsenko air cooler. However, a clear gap is still in existence on exergetic behaviour of M-cycle coolers. The significance of exergy analysis of M-cycle air coolers is highlighted when they were employed as a temperature reducer of intake air of gas-turbines in power plants to improve the efficiency of the system. Obviously, economic analysis of any thermodynamic system underlines the exergetic evaluations of the whole parts of the system which has been resulted in the emergence of professional expressions such as “exergoeconomic” and “thermoeconomic”. This paper reports a comprehensive exergetic formulation and analysis of regenerative M-cycle air cooler which can be employed in air conditioning industry and other applications of M-cycle cooler for better decision making. Higher inlet air mass flow rate, inlet air temperature and air flow ratio between two channels caused further exergy destruction. Exergetic efficiency of humid air is found more than the exergetic efficiency of dry air in M-cycle coolers. In order to prevent the severe exergy destruction through the cooler, the air velocity along the channels should not have large value. It is noted that, in the same total inlet air flow rate, the air velocity along the channels can be controlled by the numbers of the employed parallel plates in the designing process of M-cycle based on the second law of thermodynamics.

1. Introduction

The maximum useful work that can be obtained from a system as the system comes into equilibrium with the surrounding is termed exergy. Contrary to the energy, exergy can generate and destroy through a thermodynamic process. Exergy depends on the specifications of the external environment (such as temperature, chemical composition and electric potential). In other words, the availability of exergy is defined by the contrast between the thermodynamic system and its environment. Hence, higher difference between the system and its environment (in terms of temperature, gravitational, electrical or chemical potential) means greater exergy of the mentioned thermodynamic system. Moreover, different energy sources with identical energy potentials may have different values of exergy. The energy in the form of heat has less exergy than the same energy in the form of electricity (in an identical value). In other words, 1KJ of electrical energy exactly corresponds to 1KJ of exergy. Any irreversibility (such as finite temperature difference or heat transfer causes exergy destruction in the processes.

It is noted that, heat transfer is one of the major reasons of the exergy destruction. On the other hand, the main role of any heat exchanger (such as cooler) is heat transfer. Hence, it seems that, any improvement of thermal performance of heat exchangers (advantage) results in exergy destruction (disadvantage). Nonetheless, exergetic

* Corresponding authors.
E-mail addresses: HamedSadighiDizaji@gmail.com (H. Sadighi Dizaji), Eric.Hu@adelaide.edu.au (E.J. Hu).

https://doi.org/10.1016/j.applthermaleng.2019.02.067
Received 22 November 2018; Received in revised form 9 February 2019; Accepted 15 February 2019
Available online 18 February 2019
1359-4311/

Nomenclature

a	geometry in Fig. 3
b	geometry in Fig. 3
A	area (m^2)
c	specific heat (KJ/kg °C)
$c_{p,da}$	specific heat of dry air (KJ/kg °C)
c_v	specific heat of water vapor (KJ/kg °C)
d_h	hydraulic diameter (m)
e	specific exergy (KJ/kg)
e	constant in assumption 3
$\dot{E}x$	total exergy (KW)
F	defined in assumption 3
h	specific enthalpy of primary air
$h_f(T)$	enthalpy of saturated water at T
$s_f(T)$	entropy of saturated water at T
i_v	specific enthalpy of water vapor (KJ/kg)
i_{fg}	evaporation heat of water at 0 °C
c_f^*	$\frac{\dot{m}_1 c_1}{\dot{m}_2 c_a}$
c_w^*	$\frac{\dot{m}_w c_w}{\dot{m}_2 c_a}$
k_p	thermal conductivity of plate $_{(W/m^{2\circ}C)}$
L	length (m)
L_a, L_b	lengths in Fig. 3 (m)
Le	Lewis factor
NTU	number of heat transfer units
Nu	Nusselt number
P	pressure (Pas)
$p_{sat}(T)$	saturated water pressure at T
$P_{w,0}$	partial pressure of water at reference temperature
Pr	Prandtl Number
q	heat transfer rate (W)
Rd_a	specific ideal gas constant of air (KJ/kg K)
r	$\frac{UA_1}{\alpha_2 A_2}$
Re	Reynolds number
R_{cw}	$\frac{c_w}{c_a}$
R	thermal resistance (m^2 K/W)
$\dot{s}$	entropy generation (KW/K)
T	temperature (°C)
T_f	water film temperature (°C)
U	overall heat transfer coefficient (KW/m^2 °C)
V	velocity (m/s)
$\dot{m}$	mass transfer rate (kg/s)
P	atmospheric pressure of moist air
p_v	partial pressure of water vapor
R_v	specific ideal gas constant of water vapor
w_{eq}	humidity ratio of moist air in equilibrium with water surface (kg moisture/kg dry air)

Special characters

ε	mass transfer ratio between working and primary air
δ_p	thickness of the plate (m)
δ_w	thickness of water film (m)
α	convective heat transfer coefficient (KW/m^2 °C)
β	convective mass transfer coefficient (W/m K)
σ	wettability factor
ρ	density (kg/m^3)
ω	humidity ratio (kg moisture/kg dry air)
$\bar{\omega}$	mole fraction ration of air
Ψ	exergetic efficiency

Subscripts

des	destruction
in, da	inlet of dry air
in, w	inlet of water
out, da	outlet of dry air
out, ha	outlet of humid air
out, w	outlet of water
0	reference condition (25 °C)
1 or Pa	primary air (product air)
2 or wa	working air (secondary air)
f	water film
wb	wet-bulb
w	water
A, B	point A, B in Fig. 3

Superscripts

′	inlet
″	outlet

analysis of heat exchangers is required as one of the main components of energy production processes (in power plants). The exergy analysis of a whole power plant for example, provides information on useful accessible work which is consumed by the process.

Maisotsenko cycle (M-cycle) is an indirect evaporative mechanism which is employed to reduce the temperature of air fluid without adding humid to the product air. The application of M-cycle has been expanded to different engineering area including, cooling of electronic devices, air temperature reducer of gas turbines etc. Generally, a single unit of M-cycle comprises of two parallel channels one of which is wet channel (because of the sprayed water) and the other is dry channel. The air comes inside the cooler from the inlet of dry channel and its temperature is gradually reduced because of the latent and sensible heat transfer with wet channel (see Fig. 1 in Section 2). At the end of the dry channel, a portion of the cooled air is discharged into the wet channel. The enthalpy of discharged air (not necessarily its temperature) is continuously increased along the wet channel and finally goes to the surrounding (outside of the room). The outlet air from dry channel is employed as the product air. As there is no contact between primary air and water fluid, the humidity ratio of the primary air remains constant along the all cooling process.

Due to the widespread application of M-cycle cooling technology,

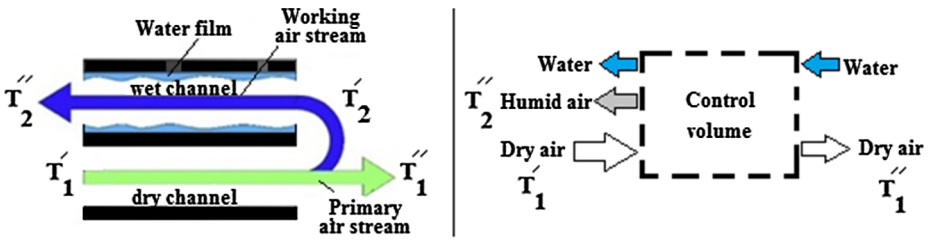

Fig. 1. Regenerative M-cycle cooler and related control volume.

great thermal researches (numerical, experimental and analytical) have been presented by many investigators. As the thermal evaluations of M-cycle is not the main aim of present research, the researches in this regard are briefly illustrated in Table 1. All thermal investigations of M-cycle was previously reviewed by Mahmood et al. [1] and recently by Sadighi Dizaji et al. [2]. The exergetic evaluations of indirect evaporative cooling is summarized in the following.

Caliskan et al. [3,4] studied the thermodynamic performance of a novel form of Maisotsenko coolers. They evaluated the effect of dead state condition on various thermodynamic parameters of M-cycle cooler. However, it seems that they have employed direct evaporative control volume for M-cycle cooler (which is indirect evaporative cooling). In other words, M-cycle cooler contains two input streams (dry air and water flow) and three output streams (dry air, humid air and water). They have not considered exergy output by dry air in their control volume and humid air is going inside the room (Fig. 1 in [3]). Eslamian [5] studied the cross flow M-cycle cooler using entropy generation minimisation analysis. Both tube type and plate type indirect evaporative coolers were investigated. Exergetic study of indirect evaporative cooling by CFD simulation was carried out by Chengqin [6]. Chen et al. [7] and Ren et al [8] showed that the exergetic efficiency of indirect evaporative cooling process is higher that the exergetic efficiency obtained in direct evaporative cooling process. Farmahini-Farahani et al. [9] experimentally investigated the exergetic characteristics of both direct and indirect evaporative coolers for different cities (climate conditions) of Iran. An independent fan was employed to provide the secondary air of indirect evaporative cooler (conventional indirect evaporative coolers) which means that it does not work based on M-cycle concept in which a portion of cooled outlet primary air is employed as the secondary air. Hence, obviously its exergetic behaviour will be different from M-cycle which is studied in present study.

The emergence of some professional expressions such as “exergoeconomic” or “thermoeconomic” implies the importance of exergetic analysis of any thermodynamic system. However, as described above, extremely few studies have been carried out for the evaluation of M-cycle technology from the view point of second law of thermodynamics. No investigation of the exergetic evaluation of regenerative M-cycle cooler and also no analytical sensitivity analysis of input thermal/fluid parameters on exergetic characteristics of M-cycle cooler have ever been reported. That is why a comprehensive exergetic analysis including formulation and sensitivity analysis are presented for regenerative Maisotsenko air cooler in this research. The required outlet specifications of cooler to calculate the exergetic parameters were obtained via thermal analytical solution of M-cycle cooler.

2. Formulations of exergetic characteristics

Fig. 1 shows a regenerative M-cycle cooler. The whole cooler is considered as a control volume as shown in Fig. 1. Inlet dry air and inlet water flow import exergy into the control volume. Outlet dry air (product air), outlet humid air (working air) and outlet water flow exit the exergy from the control volume. Hence, exergy balance for regenerative M-cycle cooler is illustrated as below.

$$\dot{E}x_{des} = \dot{E}x_{in} - \dot{E}x_{out} - \dot{E}x_{loss} \quad (1)$$

where $\dot{E}x_{des}$, $\dot{E}x_{in}$ and $\dot{E}x_{loss}$ are exergy destruction rate, total exergy input rate (by inlet dry air and inlet water flow) and total exergy output rate (by outlet dry air, outlet humid air and outlet water flow) and $\dot{E}x_{loss}$ is exergy losses rate. Hence, Eq. (1) can be rewritten as below.

$$\dot{E}x_{des} = [\dot{E}x_{in,da} + \dot{E}x_{in.w}] - [\dot{E}x_{out,da} + \dot{E}x_{out,ha} + \dot{E}x_{out.w}] - \dot{E}x_{loss} \quad (2)$$

where $\dot{E}x_{in,da}$ and $\dot{E}x_{in.w}$ are exergy input rate of dry air and exergy input rate of water. $\dot{E}x_{out,da}$, $\dot{E}x_{out,ha}$ and $\dot{E}x_{out.w}$ are exergy output rate of dry air, exergy output rate of humid air and exergy output rate of water flow respectively. Total exergies (E) are multiplication of mas flow rate and specific exergy ($E = \dot{m} \times e$). Thus, Eq. (2) is rewritten as Eq. (3).

$$\dot{E}x_{des} = [\dot{m}_{in,da}e_{in,da} + \dot{m}_{w,in}e_{w,in}] - [\dot{m}_{out,da}e_{out,da} + \dot{m}_{ha}e_{out,ha} + \dot{m}_{w,out}e_{w,out}] - \dot{E}x_{loss} \quad (3)$$

where $e_{in,da}$ and $e_{w,in}$ are specific input flow exergy of dry air. $e_{out,da}$, $e_{out,ha}$ and $e_{w,out}$ are specific output flow exergy of dry air, specific output flow exergy of humid air and specific output flow exergy of water flow respectively. Water outlet flow rate is calculated from $\dot{m}_{out,da} = \dot{m}_{w,in} - \dot{m}_{ha}(\omega_2'' - \omega_2')$. Specific flow exergy of any humid air (e_{ha}) at temperature (T) is calculated by Eq. (4). Indeed, as described by Shukuya et al. [41], the specific total flow exergy of humid air can be obtained by definition of the physical flow exergy applied to a mixture of ideal gases ([41] and Bejan, 1988 [42]).

Table 1
Numerical and experimental investigations of M-cycle coolers.

References	Studying on	Evaluation method
[10–12]	Effect of geometry on M-cycle performance	Numerical ε-NTU method
[13]	Effect of flow parameters on M-cycle performance	Numerical ε-NTU method
[14]	Comparison between eight types of Coolerado M-cycle coolers	Numerical ε-NTU method
[15–17]	Effect of flow/geometric parameters on M-cycle performance	Numerical finite element method
[18–20]	Cross flow configuration of M-cycle	Numerical finite difference method
[21,22]	General study on M-cycle	Numerical finite volume method
[23,24]	General study on M-cycle	Statistical tools (RSM)
[25]	General study on M-cycle	Statistical tools (Neural network)
[26]	Experimental research of a novel indirect evaporative air cooler	Experimental
[27]	Counter-flow and cross-flow configurations are compared with each other	Experimental
[28]	Analysis of a commercialized M-cycle cooler	Experimental
[29]	Application of liquid desiccant for M-cycle coolers	Experimental
[30]	Analysis of M-cycle air cooler under Greek climate condition	Experimental
[31]	Proposing and analysis of a counter flow exchanger for Maisotsenko coolers	Experimental
[32]	Studying of an modified Maisotsenko cooler under low velocity condition	Experimental
[33]	Analysis of M-cycle air cooler under china climate condition	Experimental
[34]	Investigation of the cross-flow exchanger of M-cycle	Experimental
[35]	Providing an innovative exchanger for Maisotsenko coolers	Experimental
[36]	Operational performance and impact factors of a counter-flow regenerative M-cycle	Experimental
[37]	Consideration of wettability factor on M-cycle exchangers	Experimental
[38]	Impact of dehumidification on cross-flow exchangers of Maisotsenko cooler	Experimental
[39]	Application of solid desiccant for cross flow exchangers of Maisotsenko cooler	Experimental
[40]	Analytical thermal solution of multi-stage M-cycle cooler	Analytical

$$e_{ha} = (c_{p,da} + \omega c_{p_v})T_0\left[\frac{T}{T_0} - 1 - \ln\frac{T}{T_0}\right] + (1+\bar{\omega})R_{da}T_0\ln\frac{p}{p_0} + R_{da}T_0[(1+\bar{\omega})\ln\frac{1+\bar{\omega}_0}{1+\bar{\omega}} + \bar{w}\ln\frac{\bar{\omega}}{\bar{\omega}_0}] \quad (4)$$

where $c_{p_{da}}$ is specific heat of dry air (1.003 KJ/kg K), ω is humidity ratio (specific humidity) which represents the number of kilograms of water to 1 kg of dry air in the given mixture, c_{p_v} is specific heat capacity of water vapor (1.872 KJ/kg K), T_0 is reference temperature (dead state temperature = 25 °C), T is dry-bulb temperature of air, $\bar{\omega}$ is mole fraction ratio of air which represents the number of moles of water corresponding to 1 mol of dry air in the given mixture ($\approx 1.608\,\omega$), Rd_a is specific ideal gas constant of dry air (0.287 KJ/kg K), P is pressure of air, p_0 is reference pressure (dead state pressure = 1 atm) and $\bar{\omega}_0$ is mole fraction ratio of the dead state condition ($1.608\,\omega_0 = 1.608\frac{0.622}{\left(\frac{p_0}{\varphi_0 P_{sat}(T_0)}\right)-1} = 0.0040$). Specific flow exergy of any dry air (e_{da})at temperature (T) is deduced by setting "ω" and "$\bar{\omega}$" to zero in Eq. (4). Therefore, specific flow exergy of dry air is evaluated from Eq. (5).

$$e_{da} = (c_{p,da})T_0\left[\frac{T}{T_0} - 1 - \ln\frac{T}{T_0}\right] + R_{da}T_0\ln\frac{p}{p_0} + R_{da}T_0\mathrm{Ln}(1+\bar{\omega}_0) \quad (5)$$

Specific flow exergy of liquid water (e_w) at temperature T is calculated by (Bejan, 1988 [42]):

$$e_w = h_f(T) - h_g(T_0) - T_0(s_f(T) - s_g(T_0)) + (p - p_{sat}(T))\upsilon_f(T) - R_vT_0\ln(\frac{P_{w,0}}{P_{sat(T_0)}}) \quad (6)$$

It is noted that, $\frac{P_{w,0}}{P_{sat(T_0)}}$ is $\varphi_0$and the value of $(p- p_{sat}(T))\upsilon_f(T)$ is negligible compared to the $R_vT_0\ln(\frac{P_{w,0}}{P_{sat(T_0)}})$. Hence, specific exergy of liquid water can be approximated via following correlation.

$$e_w = h_f(T) - h_g(T_0) - T_0(s_f(T) - s_g(T_0)) - R_vT_0\ln(\varphi_0) \quad (7)$$

where $h_f(T)$ is Enthalpy of saturated water at temperature T, $h_g(T_0)$ is Enthalpy of saturated water vapor at reference temperature, $s_f(T)$ is Entropy of saturated water at temperature T, $s_g(T_0)$ is Entropy (gas) of saturated water vapor at reference temperature, $p_{sat}(T)$ is Saturated water pressure at temperature T, $\upsilon_f(T)$ is specific volume rate of saturated water at temperature T, R_v is Specific ideal gas constant of water vapor (0.4165 KJ/kgK), $P_{w,0}$ is partial pressure of water at reference temperature. Moreover, $\dot{E}x_{loss}$ in Eq. (3) is evaluated from Eq. (8) [4].

$$\dot{E}x_{loss} = \dot{Q}_{cooling}(1 - \frac{T_0}{T_1'}) \quad (8)$$

$$\dot{Q}_{cooling} = \dot{m}_{out,da}(h_{in,da} - h_{out,da}) \quad (9)$$

Specific enthalpy of primary air (dry air) is calculated from Eqs. (10) and (11) in inlet and outlet ($h_{in,da}$and$h_{out,da}$).

$$h_{in,da} = (c_a + \omega_1'c_\upsilon)T_{in,da} + \omega_1'h_{fg} \quad (10)$$

$$h_{in,da} = (c_a + \omega_1'c_\upsilon)T_{out,da} + \omega_1'h_{fg} \quad (11)$$

According to Eqs. (4)–(6), specific exergy of dry air (inlet and outlet), humid air (outlet) and water flow (inlet and outlet) in Eq. (3) are evaluated via below correlations.

$$e_{in,da} = c_{p_{da}}T_0\left[\frac{T_1'}{T_0} - 1 - \ln\frac{T_1'}{T_0}\right] + R_{da}T_0\ln\frac{p_1'}{p_0} + R_{da}T_0\ln(1+\bar{\omega}_0) \quad (12)$$

$$e_{out,da} = c_{p_{da}}T_0\left[\frac{T_1''}{T_0} - 1 - \ln\frac{T_1''}{T_0}\right] + R_{da}T_0\ln\frac{p_1''}{p_0} + R_{da}T_0\ln(1+\bar{\omega}_0) \quad (13)$$

$$e_{out,ha} = (c_{p_{da}} + \omega_2''c_{p_v})T_0\left[\frac{T_2''}{T_0} - 1 - \ln\frac{T_2''}{T_0}\right] + (1+\overline{\omega_2''})R_{da}T_0\ln\frac{p_2''}{p_0} + Rd_aT_0[(1+\omega_2'')\ln\frac{1+\bar{\omega}_0}{1+\overline{\omega_2''}} + \overline{\omega_2''}\ln\frac{\overline{\omega_2''}}{\bar{\omega}_0}] \quad (14)$$

$$e_{w,in} = h_f(T_{w,in}) - h_g(T_0) - T_0(s_f(T_{w,in}) - s_g(T_0)) - R_vT_0\ln(\varphi_0) \quad (15)$$

$$e_{w,out} = h_f(T_{w,out}) - h_g(T_0) - T_0(s_f(T_{w,out}) - s_g(T_0)) - R_vT_0\ln(\varphi_0) \quad (16)$$

The ratio of exergy destruction to dead state is termed entropy generation ($\dot{s}$) and is evaluated via Eq. (17). The Exergetic efficiency of M-cycle cooler is defined as Eq. (18). A brief view of exergetic calculations is schematically shown in Fig. 2 (relative humidity, temperature

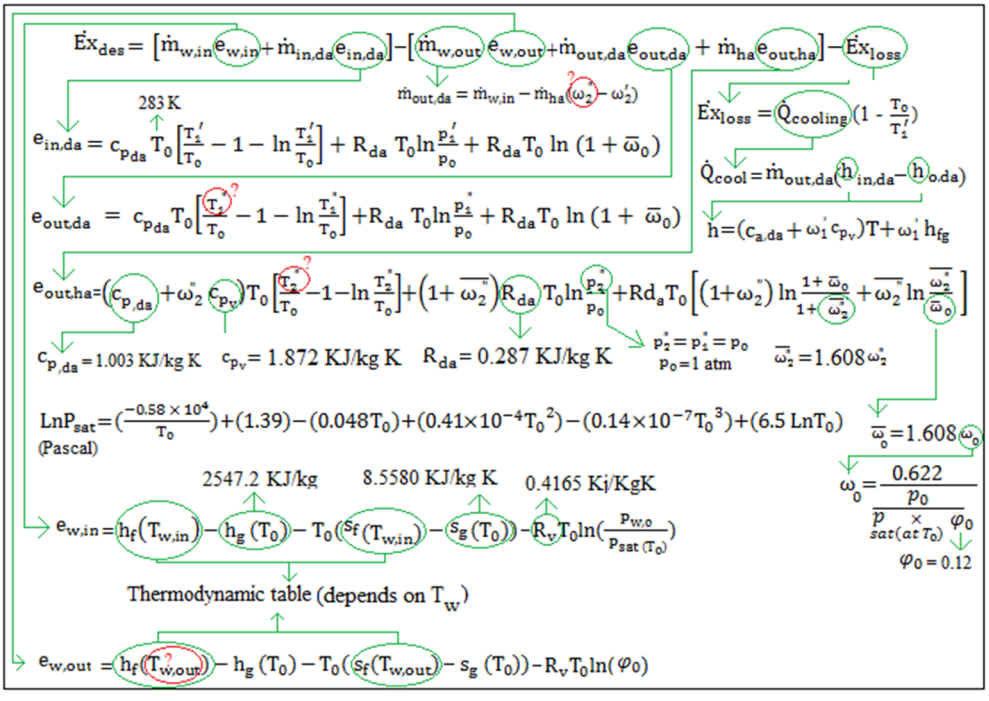

Fig. 2. A brief view of exergetic formulation of exergy destruction.

and pressure of dead state condition are 0.12, 273 K and 1Atmosfere respectively).

$$\dot{s} = \frac{\dot{E}x_{des}}{T_0} \tag{17}$$

$$\Psi = \frac{\dot{E}x_{out}}{\dot{E}x_{in}} \tag{18}$$

As shown in Fig. 2, calculation of exergetic characteristics of M-cycle cooler depends on only inlet and outlet parameters (including inlet/outlet temperature and humidity). Although inlet parameters of any given cooler are available, the outlet characteristics of the cooler (T''_2, w''_2, T''_1 and $T_{w,out}$) are not available. Hence, in order to provide a sensitivity exergetic analysis of M-cycle cooler (by changing of inlet/geometric/flow parameters), the outlet parameters should be calculated for any value of input parameters. Outlet characteristics (which is related to thermal analysis) are calculated via analytical solution presented in appendix A. As explained in the appendix A, the analytical thermal model of regenerative M-cycle results in following non-homogeneous system of first order linear differential equations with constant coefficients (Eq. (18)) that can be solved analytically via different methods such as Euler method or Laplace transformations technique. The model was developed with below assumptions for M-cycle cooler shown in Fig. 3.

Assumptions.

1. No thermal diffusivity parallel to the flow direction and cooler is insulated
2. Heat/mass transfer coefficients are constant along the exchanger
3. "w_{eq}" has a linear function with water surface temperature ($w_{eq} = F + eT_w$)
4. The system works on wet-surface mechanism which means that water mass flow rate is negligible compare to the air flow rate ($\dot{m}_w << \dot{m}_2$) which results in variant wet-wall temperature.
5. The plate is completely wetted ($\sigma = 1$) and Lewis factor is satisfied which means $\frac{\sigma}{Le_f} = 1$.

$$\text{Differential equations} \begin{cases} \frac{dT_1}{d\bar{x}_1} = G + Hw_2 + IT_2 + JT_1 \\ \frac{dT_2}{d\bar{x}_1} = K + Lw_2 + MT_2 + NT_1 \,|0<\bar{x}_1 < 1 \\ \frac{dW_2}{d\bar{x}_1} = O + Zw_2 + VT_2 + QT_1 \end{cases} \tag{18}$$

$$\text{Boundary conditions} \begin{cases} T_1(\bar{x}_1 = 0) = T_{inlet} = T'_1 \\ T_2(\bar{x}_1 = 1) = T_1(\bar{x}_1 = 1) \\ W_2(\bar{x}_1 = 1) = W_1(\bar{x}_1 = 1) \end{cases} \tag{19}$$

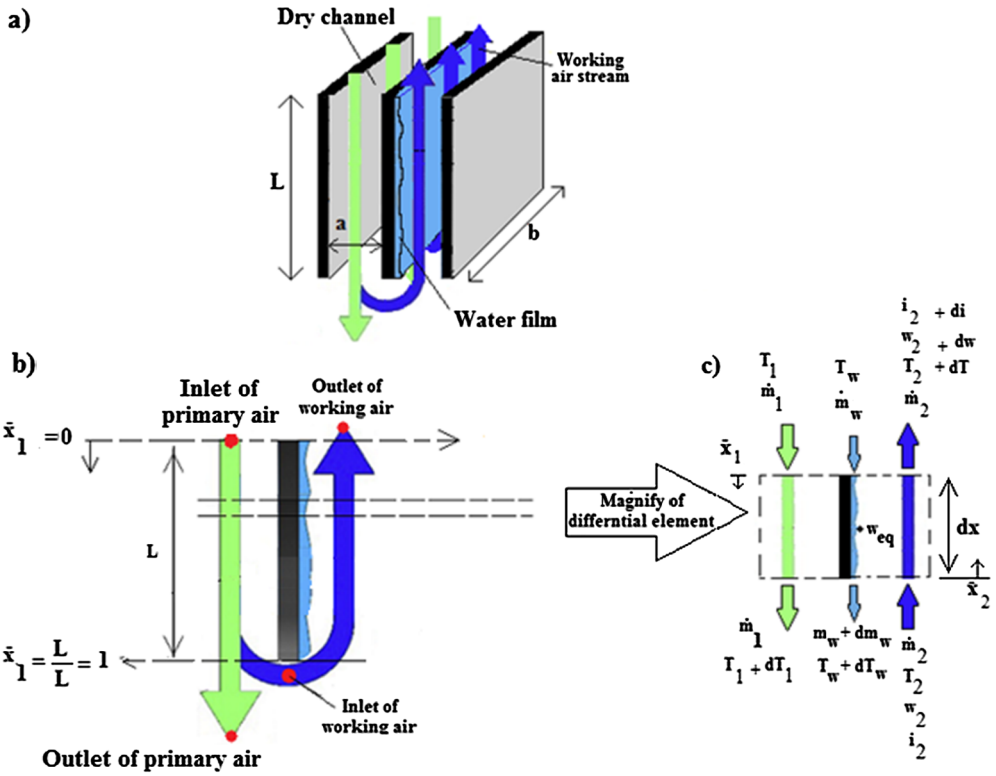

	Inlet of Primary air	Outlet of Primary air	Inlet of working air	Outlet of working air
Temperature	T'_1	T''_1	$T'_2 = T''_1$	T''_2
Humidity ratio	W'_1	$W''_1 = W'_1$	$W'_2 = W''_1 = W'_1$	W''_2
Mass flow rate	$\dot{m}'_1$	$\dot{m}''_1 = \dot{m}'_1(1-\varepsilon)$	$\dot{m}'_2 = \varepsilon\,\dot{m}'_1$	$\dot{m}''_2 = \varepsilon\,\dot{m}'_1$

Fig. 3. Schematic view of regenerative M-cycle cooler.

$$\text{Constants}\begin{cases} G=\frac{-r}{C_f^*(r+\eta)}NTU\,\bar{i}_{fg}F, \quad H=\frac{r}{C_f^*(r+\eta)}NTU\,\bar{i}_{fg} \\ I=\frac{r}{C_f^*(r+\eta)}NTU, \quad J=\frac{-r\eta}{C_f^*(r+\eta)}NTU \\ K=\bar{i}_{fg}\frac{F}{(r+\eta)}NTU, \quad L=\bar{i}_{fg}\frac{-1}{(r+\eta)}NTU \\ M=\frac{-(1-r-\eta)}{(r+\eta)}NTU, \quad N=\frac{-r}{(r+\eta)}NTU \\ O=F\left(\bar{i}_{fg}-\frac{r+\eta}{e}\right)\frac{e}{(r+\eta)}NTU, \quad Z=(\bar{i}_{fg}-\frac{r+\eta}{e})\frac{-e}{(r+\eta)}NTU \\ V=\frac{-e}{(r+\eta)}NTU, \quad Q=\frac{-er}{(r+\eta)}NTU \end{cases} \tag{20}$$

For any given cooler, the values of all constant coefficients (G, …, L) in Eq. (18) can be calculated with input parameters. The analysis procedure (and cooler characteristics) is shown in Table 2. It is noted that, inlet temperature and humidity ratio are related to boundary conditions and do not have effect on the values of constant coefficients (G, …, L).

A general brief view of the exergetic analysis process of M-cycle is shown in Fig. 4. As was described, inlet and outlet parameters of cooler (including inlet/outlet temperatures and humidity) are required to evaluate the exergetic characteristics of M-cycle and therefore the outlet parameters are calculated first by analytical solution from given inlet parameters (for a given cooler) and then the exergetic characteristics are calculated using inlet and obtained outlet parameters. The process is repeated with new values of inlet parameters to provide exergetic sensitivity analysis.

3. Solvation and sensitivity exergetic analysis

3.1. Effect of air inlet temperature and humidity ratio

In this section, the inlet air temperature/humidity are varied while all other parameters are constant (as shown in Table 2) and the effect of inlet air temperature/humidity on exergetic parameters are studied and discussed.

If the required constant coefficients (Eq. (20)) are evaluated for the first/second raw of Table 2, the Eqs. (18) and (19) will be transformed in the form of Eq. (21). It is noted that, inlet temperature and humidity do not have effect of the values of constant coefficients and they related to boundary conditions only. Hence, Eq. (21) will be solved for a boundary condition in which the value of air inlet temperature and humidity are variant parameters (see Eq. (22)). In other words, air inlet temperature and humidity in boundary conditions are substituted by parameter T'_1 and W'_1 respectively and outlet characteristics are obtained as the functions of mentioned parameters. Any arbitrary value of T'_1 and W'_1 can be then replaced in final outcome.

$$\text{Differential equations}\begin{cases} \frac{dT_1}{d\bar{x}_1}=-6.83+247.26w_2+0.1T_2-0.51T_1 \\ \frac{dT_2}{d\bar{x}_1}=6.5-235w_2+0.8T_2+0.4T_1 \\ \frac{d\omega_2}{d\bar{x}_1}=-0.013+0.5\omega_2-0.00015T_2-0.00067T_1 \end{cases}$$
$$|0<\bar{x}_1<1 \tag{21}$$

$$\text{Boundary conditions}\begin{cases} T_1(\bar{x}_1=0)=T'_1 \\ T_2(\bar{x}_1=1)=T_1(\bar{x}_1=1) \\ \omega_2(\bar{x}_1=1)=\omega_1(\bar{x}_1=1)=0.01 \end{cases} \tag{22}$$

If the Eq. (21) is solved (via analytical methods, Maple software was employed), temperature of primary air (T_1), temperature of working air T_2 and humidity of working air (W_2) are achieved as the functions of $\bar{x}_1$ (see appendix B for the answer of Eq. (21)). As only the inlet/outlet characteristics are required for exergetic evaluations, $\bar{x}_1=0$ or $\bar{x}_1=1$ is replaced in the said functions which results in Eq. (23) (it is noted that the outlet characteristics are occurred at $\bar{x}_1=0$ for working air and at$\bar{x}_1=1$ for working air (see Fig. 3(b)).

As described above, by replacing $\bar{x}_1=0$ or $\bar{x}_1=1$ in those functions, final equations (outcome) of outlet characteristics are obtained as shown in the following equation.

$$\text{Results (outlets)}\begin{cases} T''_1=0.67T'_1+178.34W'_1-4.99 \\ T''_2=0.11T'_1+189.69W'_1-5.33 \\ \omega''_2=0.00048T'^{2}_1+0.67W'_1+0.0083 \end{cases} \tag{23}$$

The outlet characteristics for any value of inlet air temperature and inlet air humidity are available now, ant it is possible to analyze the effect of air inlet temperature/humidity on exergetic parameters. The value of $e_{in,da}$, $e_{out,da}$, $e_{out,ha}$ and $\dot{E}x_{loss}$ in Eq. (3) are evaluated using Eqs. (12)–(14) and Eq. (8) respectively. It is noted that, the obtained unit of temperature in Eq. (23) is Celsius (temperature units in exergy correlations (Eqs. (12)–(14)) is Kelvin). If the correlation of all parameters are replaced in Eq. (3) the below total correlation is obtained.

$$\begin{aligned} \dot{E}x_{des}=&\{\dot{m}_{in,da}[c_{p_{da}}T_0(\frac{T'_1}{T_0}-1-\ln\frac{T'_1}{T_0})+R_{da}T_0\ln\frac{p'_1}{p_0}+R_{da}T_0\ln(1+\bar{\omega}_0)]\} \\ &+\{\dot{m}_{in,w}[h_f(T_{w,in})-h_g(T_0)-T_0(s_f(T_{w,in})-s_g(T_0)) \\ &-R_vT_0\ln(\varphi_0)]\}-\{\dot{m}_{out,da}[c_{p_{da}}T_0(\frac{T''_1}{T_0}-1-\ln\frac{T''_1}{T_0})+R_{da}T_0\ln\frac{p''_1}{p_0} \\ &+R_{da}T_0\ln(1+\bar{\omega}_0)]\}-\{\dot{m}_{ha}[(c_{p,da}+\omega''_2c_{p_v})T_0(\frac{T''_2}{T_0}-1-\ln\frac{T''_2}{T_0}) \\ &+(1+\overline{\omega''_2})R_{da}T_0\ln\frac{p''_2}{p_0}+Rd_aT_0((1+\omega''_2)\ln\frac{1+\bar{\omega}_0}{1+\overline{\omega''_2}}+\overline{\omega''_2}\ln\frac{\overline{\omega''_2}}{\bar{\omega}_0})]\} \\ &-\{\dot{m}_{out,w}[h_f(T_{w,out})-h_g(T_0)-T_0(s_f(T_{w,out})-s_g(T_0) \\ &-R_vT_0\ln(\varphi_0)]\}-\{\dot{m}_{out,da}(h_{in,da}-h_{out,da})(1-\frac{T_0}{T'_1})\} \end{aligned} \tag{24}$$

If the final value of each parameter is substituted (using Fig. (2), Eq. (23) and Table 2), the value of $\dot{E}x_{des}$ is obtained for any input value of T'_1 or W'_1 shown in Fig. 5 (input values of T'_1 and W'_1 can be seen in Table 2.

According to Fig. 5, increment of inlet air temperature increases the value of exergy destruction. Contrary to inlet temperature, increment of air inlet humidity reduces the exergy destruction of M-cycle cooler. Based on previous researches, the thermal performance of Maisotsenko coolers in hot-dry weathers is better which means that the temperature reduction of primary air through dry channel (and working air through wet-channel) is increased with increment of inlet air temperature. Fig. 6(a) shows the temperature reduction of primary air and working air for different values of inlet air temperature. It is clear that, the M-

Table 2
Exergetic procedure of regenerative M-cycle (variant parameters are bold).

	Thermal/flow parameters				Geometric parameters		
	T'_1 (°C)	W'_1 (kg/g)	$\dot{m}'_1$ (kg/s)	ε	a (mm)	b (m)	L (m)
Impact of T'_1	***25–60***	10	0.009	0.25	5	0.2	1
Impact of W'_1	40	***5–25***	0.009	0.25	5	0.2	1
Impact of $\dot{m}'_1$	40	10	**0.01–0.09**	0.25	5	0.2	1
Impact of ε	40	10	0.009	***0.25–0.75***	5	0.2	1

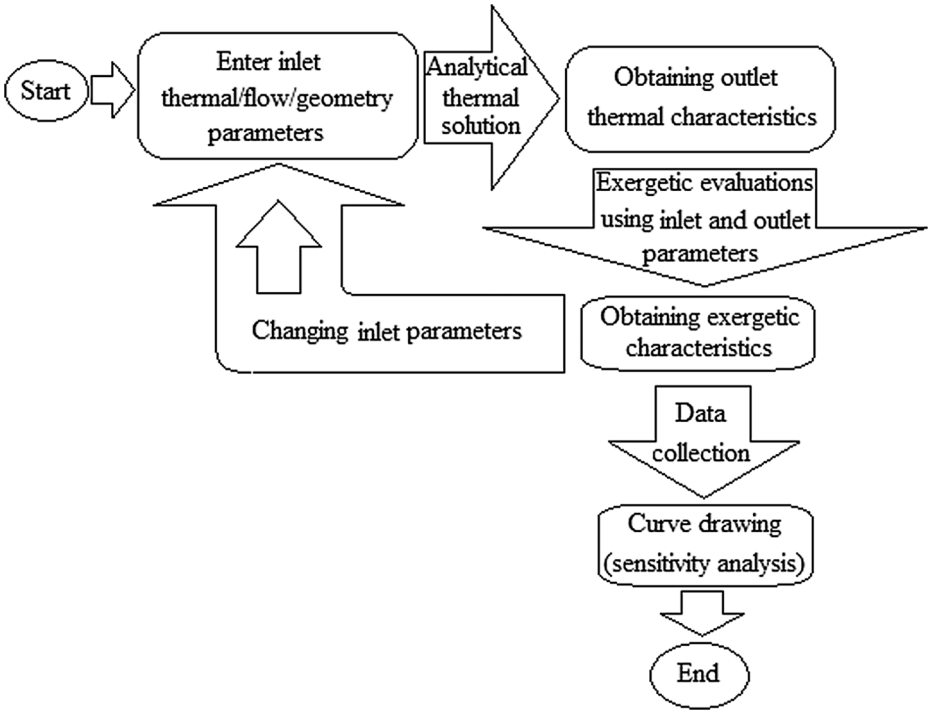

Fig. 4. A brief general view of exergetic analysis procedure.

cycle cooler can further decrease the air temperature for higher air inlet temperature. It can be concluded that, the average temperature difference between two channels (dry and wet channel) is increased by increment of air inlet temperature. The mentioned average temperature difference between two channels ($\frac{(T_{dry,inlet}+T_{dry,outlet})}{2}-\frac{(T_{wet,inlet}+T_{wet,outlet})}{2}$) is provided in Fig. 6(b). As the finite temperature difference is one of the main reasons of exergy destruction in any thermodynamic process, mentioned temperature difference has been caused further exergy destruction in M-cycle coolers. Although the M-cycle thermal efficiency is higher for warmer weathers, exergetic efficiency behaves vice versa which shows the importance of exergetic evaluation in addition to the first law analysis.

Based on Fig. 5(b), higher humidity ratio reduces the exergy destruction during the cooling process. In addition to the finite temperature difference which was discussed as one of the reasons of exergy destruction, humidity and water flow are other key factors of exergy transfer and destruction (see Eq. (3)) through the cooler. However, they do not seem independent from temperature role. In other words, humidity and water flow influence the temperature distribution which is the reason of exergy destruction. Variation of "exergy output by humid air" ($\dot{E}x_{out,ha}$) and "exergy output by water flow" ($\dot{E}x_{out.w}$) with air inlet humidity are presented in Fig. 7(a). Higher humidity ratio causes higher $\dot{E}x_{out,ha}$ and $\dot{E}x_{out.w}$which means that lower amount of input exergy by fluids has interfered in heat/mass transfer (which results in smaller exergy destruction). It is noted that, higher humidity of inlet air reduces the water evaporation rate in the wet channel which increases the water outlet mass flow rate (because a higher percentage of inlet

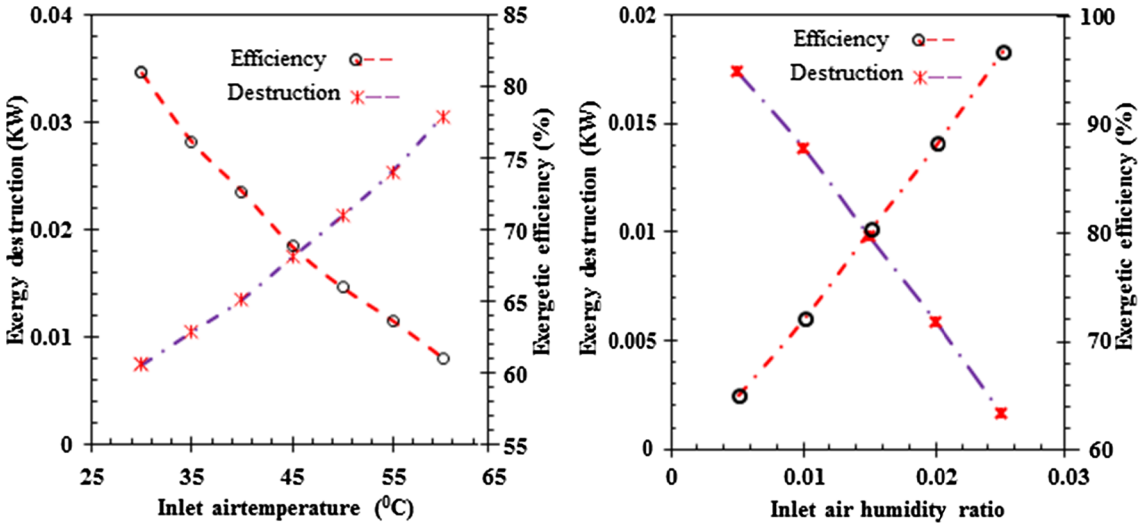

Fig. 5. (a) Variation of exergy destruction with inlet air temperature and (b) variation of exergy destruction with inlet air humidity ratio.

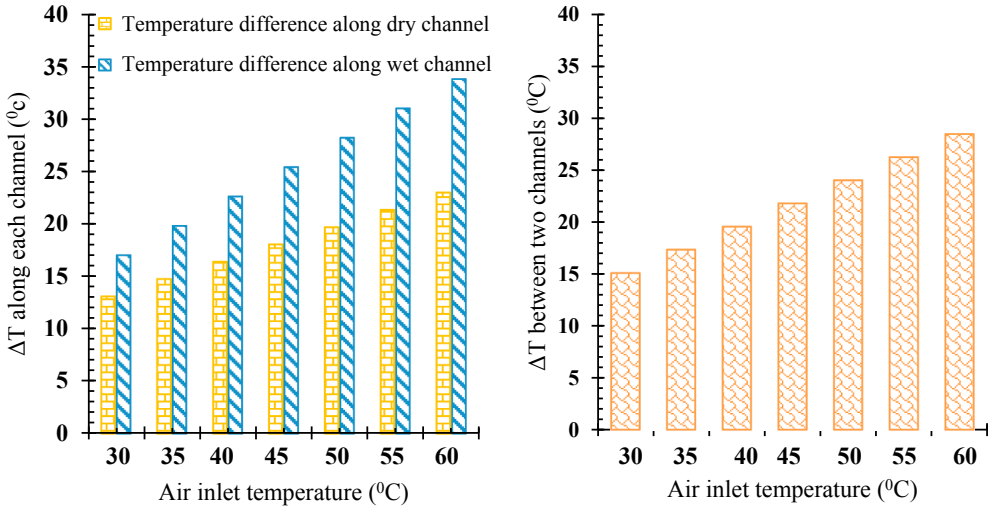

Fig. 6. (a) Temperature reduction along each channel and (b) Average temperature difference between two channels.

water flow rate leave the cooler without interfering in evaporation process, (Fig. 7(b) shows the outlet water flow rate against air inlet humidity). Obviously, reduction of water evaporation means poor heat transfer rate and consequently less exergy destruction.

As can be seen in Fig. 5, the curve trends of the exergetic efficiency and exergy destruction are vice versa (in both the impact of inlet temperature and impact of inlet humidity). In other words, increment of air inlet temperature increases the exergy destruction but it decreases the exergetic efficiency. Moreover, higher inlet humidity reduces the exergy destruction and provides higher exergetic efficiency. As described above and based on Eq. (1), higher exergy destruction means smaller value of $\dot{E}x_{out}$. Indeed, as the exergy of input air fluid is destructed along the cooler, the exergy of outlet fluid is less than the inlet fluid and that is why higher exergy destruction means smaller value of $\dot{E}x_{out}$. On the other hand, according to definition of the exergetic efficiency (Eq. (18)), reduction of $\dot{E}x_{out}$ reduces the exergetic efficiency and increment of $\dot{E}x_{out}$ increases the exergetic efficiency. Irrespective to the formula justification, it is clear that the exergy destruction implies a negative concept while the exergy efficiency induce a positive feature. Thereupon, any reason of exergy destruction causes reduction of exergetic performance.

3.2. Effect of air mass flow rate ($\dot{m}$) and air mass flow ratio (ε)

In this section, the inlet air mass flow rate or air mass flow ratio are varied while all other parameters are constant as was shown in Table 2. Similar to previous section, Eq. (18) should be solved for any value of mass flow rate of mass flow ratio in order to fined outlet characteristics of the cooler. It is noted that, as the value of mass flow rate and mass flow ratio affects the values of constants coefficients of Eq. (18), that equation (Eq. (18)) should be solved for each value of mentioned parameters separately which causes longer calculation process.

The effect of inlet air mass flow rate and mass flow ratio between two channels are shown in Fig. 8. It is clear that the increment of both mass flow rate and mass flow ratio increases the exergy destruction through the cooler. Subsequently, exergetic efficiency is reduced by enhancement of mentioned parameters. It is mentioned that the slope of exergy destruction due to the increment of mas flow ratio is reduced after $\varepsilon = 0.25$ (see Fig. 8(b)). In order to clarify the increment reason of exergy destruction due to the increment of mass flow rate or mass flow ratio, the exergy output by dry air and exergy output by humid air are determined separately in Fig. 9. According to Fig. 9 all effective parameters in total exergy destruction i.e. $E_{in,da}$, $E_{out,da}$ and $E_{out,ha}$ are

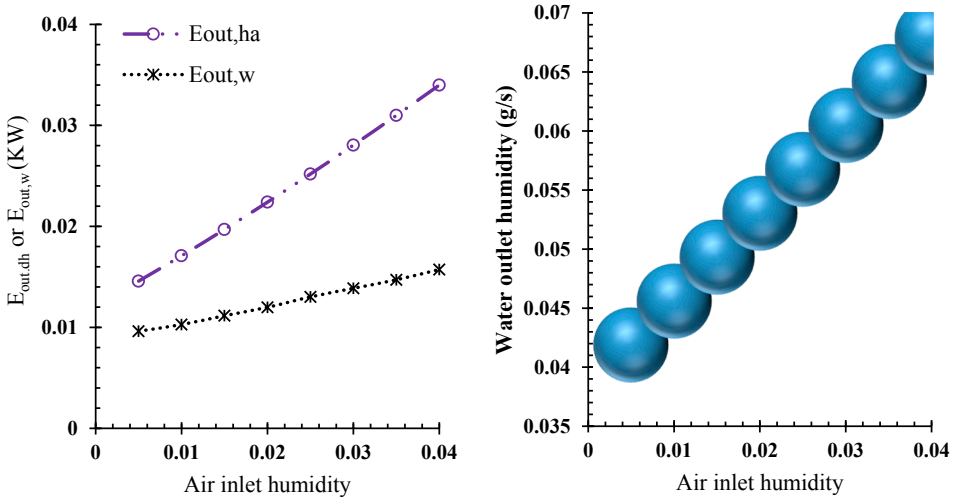

Fig. 7. (a) Variation of $\dot{E}x_{out,ha}$ and $\dot{E}x_{out.w}$ with air inlet humidity.

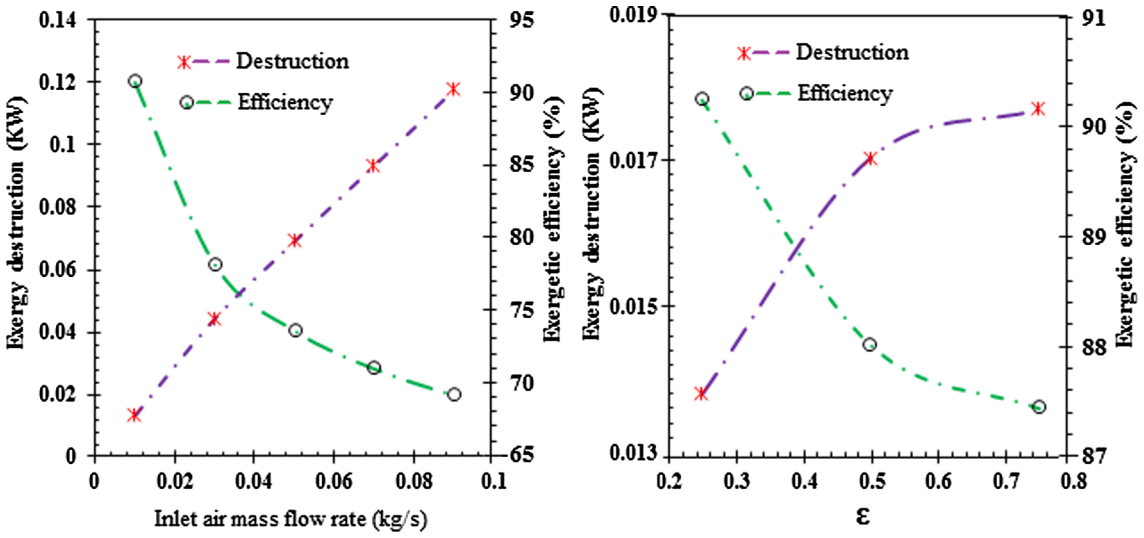

Fig. 8. Effect of air inlet mass flow rate and mass flow ratio on total exergy destruction.

enhanced by increment of air inlet mass flow rate. However, the enhancement slope of $E_{in,da}$ (exergy input) is severer than the enhancement slope of both $E_{out,da}$ and $E_{out,ha}$ which results in further exergy destruction by increment of inlet mass flow rate. It is noted that, higher air flow rate means higher fluid velocity along the heat exchanger which reduces the temperature drop (not necessarily heat transfer rate) along the wet channel (because of increment of fluid residential time through the channel). Curve behavior of $E_{in,da}$, $E_{out,da}$ and $E_{out,ha}$ in Fig. 9(b) (effect of ε) is different from Fig. 9(a). In Fig. 9(b), as the total air mass flow rate is constant, the value of $E_{in,da}$ is the same for all amounts of mass flow ratio. $E_{out,ha}$ and $E_{out,da}$ is increased and decreased respectively by increment of mass flow ratio. It is noted that, increment/reduction of exergy (E) does not necessarily mean increment/reduction of specific exergy (e) as well. For example, despite the increment of $E_{out,ha}$ by increment of inlet air mass flow rate, specific exergy ($e_{out,ha}$) is reduced by increment of air mass flow rate which its reason is related to the direct effect of mass flow rate on E ($E = \dot{m} \times e$). Although the value of $e_{out,ha}$ is reduced by increment of air mass flow rate, the value of $\dot{m}$ is increased (with stronger slope) which is shown in Fig. 10. Hence, the multiplication of $\dot{m}$ and e (i.e. E) is increased. It is concluded that it is betted choose smaller value of air velocity through the channel to reduce the exergy destruction of fluid flow along the M-cycle cooler which means using further number of parallel plates

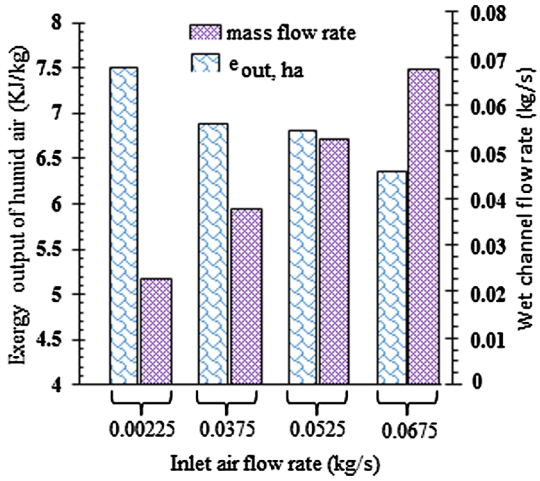

Fig. 10. Variation of specific exergy output of humid air and wet channel flow rate with air inlet flow rate.

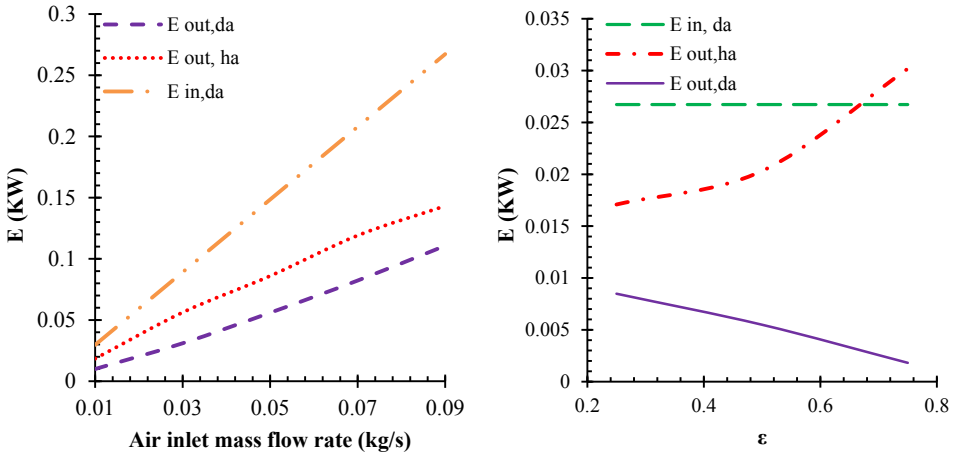

Fig. 9. Effect of air inlet mass flow rate and mass flow ratio on exergy input or output.

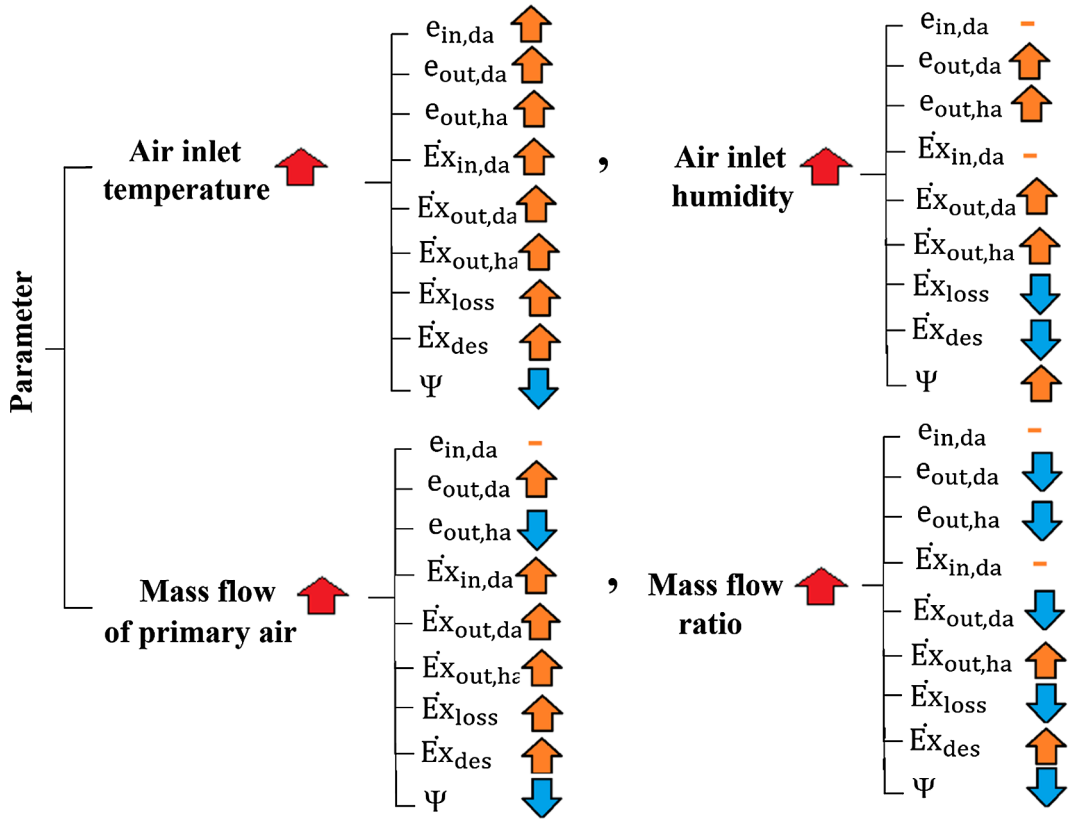

Fig. 11. A brief general view of all investigated parameters and their impacts.

instead of long plates (with lower numbers). It is clear that, reduction of air mass flow rate dos not necessarily requires reduction of air-fan power. It can be controlled in design process of the cooler by optimizing of the number of channels and other effective factors. A general view of all investigated parameters and their impact is illustrated in Fig. 11.

4. Conclusion

Exergetic analysis of regenerative M-cycle cooler was performed in present paper. Exergetic formulation was provided in detail for this type of air cooler. Outlet characteristics of the cooler (for any given value of inlet characteristics) were evaluated via analytical solution and then exergetic specifications were calculated using inlet and outlet characteristics. Exergy destruction, exergetic efficiency, exergy input/output by dry air, humid air and water fluid were evaluated and their behaviour by changing of main inlet thermal-flow factors was discussed. Inlet air temperature, inlet air humidity ratio, inlet air mass flow rate and mas flow ratio between two channels were considered as variant parameters. As the increment of air mass flow rate and mass flow ratio between two channels increased the exergy destruction through cooling process, it is recommenced to employ an optimum number of channels in the designing process of the cooler to allocate a logical value of air mass flow rate for any individual channel. Indeed, in the same total inlet air flow rate, the air velocity along the channels can be controlled by the employed numbers of parallel channels in the designing process of M-cycle based on the second law of thermodynamics. In other words, in a constant air inlet flow rate, it is possible to increase the plate numbers and increase the exergetic efficiency without reduction of thermal efficiency of the cooler. Humid air caused smaller value of exergy destruction and augmented the exergetic efficiency. Exergetic efficiency was enhanced by reduction of air inlet temperature, air inlet flow rate and mass flow ratio.

Appendix A. Analytical thermal solution of regenerative M-cycle

The preliminary governing equations for parallel flow indirect evaporative cooler are presented in the following.

$$\begin{cases} \textit{Energy balance of primary air}: \ \dot{m}_1 c_1 dT_1 = U(T_w - T_1)A_1 d\bar{x} \\ \textit{Mass balance of working air}: \ \dot{m}_2 dw_2 = \beta(w_{eq} - w_2)\sigma A_2 \frac{dx_2}{L} \ \textit{and} \ d\dot{m}_w = -\dot{m}_2 dw_2 \\ \textit{Energy balance of wet channel}: \ \dot{m}_2 di_2 = [\alpha_2(T_w - T_2) + i_v\beta(w_{eq} - w_2)\sigma]A_2\frac{dx_2}{L_{wa}} \\ \textit{Energy balance for differential element}: \ \dot{m}_w c_w dT_w + c_w T_w d\dot{m}_w + \dot{m}_1 c_1 dT_1 + \dot{m}_2 di_2 = 0 \\ w_{eq} \textit{ has a linear function with water surface temperature}: \ w_{eq} = F + eT_w \end{cases} \quad (1)$$

After some mathematical operations (similar to Eqs. (1)–(48) in [2]), the following equation was obtained.

$$\begin{cases} dT_1 = (T_w - T_1)\frac{r}{C_f^*}NTUd\bar{x} \\ dT_2 = (T_w - T_2)NTUd\bar{x} \\ dw_2 = \frac{\sigma}{Le_f}(w_{eq} - w_2)NTUd\bar{x} \\ dT_w = [-\frac{i_{fg}}{c_a}\frac{\sigma}{Le_f}(w_{eq} - w_2) + r(T_1 - T_w) - (T_w - T_2)]\frac{1}{C_w^*}NTUd\bar{x} \\ dw_{eq} = [-\frac{i_{fg}}{c_a}\frac{\sigma}{Le_f}(w_{eq} - w_2) + r(T_1 - T_w) - (T_w - T_2)]\frac{e}{C_w^*}NTUd\bar{x} \end{cases} \quad (2)$$

The concept of assumption "4" is that the value of $C_w^* = \frac{\dot{m}_w c_w}{\dot{m}_2 c_a}$ tends to zero. Besides, the amount of $\frac{\sigma}{Le_f}$ is unity based on assumption "5". Under these conditions, above equaiotn is rewritten as below. Moreover, w_{eq} in the last equation of the system can be replaced by assumption "3". Thus,

$$\begin{cases} dT_1 = (T_w - T_1)\frac{r}{C_f^*}NTUd\bar{x} \\ dT_2 = (T_w - T_2)NTUd\bar{x} \\ dw_2 = (F + eT_w - w_2)NTUd\bar{x} \\ -\frac{i_{fg}}{c_a}\frac{\sigma}{Le_f}(F + eT_w - w_2) + r(T_1 - T_w) - (T_w - T_2) = 0 \end{cases} \quad (3)$$

The fourth relation in Eq. (4) can be rearranged based on T_w as shown below.

$$T_w = \frac{-1}{(r+\eta)}[\bar{i_{fg}}(F - w_2) - T_2 - rT_1] \quad (4)$$

where

$$\eta = 1 + e\bar{i_{fg}} \quad (5)$$

$$\bar{i_{fg}} = \frac{i_{fg}}{c_a} \quad (6)$$

Now, if the parameters T_w and w_{eq} in the first three relations are replaced with Eq. (5) and assumption "3″ respectively, Eq. (4) is transformed into a 3-differential equation as shown in the following.

$$\begin{cases} \frac{dT_1}{d\bar{x}} = \{\bar{i_{fg}}F - \bar{i_{fg}}w_2 - T_2 + \eta T_1\}\frac{-r}{C_f^*(r+\eta)} \\ \frac{dT_2}{d\bar{x}} = \{\bar{i_{fg}}F - \bar{i_{fg}}w_2 - (1 - r - \eta)T_2 - rT_1\}\frac{-1}{(r+\eta)}NTU \\ \frac{dw_2}{d\bar{x}} = \{F(\bar{i_{fg}} - \frac{(r+\eta)}{e}) - (\bar{i_{fg}} - \frac{(r+\eta)}{e})w_2 - t_2 - rt_1\}\frac{-e}{(r+\eta)}NTU \end{cases} \quad (7)$$

It should be noted that, Eq. (7) was expanded for the general parallel flow indirect flow configuration. As regenerative M-cycle air cooler works based on counter-flow configuration, the second and third relation ($\frac{dT_2}{d\bar{x}}$ and $\frac{dw_2}{d\bar{x}}$) of Eq. (7) should be multiplied to "-1". Indeed, as $dx_2 = -dx_1$, for regenerative M-cycle exchanger, differential equations are written as below based on $\bar{x}_1$.

$$\begin{cases} \frac{dT_1}{d\bar{x}_1} = \{\bar{i_{fg}}F - \bar{i_{fg}}w_2 - T_2 + \eta T_1\}\frac{-r}{C_f^*(r+\eta)}NTU \\ \frac{dT_2}{d\bar{x}_1} = \{\bar{i_{fg}}F - \bar{i_{fg}}w_2 - (1 - r - \eta)T_2 - rT_1\}\frac{1}{(r+\eta)}NTU \\ \frac{dw_2}{d\bar{x}_1} = \{F(\bar{i_{fg}} - \frac{(r+\eta)}{e}) - (\bar{i_{fg}} - \frac{(r+\eta)}{e})w_2 - t_2 - rt_1\}\frac{e}{(r+\eta)}NTU \end{cases} \quad (8)$$

The validation of the model was performed with numerical solvation for below condition (Table A1) and the result is provided in Table A2 and Fig. A1 (in appendix).

Table A1
Characteristics for which the model was solved numerically and analytically.

Parameter	Value
a (m)	0.005
b (m)	0.2
L (m)	1
T'_1(C)	40, 35, 30, 25
W'_1kg/kg	0.016
$\dot{m}'_1$(Kg/s)	0.009
ε	0.5
k_p	0.00250 KW/m^2 C
δ_p	0.0005 m
k_w	0.6×10^{-3} KW/m^2 C
δ_w	0.0001 m

Table A2
Results from analytical and numerical solution.

$T_1^{'}$	$T_1^{''}$	$T_2^{''}$	$W_2^{''}$
Analytical			
45	27.53	12.06	0.031
40	24.21	10.45	0.029
35	20.91	8.86	0.028
30	17.6	7.26	0.026
25	14.3	5.66	0.025
Numerical			
45	27.48	12.26	0.031
40	24.18	10.64	0.030
35	20.88	9.02	0.028
30	17.58	7.39	0.026
25	14.28	5.77	0.025

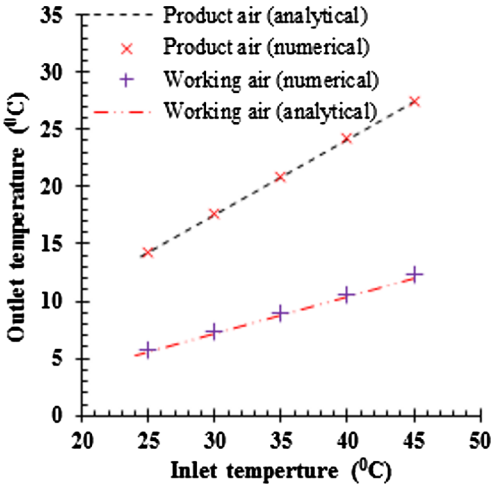

Fig. A1. Validation of analytical model with numerical solution.

Appendix B

The obtained functions by solving Eq. (21) via Laplace transformations technique:

$$\begin{cases} T_1(\bar{x}_1) = (0.62 + 0.001T_1^{'})e^{0.89\bar{x}_1} + (-183.34 + 1.06T_1^{'})e^{-0.34\bar{x}_1} + (-170.9 - 0.06T_1^{'})e^{0.23\bar{x}_1} + 354.25 \\ T_2(\bar{x}_1) = (20.98 + 0.35T_1^{'})e^{0.89\bar{x}_1} + (35.49 - 0.2T_1^{'})e^{-0.34\bar{x}_1} + (-81.14 - 0.32T_1^{'})e^{0.23\bar{x}_1} + 33.51 \\ \omega_2(\bar{x}_1) = (-0.0081 - 0.00013T_1^{'})e^{0.89\bar{x}_1} + (-0.14 + 0.00081T_1^{'})e^{-0.34\bar{x}_1} + (-0.48 - 0.00019T_1^{'})e^{0.23\bar{x}_1} + 0.74 \end{cases}$$

References

[1] M.H. Mahmood, M. Sultan, T. Miyazaki, S. Koyama, V.S. Maisotsenko, Overview of the Maisotsenko cycle – a way towards dew point evaporative cooling, Renew. Sustain. Energy Rev. 1 (66) (2016 Dec) 537–555.
[2] H.S. Dizaji, E.J. Hu, L. Chen, A comprehensive review of the Maisotsenko-cycle based air conditioning systems, Energy 1 (156) (2018 Aug) 725–749.
[3] H. Caliskan, I. Dincer, A. Hepbasli, A comparative study on energetic, exergetic and environmental performance assessments of novel M-Cycle based air coolers for buildings, Energy Convers. Manage. 1 (56) (2012 Apr) 69–79.
[4] H. Caliskan, A. Hepbasli, I. Dincer, V. Maisotsenko, Thermodynamic performance assessment of a novel air cooling cycle: maisotsenko cycle, Int. J. Refrig. 34 (4) (2011 Jun 1) 980–990.
[5] A. Abbassi, M. Aliehyaei, Exergy method of optimisation of a wavy plate indirect evaporative cooler, Int. J. Exergy 1 (3) (2004 Jan 1) 350–362.
[6] D.J. Chengqin, Exergy analysis of an indirect evaporative cooler based on CFD method, Refrig. Air-Cond. 4 (2006) 004.
[7] J.P. Chen, X. Huang, Y.M. Xuan, Exergy analysis of dew point indirect evaporative cooler, Fluid Mach. 11 (2007) 021.
[8] C.Q. Ren, M.J. Peng, The exergy efficiency analysis of an indirect evaporative heat exchanger, Ind. Heating-Xian 34 (3) (2005) 7.
[9] M. Farmahini-Farahani, S. Delfani, J. Esmaeelian, Exergy analysis of evaporative cooling to select the optimum system in diverse climates, Energy 40 (1) (2012 Apr 1) 250–257.
[10] S. Anisimov, D. Pandelidis, Numerical study of perforated indirect evaporative air cooler, Int. J. Energy Clean Environ. 12 (2–4) (2011).
[11] S. Anisimov, D. Pandelidis, Numerical study of the Maisotsenko cycle heat and mass exchanger, Int. J. Heat Mass Transf. 31 (75) (2014 Aug) 75–96.
[12] D. Pandelidis, S. Anisimov, Numerical analysis of the selected operational and geometrical aspects of the M-cycle heat and mass exchanger, Energy Build. 1 (87) (2015 Jan) 413–424.
[13] S. Anisimov, D. Pandelidis, J. Danielewicz, Numerical study and optimization of the combined indirect evaporative air cooler for air-conditioning systems, Energy 1 (80) (2015 Feb) 452–464.
[14] D. Pandelidis, S. Anisimov, Numerical analysis of the heat and mass transfer processes in selected M-Cycle heat exchangers for the dew point evaporative cooling, Energy Convers. Manage. 15 (90) (2015 Jan) 62–83.
[15] C. Zhan, X. Zhao, S. Smith, S.B. Riffat, Numerical study of a M-Cycle cross-flow heat exchanger for indirect evaporative cooling, Build Environ. 46 (2011) 657–668.
[16] X. Cui, M.R. Islam, B. Mohan, K.J. Chua, Developing a performance correlation for counter-flow regenerative indirect evaporative heat exchangers with experimental validation, Appl. Therm. Eng. 5 (108) (2016 Sep) 774–784.
[17] X. Cui, K.J. Chua, M.R. Islam, K.C. Ng, Performance evaluation of an indirect pre-cooling evaporative heat exchanger operating in hot and humid climate, Energy Convers. Manage. 15 (102) (2015 Sep) 140–150.
[18] H.Q. Khafaji, A.L. Ekaid, V.I. Terekhov, A numerical study of direct evaporative air cooler by forced laminar convection between parallel-plates channel with wetted walls, J. Eng. Thermophys. 24 (2) (2015 Apr 1) 113–122.

[19] G. Heidarinejad, S. Moshari, Novel modeling of an indirect evaporative cooling system with cross-flow configuration, Energy Build. 1 (92) (2015 Apr) 351–362.
[20] S. Moshari, G. Heidarinejad, Numerical study of regenerative evaporative coolers for sub-wet bulb cooling with cross-and counter-flow configuration, Appl. Therm. Eng. 5 (89) (2015 Oct) 669–683.
[21] H. Jafarian, H. Sayyaadi, F. Torabi, A numerical model for a dew-point counter-flow indirect evaporative cooler using a modified boundary condition and considering effects of entrance regions, Int. J. Refrig 1 (84) (2017 Dec) 36–51.
[22] Y. Wan, C. Ren, Z. Wang, Y. Yang, L. Yu, Numerical study and performance correlation development on counter-flow indirect evaporative air coolers, Int. J. Heat Mass Transf. 1 (115) (2017 Dec) 826–830.
[23] D. Pandelidis, S. Anisimov, Numerical study and optimization of the cross-flow Maisotsenko cycle indirect evaporative air cooler, Int. J. Heat Mass Transf. 31 (103) (2016 Dec) 1029–1041.
[24] A. Sohani, H. Sayyaadi, S. Hoseinpoori, Modeling and multi-objective optimization of an M-cycle cross-flow indirect evaporative cooler using the GMDH type neural network, Int. J. Refrig 30 (69) (2016 Sep) 186–204.
[25] D. Buyadgie, O. Buyadgie, O. Drakhnia, Y. Sladkovskyi, S.V. Artemenko, A. Chamchine, Theoretical study of the combined M-cycle/ejector air-conditioning system, Int. J. Energy Clean Environ. 12 (2–4) (2011).
[26] B. Riangvilaikul, S. Kumar, An experimental study of a novel dew point evaporative cooling system, Energy Build 42 (2010) 637–644.
[27] C. Zhan, Z. Duan, X. Zhao, S. Smith, H. Jin, S. Riffat, Comparative study of the performance of the M-cycle counter-flow and cross-flow heat exchangers for indirect evaporative cooling–paving the path toward sustainable cooling of buildings, Energy 36 (12) (2011 Dec 31) 6790–6805.
[28] D. Zube, L. Gillan, Evaluating Coolerado Corportion's Heatâ€ mass exchanger performance through experimental analysis, Int. J. Energy Clean Environ. 12 (2–4) (2011).
[29] W.Z. Gao, Y.P. Cheng, A.G. Jiang, T. Liu, K. Anderson, Experimental investigation on integrated liquid desiccant–Indirect evaporative air cooling system utilizing the Maisotesenko-Cycle, Appl. Therm. Eng. 5 (88) (2015 Sep) 288–296.
[30] E.D. Rogdakis, I.P. Koronaki, D.N. Tertipis, Experimental and computational evaluation of a Maisotsenko evaporative cooler at Greek climate, Energy Build. 28 (70) (2014 Feb) 497–506.
[31] O. Khalid, Z. Butt, W. Tanveer, H.I. Rao, Design and experimental analysis of counter-flow heat and mass exchanger incorporating (M-cycle) for evaporative cooling, Heat Mass Transf. 53 (4) (2017 Apr 1) 1391–1403.
[32] O. Khalid, M. Ali, N.A. Sheikh, H.M. Ali, M. Shehryar, Experimental analysis of an improved Maisotsenko cycle design under low velocity conditions, Appl. Therm. Eng. 25 (95) (2016 Feb) 288–295.
[33] Z. Duan, X. Zhao, C. Zhan, X. Dong, H. Chen, Energy saving potential of a counter-flow regenerative evaporative cooler for various climates of China: experiment-based evaluation, Energy Build. 1 (148) (2017 Aug) 199–210.
[34] S. De Antonellis, C.M. Joppolo, P. Liberati, S. Milani, L. Molinaroli, Experimental analysis of a cross flow indirect evaporative cooling system, Energy Build. 1 (121) (2016 Jun) 130–138.
[35] P. Xu, X. Ma, X. Zhao, K. Fancey, Experimental investigation of a super performance dew point air cooler, Appl. Energy 1 (203) (2017 Oct) 761–777.
[36] Z. Duan, C. Zhan, X. Zhao, X. Dong, Experimental study of a counter-flow regenerative evaporative cooler, Build. Environ. 1 (104) (2016 Aug) 47–58.
[37] S. De Antonellis, C.M. Joppolo, P. Liberati, S. Milani, F. Romano, Modeling and experimental study of an indirect evaporative cooler, Energy Build. 1 (142) (2017 May) 147–157.
[38] J. Lin, R.Z. Wang, M. Kumja, T.D. Bui, K.J. Chua, Modelling and experimental investigation of the cross-flow dew point evaporative cooler with and without dehumidification, Appl. Therm. Eng. 5 (121) (2017 Jul) 1–3.
[39] M.K. Shahzad, G.Q. Chaudhary, M. Ali, N.A. Sheikh, M.S. Khalil, T.U. Rashid, Experimental evaluation of a solid desiccant system integrated with cross flow Maisotsenko cycle evaporative cooler, Appl. Therm. Eng. 5 (128) (2018 Jan) 1476–1487.
[40] H.S. Dizaji, E.J. Hu, L. Chen, S. Pourhedayat, Development and validation of an analytical model for perforated (multi-stage) regenerative M-cycle air cooler, Appl. Energy 15 (228) (2018 Oct) 2176–2194.
[41] M. Shukuya, A. Hammache, Introduction to the concept of exergy-for a better understanding of low temperature heating and high temperature cooling systems, in: LowEx Espoo 2002, VTT Research Notes 2158, ISBN 951-38-6075-2, 2002, < http://www.vtt. fi/inf/pdf/tiedotteet/2002/T2158.pdf > (accessed 05.06.10).
[42] A. Bejan, Advanced Engineering Thermodynamics, A Wiley – Interscience Publication, John Wiley & Sons, 1988.

Chapter 6

Application of M-cycle in the cooling of gas turbine inlet air

This chapter has been published as

> Dizaji HS, Hu EJ, Chen L, Pourhedayat S. Using novel integrated Maisotsenko cooler and absorption chiller for cooling of gas turbine inlet air. Energy Conversion and Management. 2019 Sep 1;195:1067-78. (DOI: 10.1016/j.enconman.2019.05.064).

This chapter provides a new industrial application of M-cycle and provides a novel hybrid cycle of M-cycle and absorption chiller which can be used to reduce the air inlet temperature of gas turbine power plants. Air temperature reduction causes increment of electrical power production by gas turbine.

It was found that the proposed hybrid cycle is able to efficiently reduce the inlet air temperature of the gas turbine. The air fluid is first cooled through the M-cycle cooler (up to dew-point temperature) and then is further cooled on saturation line by the absorption chiller. The condensed water through the cooling process on saturation line can be employed as the required water by M-cycle. If all mentioned cooling process is performed by absorption refrigeration systems, extremely huge capacity of absorption chiller is required which increases the capital and maintenance costs due to their more complicated structures.

Statement of Authorship

Title of Paper	Using novel integrated Maisotsenko cooler and absorption chiller for cooling of gas turbine inlet air
Publication Status	☑ Published ☐ Accepted for Publication ☐ Submitted for Publication ☐ Unpublished and Unsubmitted w ork w ritten in manuscript style
Publication Details	Dizaji HS, Hu EJ, Chen L, Pourhedayat S. Using novel integrated Maisotsenko cooler and absorption chiller for cooling of gas turbine inlet air. Energy Conversion and Management. 2019 Sep 1;195:1067-78. (DOI: 10.1016/j.enconman.2019.05.064).

Principal Author

Name of Principal Author (Candidate)	Hamed Sadighi Dizaji		
Contribution to the Paper	Proposing a new hybrid cycle for gas turbine based power plants. Developing related model, writing the manuscript and data analysis.		
Overall percentage (%)	70%		
Certification:	This paper reports on original research I conducted during the period of my Higher Degree by Research candidature and is not subject to any obligations or contractual agreements with a third party that would constrain its inclusion in this thesis. I am the primary author of this paper.		
Signature		Date	

Co-Author Contributions

By signing the Statement of Authorship, each author certifies that:

i. the candidate's stated contribution to the publication is accurate (as detailed above);

ii. permission is granted for the candidate in include the publication in the thesis; and

iii. the sum of all co-author contributions is equal to 100% less the candidate's stated contribution.

Name of Co-Author	Eric Hu		
Contribution to the Paper	Supervising the work, continuous recommendations and assistances through the developing process of the model. Review and editing of the manuscript.		
Signature		Date	

Name of Co-Author	Lei Chen		
Contribution to the Paper	Supervising the work, continuous recommendations and assistances through the developing process of the model. Review and editing of the manuscript.		
Signature	Ley Chen Digitally signed by Ley Chen DN: cn=Ley Chen, o, ou, email=Ley.chen@eng.adelaide.edu.au, c=AU Date: 2021.01.12 16:23:45 +10'30'	Date	

Name of Co-Author	Samira Pourhedayat		
Contribution to the Paper	Assisting in the developing of the model and programming.		
Signature		Date	

Energy Conversion and Management 195 (2019) 1067–1078

Contents lists available at ScienceDirect

Energy Conversion and Management

journal homepage: www.elsevier.com/locate/enconman

Using novel integrated Maisotsenko cooler and absorption chiller for cooling of gas turbine inlet air

Hamed Sadighi Dizaji*, Eric Jing Hu*, Lei Chen, Samira Pourhedayat

School of Mechanical Engineering, The University of Adelaide, Adelaide, SA 5005, Australia

ARTICLE INFO

Keywords:
Maisotsenko cycle
Absorption chiller
Gas turbine power plant
M-cycle

ABSTRACT

Performance reduction of gas turbine power plants during the hot seasons has persuaded the specialists to propose different inlet air temperature reducer techniques. Accessible free heat at the exhaust of the turbine justifies the absorption chiller as a potential solution. However, based on the evaluations of present research, almost for all climate conditions a huge capacity/size/number of absorption chillers are required to reach the ISO condition (15 °C and RH 100% which is the design point of gas turbine) which means considerable amount of initial, operating and maintenance cost. As the M-cycle cooler (which has very simpler structure and lower costs) is able to reduce the air temperature toward the dew point temperature without adding any moisture, present research proposes an integrated cycle of M-cycle and absorption chiller (which notably reduces the whole cost of the cooling process) for said aim. In present novel cycle, the air is precooled by M-cycle toward its dew point temperature before entering to the absorption chiller which significantly reduces the required capacity of absorption chiller for the rest of the cooling process. The most amazing feature of the integrated cycle is that the condensed water from the air during the cooling process by absorption chiller can be employed as the M-cycle water consumption. For some climate conditions, M-cycle is able to provide ISO condition (or colder temperatures) without the requirement of absorption chiller. Many other outstanding results are obtained which can be used in real industrial applications.

1. Introduction

During the hot seasons of the year, gas turbine based power plants deal with two major challenges. First, the electricity demand is sharply increased which is commonly due to the simultaneous use of air conditioning systems by all domestic and industrial customers. Second, the efficiency and subsequently the electricity production capacity by power plants are reduced in hot days of the years. Indeed, the performance of gas turbines is reduced by increment of the air inlet temperature into the compressor. Researchers have proposed different techniques to reduce the inlet air temperature to the compressor of gas turbine power plants. Fogging, swirl-Flash, media cooling method, ice storage and absorption chiller are the main suggested air inlet cooling techniques. Among mentioned methods, absorption chiller does not add any moisture (or water droplets) to the air fluid and that is why it does not have any negative effect such as erosion, corrosion etc. on blades and other parts of gas turbine. Moreover, the energy required by absorption chiller can be obtained from the wasted heat at the outlet of the turbine. However, as a huge size and capacity of absorption chiller is required for this aim, initial, maintenance and operation cost of absorption chiller are higher than the other methods. Normally, several jointed large commercial size absorption chillers should work simultaneously to provide ISO inlet condition.

Most recently, some researchers proposed the Maisotsenko coolers as the novel air inlet temperature reducers in gas turbines. Contrary to the other methods which work based on direct water evaporation mechanism, M-cycle is an indirect evaporative cooler and it does not add any water droplets into the air fluid stream. Nonetheless, it is not able to reduce the air temperature below the dew-point temperature of ambient air. Dew-point temperature of most climate conditions is higher (warmer) than the 15 °C (ISO condition) which will be discussed in detail in the next sections. Irrespective of said limited cooling capacity of M-cycle, it requires a considerable amount of water for this application (gas turbine) in which the air flow rate is high. The investigations of absorption chiller in gas turbines and also the researches of the application of M-cycle in gas turbine power plants are reviewed in the following to provide the recent developments and progresses in this regard and then the main aims of present research will be explained.

Hadik [1] studied the impact of various weather parameters

* Corresponding authors.
E-mail addresses: Hamed.SadighiDizaji@adelaide.edu.au (H. Sadighi Dizaji), Eric.Hu@Adelaide.edu.au (E.J. Hu).

https://doi.org/10.1016/j.enconman.2019.05.064
Received 29 January 2019; Received in revised form 19 May 2019; Accepted 20 May 2019
Available online 31 May 2019
0196-8904/

Nomenclature

H	Specific enthalpy (KJ/kg)	$\dot{q}$	Heat transfer rate (W)
h_{vapor}	Enthalpy of saturated vapor (KJ/kg)	T	Temperature (°C)
$\dot{m}$	Mass flow rate (kg/s)	ω	Humidity ratio (kg moisture/kg dry air)
P	Pressure (Pa)	φ	Relative humidity (%)
p_g	Saturation pressure (Pa)	ν	Specific volume $\left(\frac{m^3}{kg}\right)$

including ambient temperature, relative humidity and ambient pressure on gas turbine efficiency. It was concluded that the pressure and relative humidity have negligible effects while the impact of temperature on turbine efficiency is significant. Najjar [2] studied the application of the absorption chiller as a precooling technique in gas turbine. A heat recovery boiler was utilized to recover the heat at the exhaust and inject it into the generator of the chiller. Up to 30% efficiency improvement was reported in said research. Ameri and Hejazi [3] worked on the application of absorption chiller in the Chabahar gas turbine power plant. Installation of the absorption chiller enhanced the output power of the whole system around 11%. They also estimated that the payback period will be around four years. Boonnasa et al. [4] investigated the combined cycle power plant in which an absorption chiller was employed to boost the performance of the power plant. They indicated that the best air fluid conditions before entering the air compressor are 15 °C (ISO) and 100% RH which were considered in their calculations. Power output of gas turbine was enhanced around 10.5% based on their study and payback period was obtained about 3.8 years. Sa and Zubaidy [5] provided an empirical correlation between the ambient temperature and gas turbine power output. According to their findings, 1 °C increment of ambient air temperature causes reduction of gas turbine power output around 1.5 MW. Exergy-economic analysis of absorption chiller used in gas turbine was presented by Ehyaei et al. [6]. The exergetic efficiency was enhanced around 30% by employment of absorption chiller in gas turbine power plants. Ahmadi et al. [7] provided a thermodynamic model and then worked on optimization of gas turbine with absorption chiller. Another research on the application of absorption chiller on gas turbines was performed by Kwon et al. [8] in which the thermal performance augmentation of gas turbine was reported around 16%. Mohammadi et al. [9] proposed and analysed a combined gas turbine, ORC cycle and absorption chiller for a CCHP system. The mentioned hybrid system is able to provide electrical power, cooling and also hot water with an efficiency of 67.6%. Based on their results, gas turbine inlet temperature is the most influential parameter on the performance of the systems. Kwon et al. [10] provided a comparative study between the application of absorption chiller and mechanical chiller. The power boost by absorption chiller was found larger than the mechanical one. Besides, they presented an economic analysis as well which showed the feasibility of their proposed dual cooling system. Among the different systems studied in that research, the maximum power enhancement was achieved around 8.2%. Recently, Radchenko et al. [11] studied the effect of absorption-ejector chiller on performance of gas turbine. They believe that the excessive cooling capacity is obtained by this cycle compared to the unite absorption chiller. Sohani et al. [12] suggested the employment of M-cycle cooler as a pre-cooling method in gas-turbine power plants. They also worked on the best investment strategy in this regard. According to their results, the M-cycle inlet air cooler for pre-cooling of gas turbine power plant is able to increase the annual generated power around 9%. Saghafifar and Gadalla [13–14] employed integrated solid desiccant and Maisotsenko cooler as an innovative technology for air inlet cooling process in gas turbine power plants. They believe that the M-cycle system with life span of 25 years is the most economically justified air cooler technology for gas turbines. Zhu et al. [15] compared a CCHP system primed with M-cycle cooler with a simple gas turbine with recuperator. They also provided analysis of M-cycle open gas turbine power cycle in another research [16]. They discussed the advantages and disadvantages of M-cycle for this aim and performed a comparison between the M-cycle and humid air gas turbine cycle. Some studies on other methods of air inlet cooling of gas turbine power plants are presented in the following as well. Moon et al. [17] suggested the coolant inter cooling as a method to boost the performance of the gas turbine. Najjar et al. [18] employed

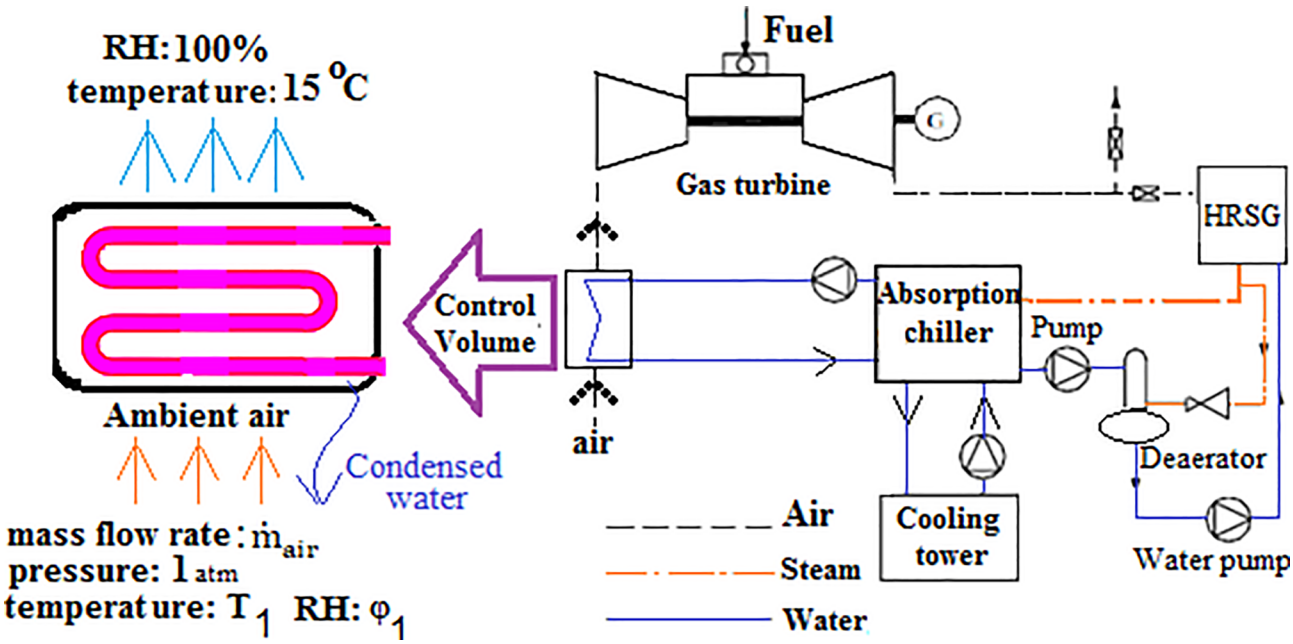

Fig. 1. Air stream on the cooling coil of absorption chiller (evaporator).

Table 1
The air inlet conditions of gas turbine.

φ_1 %	T_1 (°C)							
φ_1 = 15%	20	25	30	35	40	45	50	55
φ_1 = 25%	20	25	30	35	40	45	50	55
φ_1 = 35%	20	25	30	35	40	45	50	55
φ_1 = 45%	20	25	30	35	40	45	50	55
φ_1 = 55%	25	20	25	30	35	40	45	50
φ_1 = 65%	20	25	30	35	40	45	50	55

the wasted heat from the turbine to reduce the air inlet temperature to the compressor of gas turbine. Their system comprises of organic Rankine cycle and gas refrigeration. The system reduced the temperature around 15 °C and the overall efficiency of the power plant was enhanced around 50%. A comparison between two conventional cooling technique including evaporative media and a mechanical chiller and a novel technique was performed by Farzane-Gord and Deymi-Dashtebayaz [19]. Barakat et al. [20] employed the earth to air heat exchanger (EAHE) as an air cooler technology for gas turbines. They numerically evaluated the performance, net power and fuel consumption of the power plant under EAHE application. Thermal

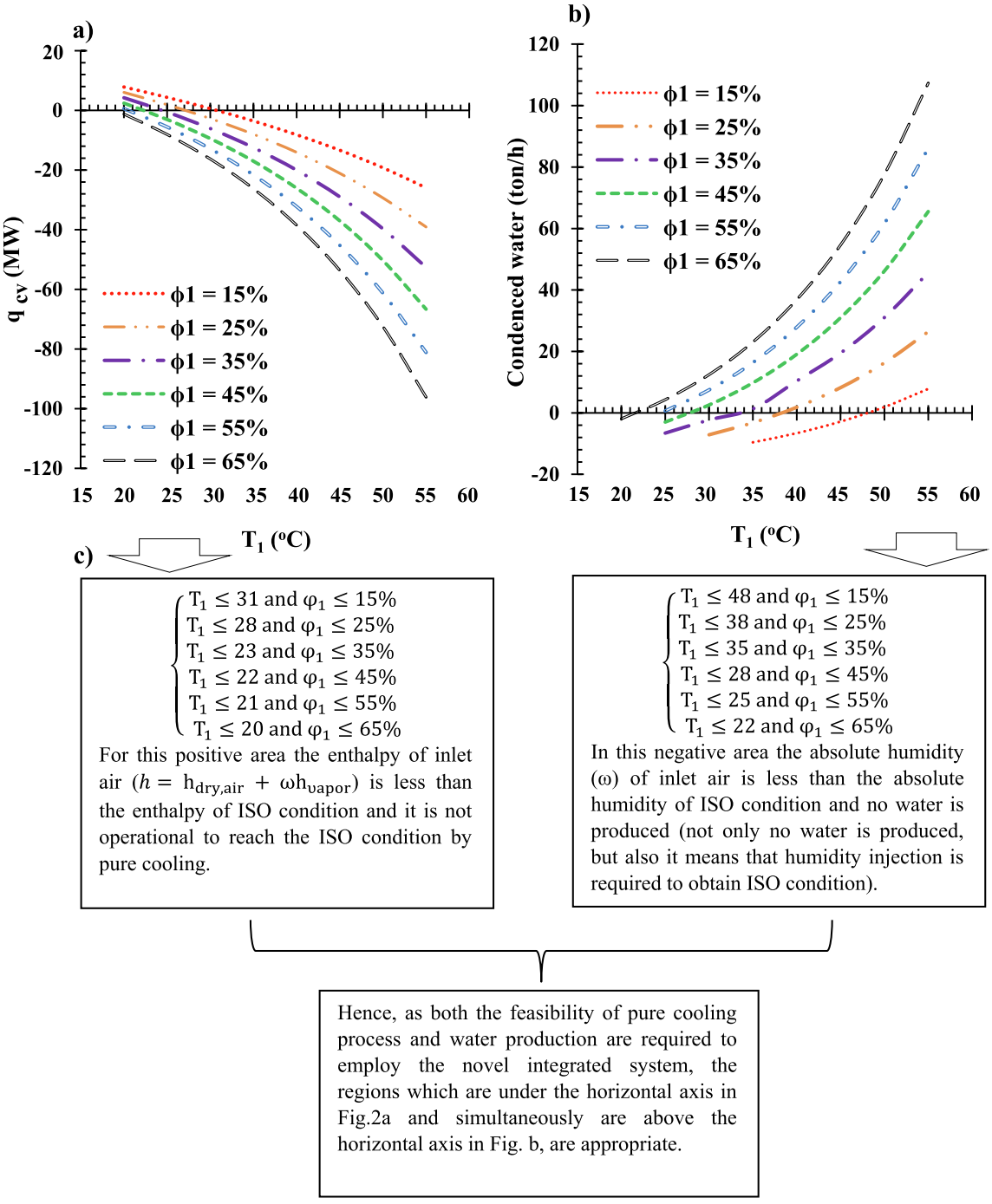

Fig. 2. a) Required cooling capacity to reach ISO condition at the inlet of compressor and b) produced condensed water during this cooling process and c) a quick brief analysis.

Table 2
Selected commercial absorption chiller for different climate conditions.

φ_1 (%)	T_1 (°C)	q_{cv}(MW)	Selected commercial absorption chiller	Number of chillers	Condensed water (ton/h)
15%	50	19	One 3307H2 model and one 1984H2 model	2	1.9
	55	25	Two 3307H2 model and one 661H2 model	3	7.8
25%	40	14	One 3307H2 model and one 661H2 model	2	1.8
	45	21	Two 3307H2 model	2	8.2
	50	29	Two 3307H2 model and one 1653H2 model	3	16.2
	55	39	Three 3307H2 model and one 1157H2 model	4	26.4
35%	35	12	One 2646H2 model and one 827H2 model	2	1.3
	40	20	Two 3307H2 model	2	10.3
	45	28	Two 3307H2 model and one 1653H2 model	3	19.4
	50	39	Three 3307H2 model and one 1157H2 model	4	31
	55	52	Four 3307H2 model and one 1488H2 model	5	45.6
45%	30	19	One 3307H2 model and one 2646H2	2	2.5
	35	17	One 3307H2 model and one 1488H2	2	9.7
	40	26	Two 3307H2 model and one 1157H2 model	3	19
	45	37	Three 3307H2 model and one 661H2 model	4	30.9
	50	50	Four 3307H2 model and one 992H2	5	46
	55	66.5	Five 3307H2 model and one 2646H2 model	6	65.5
55%	25	5.5	One 1653H2 model	1	0.6
	30	12.8	One 2646H2 model and one 827H2 model	2	7.4
	35	21.6	Two 3307H2 model	2	16.3
	40	32.2	Three 3307H2 model	3	27.8
	45	45.2	Four 3307H2 model	4	42.6
	50	61.2	Five 3307H2 model and one 992H2 model	6	61.7
	55	81.1	Seven 3307H2 model	7	86
65%	25	8	One 2646H2 model	1	4.2
	30	16.2	One 3307H2 model and one 1488H2 model	2	12.4
	35	26.2	Two 3307H2 model and one 827H2 model	3	23
	40	38.4	Three 3307H2 model and one 1157H2 model	4	36.8
	45	53.58	Four 3307H2 model and one 1984H2 model	5	54
	50	72.43	Six 3307H2 model and one 744H2 model	7	77.6
	55	97	Eight 3307H2 model and one 1157H2 model	9	107.3

Model	ST-	661H2	744H2	827H2	992H2	1157H2	1323H2	1488H2	1653H2	1984H2	2646H2	3307H2
Cooling Capacity	kW	2330	2620	2910	3490	4070	4650	5230	5820	6980	9300	11630
	10^4kcal/h	200	225	250	300	350	400	450	500	600	800	1000
	USRt	661	744	827	992	1157	1323	1488	1653	1984	2646	3307

Fig. 3. Various models of steam-operated single effect lithium bromide absorption chiller based on cooling capacity [22].

performance of the system was increased 4.8% by their technique. Al-Ansary et al. [21] investigated the effect of the application of a hybrid turbine inlet air cooling for arid climates.

In present research, an integrated cycle is proposed in which both M-cycle cooler and absorption chiller are simultaneously employed as a novel air inlet cooling technology for gas turbine power plants. Present novel cycle overcomes all defectiveness of sole application of absorption chiller and sole application of M-cycle. In this cycle, the air fluid is firstly precooled by Maisotsenko cooler toward its dew point temperature and then is cooled again through absorption chiller up to ISO condition. It is noted that, if the whole cooling process until ISO condition is performed by only absorption chiller, huge amount of chiller cooling capacity will be required which means further initial, operating and maintenance cost (some clime conditions require more than five commercial size absorption chiller which is not logical). It is not possible to reach ISO condition only by M-cycle cooling technology for most clime conditions as well because dew-point is the minimum achievable temperature in M-cycle cooler. Irrespective of cooling limitation of M-cycle, huge amount of water flow is required. However, in the novel present cycle all mentioned issues are solved and the condensed water through the cooling process in the absorption chiller will be used as the required water by M-cycle cooler which is one of the remarkable and interesting features of the new proposed cycle. At the first step of this research, required cooling capacity (and related absorption chiller) is evaluated for gas turbine under different inlet ambient conditions toward to ISO condition (15 °C and 100%RH) and the results are discussed. At the second step, the new integrated cycle is presented and the required capacity of absorption chiller and produced condensed water, required water by M-cycle etc. are discussed, analysed and compared with the first step.

2. Application of sole absorption chiller

2.1. Thermodynamic model (required cooling capacity and volume of condensed water)

In this section a mathematical calculation is provided by which the required capacity of absorption chiller is clarified to reduce the air temperature from any given ambient condition to ISO condition. It is tried to clarify the number (capacity) of required absorption chiller for any climate condition from commercial brochure. The condensed water is evaluated as well which may be employed in M-cycle integrated system. As described by [4], the most efficient condition of air intake to the compressor is 15 °C and 100% RH which is the design point of gas turbine and is considered as the calculations criteria in present study. However, more power output can be obtained in lower temperatures.

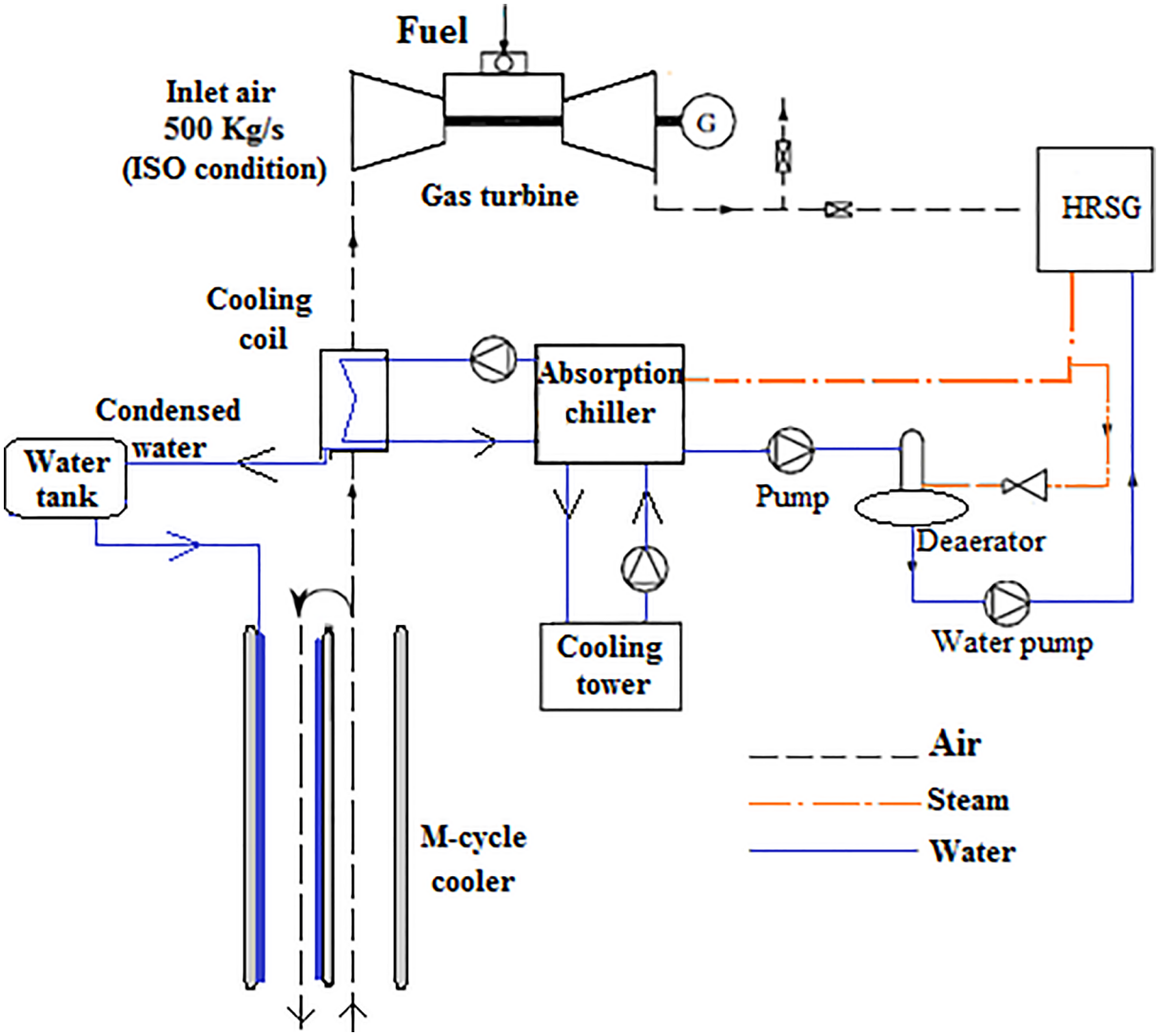

Fig. 4. A general view of the proposed novel integrated cycle.

Nonetheless, it is noted that, the inlet air temperature can be reduced until occurrence of icing phenomenon. The icing usually occurs at 5 °C and may be considered as another interested principle as well. A view of the application of absorption chiller on gas turbines is shown in Fig. 1.

Required cooling capacity by which the inlet air flow reaches to 15 °C with 100% relative humidity is calculated. The conservation of mass and also the first law of thermodynamics are written for the air fluid for the selected control volume shown in Fig. 1.

Conservation of mass for dry air:

$$\dot{m}_{air,\,1} = \dot{m}_{air,\,2} = \dot{m}_{air} \tag{1}$$

Conservation of mass for existent vapor in the air fluid:

$$\dot{m}_{vapor,\,1} = \dot{m}_{vapor,\,2} + \dot{m}_{condensed\ water} \tag{2}$$

The first law of thermodynamics:

$$\dot{q}_{C.V} + \dot{m}_{air} h_{air,\,1} + \dot{m}_{vapor,\,1} h_{vapor,\,1} = \dot{m}_{air} h_{air,\,2} + \dot{m}_{vapor,\,2} h_{vapor,\,2} + \dot{m}_{water} h_{water} \tag{3}$$

Eq. (3) is divided to $\dot{m}_{air}$ and rewritten as Eq. (4).

$$\frac{\dot{q}_{C.V}}{\dot{m}_{air}} + h_{air,1} + \frac{\dot{m}_{vapor,\,1}}{\dot{m}_{air}} h_{vapor,\,1} = h_{air,\,2} + \frac{\dot{m}_{vapor,\,2}}{\dot{m}_{air}} h_{vapor,\,2} + \frac{\dot{m}_{water}}{\dot{m}_{air}} h_{water} \tag{4}$$

It is noted that $\frac{\dot{m}_{vapor,\,1}}{\dot{m}_{air}}$ and $\frac{\dot{m}_{vapor,\,2}}{\dot{m}_{air}}$ are the humidity ratio (ω) at the inlet and outlet of the cooling coil respectively. Thus, Eq. (4) is re-written as below.

$$\frac{\dot{q}_{C.V}}{\dot{m}_{air}} = (h_{air,\,2} - h_{air,\,1}) + \omega_2 h_{vapor,\,2} - \omega_1 h_{vapor,\,1} + (\omega_1 - \omega_2) h_{water} \tag{5}$$

If the air is assumed as an ideal gas, the humidity ratio can be calculated from Eqs. (6) and (7) in which p_v is partial pressure of water vapor existent in the fluid and p_{air} is pressure of dry air.

$$\omega_1 = 0.622 \frac{p_{v1}}{p_{air\,1}} \tag{6}$$

$$\omega_2 = 0.622 \frac{p_{v2}}{p_{air\,2}} \tag{7}$$

$$p_{v1} = \varphi_1 p_{g1} \tag{8}$$

$$p_{v2} = \varphi_2 p_{g2} \tag{9}$$

$$p_{air1} = p_{total} - p_{v1} \tag{10}$$

$$p_{air2} = p_{total} - p_{v2} \tag{11}$$

If Eqs. (8)–(11) are substituted in Eqs. (9)–(7), Eqs. (12) and (13) are obtained.

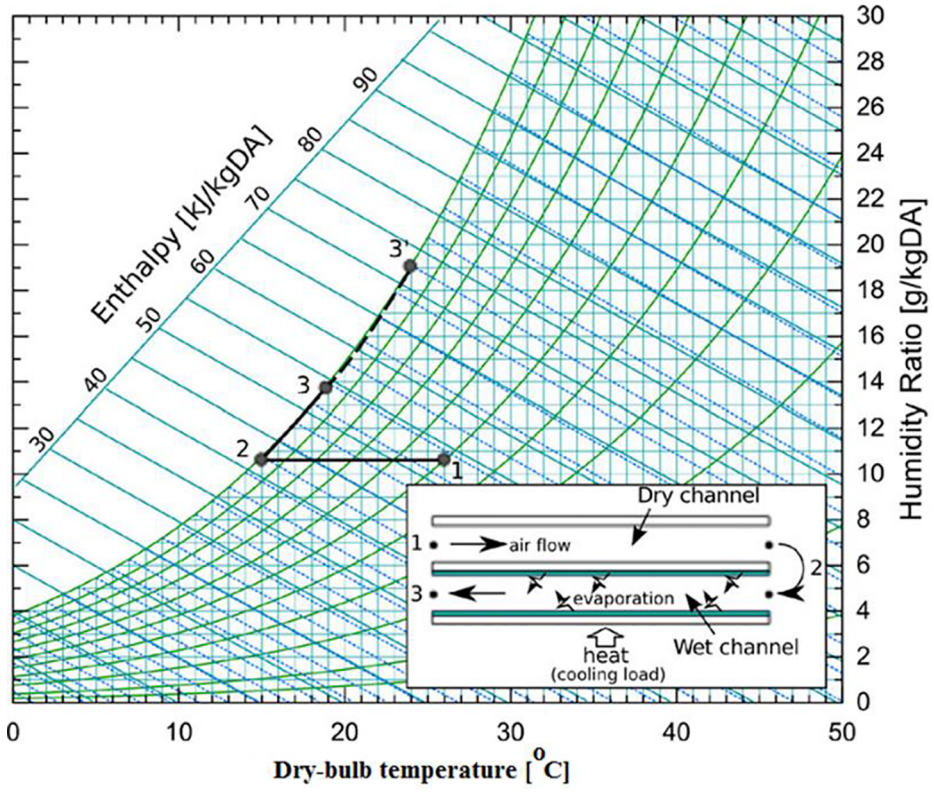

Fig. 5. Working principle of M-cycle cooler [23–27].

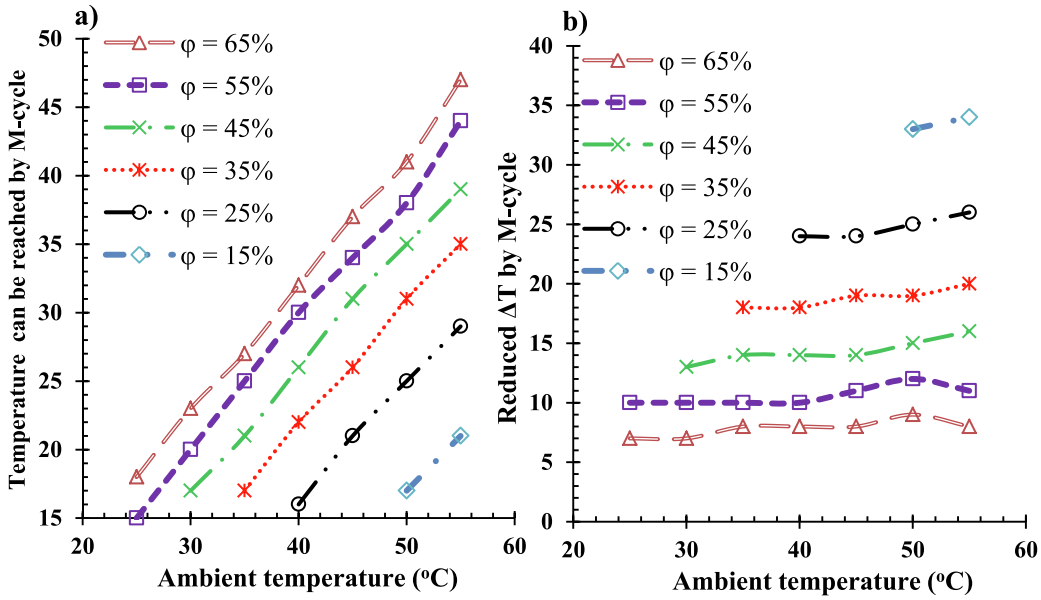

Fig. 6. (a). Temperature that can be reached by M-cycle for different climate condition and b) reduced temperature by M-cycle.

$$\omega_1 = 0.622\frac{\varphi_1 p_{g1}}{p_{total} - (\varphi_1 p_{g1})} \tag{12}$$

$$\omega_2 = 0.622\frac{p_{g2}}{p_{total} - p_{g2}} \tag{13}$$

It is noted that, p_g is saturation pressure and can be obtained from thermodynamic tables for any temperature. Furthermore, h_{vapor} (enthalpy of saturated vapor) can be red from thermodynamic table as well. The value of $h_{air,2} - h_{air,1}$ in Eq. (5) can be evaluated from Eq. (14).

$$h_{air,2} - h_{air,1} = c_p(T_2 - T_1)) \tag{14}$$

Now, Eq. (5) can be written as below.

$$\frac{\dot{q}_{C.V}}{\dot{m}_{air}} = c_p(T_2 - T_1) + \omega_2 h_{varpor,2} - 0.622\frac{h_{varpor,1}\varphi_1 p_{g1}}{p_{total} - (\varphi_1 p_{g1})} + h_{water}\left(\frac{0.622\varphi_1 p_{g1}}{p_{total} - (\varphi_1 p_{g1})} - \omega_2\right) \tag{15}$$

Eq. (15) is based on per kilogram of mass flow rate. Eq. (15) is

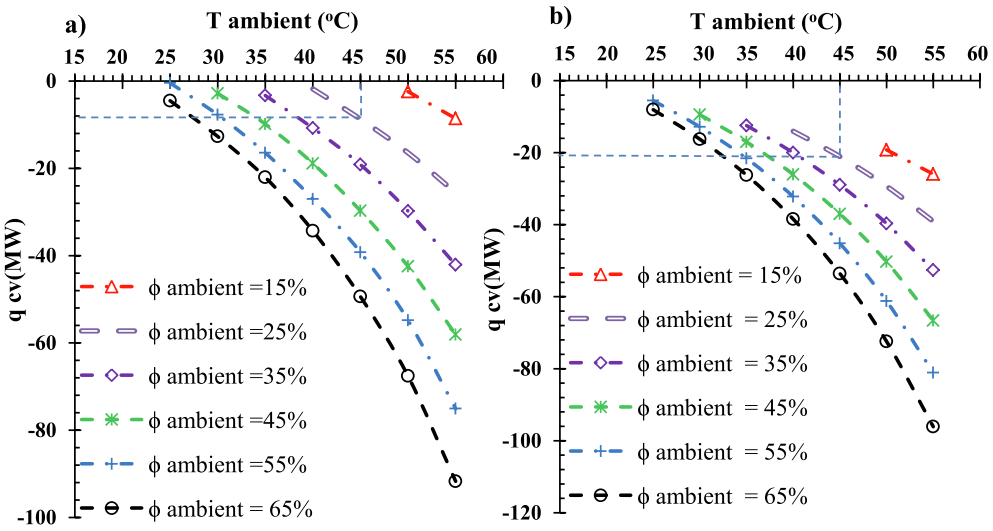

Fig. 7. (a). Required cooling capacity of absorption chiller for integrated cycle and b) required cooling capacity of absorption chiller for usual cycle shown in Fig. 1.

written as blow. The unit of obtained value for $\dot{q}_{C.V}$ from Eq. (16) is KW.

$$\dot{q}_{C.V} = \dot{m}_{air}\left[c_p(T_2 - T_1) + \omega_2 h_{varpor,2} - 0.622\frac{h_{varpor,1}\varphi_1 p_{g1}}{p_{total} - (\varphi_1 p_{g1})} + h_{water}\left(\frac{0.622\varphi_1 p_{g1}}{p_{total} - (\varphi_1 p_{g1})} - \omega_2\right)\right] \quad (16)$$

Produced condensed water during the cooling process by chiller can be estimated from Eq. (17).

$$\dot{m}_{con,\,water} = \dot{m}_{air}(\omega_1 - \omega_2) \quad (17)$$

Now, for any inlet condition (ambient condition) the cooling capacity of required absorption chiller (or any other cooling method) can be determined via Eq. (16). For different ambient conditions (presented in Table 1) the amount of $\dot{q}_{C.V}$ (MW) and also the amount of produced condensed water during the cooling process (ton/hour) are evaluated and the results are illustrated in Fig. 2.

Fig. 2(a) shows the required cooling capacity to reach the ISO condition from various climate conditions. Fig. 2(b) illustrates the produced condensed water during cooling process. According to Eq. (4) positive cooling capacity (above the horizontal axis) indicates that the total specific enthalpy of inlet air $\left(h_{air,1} + \frac{\dot{m}_{vapor,1}}{\dot{m}_{air}}h_{vapor,1}\right)$ is less than the specific enthalpy of ISO condition and therefore it is not possible to reach the ISO condition by pure cooling process. Based on Fig. 2(a) higher humidity or higher temperature increases the required cooling capacity. For example, required cooling capacity for humidity ratio of 65% (in temperature of 55 °C) is around 100 MW while in humidity ratio of 15% (in the same temperature) the required cooling capacity is around 20 MW. According to Eq. (17), negative water production in Fig. 2(b) means that the absolute humidity of inlet air is less than the absolute humidity of outlet air and no water is condensed. Based on Fig. 2(b), higher inlet temperature or higher inlet humidity ratio causes enhancement of condensed water production during the cooling process.

2.2. Selection of absorption chiller

Based on the calculated cooling capacity, the commercial existent absorption chiller can be selected from the available brochures. Required absorption chiller is presented in Table 2 for various climate conditions (the climate conditions in which no condensed water is produced were removed). The chillers were selected from SHUANGLIANG catalogue. Between different kinds of absorption chiller (direct fired, steam operated, hot water operated and fuel gas operated), Steam-Operated Single Effect Lithium Bromide Absorption Chiller is appropriate for present aim (steam can be provided as shown in Fig. 4). Indeed, as described in the catalogue, steam-operated lithium bromide absorption chiller is a kind of large-size refrigeration facility with low pressure steam as the driving energy and lithium bromide solution as the absorbent and water as refrigerant. Moreover, Steam Effect chiller, using steam or waste steam as the energy source, not only reduces greatly the cost for electricity but also possess great economic potential in applications where this source of energy is available [22]. Different model of mentioned chiller is shown in Fig. 3 (based on cooling capacity).

As can be seen in Table 2, most climate conditions require more than one commercial size absorption chiller to reach the ISO condition at the inlet of compressor of the GT power plants. Usually, simultaneous employment of more than three unit absorption chiller is not logical and affordable from the view point of economic condition, operational condition, maintenance cost, required space etc.

3. Novel integrated cycle (absorption chiller and Maisotsenko cooler)

3.1. General evaluations and comparison with previous section

A general view of the proposed novel integrated cycle is presented in Fig. 4. The air fluid is precooled by M-cycle cooler toward its dew point temperature by M-cycle before entering to the absorption chiller. The water of M-cycle is provided from the condensed water from the air in the cooling coil of absorption chiller.

Required capacity of absorption chiller in this new system is compared with previous section (in which only absorption chiller was employed to reduce the air inlet temperature). As the M-cycle cooler reduces the air temperature toward the dew point temperature of its inlet air temperature (see Fig. 5), at the first step, the dew point

Table 3
Selected commercial absorption chiller based on novel integrated cycle.

φ_1 %	T_1	Required q_{cv} for absorption chiller (MW)			Selected absorption chiller (for novel integrated cycle)	Number of chillers
		Former	Novel	Reduction ⬇%		Integrated cycle
15	50	19	2.4	87%	One 744H2 model	1
	55	25	8.5	66%	One 26467H2 model	1
25	40	14	1.7	88%	One 661H2 model	1 or 0
	45	21	8.7	58%	One 2646H2 model	1
	50	29	16.4	43%	One 3307H2 model and one 1488H2 model	2
	55	39	24	36%	Two 3307H2 model	2
35	35	12	3.3	72%	One 992H2 model	1
	40	20	10.7	46%	One 3307H2 model	1
	45	28	19.1	32%	Two 26467H2 model	2
	50	39	29.7	24%	Three 2646H2 model	3
	55	52	42.1	19%	Three 3307H2 model and one 3646H2	4
45	30	19	2.8	85%	One 827H2 model	1
	35	17	9.8	42%	One 3307H2 model	1
	40	26	18.8	28%	One 3307H2 model and one 198H2 model	2
	45	37	29.7	20%	Three 2646H2 model	3
	50	50	42.4	15%	Three 3307H2 model and one 2646H2	4
	55	66.5	58.1	12%	Five 3307H2 model	5
55	25	5.5	0.4	92%	One 661H2 model	0
	30	12.8	7.7	40%	One 2646H2 model	1
	35	21.6	16.4	24%	One 3307H2 model and one 14884H2	2
	40	32.2	27	16%	Three 2646H2 model	3
	45	45.2	39.2	13%	Three 3307H2 model and one 1653H2	4
	50	61.2	54.8	10%	Five 3307H2 model	5
	55	81.1	75	7%	Seven 3307H2 model	7
65	25	8	4.5	44%	One 1323H2 model	1
	30	16.2	12	22%	One 3307H2 model	1
	35	26.2	22	16%	Two 3307H2 model	2
	40	38.4	34	11%	Three 3307H2 model	3
	45	53.5	49	8%	Four 3307H2 model	4
	50	72.4	67.5	7%	Six 3307H2 model	6
	55	97	91.7	6%	Eight 3307H2 model	8

temperature of considered climate conditions (investigated in previous section) are presented to clarify the possible temperature reduction of any climate condition by M-cycle. Note that, it is assumed that both absorption chiller and M-cycle work with their nominal capacity in this research. The temperature that can be reached by M-cycle cooler (T_{outlet}) and the amount of $T_{inlet} - T_{outlet}$ for any climate condition is illustrated in Fig. 6(a) and (b) respectively (point 1 in Fig. 5 is ambient air and point 2 is going to absorption chiller). It is noted that φ in Fig. 6 is inlet relative humidity to the M-cycle cooler (ambient condition).

The outlet air temperature from M-cycle (which is going into the absorption chiller) is now available and the required cooling capacity of absorption chiller can be calculated by Eq. (16) for the new conditions. It is mentioned that, as no humidity is added to the product air in M-cycle cooler, humidity ratio (ω) of the air remains constant as shown in Eq. (18). According to Eq. (12), Eq. (18) can be written as Eq. (19). In the novel integrated cycle, the outlet temperature of the M-cycle (in Fig. 6) plays the role of T_1 (inlet temperature to the absorption chiller) in Eq. (16). It is noted that, by employment of Eq. (19), it is not required to separately calculate the relative humidity of the air at the inlet of the absorption chiller because the value of $\frac{\varphi P_g}{101-(\varphi P_g)}$ has been remained constant through the M-cycle. However, $h_{vapor,\,1}$ should be extracted for the new T_1 (into the absorption chiller) from the thermodynamics tables. The new $\dot{q}_{C.V}$ (required cooling capacity of absorption chiller for integrated cycle) are illustrated in Fig. 7(a). Moreover, Fig. 7(b) is related to the previous section (sole absorption chiller) that can be compared with Fig. 7(a) simultaneously now. Table 3 shows the selected absorption chiller for different climate conditions for the integrated cycle. Previous and new cooling capacity and also number of required commercial absorption chiller can be compared with each other in Table 3.

$$\omega_{ambient} = \omega_{inlet\ to\ M-cycle} = \omega_{oulet\ of\ M-cycle} = \omega_{inlet\ to\ the\ absorption\ chiller} \tag{18}$$

$$\underbrace{\frac{\varphi_{inlet} P_{g,inlet}}{101-(\varphi_{inlet} P_{g,inlet})} = \frac{\varphi_{outlet} P_{g,outlet}}{101-(\varphi_{outlet} P_{g,outlet})}}_{\text{In M-cycle cooler}} = \underbrace{\frac{\varphi_{inlet} P_{g,inlet}}{101-(\varphi_{inlet} P_{g,inlet})}}_{\text{Absorption chiller}} \tag{19}$$

According to Eqs. (17) and (18), the condensed water in the new cycle should be the same as previous cycle. Indeed, as the temperature does not go under the dew point temperature in M-cycle cooler, no vapor is condensed through M-cycle cooling. Thus, all condensed water is generated through cooling process of absorption chiller.

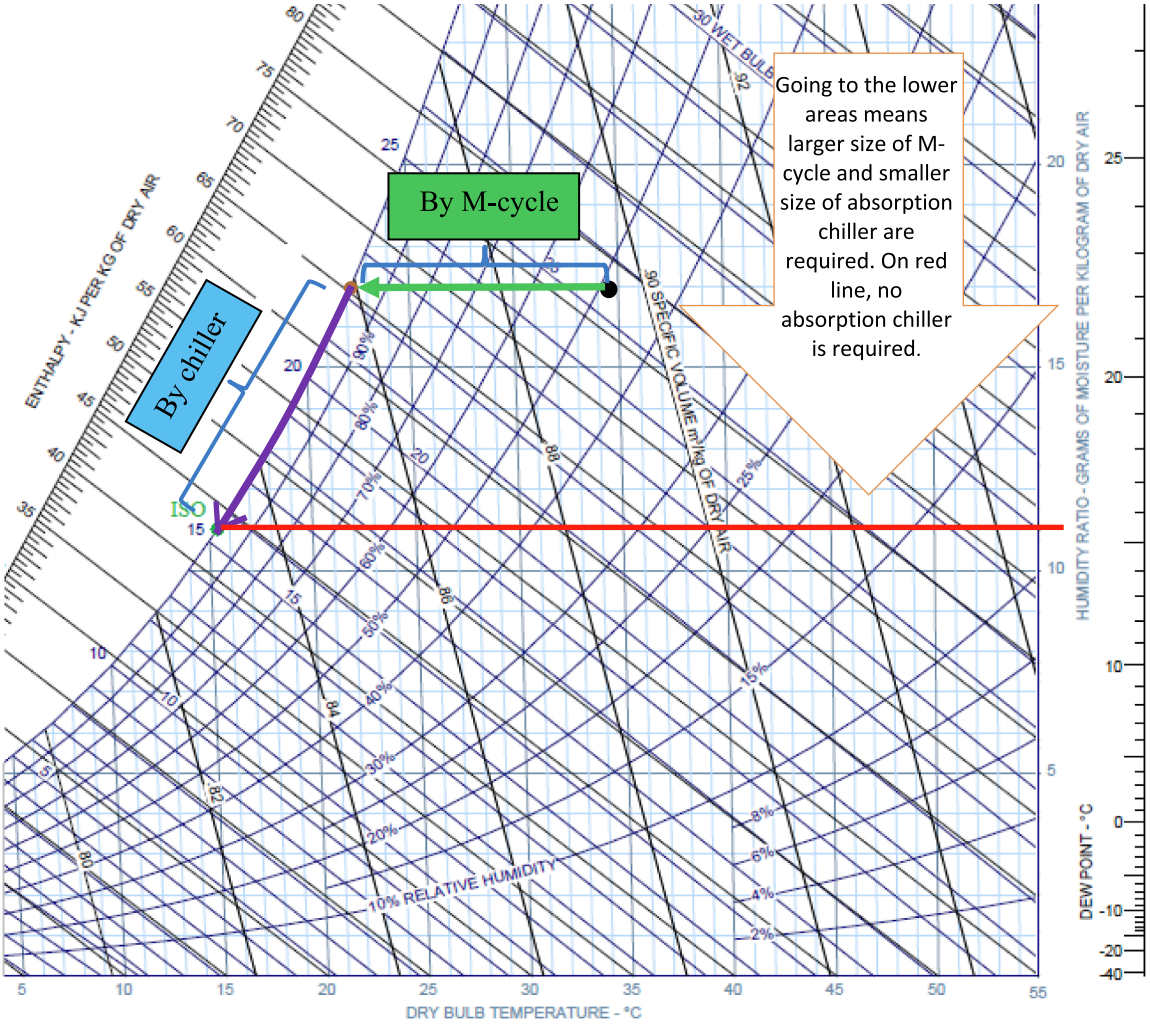

Fig. 8. (a). A brief of the outcome of the research and the conceptual operation of the novel integrated cycle.

As can be seen in Table 3, the novel integrated cycle has significantly reduced the required cooling capacity of absorption chiller. This reduction of cooling capacity reduces the required number/capacity/size of absorption chiller. Three number of absorption chillers (irrespective of their capacity) seems the maximum logical number that can be employed which are available for most climate conditions (green colour in Table 3) by integrated cycle.

It is mentioned that, for some of the regions no absorption chiller is required and M-cycle is able to obtain ISO condition or close to the ISO condition. The climate conditions for which no absorption chiller is required and M-cycle capability is enough to reach ISO condition is shown in Fig. 8 (all points on red line). However, even for these areas, it can be still obtained colder temperatures (less than ISO condition) by adding an absorption chiller. Integrated cycle is appropriate for all points above the red line (an example is shown on the Psychrometric chart). For extreme right regions (above the red line) the percentage of cooling by M-cycle is increased compared to the absorption chiller. By moving (on a vertical line) toward the top side of the chart (humid weathers), bigger size of absorption chiller and smaller size of M-cycle are required. It is clear that, the humidity ratio (ω) of the all points below the red line is lower than the humidity ratio of ISO condition and therefore it is impossible to reach the ISO point without adding moisture to the air; and pure cooling process (without adding any moisture) will provide colder temperatures i.e. less than ISO temperature (which is not necessarily negative feature especially from the net output power viewpoint).

3.2. Water consumption by M-cycle comparison with condensed water by absorption chiller

As described before, one of the remarkable features of novel integrated cycle is that the condensed water from the air during the cooling process through the absorption chiller can be employed as the required water consumption by the Maisotsenko cooler. However, the water consumption of the M-cycle (which depends on the cooling capacity of the M-cycle cooler) should be evaluated and compared with

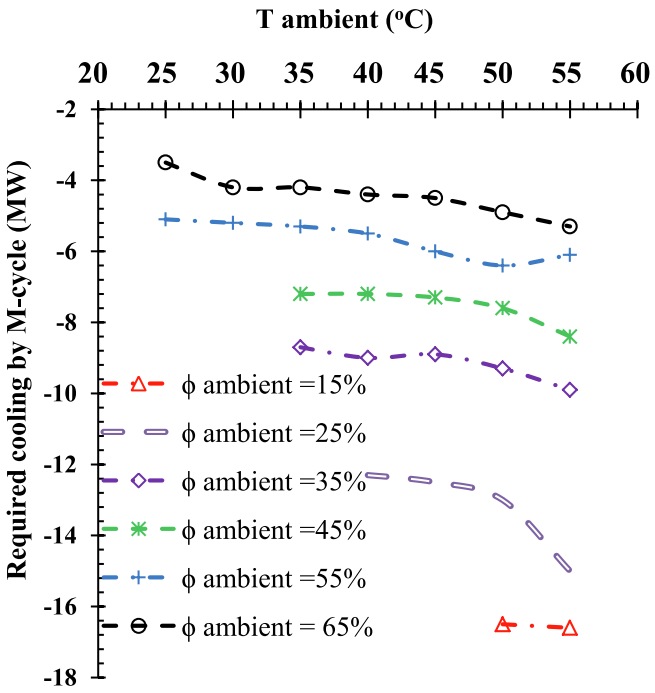

Fig. 9. Required cooling capacity of M-cycle for any climate condition (to reach the dew-point temperature of the ambient air).

the volume of the condensed water which was presented in Table 2. In order to calculate the water consumption by M-cycle cooler for any climate condition, the required cooling capacity of M-cycle should be first determined. Total required cooling capacity for any clime condition (to reach ISO condition) was calculated and presented in Table 2 in which all cooling process was assumed to be performed by absorption chiller. Also, required cooling capacity of absorption chiller in integrate cycle was presented in Table 3. Hence, the difference between these two cooling capacities should be provided by M-cycle cooler. Required cooling capacity for any climate condition is illustrated in Fig. 9.

Based on the provided information by Coolerado Corporation [28] (which is the pioneer in the development of M-cycle coolers), the water consumption by M-cycle coolers is is approximately two gallons (3.7 kg water) per ton-hour (3.5 kW-hour) of cooling. Hence, the water consumption of M-cycle cooler can be evaluated for any climate condition based on required cooling capacity by M-cycle. As explained in Fig. 9 as well, required cooling capacity by M-cycle is increased by reduction of humidity ratio (for a given ambient temperature). Obviously, for a given humidity ratio, higher ambient temperature requires larger capacity of M-cycle cooler. The water consumption by M-cycle cooler in the novel integrated cycle is presented in Fig. 10 per one hour working of the whole system.

According to Fig. 10, for most climate conditions the condensed water in the cooling process through the absorption chiller is so higher than the required water by M-cycle for the integrated cycle which is a strong aspect of the novel integrated cycle. The remaining produced water can be used in other parts of the power plant. For the regions under the red line (see Fig. 9) it is possible to reduce the air temperature toward the 15 °C (but not RH 100%) by either absorption chiller or M-cycle. However, for these regions, the application of absorption chiller seems to be more logical compared to the M-cycle because no condensed water is available to be used in M-cycle. Hence, other sources should be provided for water consumption of the M-cycle. Nonetheless, if the water source is available (such as a river etc.), the application of M-cycle is suggested instead of absorption chiller because of simpler structure, lower initial and operation cost.

4. Conclusion

In this study, a novel integrated absorption chiller and Maisotsenko cycle is proposed as an air inlet temperature reducer technique in gas turbine power plants. The air fluid is precooled first by M-cycle toward its dew point temperature and then enters into the absorption chiller. If the whole of this cooling process is done by sole absorption chiller, very huge capacity/size of commercial absorption chiller will be required. The condensed water from the air through the cooling process in the absorption chiller can be used as the required water by M-cycle which is one of the most positive features of the integrated cycle. For some climate conditions, it is possible to obtain ISO condition by only M-cycle application. However, the water should be available for the cooling process by M-cycle. Integrated cycle was found as an appropriate cooling technology in gas turbine power plants. For most climate conditions, maximum three commercial absorption chillers will be enough for the integrated cycle. Sole application of M-cycle is not viable because it is not able to reduce the air temperature less than dew point. All these disadvantages of sole application of M-cycle or sole application of absorption chiller overcome in the novel integrated cycle.

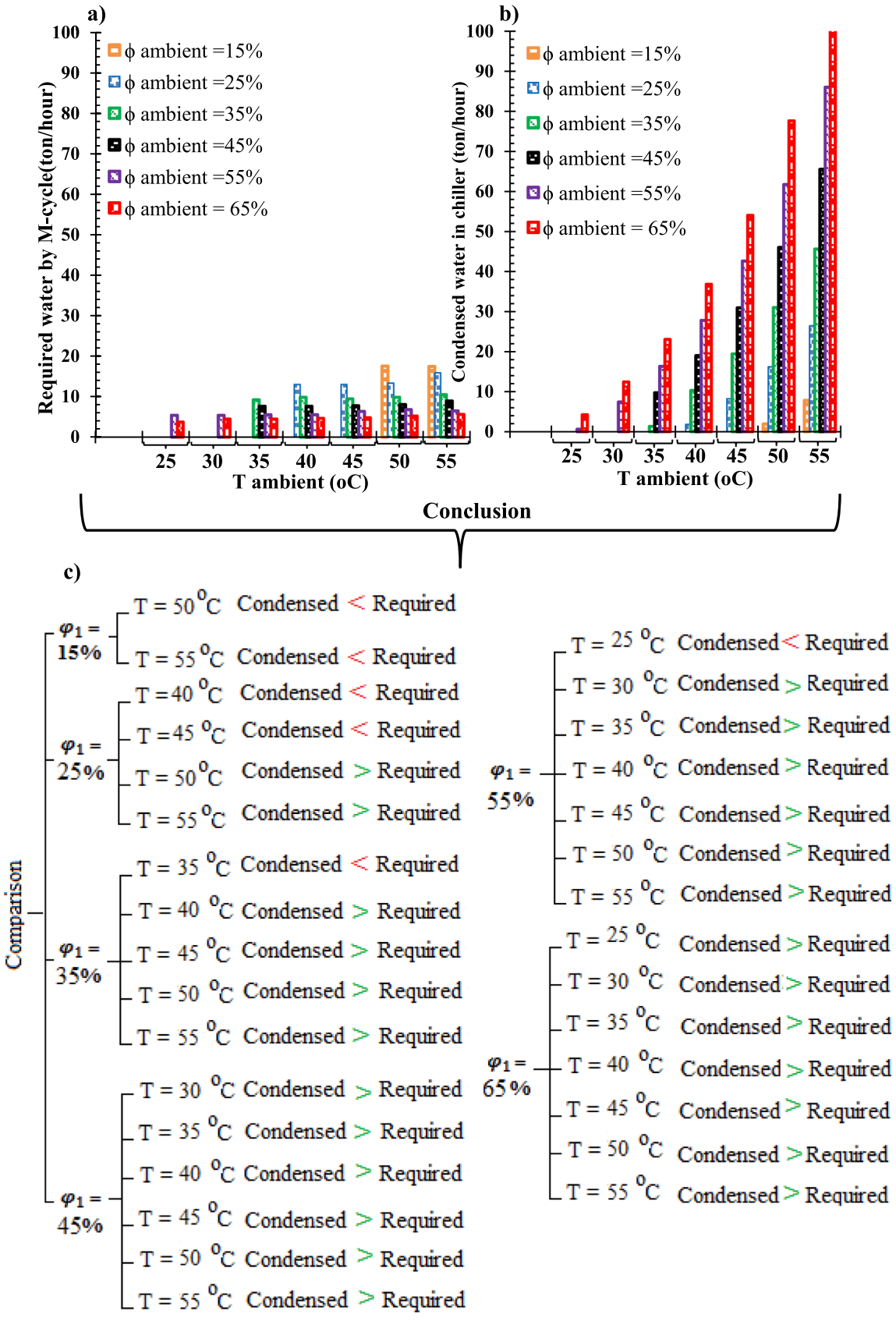

Fig. 10. a) Required water by M-cycle cooler and b) Condensed water in by absorption chiller and c) Comparison between "a" and "b".

Declaration of Competing Interest

The authors confirm that there are no conflicts of interest associated with this paper.

References

[1] El-Hadik AA. The impact of atomospheric conditions on gas turbine performance. Trans ASME 1990;112:590–6.
[2] Najjar YN. Enhancement of performance of gas turbine engines by inlet air cooling and cogeneration system. Appliedthermal Eng 1996;16(2):163–73.
[3] Ameri M, Hejazi SH. The study of capacity enhancement of the chabahar gas turbine installation using an absorption chiler. Scienccdirectvol 2004;24:59–68.
[4] Boonnasa S, Namprakai P, Muangnapoh T. Performance improvement of the combined cycle power plant by intake air cooling using an absorption chiller. Energy 2006;31:2036–46.
[5] Sa A, Zubaidy S. Gas turbine performance at varying ambient temperature. Appl Therm Eng 2011;31:2735–9.
[6] Ehyaei MA, Hakimzadeh S, Enadi N, Ahmadi P. Exergy, economic and environment (3E) analysis of absorption chiller inlet air cooler used in gas turbine power plants. Int J Energy Res 2012;36(4):486–98.
[7] Ahmadi P, Enadi N, Avval HB, Dincer I. Modelling and exergoeconomic optimisation of a gas turbine with absorption chiller using evolutionary algorithm. Int J Exergy 2012;11(1):1–8.
[8] Kwon HM, Kim JH, Kim TS. Gas Turbine Performance Enhancement by Inlet Air Cooling and Coolant Pre-Cooling Using an Absorption Chiller. InASME Turbo Expo 2016: Turbomachinery Technical Conference and Exposition 2016 Jun 13 (pp. V003T06A022-V003T06A022). American Society of Mechanical Engineers.
[9] Mohammadi A, Kasaeian A, Pourfayaz F, Ahmadi MH. Thermodynamic analysis of a combined gas turbine, ORC cycle and absorption refrigeration for a CCHP system. Appl Therm Eng 2017 Jan;25(111):397–406.
[10] Kwon HM, Kim TS, Sohn JL. Performance improvement of gas turbine combined cycle power plant by dual cooling of the inlet air and turbine coolant using an absorption chiller. Energy 2018;15(163):1050–61.
[11] Radchenko R, Radchenko A, Serbin S, Kantor S, Portnoi B. Gas turbine unite inlet air cooling by using an excessive refrigeration capacity of absorption-ejector chiller in booster air cooler. InE3S Web of Conferences 2018 (Vol. 70, p. 03012). EDP Sciences.
[12] Sohani A, Farasati Y, Sayyaadi H. A systematic approach to find the best road map for enhancement of a power plant with dew point inlet air pre-cooling of the air compressor. Energy Convers Manage 2017 Oct;15(150):463–84.
[13] Saghafifar M, Gadalla M. Innovative inlet air cooling technology for gas turbine power plants using integrated solid desiccant and Maisotsenko cooler. Energy 2015;1(87):663–77.
[14] Saghafifar M, Gadalla M. Analysis of Maisotsenko open gas turbine bottoming cycle. Appl Therm Eng 2015 May;5(82):351–9.
[15] Zhu G, Chow TT, Fong KF, Lee CK, Luo XJ. Design optimization and performance appraisal of a combined cooling, heating and power system primed with Maisotsenko combustion turbine cycle. Energy Convers Manage 2018 Dec;1(177):91–106.
[16] Saghafifar M, Gadalla M. Analysis of Maisotsenko open gas turbine power cycle with a detailed air saturator model. Appl Energy 2015 Jul;1(149):338–53.
[17] Moon SW, Kwon HM, Kim TS, Sohn JL. A novel coolant cooling method for enhancing the performance of the gas turbine combined cycle. Energy. 2018 Oct;1(160):625–34.
[18] Najjar YS, Abubaker AM, El-Khalil AF. Novel inlet air cooling with gas turbine engines using cascaded waste-heat recovery for green sustainable energy. Energy 2015 Dec;15(93):770–85.
[19] Farzaneh-Gord M, Deymi-Dashtebayaz M. Effect of various inlet air cooling methods on gas turbine performance. Energy 2011;36(2):1196–205.
[20] Barakat S, Ramzy A, Hamed AM, El Emam SH. Enhancement of gas turbine power output using earth to air heat exchanger (EAHE) cooling system. Energy Convers Manage 2016 Mar;1(111):137–46.
[21] Al-Ansary HA, Orfi JA, Ali ME. Impact of the use of a hybrid turbine inlet air cooling system in arid climates. Energy Convers Manage 2013 Nov;1(75):214–23.
[22] http://www.simonsgreenenergy.com.au.
[23] Anisimov S, Pandelidis D, Danielewicz J. Numerical analysis of selected evaporative exchangers with the Maisotsenko cycle. Energy Convers Manage 2014 Dec;31(88):426–41.
[24] Miyazaki T, Akisawa A, Nikai I. The cooling performance of a building integrated evaporative cooling system driven by solar energy. Energy Build 2011;43(9):2211–8.
[25] Dizaji HS, Hu EJ, Chen L. A comprehensive review of the Maisotsenko-cycle based air conditioning systems. Energy 2018;1(156):725–49.
[26] Dizaji HS, Hu EJ, Chen L, Pourhedayat S. Development and validation of an analytical model for perforated (multi-stage) regenerative M-cycle air cooler. Appl Energy 2018 Oct;15(228):2176–94.
[27] Dizaji HS, Jafarmadar S, Khalilarya S, Pourhedayat S. A comprehensive exergy analysis of a prototype Peltier air-cooler; experimental investigation. Renew Energy 2019 Feb;1(131):308–17.
[28] www.coolerado.com/news/coolerados-super-efficient-air-conditioning-expanded-to-include-small-residences/.

Chapter 7

Conclusion and Future Work

7.1. Conclusions

Indirect evaporative cooler is a cooling mechanism in which the temperature of product air is reduced via water evaporation without adding moisture to the product air. M-cycle type of indirect evaporative coolers is able to reduce the air temperature below the wet-bulb temperature towards the dew-point temperature of ambient air. Indirect evaporative cooler consists of two main parts including dry channel and wet channel. These two channels are separated from each other using an ultra-thin plate (to minimize the thermal conductivity resistance). The working principle of the cooler is associated with sensible heat transfer, latent heat transfer, water evaporation, mass transfer and prose surface (material of the channels' separator) which significantly complicates the numerical simulation of the cooling processes by M-cycle (however, in the absence of analytical solution (model) for any thermodynamic process, employment of numerical solutions is unavoidable). In this thesis, a high accurate quick solving analytical model was developed for multi-stage M-cycle based air conditioning systems.

Previous simplified models are only valid for single stage conventional indirect evaporative coolers (with constant wall temperature which is not real) and provides only outlet temperature/humidity of the cooler. However, current model was developed for multi-stage M-cycle type of indirect evaporative coolers (much more efficient comparted to the conventional coolers) which works based on real working condition (variant wall temperature, wet-surface theory) and it was able to provide temperature/humidity distributions through the cooler (in addition to the outlet parameters). All previous evaluations of multi-stage M-cycle cooler were carried

out only via cumbersome sophisticated numerical simulations because of lack of analytical model. The proposed models are applicable for M-cycle dew point coolers. However, mathematically, the difference between traditional indirect evaporative cooler and M-cycle cooler, is their boundary conditions. Hence, the new high-accurate quick analytical model can also be employed for traditional coolers by modifying the boundary conditions through the beginning of the programing code.

The proposed model is able to generate the characteristics of the cooler for a set of given inlet parameters. Moreover, the temperature and humidity distribution through the dry channel, wet channel and middle separator curtain are provided by the model as a function of "x" which makes the model as strong analysis/designing tool of M-cycle coolers. The solution time of the cooler using the proposed analytical model is significantly shorter than the numerical simulation without the reduction of accuracy. The model was validated with experimental data and employed to perform a comprehensive sensitivity analysis of multi-stage M-cycle cooler. The model also was employed to evaluate the cooler from the second law of thermodynamic viewpoint. The main conclusions of this research are summarized in the following.

7.1.1. Analytical model based on sprayed-water mechanism

Working principle of indirect evaporative cooler can be classified into two main categories including sprayed-water mechanism and wet-surface mechanism. Both of these mechanisms can be employed in the cooler depending on the application of the cooler (indoor cooler, outdoor cooling, size of the cooling environment), size of the cooler, expected temperature reduction of the air, availability of the water, pressure drop through the channels, production cost of the cooler and so on. In

sprayed-water mechanism the water fluid comes down from the top side of the cooler (and recirculated from the bottom side again) with roughly large value of water mass flow rate. The water fluid continuously comes flows and creates continuous water streams on the middle surface (separator surface between wet and dry channel). That is why, the middle surface is not supposed to have specific material (such as porous media or tissue-like materials to absorb the water) which reduces the price of the cooler. This working condition is appropriate for high temperature range of weather conditions, big halls and outdoor cooling (this method has been used in most conventional type of indirect evaporative coolers). As the most portion of thermal process occurs in sensible heat transfer form, the cooling capacity of cooler is low (compared to the wet-surface mechanism). The first analytical model was developed under this working condition. As the water fluid is sprayed with high mass flow rate, it dominates the temperature of the middle surface. The temperature of the middle surface is almost the same as water inlet temperature through the whole surface and that is what the inlet temperature of the water should be colder than the ambient air temperature. Otherwise, the cooler is not be able to cool the air. The latent heat transfer mechanism does not have significant role in the sprayed-water mechanism. The created noise due to the the high pressure sprayed-water system may make them unsuitable for inside-room applications.

7.1.2. Analytical model based on wet-surface mechanism

Contrary to the sprayed-water mechanism, the water flow rate in wet-surface theory should be as possible as small. In this systems, the water is absorbed by the middle surface to create a continuous wet-surface. That is why the material of the middle surface is important if this mechanism. The wet-side of the middle ultra-thin

surface should be tissue-like (porous) to absorb the water and keep the surface wetly all the time while the dry side of the middle surface should be impermeable (nylon like). The material with mentioned specifications is employed in recent generations of M-cycle coolers. Theoretically, the water flow rate is the same as evaporated water and is replaced immediately and without the creation of any water stream. The M-cycle under this working condition achieves its maximum cooling capacity. However, water distribution system causes some limitations in real cooler as it is not possible to replace the evaporated water with small water flow rates. Any further water flow rate (and creation of water streams on the surface) is reduced the cooling capacity of the cooler. Thus, in real coolers, the idea of the water distribution system will play a key role on the performance of the cooler. Because of the major role of latent heat transfer in this mechanism, the cooler is able to reduce the air temperature even if the water inlet temperature is the same as air inlet (ambient) temperature. Contrary to the sprayed-water mechanism, the temperature of the middle surface varies through the "x" and its temperature is dominated with fluid flow conditions through the channels (not water inlet temperature). In other words, the surface evaporation of the ultra-thin water film (evaporation rate depends on fluid flow condition through the both channels) dominates the temperature distribution through the middle surface. Innovative materials which can absorb the water and spread it through the whole surface quickly makes the performance of the real cooler to the theoretical performance. Nonetheless, it is noted that, the dew-point temperature of the ambient temperature is the minimum achievable temperature for any type of indirect evaporative coolers. The second analytical model was developed based on the mentioned wet-surface theory. The model is able able to provide the outlet characteristics of the cooler and also temperature/humidity

distribution along the dry/wet channel and middle surface. Required experimental test-rig was designed to validate the analytical model with experimental data. The M-cycle cooler under wet-surface mechanism can be employed in any room size through a wide range of weather conditions.

All thermal/fluid and geometric parameters were then changed to provide a comprehensive sensitivity analysis using the analytical model with below conclusions.

- ✓ Although the increment of the ambient temperature increases the outlet temperature of the product air, the temperature-drop is enhanced which means higher cooling efficiency for warmer ambient temperatures.
- ✓ Changing of the discharged air into the wet channel, can increase or decrease the outlet product temperature depending on the created Reynolds number for each part of the cooler which varies based on mass flow ratios.
- ✓ Smaller channel gap provides colder outlet temperature with a sharp curve behavior. However, channel height does not impress the cooling capacity as severity as channel gap.
- ✓ By moving the middle perforation towards the end of the dry channel, the outlet temperature of product air is first increased and then decreased so that the maximum (warmer) temperature occurs when the perforation is in the middle of the channel.

7.1.3. Exergetic viewpoint of M-cycle cooler

Exergy analysis of any thermodynamic process is important as it is associated with economic analysis of the engineering systems. The emergence of some specific expressions such as exergoeconomic and thermoeconomic further reveals the significance of exergy analysis of systems. Exergoeconomy is strong tool to

optimize the engineering systems from cost-efficiency and economic viewpoints. Moreover, exergy analysis of any individual unit (system) is required when it works as a subset of a large whole system (such as power plant) to provide general economic considerations and marketing related decision-makings. That is why, as M-cycle cooler can be employed in a wide range of cooling applications, an strategy for exergetic analysis of M-cycle is required which was provided in this research as well. It was showed how the provided analytical model can be expanded and employed for exergetic analysis of M-cycle cooler. The impact of key operational and design parameters on exergetic characteristics of the cooler was evaluated and discussed.

Increment of air mass flow rate and mass flow ratio between two channels increased the exergy destruction through cooling process. Hence, it is recommenced to employ an optimum number of channels in the designing process of the cooler to allocate a logical value of air mass flow rate for any individual channel. Indeed, in the same total inlet air flow rate, the air velocity along the channels can be controlled by the numbers of parallel channels in the designing process of M-cycle based on the second law of thermodynamics. In other words, in a constant air inlet flow rate, it is possible to increase the plate numbers and increase the exergetic efficiency of the cooler without reduction of thermal efficiency of the cooler. Humid air reduced the exergy destruction and augmented the exergetic efficiency of M-cycle cooler. Exergetic efficiency were enhanced by reduction of air inlet temperature, air inlet flow rate and mass flow ratio. Based on the application of M-cycle cooler (as an air conditioning systems or other applications), the cooler can be designed in a manner to meet the required exergetic characteristics of the cooler.

7.1.4. Other potential application of M-cycle cooler

Although Maisotsenko-cycle based air coolers was firstly developed as air conditioning systems, many other potential applications of M-cycle cooler lately were proposed by researchers. As the M-cycle working principle was comprehensively investigated in this research, other innovative probable applications of M-cycle was considered as well. Most recently, the M-cycle cooler was proposed as a pre-cooler technology for gas turbine based power plants. Generally, the output power of gas turbines is significantly reduced during the hot days of the year (because of lower density and subsequently low air mass flow rate of intake air to the gas turbine). Exhaust hot gas at the outlet of the turbine is a potential source for running the absorption chiller and that is why this mechanism is mainly employed for the mentioned aim. However, the required size/capacity of absorption chiller is high which leads to higher initial/operation/maintenance cost. That is why, the combination of M-cycle and absorption chiller (hybrid cycle) is a promising solution which is proposed as the last part of this research. In this hybrid cycle, the air fluid is first pre-cooled by M-cycle cooler before entering to the absorption chiller. Hence, the required capacity and size of the absorption chiller is significantly reduced. One significant feature of the hybrid cycle is that a large portion of the required water for M-cycle cooler can be supplied from the condensed water through the cooling process by absorption chiller. For some climate conditions, the application of M-cycle would be enough without the requirement of any absorption chiller. Obviously the working principle of M-cycle is so simpler than the absorption chiller and its general costs is lower. It is noted that, direct evaporative cooler can not be employed for this application because of the probable issues (due to the water droplets) such as erosion and corrosion. The results of this

part of the research showed the applicability of proposed hybrid cycle for gas turbine intake air pre-cooler.

7.2. Future Work

The proposed hybrid cycle at the last part of this research needs further consideration from different viewpoints. Although the general idea was qualitatively proposed, it is still unclear how many MW quantitatively can be increased by the employment of this cycle for gas turbine power plants. Hence, it is proposed as a future work to focus on the application of M-cycle for gas turbine based power plants and identify its characteristics.

As described in the wet-surface theory, the water flow rate is as possible as small to create a wet-surface. However, in real practical M-cycle coolers, the water mass flow rate is neither such small (such as wet-surface theory) nor large. Thus, it is proposed to modify the current analytical model with consideration of any arbitrary limit water mass flow rate. Mathematically, the ratio of water mass flow rate to the air flow rate should be tend for a constant vale rather than zero (in wet-surface theory). The modified model will be more complicated to solve but with more accurate results compared to the real working condition of the M-cycle cooler. However, it is noted that, the maximum cooling of the cooler is occurred in under wet-surface mechanism. However, it is impossible (at least with current water distribution systems) to practically apply the wet-surface mechanism.

Appendix A, Programming code of wet-surface theory

```
restart;

Round := proc (x, n) options operator, arrow; parse(sprintf("%.*f", n, x)) end

proc;

parameters(TC, WC);

ThicknessOfPlate := 0.5e-3;

PlateThermalConductivity := 0.25e-2;

WaterFilmThicness := 0.1e-3;

P := 101325;

a := 0.5e-2;

b := .2;

L := 1;

LatoL := .75;

Nesbat := LatoL;

La := Nesbat*L;

Lb := L-La;

InletAirTem := 25;

InletHumidity := 0.15e-1;

InletairMassflow := 0.1e-1;

InletWaterTem := 30;

Ea := .2;

Eb := .2;

mdat1La := InletairMassflow;

mdat1Lb := InletairMassflow*(1-Ea);

mdat2La := InletairMassflow*(Ea+Eb);
```

```
mdat2Lb := InletairMassflow*Eb;

ca := 1.0029+5.4*InletAirTem*10^(-5);

cv := 1.856+2*InletAirTem*10^(-4);

c1 := ca/(1+InletHumidity)+cv*InletHumidity/(1+InletHumidity);

ifg := 2501;

ibarfg := ifg/ca;

Miuoo := 1.8*10^(-5);

Pr := .7;

K := 0.26e-1/1000;

dh := 2*a*b/(a+b);

Kwater := .6/1000;

Ro :=

101325*(1+InletHumidity)/((461.56*(.62195+InletHumidity))*(InletAirTem+273

.15));

V1La := mdat1La/(Ro*a*b);

V1Lb := mdat1Lb/(Ro*a*b);

V2La := mdat2La/(Ro*a*b);

V2Lb := mdat2Lb/(Ro*a*b);

Re1La := Ro*V1La*dh/Miuoo;

Re1Lb := Ro*V1Lb*dh/Miuoo;

Re2La := Ro*V2La*dh/Miuoo;

Re2Lb := Ro*V2Lb*dh/Miuoo;

ALa := b*La;

Alb := b*Lb;
```

if Re2Lb > 3000 or Re2Lb = 3000 then f2La := 1/(.79*ln(Re2La)-1.64)^2; f2Lb := 1/(.79*ln(Re2Lb)-1.64)^2; Nu2La := (1/8)*f2La*Pr*(Re2La-1000)/(1+(12.7*(Pr^(2/3)-1))*((1/8)*f2La)^.5); Nu2Lb := (1/8)*f2Lb*Pr*(Re2Lb-1000)/(1+(12.7*(Pr^(2/3)-1))*((1/8)*f2Lb)^.5); Alfa2La := K*Nu2La/dh; Alfa2Lb := K*Nu2Lb/dh; NTU2La := Alfa2La*ALa/(mdat2La*ca); NTU2Lb := Alfa2Lb*Alb/(mdat2Lb*ca) else Nu2Lb := 4.36; Alfa2Lb := K*Nu2Lb/dh; NTU2Lb := Alfa2Lb*Alb/(mdat2Lb*ca); if Re2La > 3000 or Re2La = 3000 then f2La := 1/(.79*ln(Re2La)-1.64)^2; Nu2La := (1/8)*f2La*Pr*(Re2La-1000)/(1+(12.7*(Pr^(2/3)-1))*((1/8)*f2La)^.5); Alfa2La := K*Nu2La/dh; ALa := b*La; NTU2La := Alfa2La*ALa/(mdat2La*ca) else Nu2La := 4.36; Alfa2La := K*Nu2La/dh; NTU2La := Alfa2La*ALa/(mdat2La*ca) end if end if;
if Re1La < 3000 then Nu1La := 4.36; Nu1Lb := 4.36; Alfa1La := K*Nu1La/dh; Alfa1Lb := K*Nu1Lb/dh; U1La := 1/(1/Alfa1La+ThicknessOfPlate/PlateThermalConductivity+WaterFilmThicness/Kwater); U1Lb := U1La else f1La := 1/(.79*ln(Re1La)-1.64)^2; Nu1La := (1/8)*f1La*Pr*(Re1La-1000)/(1+(12.7*(Pr^(2/3)-1))*((1/8)*f1La)^.5); Alfa1La := K*Nu1La/dh; if Re1Lb < 3000 then Nu1Lb := 4.36; Alfa1Lb := K*Nu1Lb/dh else f1Lb := 1/(.79*ln(Re1Lb)-1.64)^2; Nu1Lb := (1/8)*f1Lb*(Re1Lb-1000)*Pr/(1+12.7*((1/8)*f1Lb)^.5*(Pr^(2/3)-1)); Alfa1Lb := K*Nu1Lb/dh end if; U1La := 1/(1/Alfa1La+ThicknessOfPlate/PlateThermalConductivity+WaterFilmThicness/Kwater); U1Lb := 1/(1/Alfa1Lb+ThicknessOfPlate/PlateThermalConductivity+WaterFilmThicness/Kwater) end if;

RLa := U1La/Alfa2La;

RLb := U1Lb/Alfa2Lb;

CstarFLa := mdat1La*c1/(ca*mdat2La);

CstarfLb := mdat1Lb*c1/(ca*mdat2Lb);

twmin := InletWaterTem;

twmax := twmin+1;

Psatmin := 2.7182^(-.58002206*10^4/(twmin+273.15)+1.39149-0.48640239e-

1*(twmin+273.15)+.417647*10^(-4)*(twmin+273.15)^2-.14452*10^(-

7)*(twmin+273.15)^3+(.654596*10)*ln(twmin+273.15));

Psatmax := 2.7182^(-.58002206*10^4/(twmax+273.15)+1.39149-0.48640239e-

1*(twmax+273.15)+.417647*10^(-4)*(twmax+273.15)^2-.14452*10^(-

7)*(twmax+273.15)^3+(.654596*10)*ln(twmax+273.15));

weqmin := .621945*Psatmin/(P-Psatmin);

weqmax := .621945*Psatmax/(P-Psatmax);

weqmean := (weqmin+weqmax)*(1/2);

e := (weqmax-weqmin)/(twmax-twmin);

F := (2*(weqmin+weqmean)-weqmax)/(-e*twmin+3);

eta := e*ibarfg+1;

GLa := Round(-RLa*NTU2La*ibarfg*F/(CstarFLa*(RLa+eta)), 2);

HLa := Round(-GLa/F, 2);

ILa := Round(-GLa/(F*ibarfg), 2);

JLa := Round(GLa*eta/(F*ibarfg), 2);

KLa := Round(ibarfg*NTU2La*F/(RLa+eta), 2);

LLa := Round(-KLa/F, 2);

MLa := Round(-(1-RLa-eta)*NTU2La/(RLa+eta), 2);

```
NLa := Round(ILa*CstarFLa, 2);

OLa := Round(F*NTU2La*e*(ibarfg-(RLa+eta)/e)/(RLa+eta), 4);

ZLa := Round(-OLa/F, 4);

VLa := Round(-NTU2La*e/(RLa+eta), 5);

QLa := Round(-NTU2La*RLa*e/(RLa+eta), 4);

GLb := Round(-RLb*NTU2Lb*ibarfg*F/(CstarfLb*(RLb+eta)), 2);

HLb := Round(-GLb/F, 2);

ILb := Round(-GLb/(F*ibarfg), 2);

JLb := Round(GLb*eta/(F*ibarfg), 2);

KLb := Round(ibarfg*NTU2Lb*F/(RLb+eta), 2);

LLb := Round(-KLb/F, 2);

MLb := Round(-(1-RLb-eta)*NTU2Lb/(RLb+eta), 2);

NLb := Round(ILb*CstarfLb, 2);

OLb := Round(F*NTU2Lb*e*(ibarfg-(RLb+eta)/e)/(RLb+eta), 4);

ZLb := Round(-OLb/F, 4);

VLb := Round(-NTU2Lb*e/(RLb+eta), 5);

QLb := Round(-NTU2Lb*RLb*e/(RLb+eta), 4);

sys_odeLa := diff(T1(x), x) = GLa+HLa*W2(x)+ILa*T2(x)+JLa*T1(x),

diff(T2(x), x) = KLa+LLa*W2(x)+MLa*T2(x)+NLa*T1(x), diff(W2(x), x) =

OLa+ZLa*W2(x)+VLa*T2(x)+QLa*T1(x);

bcsLa := T1(0) = InletAirTem, T2(Nesbat) = Tc, W2(Nesbat) = Wc;

sLa := evalf(simplify(evalf(simplify(dsolve({bcsLa, sys_odeLa})))));

sLa := subs(I = 0, sLa);

xx := T1(x);

T1 := subs(sLa, xx);
```

```
T1nesbat := subs(x = Nesbat, T1);

M1 := TA-T1nesbat = 0;

yy := T2(x);

T2 := subs(sLa, yy);

T20 := evalf(subs(x = 0, T2));

M2 := Tzegon2-T20 = 0;

zz := W2(x);

W2 := subs(sLa, zz);

W20 := evalf(subs(x = 0, W2));

M3 := Wzegon2-W20 = 0;

sys_odeLb := diff(t1lb(x), x) = GLb+HLb*w2lb(x)+ILb*t2lb(x)+JLb*t1lb(x),

diff(t2lb(x), x) = KLb+LLb*w2lb(x)+MLb*t2lb(x)+NLb*t1lb(x), diff(w2lb(x), x)

= OLb+ZLb*w2lb(x)+VLb*t2lb(x)+QLb*t1lb(x);

bcsLb := t1lb(1) = t2lb(1), t1lb(Nesbat) = TA, w2lb(1) = InletHumidity;

sLb := evalf(simplify(evalf(simplify(dsolve({bcsLb, sys_odeLb})))));

sLb := subs(I = 0, sLb);

xxx := t1lb(x);

t1lb := subs(sLb, xxx);

t11lb := evalf(subs(x = 1, t1lb));

M4 := Tzegon1-t11lb = 0;

yyy := t2lb(x);

t2lb := subs(sLb, yyy);

T2Nesbat := evalf(subs(x = Nesbat, t2lb));

M5 := TB-T2Nesbat = 0;

zzz := w2lb(x);
```

```
w2lb := subs(sLb, zzz);

W2nesbat := evalf(subs(x = Nesbat, w2lb));

M6 := WB-W2nesbat = 0;

M7 := Wc-(Ea*InletHumidity+Eb*WB)/(Ea+Eb) = 0;

aaa := (cv*InletHumidity+ca)*TA;

bbb := (ifg*InletHumidity+aaa)*Ea;

ccc := (WB*cv+ca)*TB;

ddd := WB*ifg;

eee := (ccc+ddd)*Eb;

fff := (Ea+Eb)*Wc*ifg;

ggg := (Ea+Eb)*(Wc*cv+ca);

hhh := (bbb+eee-fff)/ggg;

M8 := Tc-hhh = 0;

M := M1, M2, M3, M4, M5, M6, M7, M8;

Results := solve({M}, {TA, TB, Tc, Tzegon1, Tzegon2, WB, Wc, Wzegon2});

qq := Tzegon1;

ww := TB;

tt := WB;

uu := Wc;

ii := Tc;

oo := TA;

pp := Tzegon2;

aa := Wzegon2;

Tzegon1 := subs(Results, qq);

TB := subs(Results, ww);
```

```
WB := subs(Results, tt);

Wc := subs(Results, uu);

Tc := subs(Results, ii);

TA := subs(Results, oo);

Tzegon2 := subs(Results, pp);

Wzegon2 := subs(Results, aa);

T1xLa := evalf(T1);

T2xLa := evalf(T2);

W2xLa := evalf(W2);

TwxLa := -(ibarfg*(F-W2xLa)-T2xLa-RLa*T1xLa)/(RLa+eta);

T1xLb := evalf(t1lb);

T2xLb := evalf(t2lb);

W2xLb := evalf(w2lb);

TwxLb := -(ibarfg*(F-W2xLb)-T2xLb-RLa*T1xLb)/(RLb+eta);
```